



**HAL**  
open science

# Intracellular and extracellular signatures of action potentials initiated in the axon

Maria Telenczuk

► **To cite this version:**

Maria Telenczuk. Intracellular and extracellular signatures of action potentials initiated in the axon. Neurons and Cognition [q-bio.NC]. Université Pierre et Marie Curie - Paris VI, 2016. English. NNT : 2016PA066211 . tel-01425136

**HAL Id: tel-01425136**

**<https://theses.hal.science/tel-01425136>**

Submitted on 3 Jan 2017

**HAL** is a multi-disciplinary open access archive for the deposit and dissemination of scientific research documents, whether they are published or not. The documents may come from teaching and research institutions in France or abroad, or from public or private research centers.

L'archive ouverte pluridisciplinaire **HAL**, est destinée au dépôt et à la diffusion de documents scientifiques de niveau recherche, publiés ou non, émanant des établissements d'enseignement et de recherche français ou étrangers, des laboratoires publics ou privés.



**THÈSE DE DOCTORAT DE  
L'UNIVERSITÉ PIERRE ET MARIE CURIE**

Spécialité

**Neurosciences**

École doctorale Cerveau, Cognition et Comportement

Présentée par

**Maria TELEŃCZUK**

Pour obtenir le grade de  
DOCTEUR de L'UNIVERSITÉ PIERRE ET MARIE CURIE

Sujet de la thèse:

**Intracellular and extracellular signatures of action potentials  
initiated in the axon**

soutenue le 23 Septembre 2016

devant le jury composé de:

Dr. Romain BRETTE	Directeur de thèse
Dr. Alain DESTEXHE	Examineur
Pr. Gaute EINEVOLL	Rapporteur
Pr. Michele GIUGLIANO	Examineur
Dr. Jean-Marc GOAILLARD	Rapporteur
Dr. Catherine VILLARD	Examineur



mojemu mężowi Bartkowi  
oraz tacie Maciejowi



---

## Contents

---

<b>Acknowledgements</b>	<b>x</b>
<b>Summary</b>	<b>xiii</b>
1.1 Abstract . . . . .	xiii
1.2 Résumé (en français) . . . . .	xiv
<b>2 Introduction to action potential</b>	<b>1</b>
2.1 Context and objective of this work . . . . .	2
2.2 Currents during action potential . . . . .	5
2.2.1 Hodgkin and Huxley Model . . . . .	5
2.2.2 Voltage gated channels . . . . .	7
2.2.2.1 Sodium channels . . . . .	7
2.2.2.2 Potassium channels . . . . .	12
2.2.2.3 Other voltage gated channels . . . . .	16
2.2.3 Energy efficiency . . . . .	18
2.3 Role of different neuronal segments . . . . .	19
2.3.1 Soma . . . . .	20
2.3.2 Axon . . . . .	21
2.3.3 Axon initial segment . . . . .	24
2.3.4 Synapse . . . . .	27
2.3.5 Dendrite . . . . .	28
2.3.6 Impact of morphology on the firing pattern . . . . .	29
2.4 Kink at the initiation, experiments vs models . . . . .	29
2.4.1 Cooperativity Hypothesis . . . . .	30

2.4.2	Backpropagation Hypothesis . . . . .	31
2.4.3	Critical Resistive Coupling Hypothesis . . . . .	31
2.5	Signature of a single cell activity in the extracellular potential . . . . .	32
2.6	Bursts of action potentials . . . . .	33
2.7	Activity of single cell within population . . . . .	33
2.8	Sharp Waves as example of network activity . . . . .	34
2.9	Malfunction of action potential . . . . .	37
2.9.1	Epilepsy . . . . .	37
2.9.2	Stroke . . . . .	38
2.9.3	Alzheimer’s disease . . . . .	38
2.9.4	Other Disease . . . . .	39
<b>3</b>	<b>The basis of sharp spike onset in standard biophysical models</b>	<b>61</b>
3.1	Abstract . . . . .	61
3.2	Author summary . . . . .	62
3.3	Introduction . . . . .	62
3.4	Results . . . . .	64
3.4.1	Intracellular and extracellular features of sharp spike initiation in multicompartmental models . . . . .	64
3.4.2	Extracellular field at spike initiation . . . . .	64
3.4.3	Currents at spike initiation . . . . .	67
3.4.4	Excitability increases with intracellular resistivity . . . . .	70
3.4.5	Sharp spike initiation requires a large enough somatodendritic compartment . . . . .	72
3.4.6	Backpropagation does not sharpen spikes . . . . .	74
3.4.7	Active backpropagation is not necessary for sharp spike initiation . . . . .	77
3.4.8	Sharp somatic onset is reproduced by a model with two resistively coupled compartments . . . . .	79
3.5	Discussion . . . . .	81
3.6	Materials and methods . . . . .	86
3.6.1	Detailed neuron models . . . . .	86
3.6.1.1	Morphology . . . . .	87
3.6.1.2	Channel properties . . . . .	87
3.6.2	Two-compartment model . . . . .	88
3.6.3	Analysis . . . . .	88
3.6.3.1	Voltage-clamp . . . . .	88
3.6.3.2	Phase slope . . . . .	88

3.6.4	Theoretical prediction of onset rapidness . . . . .	89
3.7	Acknowledgments . . . . .	89
<b>4</b>	<b>Local field potential generated by neurons with different localisation of axon initial segment</b>	<b>95</b>
4.1	Results . . . . .	96
4.1.1	Soma-axon model . . . . .	96
4.1.2	Far-field dipole approximation . . . . .	99
4.1.3	Dipole model – near field . . . . .	102
4.1.4	Two cylinder model . . . . .	104
4.2	Discussion . . . . .	107
4.3	Methods . . . . .	108
4.3.1	Soma-axon model . . . . .	108
4.3.2	Linear Source Approximation . . . . .	108
4.3.3	Two cylinders model . . . . .	109
<b>5</b>	<b>Single CA3 pyramidal cells trigger sharp waves <i>in vitro</i> by exciting interneurones</b>	<b>113</b>
5.1	Abstract . . . . .	113
5.2	Introduction . . . . .	114
5.3	Methods . . . . .	115
5.3.1	Slice preparation . . . . .	115
5.3.2	Drugs . . . . .	115
5.3.3	Recordings . . . . .	116
5.3.4	Signal analysis . . . . .	116
5.3.5	Statistical analysis . . . . .	118
5.4	Results . . . . .	120
5.4.1	Single pyramidal cells initiate SPWs and field IPSPs . . . . .	120
5.4.2	fIPSPs from perisomatic interneurones are repeated in SPW fields	120
5.4.3	Excitation of interneurons by single pyramidal cells . . . . .	122
5.4.4	Comparison of spontaneous SPWs and SPWs initiated by single cells	125
5.4.5	Patterns of SPW spread and the activity of identified interneurons	127
5.5	Discussion . . . . .	129
5.5.1	Advantages of an <i>in vitro</i> study . . . . .	129
5.5.2	Initiating pyramidal cells excite perisomatic interneurones . . . . .	130
5.5.3	Continuation, spread and cellular components of SPWs . . . . .	130

<b>6</b>	<b>Conclusions</b>	<b>137</b>
6.1	Uniqueness of Action Potential . . . . .	138
6.2	Role of the axon in neuronal coding . . . . .	139
<b>A</b>	<b>Recurrent synapses and circuits in the CA3 region of the hippocampus: an associative network</b>	<b>143</b>
A.1	Abstract . . . . .	143
A.2	Recurrent excitatory synapses between CA3 cells: emergence . . . . .	144
A.3	Axonal distributions of CA3 pyramidal cells . . . . .	145
A.4	CA3 pyramidal cell axon physiology . . . . .	146
A.5	CA3 pyramidal cell terminals: numbers, form, contents, channels and release	146
A.6	Pre- meets post: synapses made by CA3 pyramidal cells with other CA3 cells . . . . .	148
A.7	Pre- meets post in dual records . . . . .	149
A.8	Short-term and long-term synaptic plasticity in double recordings . . . . .	151
A.9	Transmission of recurrent excitatory signals on the membrane of a post- synaptic cell . . . . .	152
A.10	Recurrent excitatory contributions to population activities in the CA3 region	153
A.11	Interictal epileptiform rhythm . . . . .	155
A.12	Sharp-wave rhythm . . . . .	156
A.13	Theta and gamma rhythms . . . . .	156
A.14	Comparison of recurrent connectivity in CA3 and other cortical regions . . . . .	157
A.15	The CA3 recurrent system as an associative network . . . . .	158
	<b>List of Figures</b>	<b>173</b>
	<b>List of Tables</b>	<b>175</b>



---

## Acknowledgements

---

I am truly indebted to my PhD supervisor Romain Brette who gave me an opportunity to work on this project and provided his support when my academic career seemed to be falling apart. I would not complete this thesis without his scientific guidance, which gave me the best example of scholarly work.

This thesis would also not exist without friendly support of Pierre Yger who in difficult moments reached out his helpful hand.

I would like to thank Richard Miles, whose work and encouragement brought me to join the scientific community of Paris.

I am eternally grateful to Valérie Bercier who offered her gracious help when I needed it most and spent countless hours on reading my thesis and laboriously correcting all the English mistakes. I am also thankful to Mariana Ramos and Stefan Percoco for jointly translating the abstract to French.

I am obliged to many of my colleagues who have not yet been mentioned, and who supported, encouraged and educated me: Marcel Stimberg, Jean Simonnet, Charlotte Le Mouel, Katia Lehongre, Mérie Nassar, Desdemona Fricker, Caroline Le Duigou, Etienne Savary, Michaël Bazelot, Marta Kołodziejczak, Vasilisa Skvortsova and Jenna Stimberg. I have always enjoyed and learnt from discussing with them scientific and non-scientific topics.

I would also like to acknowledge the support I received from members of my family who believed in me throughout years of my PhD and to my daughter Weronika who taught me science in everyday life and brought more life to my science.

I would like to thank members of my dissertation committee for their time and help as well as the anonymous reviewers of the articles which are part of this work.

I would not be able to devote to scientific research without the financial support I have

received from the l'École des Neurosciences de Paris, Domaines d'Intérêt Majeur – Île de France and l'Agence Nationale de la Recherche. In addition, I would like to acknowledge administrative help of Yvette Henin, Laura Peeters and Deborah Deslierres.

Above all, I would like to thank my husband, Bartosz Teleńczuk who was always there throughout the course of my studies as a best friend and scientific guide and without whose support and confidence I would never be able to complete this thesis.



## 1.1 Abstract

The action potential is considered one of the major signalling events in the brain and malfunction of firing of action potentials might lead to various neurological diseases. Although it has been studied for years, many questions remain unanswered. The present work is dedicated to the study of action potential generation, its impact on extracellular field and local network establishment. We considered three questions: Firstly, (i) we asked why mammalian neurons often have characteristically sharp onset in the somatic recordings of action potentials. Until recently, researchers debated on the causes of this so-called ‘kink’. We tested different hypotheses by means of computational modelling. We show that the Critical Resistive Coupling Hypothesis is sufficient to explain how the action potential is initiated in the axon initial segment to provide for the ‘kink’ in the soma, while the Backpropagation Hypothesis is not sufficient to explain it. Next, (ii) we asked how the placement of the axon initial segment might affect the extracellular field. Experimental recordings reveal that the location of the axon initial segment varies in different cell types and might be altered by elevated activity. We provide theoretical evidence that those differences are reflected extracellularly. Most importantly, we show that the impact of the axon initial segment position on the shape and amplitude of extracellular action potential depends on the distance between the recording site and the axon and on its position along the soma–axon initial segment axis. Finally, (iii) we inquired if a single action potential might have an effect on the network activity as the impact of a single action potential on the local network is often questioned. So-called sharp-wave ripple complexes are hippocampal network events identified in the extracellular activity which are believed to be responsible for memory consolidation. We show that a single action

potential from a single pyramidal neuron in the hippocampus can trigger sharp-wave ripple activity consisting of the firing of multiple interneurons.

Altogether, our results show that action potentials are complex events shaped by the biochemistry of the neuronal membrane and morphology of the axon. In addition these features strongly modulate the neuron's impact on the extracellular field and network activity.

## 1.2 Résumé (en français)

Le potentiel d'action est un des événements de signalisation majeurs du cerveau. Des défauts dans ce processus peuvent entraîner des maladies neurologiques. Même si le potentiel d'action a beaucoup été étudié, plusieurs questions restent sans réponse. Ce travail est dédié à l'étude de la génération du potentiel d'action, et son impact dans le potentiel extracellulaire ainsi que dans le réseau local. Pour ce faire nous avons abordé trois questions principales.

Premièrement, nous nous sommes intéressés à comprendre pourquoi les potentiels d'action ont souvent un début brutal ('kink') dans les enregistrements somatiques des neurones de mammifères. L'origine de ce phénomène, est actuellement en débat. Nous avons testé différentes hypothèses par modélisation informatique, et nous avons montré que l'hypothèse du couplage résistif critique explique comment le potentiel d'action est initié dans le segment initial de l'axone pour fournir le 'kink' dans le soma, alors que l'hypothèse de la retropropagation n'est pas suffisante pour expliquer ce phénomène.

Deuxièmement, nous avons évalué l'impact de la position du segment initial sur le potentiel extracellulaire. Des enregistrements expérimentaux révèlent que la localisation du segment initial varie entre différents types cellulaires et peut être modifiée par l'activité. Nous fournissons des preuves théoriques qui suggèrent que ces différences se reflètent de façon extracellulaire. De façon importante, nous démontrons que l'impact de la position du segment initial axonal dans la forme et l'amplitude du potentiel d'action dépend de la distance entre le site d'enregistrement et l'axone, et de sa position par rapport à l'axe soma-segment initial axonal.

Finalement, nous avons exploré l'impact d'un seul potentiel d'action dans l'activité de réseau, car cet effet est souvent questionné. Les complexes "sharp-wave ripple" sont des événements de réseau identifiés dans l'activité extracellulaire de l'hippocampe, et sont responsables de la consolidation de la mémoire. Nous montrons qu'un seul potentiel d'action d'un neurone pyramidal hippocampique peut commencer l'activité "sharp-wave ripple" qui consiste en l'activation de multiples interneurons.

L'ensemble de nos résultats montre que les potentiels d'action sont des événements

complexes modelés par la biochimie de la membrane neuronale et la morphologie de l'axone. De plus, ces caractéristiques neuronales modulent fortement leur impact dans le champ extracellulaire et l'activité de réseau.



---

## Introduction to action potential

---

The brain has fascinated people since ancient times and many have tried to understand its secrets. However, the nerve cell in the brain was not described until the XIXth century by Johannes Purkinje (1787–1869). Later came the pioneering discovery by Camillo Golgi (1843–1956) who developed method for visualization of neurons which lead Santiago Ramón y Cajal (1852–1934) to propose the concept that the nervous system is made of individual units and not just continuous mass of tissue (neuron doctrine) (Ramon y Cajal, 1888). To him, neurons in the brain appeared to be of complex and variable structure with many processes extending from the cell body and they quickly gathered a lot of interest.

Although recording intracellular electrical activity posed technical difficulty, already in 1939 the first trace of intracellular action potential from an animal cell was published (Fig 2.1A) (Hodgkin and Huxley, 1939). Since then many researchers have thoroughly studied the action potential: its shape (e.g. Barthó et al. (2004); Brette (2013); McCormick et al. (1985)), origin (e.g. Hodgkin and Huxley (1952)) and function (e.g. Houweling and Brecht (2008); Li et al. (2009)).

The action potential can be described as a rapid and short-lasting rise in electric potential in the cell. It has a distinct shape (Fig 2.1A and B, black) which has its origin in the underlying mechanism of its generation; Hodgkin and Huxley were able to fit their measurements of action potentials to changes in  $\text{Na}^+$  and  $\text{K}^+$  conductances as a function of membrane potential and time.

At the resting potential the cell membrane is not permeable to sodium ( $\text{Na}^+$ ) which mostly remains in the extracellular medium, while potassium ( $\text{K}^+$ ) is mostly concentrated inside the cell. If a neuron is sufficiently depolarized, some of the voltage-gated sodium channels ( $\text{Na}_v$ ) open, enabling  $\text{Na}^+$  to flow into the cell (example of  $\text{Na}^+$  current during

action potential, Fig 2.1, red). This inflow causes further depolarization and as a result, even more  $\text{Na}_v$  channels open. This forms a positive feedback cycle which eventually drives the membrane potential of the cell to positive values and to the peak of the action potential. The amplitude of the electrical potential during an action potential is roughly 100 mV and it lasts about 1 ms (Dayan and Abbott, 2001). The generation of an action potential also depends on the cell's previous firing activity. It is known to be impossible to evoke an action potential in the first few milliseconds (the absolute refractory period) following an action potential, and more difficult up to next tens of milliseconds (relative refractory period) after one. After the action potential reaches its peak, membrane potential is brought to resting values. This is achieved reliably and rapidly because sodium channels become inactivated soon after generating action potential, and because voltage-gated potassium ( $\text{K}_v$ ) channels open to accelerate repolarization (example of  $\text{K}^+$  current during action potential, Fig 2.1, blue) (Kandel et al., 2000).

The process of action potential generation described above fascinates with its beauty and seeming simplicity. However, the details are more complex. Specifically, sodium and potassium channels have multiple subtypes which differ in many ways, such as the time courses of their activation and inactivation. Furthermore, their concentration and localisation differ within neuronal segments enabling them to impact action potential in a variety of ways, and in different cell compartments. Finally, cells themselves vary largely in their morphology: the size of the soma, the extent of the axon, and the morphology of the dendritic tree, not only across the different cell types but even within seemingly similar neurons. Therefore, we wanted to know how much these differences impact single action potential making each of them very unique.

## 2.1 Context and objective of this work

If the distribution of active channels within varied morphologies of neurons provide the uniqueness of the fired action potential, it is important to know the types of currents and ionic channels which contribute to the generation and propagation of the action potential. Thus, in section 2.2 we will talk about currents rushing through the cell during action potential, we will explain the types of  $\text{Na}_v$  and  $\text{K}_v$  which can be found in the brain, and we will highlight the existence and role of other voltage-gated channels.

Next, in section 2.3 we will describe different parts of the neuronal structure as morphology of the cell largely impacts action potential. In many mammalian cells, action potential is initiated in the axon initial segment, which is characterized by a distinct structure and ionic channel composition. Initiation in this segment might be more energy efficient compared to initiation at the soma. Most recordings of the action potential

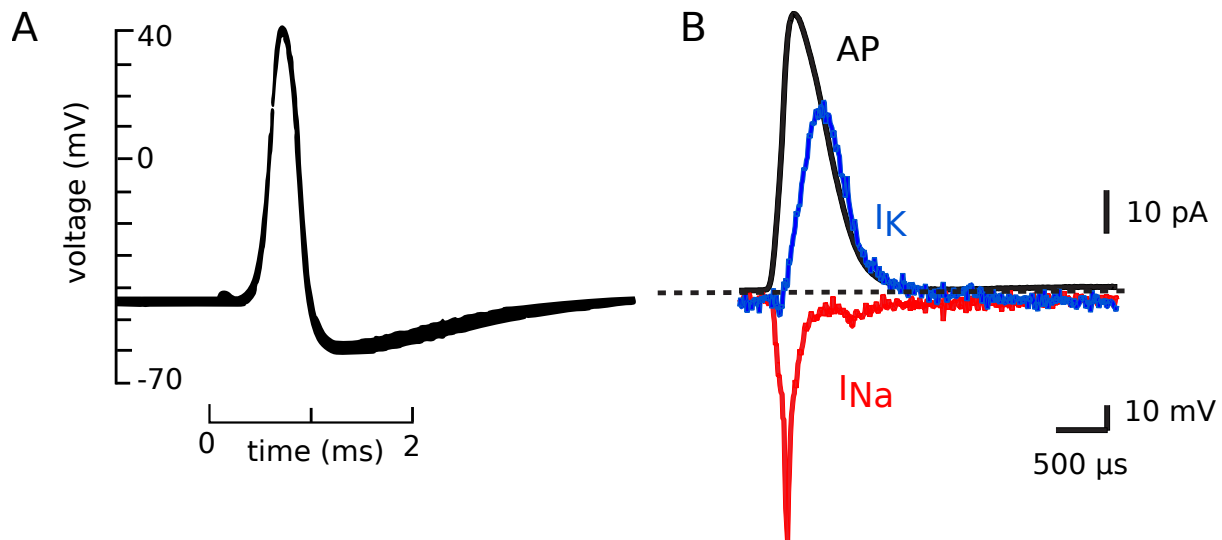


Figure 2.1: **Action potential.** **A.** The first published intracellular trace of the action potential recorded from the squid giant axon. Hodgkin and Huxley used glass capillary electrodes filled with sea water. The sea water outside is considered to be at zero potential. Adapted from [Hodgkin and Huxley \(1939\)](#). **B.** Contribution of sodium and potassium currents to action potential in the soma of thick-tufted layer 5 pyramidal neuron. Black: Action potential, blue: potassium current ( $I_k$ ), red: sodium current ( $I_{Na}$ ). Adapted from [Hallermann et al. \(2012\)](#).

show surprisingly sharp onset (called ‘kink’). For years, the origin of this characteristic pattern was debated (we explain hypotheses which tried to address this problem in section 2.4). This unsolved question motivated us to find the origin of the ‘kink’. In Chapter 3, we contribute to the discussion by showing that the initiation of the action potential in the axon initial segment is responsible for the formation of the current loop between the initiation location and the soma. As it is much larger than the axon, the soma acts as a current sink causing the current flowing into the axon initial segment to pass directly to the soma. The current coming from the axon to the soma is interpreted as the part of the action potential with the sharp onset, which sufficiently rises the potential in the soma to cause the opening of the somatic sodium channels and to generate a fully blown action potential. This explanation was proposed as the Critical Resistive Coupling Hypothesis (or Compartmentalization Hypothesis) ([Brette, 2013](#)).

The size and location of the axon initial segment have a crucial role in the initiation of an action potential. Interestingly, it is known that the axon initial segment varies in length and that it is present at different distances from the cell body in different cell types. Additionally, it is plastic: its localisation and length can be altered depending on the activity of the neuron. Since these properties have a large effect on the action potential initiation, as we show in Chapter 3, it is essential to be able to monitor their change *in vivo*. Intracellular recordings, which give access to these properties and their

effects on action potential, are hard to perform. Fortunately, the action potential is a large event that can also be recorded outside of the cell, in the extracellular medium (we discuss it further in section 2.5). These types of recordings are much easier to perform and are often the only possibility to measure the activity of multiple units. In Chapter 4, we show that the change of the location of the axon initial segment can be reflected in extracellular recordings performed near the cell but that this difference is not seen in the recordings performed far from the neuron. These findings may help us to monitor the morphological and chemical properties of the axon and how they affect the initiation of action potential *in vivo*. Since our understanding of neuronal function can only be obtained from intact neural networks, we hope that such recordings may allow us to determine the functional relevance of the axon initial segment and of sharp initiation in cortical networks.

It is possible that single action potentials carry information different from multiple action potentials fired within a short interval (such as the burst described in more detail in Section 2.6). The function of an individual action potential may depend on the local network it is embedded into. For example, it has been debated whether a single action potential could affect the entire network (Epsztein et al., 2010) or if only action potentials of the entire population encode useful information (London et al., 2010; Softky and Koch, 1993). The importance of a single action potential initiated by a single cell has also been shown (we provide more detail in section 2.7), as some of the action potentials can lead network of neurons to change their state and their firing pattern. In our work we show that single pyramidal cells in the CA3 area of the hippocampus can excite interneurons whose joint activity creates sharp wave-ripples. These sharp wave-ripples can be recorded both *in vitro* and *in vivo* and are believed to be responsible for the consolidation of the memories (more on sharp waves in section 2.8). The CA3 region is known for its recurrent connectivity (Appendix A) and therefore might support easy and quick excitation between the cells in the network.

It is to be noted that the important role of the action potential carries its risks. For example, the cell might fail to generate action potentials which in normal conditions would inhibit other neurons. This may cause over-excitation of the network as it is the case in epilepsy. Additionally, malfunctioning voltage-gated channels which do not properly carry out their function might lead to diseases collectively called channelopathies (we describe the diseases caused by the malfunction of the action potential in more detail in section 2.9).

## 2.2 Currents during action potential

Multiple currents constantly flow along the living neuron and through its membrane via ion channels. Electro-chemical gradients are largely responsible for the ion movement, but there are also other active processes supporting the function of the cell, and multiple channels which do not remain open.

Since the initial description of two voltage-dependent conductances by the Hodgkin-Huxley model in the giant-squid axon (which we will explain in more details in section 2.2.1), a large number of voltage-gated channels has been discovered in mammalian neurons and in different brain areas. This wide range of channel types allows the generation of action potentials of various shapes, frequencies and patterns (Bean, 2007; Connors and Gutnick, 1990; Nowak et al., 2003).

ion	extracellular (mM)	intracellular (mM)	reversal potential (mV)
potassium [K <sup>+</sup> ]	5	140	-89.7
sodium [Na <sup>+</sup> ]	145	5-15	61.1 – 90.7
calcium [Ca <sup>2+</sup> ]	2.5 – 5	100 – 200 (nM)	136 – 145

Table 2.1: Typical intra- and extracellular ion concentration in the mammals. Table adapted from (Johnston et al., 1995). Reversal potential was calculated from Nernst Equation  $E_s = \frac{RT}{F} \ln\left(\frac{[S]_o}{[S]_i}\right)$  for K<sup>+</sup> and Na<sup>+</sup> and  $E_{Ca} = \frac{RT}{2F} \ln\left(\frac{[Ca]_o}{[Ca]_i}\right)$  for Ca<sup>2+</sup>. Temperature was set to 37° C;  $R$  is the gas constant equal to 8.3145 (J mol<sup>-1</sup> K<sup>-1</sup>),  $T$  is a temperature (K) and  $F$  is a Faraday's constant equal to 9.6485·10<sup>4</sup> C mol<sup>-1</sup>,  $S$  is an ion type  $[S]_o$  and  $[S]_i$  are specific concentrations inside and outside of the cell respectively (mM). Here,  $\frac{RT}{F} = 26.73$  mV.

### 2.2.1 Hodgkin and Huxley Model

One of the most popular biophysical models of the action potential is the model described by Hodgkin and Huxley in 1952 (hence Hodgkin–Huxley (HH) model) (Hodgkin and Huxley, 1952). They defined the membrane current by the equation:

$$I_m = C_m \frac{dV}{dt} + I_K + I_{Na} + I_L$$

where  $I_K$  is the potassium current,  $I_{Na}$  – sodium current  $I_L$  – leak current,  $C_m$  is the membrane capacitance and  $V$  is voltage. Hodgkin and Huxley hypothesised that all those

currents obey Ohm's law, therefore the same equation can be rewritten to:

$$I_m = C_m \frac{dV}{dt} + g_K(V, t)(V - E_K) + g_{Na}(V, t)(V - E_{Na}) + g_L(V - E_L)$$

where  $E_K$ ,  $E_{Na}$  and  $E_L$  are the reversal potentials and  $g_K$ ,  $g_{Na}$  and  $g_L$  are the conductances.

Hodgkin and Huxley proposed the currently accepted idea that sodium channels are voltage sensitive and as such, they can be found in one of three different states: opened, closed or inactivated. Potassium channels on the other hand, can be either opened or closed. Channels open with various kinetics: total conductance  $g_{Na}$  and  $g_K$  through all the channels follow the power functions of the gating variables, thus in HH model:

$$g_K(V, t) = n^4 \bar{g}_K$$

and

$$g_{Na}(V, t) = m^3 h \bar{g}_{Na}$$

where  $n$ ,  $m$  and  $h$  are gating variables which follow an exponential time course and  $\bar{g}_K$  and  $\bar{g}_{Na}$  are maximum conductances

Therefore, sodium and potassium channels might be imagined as consisting of four independent subunits where the channel becomes open only if all of the subunits are opened.

It is possible to describe the kinetics of the gating variable  $n(t)$  as follows:

$$\begin{aligned} \frac{dn}{dt} &= \alpha_n(1 - n) - \beta_n n \\ \tau_n \frac{dn}{dt} &= n_\infty - n \end{aligned}$$

and  $m(t)$  and  $h(t)$  accordingly. Here,  $\alpha$  and  $\beta$  are rate coefficients,  $n_\infty$  is the activation function of the gating variable  $n$ , and  $\tau_n$  is its time constant.

Hodgkin and Huxley described their model based on multiple recordings from the giant squid axon. Furthermore, they made it isopotential by placing an electrode inside of it, but the properties of this extraordinary cable are not always applicable to mammalian species (Attwell and Laughlin, 2001; Fohlmeister, 2009; Hille et al., 2001; Shoukimas and French, 1980), and variations of the HH model have been published by multiple groups (Hallermann et al., 2012; Mainen et al., 1995). Generally we call the family of all of those models, the HH-type models. When using them, it is important to remember that action potentials in the mammalian neurons are usually initiated not inside, but adjacent to the soma, in the AIS. That is why isopotential model of HH-type consisting of single

soma cannot correctly reflect actual mammalian experimental data (Brette, 2015). We will explain the initiation process in detail in Section 2.4 and in Chapter 3.

## 2.2.2 Voltage gated channels

The cell membrane is built out of a lipid bilayer which forms a virtually impermeable barrier to ions. Ions can pass through it but only via the ion channels which are embedded in the membrane (Kandel et al., 2000). These channels have different localisation within the body regions but also within single cells and some of them are voltage sensitive and can open or close depending on the difference in voltage between the inside and the outside of the cell (Trimmer and Rhodes, 2004). When they are opened, a restricted class of ions follow the electrochemical gradient to enter or leave the cell at high rates ( $> 10^6$  ions per second) (Hille et al., 2001).

In this section we will give a basic overview of a large family of voltage-gated channels which are expressed in the adult mammalian brain. We will mostly focus on their localisation within the single cell and the role they play in the generation of action potentials.

### 2.2.2.1 Sodium channels

In physiological conditions concentration of sodium ( $\text{Na}^+$ ) inside the cell is 5 – 15 mM and 140 mM outside the cell (Table 2.1). This results in an equilibrium potential of  $\text{Na}^+$  ions ( $E_{\text{Na}}$ ) between 61.1 and 90.7 mV and at membrane resting potential it produces a large drive for  $\text{Na}^+$  to enter the cell. Therefore, when sodium channels open,  $\text{Na}^+$  rapidly enters the cell, causing the depolarization of the membrane. The rise of intracellular  $\text{Na}^+$  is responsible for the rising phase of the action potential (Catterall, 2000).

Sodium channels can generate three types of sodium currents: (1) the fast-inactivating transient  $\text{Na}^+$  current, (2) the persistent  $\text{Na}^+$  current, which slowly activates and inactivates (Crill, 1996) and (3) the resurgent  $\text{Na}^+$  current which is activated upon repolarization in sub-threshold, potentials causing membrane depolarization and enabling the cell to fire at higher frequencies (Cruz et al., 2011; Raman and Bean, 1997).

There are three families of sodium channels: voltage-gated sodium channels ( $\text{Na}_v$ ),  $\text{Na}_x$ , and non-voltage-gated sodium channels which will not be discussed here (Yu and Catterall, 2003). Voltage-gated sodium channels ( $\text{Na}_v$ ) can be found in three states: closed, opened or inactivated (Hodgkin and Huxley, 1952). It is however worth noting that  $\text{Na}_v$  channels are not perfectly discriminating for  $\text{Na}^+$ , thus when opened, they let a smaller number of other ions (such as potassium and calcium) pass through (Hille et al., 2001).  $\text{Na}_v$  channels consist of one  $\alpha$  and one or more of the smaller  $\beta$  subunits. The  $\alpha$  subunit serves as a voltage sensor while the  $\beta$  is responsible for modulation of voltage

dependence and kinetics, as well as localisation of the  $\alpha$  subunit within the cell (Catterall, 2000; Goldin et al., 2000).

There are nine known subtypes of  $\text{Na}_v1$  family of voltage-gated sodium channels:  $\text{Na}_v1.1$ - $\text{Na}_v1.9$ . Four of them are commonly found in the adult mammalian brain:  $\text{Na}_v1.1$ ,  $\text{Na}_v1.2$ ,  $\text{Na}_v1.3$  and  $\text{Na}_v1.6$  (Goldin et al., 2000; Trimmer and Rhodes, 2004) (subcellular expression of selected  $\text{Na}_v$  channels in the mammalian brain, Table 2.2). Some studies have also shown a selective expression of  $\text{Na}_v1.5$  (Donahue et al., 2000; Hartmann et al., 1999; Ren et al., 2012; Wu et al., 2002),  $\text{Na}_v1.7$  (Morinville et al., 2007) and  $\text{Na}_v1.9$  (Jeong et al., 2000) at this location although they are mostly found in other parts of the body (such as in the heart or skeletal muscles). Each of the  $\text{Na}_v$  channels play different roles in action potential initiation and propagation (Catterall et al., 2005a; Royeck et al., 2008; Yu and Catterall, 2003).

The second family of Na channels is called  $\text{Na}_x$ . It has some similarities to  $\text{Na}_v1$  channels (Catterall et al., 2005a) as members of this family have no voltage sensitivity but are responsible for sensing extracellular sodium concentration and for regulating salt intake behaviors (Hiyama et al., 2002). These channels localize to neurons and to neuroglia cells of central nervous system organs (Watanabe et al., 2000).

Sodium channels can be classified as either sensitive or resistant to pharmacological block by tetrodotoxin (TTX) (Catterall, 1980; Donahue et al., 2000; Jeong et al., 2000). The resistant channels ( $\text{Na}_v1.5$  and  $\text{Na}_v1.9$  from those found in the brain) usually generate slower currents, but recover from inactivation much faster. These channels are therefore considered good candidates for the support of sustained firing (Elliott and Elliott, 1993; Wu et al., 2002). Below we will give a brief overview of the  $\text{Na}_v$  channels found in the brain.

**$\text{Na}_v1.1$**  channels are mostly expressed in inhibitory cells (Gong et al., 1999; Lorincz and Nusser, 2008; Ogiwara et al., 2007; Tian et al., 2014; Trimmer and Rhodes, 2004). They were also detected in the pyramidal cells of the hippocampus but only at extremely low levels (Ogiwara et al., 2007). During development  $\text{Na}_v1.1$  channels mostly cluster at the axon initial segment but in the adulthood, the density of  $\text{Na}_v1.1$  drops dramatically (even up to 50%) (Gong et al., 1999). In mature animal  $\text{Na}_v1.1$  channels are expressed in the proximal part of the axon initial segment (AIS) (Leterrier, 2015; Lorincz and Nusser, 2008; Ogiwara et al., 2007; Tian et al., 2014; Van Wart et al., 2007) and in the somatodendritic compartment (Beckh et al., 1989; Gong et al., 1999; Ogiwara et al., 2007; Westenbroek et al., 1989, 1992). The possible roles they could play include integration of synaptic impulses (Yu and Catterall, 2003), initiating action potentials, and sustaining high-frequency firing of fast-spiking interneurons (Catterall et al., 2005a; Ogiwara et al., 2007).

	dend	soma	axon	AIS	NoR	terminals
<b>Na<sub>v</sub>1.1</b>	yes <sup>1-6</sup>	yes <sup>1-6</sup>	some <sup>1,4,7</sup>	rare <sup>5,8-10</sup>	rare <sup>8</sup>	
<b>Na<sub>v</sub>1.2</b>	rare, proximal <sup>1,2</sup>	rare, pyramidal cells <sup>2</sup>	yes <sup>1-4,6,8,11-14</sup>	proximal <sup>7-9,15</sup>	some, only human <sup>7</sup>	yes <sup>2,3,8,12</sup>
<b>Na<sub>v</sub>1.3</b>	only human <sup>3,4,6</sup>	human <sup>3,4,6,11,14</sup> rarely in rodent <sup>1,13,16</sup>	some, only human <sup>3,4,6</sup>			
<b>Na<sub>v</sub>1.6</b>	rare(*) <sup>3,4,6,17</sup>	some <sup>3,4,6</sup>	some, only rodent <sup>4,6</sup>	distal AIS, pyramidal cells <sup>3,5,7-9,15,18</sup>	yes <sup>3,6-8</sup>	
*	only in those pyramidal cells where AIS originates from apical dendrite					
<sup>1</sup> Beckh et al. (1989)		<sup>7</sup> Tian et al. (2014)		<sup>13</sup> Westenbroek et al. (1992)		
<sup>2</sup> Gong et al. (1999)		<sup>8</sup> Debanne et al. (2011)		<sup>14</sup> Yu and Catterall (2003)		
<sup>3</sup> Trimmer and Rhodes (2004)		<sup>9</sup> Lorincz and Nusser (2008)		<sup>15</sup> Hu et al. (2009)		
<sup>4</sup> Vacher et al. (2008)		<sup>10</sup> Ogiwara et al. (2007)		<sup>16</sup> Shah et al. (2001)		
<sup>5</sup> Van Wart et al. (2007)		<sup>11</sup> Catterall et al. (2005a)		<sup>17</sup> Lorincz and Nusser (2010)		
<sup>6</sup> Whitaker et al. (2001a)		<sup>12</sup> Westenbroek et al. (1989)		<sup>18</sup> Royeck et al. (2008)		

Table 2.2: Subcellular localisation of selected Na<sub>v</sub> channels in the mammalian brain; blue color indicates major localisation. ‘axon’ denotes non-myelinated axons, AIS: axon initial segment, NoR: nodes of Ranvier.

In humans, the loss of the gene encoding  $\text{Na}_v1.1$  is associated with a severe epileptic disorder because inhibitory cells (parvalbumin-positive) lacking  $\text{Na}_v1.1$  have problems to generate spike output (Ogiwara et al., 2007).

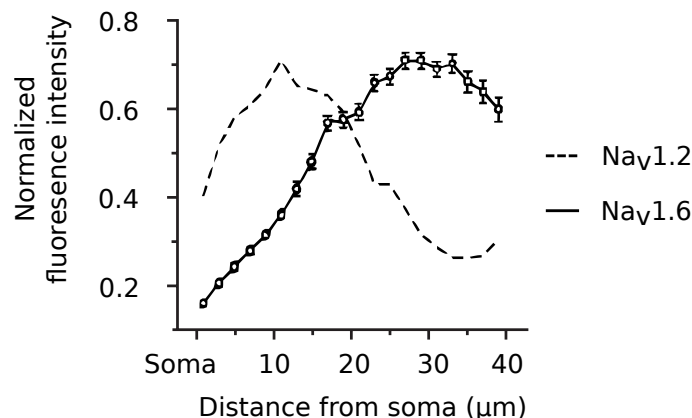


Figure 2.2: Distribution of  $\text{Na}_v1.2$  and  $\text{Na}_v1.6$  channels in the proximal part of the axon of the layer 5 pyramidal neurons. Adapted from Fig 1 from (Hu et al., 2009).

**$\text{Na}_v1.2$**  channels are very closely related to  $\text{Na}_v1.1$  channels (by their amino acid sequence) and, together with  $\text{Na}_v1.3$  and  $\text{Na}_v1.7$ , they form a close family of sodium channels (Goldin et al., 2000).  $\text{Na}_v1.2$  channel expression is high in the development stage and remains high throughout adulthood (Gong et al., 1999). The density of  $\text{Na}_v1.2$  in cortical pyramidal neurons reaches its peak in the proximal axon initial segment (around 10-20  $\mu\text{m}$  from the soma) (Hu et al., 2009; Lorincz and Nusser, 2008). In CA1 pyramidal cells it is expressed mostly in the axon while it is not expressed in the postsynaptic dendritic compartment. (Lorincz and Nusser, 2010).

Having a higher activation threshold than neighbouring  $\text{Na}_v1.6$  (Fig 2.2),  $\text{Na}_v1.2$  is responsible for the propagation of the action potential to the soma and for repetitive firing (Hu et al., 2009; Catterall et al., 2005a; Yu and Catterall, 2003).

**$\text{Na}_v1.3$**  channels are highly expressed during development stage while in adult rodents they almost disappear. However this is not the case in humans, where the high density of these channels is retained in the adult brain (Whitaker et al., 2001a; Trimmer and Rhodes, 2004). Because of their localisation in the cell body (Beckh et al., 1989; Shah et al., 2001; Westenbroek et al., 1992),  $\text{Na}_v1.3$  channels might be responsible for the integration of synaptic inputs (Yu and Catterall, 2003).

The  **$\text{Na}_v1.5$**  channel family is closely related to  $\text{Na}_v1.8$  and  $\text{Na}_v1.9$  (Goldin et al., 2000). It is mainly found in the heart, but recently various groups also reported a slightly different form of these channels to be expressed in the mammalian brain.  $\text{Na}_v1.5$  channels (as  $\text{Na}_v1.8$  and  $\text{Na}_v1.9$ ) are resistant to TTX (Donahue et al., 2000; Hartmann

et al., 1999; Ren et al., 2012; Wu et al., 2002). Functionally,  $\text{Na}_v1.5$  channels are believed to regulate excitability and rhythmic firing in the brain (Hartmann et al., 1999) and might be involved in the generation and propagation of action potentials (Catterall et al., 2005a).  $\text{Na}_v1.5$  is also a possible candidate whose defects might cause inherited epilepsy (Hartmann et al., 1999).

**$\text{Na}_v1.6$**  channels replace  $\text{Na}_v1.2$  channels during development in the maturing nodes of Ranvier (NoR) (Boiko et al., 2001; Kaplan et al., 2001).  $\text{Na}_v1.6$  channels have the highest NoR density in the adult brain, which is almost twice as high as in the axon initial segment (AIS) (Lorincz and Nusser, 2010). At the level of AIS,  $\text{Na}_v1.6$  channels are expressed in the distal part (around 30-50  $\mu\text{m}$  from the soma, Fig 2.2) (Hu et al., 2009; Lorincz and Nusser, 2008; Royeck et al., 2008) where their density increases 40 times in the first ten  $\mu\text{m}$  of AIS. In the dendrites, the density of  $\text{Na}_v1.6$  becomes lower as the distance from the soma increases (Lorincz and Nusser, 2010).

In most neurons localization of  $\text{Na}_v1.6$  channels in the AIS coincides with the initiation zone for action potential (Hu et al., 2009), a phenomenon for which  $\text{Na}_v1.6$  channels are believed to be responsible (Royeck et al., 2008). In mice lacking  $\text{Na}_v1.6$ ,  $\text{Na}_v1.2$  are sufficient for action potential (AP) initiation in the axon, although the threshold for the AP initiation is higher (Royeck et al., 2008). Higher threshold for AP is due to  $\text{Na}_v1.6$  channels having a lower threshold for activation (by around 15 mV) than the more proximal  $\text{Na}_v1.2$  channels (Hu et al., 2009; Royeck et al., 2008; Rush et al., 2005).  $\text{Na}_v1.6$  channels have also been associated with rapid burst firing (Raman et al., 1997; Royeck et al., 2008). In small dorsal root ganglia neurons  $\text{Na}_v1.6$  channels produce a large persistent current, much larger than the persistent current produced by  $\text{Na}_v1.2$  channels in the same cells (Rush et al., 2005).

**$\text{Na}_v1.7$**  channels are expressed mainly in the cell bodies of neurons in some areas of the mammalian brain (Morinville et al., 2007). To our knowledge their role in the brain with regards to action potentials has not been shown to date, however in peripheral neurons they are responsible for action potential initiation and transmission (Catterall et al., 2005a).

**$\text{Na}_v1.9$**  is TTX-resistant. It is expressed in the brains of humans (in multiple regions) (Jeong et al., 2000) and of other mammals (dorsal cochlear nucleus) (Yan et al., 2015). Its subcellular localisation and function in the brain to the best of our knowledge remains unknown. Overall,  $\text{Na}_v1.9$ , along with  $\text{Na}_v1.7$  and  $\text{Na}_v1.8$  channels play a key role in the perception of pain (Huang et al., 2014; Yu and Catterall, 2003).

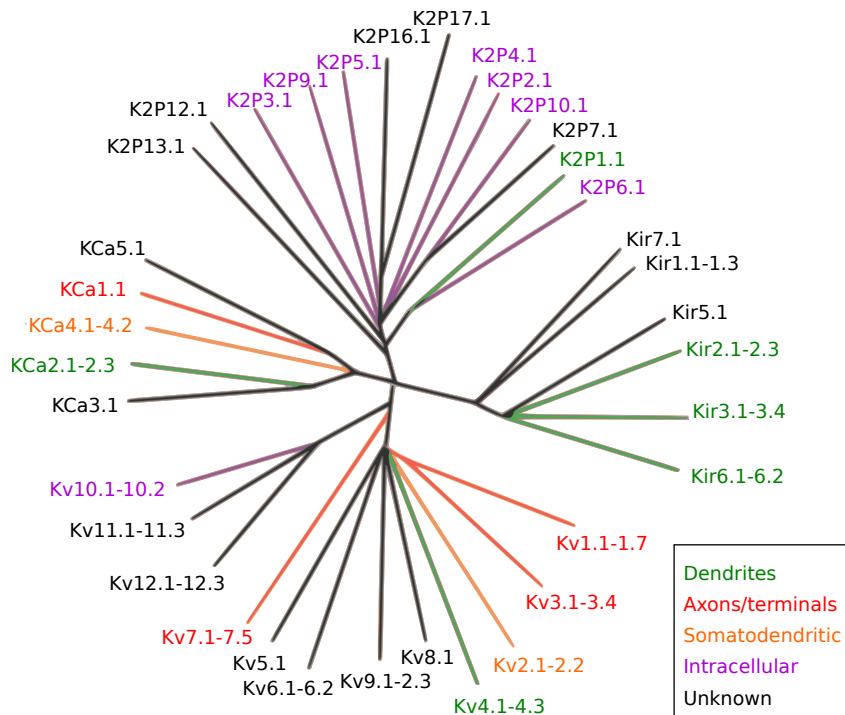


Figure 2.3: Simplified overview of family of potassium channels and their sub-cellular localization. Sub-cellular localisation is true only for certain neuron types and might differ for others. This diagram is therefore only meant as general overview. Intracellular channels are meant as nonreceptor plasma membrane ion channels which carry intracellular transmission. Adapted from Trimmer (2015).

### 2.2.2.2 Potassium channels

Potassium channels are the most variable among ion channels. In mammals they comprise more than 80 genes (Fig 2.3). They are formed from one or more (usually four)  $\alpha$  subunits and variable number of additional subunits (Jan and Jan, 2012; Lujan, 2010; Trimmer, 2015).

Potassium channels have been studied more thoroughly than  $\text{Na}_v$  channels and there are multiple reviews describing them in detail (Gutman et al., 2005; Jan and Jan, 2012; Lujan, 2010; Trimmer, 2015; Vacher et al., 2008). Here, we will focus on the voltage-sensitive potassium channels ( $\text{K}_v$ ) found in the adult mammalian brain.

The main role of potassium channels is to repolarize the membrane after action potentials and to limit the excitability of the neuron (Debanne et al., 2011). Once the membrane is sufficiently depolarized,  $\text{K}_v$  channels open rapidly ( $< 1$  ms) to let potassium ( $\text{K}^+$ ) flow out of the cell (Lujan, 2010). The equilibrium potential of  $\text{K}^+$  is around  $-70$  to  $-90$  mV (Table 2.1) (Dayan and Abbott, 2001).

There are many different  $\text{K}_v$  channels (as shown in Fig 2.3) but  $\text{K}_v1 - \text{K}_v4$  have the widest expression pattern in the brain (Gutman et al., 2005; Trimmer and Rhodes,

2004).  $K_v5$ ,  $K_v6$ ,  $K_v8$  and  $K_v9$  are electrically silent voltage-gate  $K^+$  subunits: When they are expressed on their own they do not show any function, but when co-expressed with other  $K_v$  channels, they modulate their activity, forming channels with unique biophysical properties (Bocksteins, 2016).

The  **$K_v1$**  channel family consists of three subunits which are most abundantly found in the brain:  $K_v1.1$ ,  $K_v1.2$  and  $K_v1.4$  (Rhodes et al., 1997). They regulate spike duration in the axon (Kole et al., 2007; Shu et al., 2007b).  $K_v1.1$ - $K_v1.2$  are delayed rectifiers, which means that they activate slowly or they activate at high voltages to repolarize the cell.  $K_v1.4$  is an A-type channel, meaning that they inactivate quickly and can generate transient current (Gutman et al., 2005; Jerng et al., 2004; Lujan, 2010). This type of channel is found in the axon and nerve terminals (Cooper et al., 1998; Trimmer and Rhodes, 2004; Vacher et al., 2008; Wang et al., 1993, 1994).  $K_v1.1$ - $K_v1.2$  can be found in the distal axon initial segment (they tend to be located more distally than  $Na_v1.6$  channels) where they determine some of the properties of the action potentials and repolarize the axon initial segment (AIS) after an action potential (Debanne et al., 2011; Kole et al., 2007; Rowan et al., 2014). Furthermore,  $K_v1$  channels prevent atypical transmitter release at presynaptic sites by reducing nerve terminal excitability (Ishikawa et al., 2003).  $K_v1.1$  and  $K_v1.2$  channels are responsible for maintaining membrane potential by modulating electrical excitability in neurons (also in muscle), whereas  $K_v1.4$  is responsible for afterhyperpolarization (Gutman et al., 2005). Malfunction of  $K_v1.1$  channels is believed to be causative of episodic ataxia (severe dis-coordination) syndrome type 1 (Browne et al., 1994; Gutman et al., 2005)

The channels of the  **$K_v2$**  family are widely expressed in the brain. They are a delayed rectifier type of channels and are responsible for maintaining membrane potential and modulating electrical excitability in the dendrites (Du et al., 1998; Gutman et al., 2005; Murakoshi and Trimmer, 1999). Channels from this group are mostly located at the soma and along the dendrites but not in the axon (Du et al., 1998; Trimmer and Rhodes, 2004).

In chronic hypoxic pulmonary hypertension (increased blood pressure in arteries and veins disease)  $K_v2.1$  expression is reduced (Archer et al., 1998; Gutman et al., 2005).

The  **$K_v3$**  channel family consists of the  $K_v3.1$ ,  $K_v3.2$ ,  $K_v3.3$  and  $K_v3.4$  subunits which are mostly expressed in the brain, although  $K_v3.4$  is more abundant in the skeletal muscles. They localize to the dendrites and to the axon (Lujan, 2010; Trimmer and Rhodes, 2004).  $K_v3.1$  and  $K_v3.2$  are delayed rectifiers, while  $K_v3.3$  and  $K_v3.4$  are A-type potassium channels (Gutman et al., 2005; Rudy et al., 1999).  $K_v3$  channels show a higher activation threshold than other  $K_v$  channels and they have fast kinetics, being steeply voltage-dependent, which leads to spikes with narrower width and high firing frequen-

	dend	soma	axon	AIS	NoR	terminals
<b>K<sub>v</sub>1.1</b>	yes <sup>1,2</sup>	yes <sup>2</sup>	yes <sup>1,3,4</sup>	yes <sup>4-7</sup>	yes <sup>8</sup>	yes <sup>2,4,8</sup>
<b>K<sub>v</sub>1.2</b>	yes <sup>2</sup>	yes <sup>2</sup>	yes <sup>1,3-5,9</sup>	yes <sup>4-6</sup>	yes <sup>8,9</sup>	yes <sup>2,4,8</sup>
<b>K<sub>v</sub>1.3</b>			yes <sup>1,5</sup>			yes <sup>4</sup>
<b>K<sub>v</sub>1.4</b>			yes <sup>1,10,11</sup>			excitatory cells <sup>4,10,11</sup>
<b>K<sub>v</sub>2.1</b>	proximal <sup>1,7,12</sup>	yes <sup>1,7</sup>		yes <sup>4</sup>		
<b>K<sub>v</sub>2.2</b>	yes <sup>1,7</sup>	yes <sup>1,7</sup>			yes <sup>5</sup>	yes <sup>4,7</sup>
<b>K<sub>v</sub>3.1</b>	yes <sup>1,7</sup>	yes <sup>1,7</sup>	yes <sup>1,7</sup>		yes <sup>4,13</sup>	yes <sup>7</sup>
<b>K<sub>v</sub>3.2</b>	yes <sup>1,7</sup>	yes <sup>1</sup>				yes <sup>4</sup>
<b>K<sub>v</sub>3.3</b>	yes <sup>7</sup>	yes <sup>7</sup>	yes <sup>1,5</sup>			yes <sup>4,7</sup>
<b>K<sub>v</sub>3.4</b>			yes <sup>1,5,7</sup>			yes <sup>4,7</sup>
<b>K<sub>v</sub>4.1*</b>	yes <sup>1,7</sup>	yes <sup>1,7</sup>				
<b>K<sub>v</sub>4.2</b>	yes <sup>1,7,12</sup>	yes <sup>1</sup>				
<b>K<sub>v</sub>4.3</b>	yes <sup>1,4</sup>	yes <sup>1</sup>				
<b>K<sub>v</sub>7.2</b>			yes <sup>1,5</sup>	yes <sup>4,5,14</sup>	yes <sup>14</sup>	
<b>K<sub>v</sub>7.3</b>	yes <sup>1</sup>	yes <sup>1</sup>	yes <sup>1,5</sup>	4,5,14	yes <sup>14</sup>	
<b>K<sub>v</sub>7.5</b>	yes <sup>1</sup>	yes <sup>1</sup>				
*	K <sub>v</sub> 4.1 is expressed in very low levels in mammalian brain <sup>7</sup>					

<sup>1</sup> Vacher et al. (2008)

<sup>6</sup> Lorincz and Nusser (2008)

<sup>11</sup> Jerng et al. (2004)

<sup>2</sup> Wang et al. (1994)

<sup>7</sup> Trimmer and Rhodes (2004)

<sup>12</sup> Lai and Jan (2006)

<sup>3</sup> Boiko et al. (2001)

<sup>8</sup> Wang et al. (1993)

<sup>13</sup> Devaux et al. (2003)

<sup>4</sup> Trimmer (2015)

<sup>9</sup> Van Wart et al. (2007)

<sup>14</sup> Cooper (2011)

<sup>5</sup> Debanne et al. (2011)

<sup>10</sup> Cooper et al. (1998)

Table 2.3: Subcellular localisation of selected K<sub>v</sub> channels in the mammalian brain; blue color indicates major localisation. axon: non-myelinated axons, AIS: axon initial segment, NoR: nodes of Ranvier. The cellular and subcellular localization of members of K<sub>v</sub> subfamilies K<sub>v</sub>5, K<sub>v</sub>6, and K<sub>v</sub>8-K<sub>v</sub>12 is not as well characterized as that of the members of the K<sub>v</sub>1-K<sub>v</sub>4 and K<sub>v</sub>7/KCNQ subfamily (Vacher et al., 2008).

cies (Bean, 2007; Constantinopole et al., 2009; Massengill et al., 1997; Rudy et al., 1999). They also play important role in the regulation of action potential duration in presynaptic terminals (Gutman et al., 2005; Ishikawa et al., 2003)

The **K<sub>v</sub>4** channel family has three subunits: K<sub>v</sub>4.1, K<sub>v</sub>4.2 and K<sub>v</sub>4.3 which are distributed in the brain, where they are mostly expressed in the dendrites (Serôdio and Rudy, 1998; Trimmer and Rhodes, 2004). Expression of the K<sub>v</sub>4.1 channel is overall very low. The K<sub>v</sub>4 channels have transient current (A-type) (Gutman et al., 2005; Serôdio and Rudy, 1998) and in the CA1 region of the hippocampus are responsible for dampening back-propagating action potentials (Gutman et al., 2005).

The **K<sub>v</sub>5** family consists of only one subunit: K<sub>v</sub>5.1 (Lujan, 2010). It does not have function on its own, but rather has modulatory actions on the gating properties of both K<sub>v</sub>2.1 and K<sub>v</sub>2.2 channels (Gutman et al., 2005).

The **K<sub>v</sub>6** family consists of K<sub>v</sub>6.1-K<sub>v</sub>6.4 subunits which are expressed in the human brain (Ottschytsch et al., 2002). Their localization within the cell has not yet been determined (Lujan, 2010). As it is the case for K<sub>v</sub>5, these channels also do not have an independent function. When they are expressed alone they are unable to produce any current (Ottschytsch et al., 2002), but when they are coexpressed with K<sub>v</sub>2 channels, especially K<sub>v</sub>2.1, they exhibit modulatory properties. The K<sub>v</sub>2 channels are able to modulate (suppress) currents generated by K<sub>v</sub>2.1 and K<sub>v</sub>2.2 by increasing their time constant of activation and thus slowing down their inactivation (Gutman et al., 2005; Post et al., 1996).

The **K<sub>v</sub>7** family composed of five subunits: K<sub>v</sub>7.1-K<sub>v</sub>7.5 (also known as KCNQ1-5). Aside from K<sub>v</sub>7.1 which is mostly found in the heart, these channels are mostly localized along the axon but they can also be found in the soma, dendrites and synaptic terminals (Gutman et al., 2005). K<sub>v</sub>7.2 and K<sub>v</sub>7.3 are present in high density in the axon initial segment and in the nodes of Ranvier, where they interact with ankyrin G (Devaux et al., 2004; Lai and Jan, 2006). KCNQ2 and KCNQ3 are responsible for generating M-current, which is activated at subthreshold potentials (Lai and Jan, 2006) and is known to be important for rising the threshold necessary for action potential initiation. These channels are unique as they have an “open” state at resting potentials of the membrane (Brown and Adams, 1980) and are delayed-rectifier type of channels (Gutman et al., 2005; Lai and Jan, 2006). In the hippocampus they regulate action potential firing in pyramidal cells by controlling resting potential and threshold for action potential generation (Debanne et al., 2011; Shah et al., 2008; Yue and Yaari, 2006). Mutations in the K<sub>v</sub>7 channels can lead to diseases such as epilepsy and myokymia (Devaux et al., 2004; Lai and Jan, 2006; Lujan, 2010).

The **K<sub>v</sub>8** family of channels consists of two subunits: K<sub>v</sub>8.1 and K<sub>v</sub>8.2, but only K<sub>v</sub>8.1

is expressed in the brain where it is preferentially found in excitatory cells (Hugnot et al., 1996). It is another modifier-type channel which does not have a function on its own. When coexpressed with  $K_v2.1$  or  $K_v2.2$  it can modulate their kinetics and shift the half-inactivation potential to more polarized levels; Its activity impacts membrane potential and action potential frequency (Gutman et al., 2005). Mutations in this channel can cause severe epilepsy (Jorge et al., 2011).

The  **$K_v9$**  family includes the  $K_v9.1$ ,  $K_v9.2$  and  $K_v9.3$  subunits which are all present in the mammalian brain, although  $K_v9.3$  is also expressed in other tissues (Lujan, 2010). They are modifier-type channels acting on  $K_v2.1$  and  $K_v2.2$  channels by enhancing their single-channel conductance (Gutman et al., 2005).

The  **$K_v10$**  family has two subunits:  $K_v10.1$  and  $K_v10.2$ . Both are expressed in the mammalian brain (Lujan, 2010).  $K_v10.1$  is a delayed-rectifier while  $K_v10.2$  is an outward-rectifying channel, meaning that it passes current more easily in the outward direction.

The  **$K_v11$**  family is composed of the  $K_v11.1$ ,  $K_v11.2$  and  $K_v11.3$  subunits present in the mammalian brain (Lujan, 2010; Shepard and Trudeau, 2008). They are inwardly-rectifying channels which pass current more easily in inward direction (Gutman et al., 2005).  $K_v11.1$  (encoded by ether *á-go-go* gene) is normally expressed nearly throughout the brain (specifically hippocampus, neocortex, hypothalamus, thalamus, amygdala, substantia nigra, red nucleus and cerebellum), where it is associated with schizophrenia (Atalar et al., 2010), and in the heart, where it plays a role in cardiac arrhythmias (Wang et al., 2011). It has been also found to be expressed in several somatic cancer cell lines (such as cervix cancer in humans) where it has been reported to play a role in cancer progression (Farias et al., 2004; Wu et al., 2012).

The  **$K_v12$**  family of channels consist of  $K_v12.1$ ,  $K_v12.2$  and  $K_v12.3$  which are all present in the mammalian brain (Clancy et al., 2009).  $K_v12.1$  and  $K_v12.3$  are slowly-activating and deactivating potassium channels whereas  $K_v12.2$  inactivate quickly (Engel-land et al., 1998; Shi et al., 1998). It has been reported that under-expression of  $K_v12.2$  can lead to epilepsy (Zhang et al., 2010).

### 2.2.2.3 Other voltage gated channels

Sodium and potassium voltage-gated channels seem to be most crucial for action potential generation as they are responsible for the rising and falling phases respectively. However, other channels may influence the crossing of the threshold for action potential initiation by modulating voltage level, and thus may alter the shape of the action potential. Notably voltage-sensitive **calcium channels ( $Ca_v$ )** can regulate firing properties such as the timing and threshold of action potential, as well as burst-firing (Debanne et al., 2011). They are also responsible for dendritic calcium signalling resulting from back-

	dend	soma	axon	AIS	NoR	terminals
<b>Ca<sub>v</sub>1.2</b>	yes <sup>1,2</sup>	yes <sup>1,2</sup>				
<b>Ca<sub>v</sub>1.3</b>	proximal <sub>1,2</sub>	yes <sup>1,2</sup>				
<b>Ca<sub>v</sub>2.1</b>	some <sup>2,3</sup>	some <sup>2,3</sup>	yes <sup>2,3</sup>			yes <sup>1</sup>
<b>Ca<sub>v</sub>2.2</b>	some <sup>1,2</sup>	some <sup>1,2</sup>				yes <sup>1,3</sup>
<b>Ca<sub>v</sub>2.3</b>	yes <sup>1-3</sup>	yes <sup>1-3</sup>				some <sup>1,3</sup>
<b>Ca<sub>v</sub>3.1</b>	yes <sup>1-3</sup>	yes <sup>1-3</sup>				
<b>Ca<sub>v</sub>3.2</b>	proximal <sup>1</sup>	yes <sup>1</sup>				
<b>Ca<sub>v</sub>3.3</b>	yes <sup>1</sup>	yes <sup>1</sup>				yes <sup>3</sup>

<sup>1</sup> Catterall et al. (2005b)    <sup>2</sup> Vacher et al. (2008)    <sup>3</sup> Trimmer and Rhodes (2004)

Table 2.4: Subcellular localisation of selected Ca<sub>v</sub> channels in the mammalian brain; blue color indicates major localisation. Axon: non-myelinated axons, AIS: axon initial segment, NoR: nodes of Ranvier.

propagating action potentials, synaptic plasticity, and activity-dependent modulation of gene transcription in the mammalian brain (Vacher et al., 2008; Yu and Catterall, 2004). There are ten different Ca<sub>v</sub> channels present in mammals. Of those, Ca<sub>v</sub>1.2, Ca<sub>v</sub>1.3, Ca<sub>v</sub>2.1 – Ca<sub>v</sub>2.3, Ca<sub>v</sub>3.1 – Ca<sub>v</sub>3.3 are expressed in the brain (subcellular localisation, Table 2.4) (Catterall et al., 2005b; Vacher et al., 2008). Calcium channels can enable ‘calcium spikes’ (also called Ca<sup>2+</sup> action potentials) which depend on calcium (Ca<sup>2+</sup>) rather than on Na<sup>+</sup> ions (Fig 2.9 B) (Fatt and Ginsborg, 1958; Hille et al., 2001).

The drive for calcium to enter the cell is much stronger than that for sodium (Table 2.1), with around 3 mM Ca<sup>+</sup> concentration in the extracellular medium and only around 150 nM inside the cell, leading to a reversal potential of calcium (E<sub>Ca</sub>) as high as approximately 140 mV. However, calcium channels usually require very strong depolarization to be activated (Catterall et al., 2005b) and they open slowly (Hille et al., 2001) (there are also low-voltage calcium channels which follow different behavior which we do not discuss here (Zhang et al., 2013)). The channel opening leads to calcium flowing into the cell during the falling phase of the action potential.

Surprisingly, blocking calcium channels often leads to the broadening of action potential (Faber and Sah, 2002; Sah, 1996; Shao et al., 1999); This is because calcium binds to **calcium-activated potassium channels**, which then trigger a larger outflux of potassium than the initial influx of calcium (Bean, 2007). There are three distinct types of calcium-activated potassium channels: (1) BK channels have large single-channel con-

ductances and in addition to calcium, they require membrane depolarization to open. (2) SK channels have small conductances and they are voltage insensitive. Finally, (3) IK channels have an intermediate single-channel conductances, are voltage insensitive and are sparsely distributed in the brain (Sah and Louise Faber, 2002).

Another voltage-gated channel type are the **HCN channels** (Hyperpolarization-activated cyclic nucleotide-gated channels) which are sometimes called ‘pacemaker channels’ due to their function in modulating the rhythmic activity in many cell types like the sinoatrial node cells in the heart or the relay cells in the thalamus. They generate so-called h-current ( $I_h$ ) because of their dependence on hyperpolarization (sometimes also named ‘funny’,  $I_f$  in cardiac tissue or ‘queer’,  $I_q$  in the hippocampus (Lüthi and McCormick, 1998)). HCN channels activate slowly with hyperpolarization (around -70 to -50 mV), slowly depolarize the cell and close at positive potential values; They do not inactivate. These channels pass inward current of mixed ions such as  $\text{Na}^+$  and  $\text{K}^+$  (Hille et al., 2001). In the CA1 pyramidal neurons of the hippocampus, their density increases along the somato-dendritic axis, with largest densities being furthest from the soma. This distribution shapes the time course of excitatory postsynaptic potentials and makes their summation location-independent (Magee, 1998).

In addition to voltage-gated potassium channels there are also specific pumps such as  $\text{Na}^+$ - $\text{K}^+$  pump, the  $\text{Ca}^{2+}$  pump,  $\text{Na}^+$ - $\text{Ca}^{2+}$  exchanger,  $\text{Cl}^-$ - $\text{HCO}_3^-$ -exchanger and many others (Hille et al., 2001).

A large variation of channel expression and currents produced, as well as their variable distribution within different neuronal segments and across brain regions (Nusser, 2012) makes general assumptions of ionic currents flowing through a neuron difficult. Thus, an important step in a given study is the selection of the applicable currents; In the models described in the next chapters, only passive, sodium and potassium channels are discussed. This work focuses on the action potential initiation, and how action potential may impact further activity in the network, therefore sub-threshold activity of the cell is not considered important.

### 2.2.3 Energy efficiency

The use of electro-chemical gradients alone is not sufficient for brain function. The supply of energy is crucial for this organ and when subjected to lower levels of energy, the brain is prone to anoxia or ischemia (Ames et al., 1995). The brain, just as any other organ, needs a constant external supply of energy in the form of oxygen and glucose, which are transported in the blood. Notably, increase in the supply of blood into the brain is widely used for verifying the level of brain activity. This organ uses 20% of the energy consumed by the whole-body even though it accounts for only 2% of the body’ weight (Attwell and

Laughlin, 2001). Still, with the activity of 120 billion neurons (Herculano-Houzel, 2009) it needs to use its resources efficiently. The initiation and propagation of action potentials are considerably taxing to brain metabolism (Alle et al., 2009) since they require as much as 20–47% of the total energy consumed by the brain (Attwell and Laughlin, 2001; Howarth et al., 2012). To minimize the ‘cost’ of single action potentials, the contributing currents of sodium and potassium (responsible for rising and falling phase of the action potential respectively) should overlap as little as possible (Carter and Bean, 2009).

In the popular Hodgkin-Huxley model (Hodgkin and Huxley, 1952) (explained in more detail in Section 2.2.1) action potentials are not very energy-efficient because the sodium channels remain open for some time during the falling phase of the action potential (Fohlmeister, 2009). In mammals, action potentials are reported to be more efficient but this varies largely depending on cell types (Carter and Bean, 2009) and the estimations are subject to controversy (Lennie, 2003; Attwell and Laughlin, 2001; Attwell and Iadecola, 2002).

Neurons which have myelinated axons have a much smaller capacitance and use less metabolic energy to maintain the gradient of sodium and potassium because those ions only flow at the nodes of Ranvier (NoR). In unmyelinated axons, such as the mossy fibers of hippocampus, consumption of energy is minimal because the overlap of flux from  $\text{Na}^+$  and  $\text{K}^+$  channels is minimized (Alle et al., 2009).

To increase its efficiency, the brain should limit the excessive expenditure of energy which does not lead to the desired result. Therefore, if considering the brain as an information-processing device and action potentials as messages, each of the action potentials should spend minimal energy and provide a maximum of information. It is debated whether the brain works this way or not. Nonetheless, the way action potentials are initiated (which we talk more about in the Chapter 3) is more energy-efficient than originally thought (Brette, 2013) and single action potentials may have a larger impact on the network information than believed (Chapter 5).

## 2.3 Role of different neuronal segments

The soma, axon and dendritic tree are all distinct parts of neuron which have different molecular identity and it is possible to express one of the molecular components to properly identify neuronal segment of interest (Fig 2.4 B). However, exact morphology differs depending on the brain area and the cell type (e.g. Fig 2.6).

The activity of neurons is most frequently recorded at the soma, which is the largest segment of the neuron and the easiest to access with the electrode. However, in most neurons, the action potential is not initiated at the soma but in the tiny axon initial

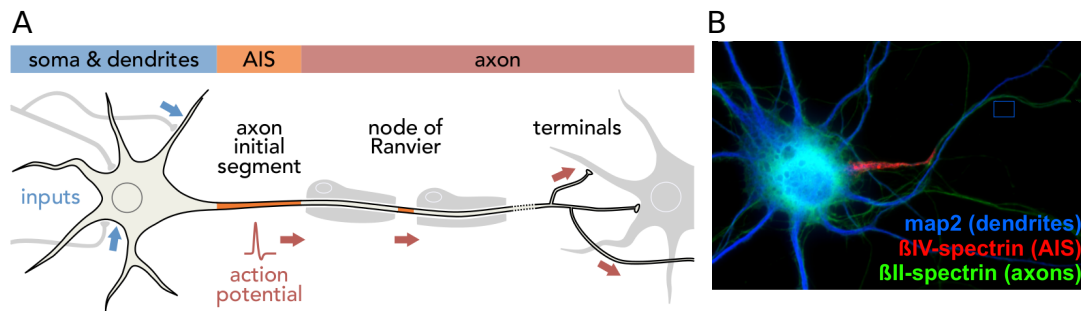


Figure 2.4: **Neuronal segments.** **A.** Graphics of the neuron showing different neuronal segments. **B.** Molecular identification of dendrites, axon initial segment (AIS) and nonmyelinated axons. Adapted from [Letierrier \(2015\)](#).

segment located in the axon 15 - 40  $\mu\text{m}$  away from the soma (Fig 2.4). In rare cases, action potential initiation may even take place away from the axon initial segment (such as at the apical and basal dendrites, soma, axon hillock, and nodes of Ranvier) ([Colbert and Johnston, 1996](#); [Debanne et al., 2011](#); [Mainen et al., 1995](#); [Milojkovic et al., 2005](#); [Stuart et al., 1997a,b](#)). After initiation, the action potential propagates through the axon to reach the pre-synaptic terminals and it develops in the soma (process which we will explain in more detail in Chapter 3) and then backpropagates further into the dendrites where it may act on synaptic plasticity ([Gong et al., 1999](#); [Stuart et al., 1997b](#)).

In the following sections we will discuss the process of action potential initiation and propagation within different neuronal segments.

### 2.3.1 Soma

The soma (cell body) of a neuron contains the cell nucleus. Most of the proteins are produced at this site and are later distributed throughout the whole cell. The soma gives rise to the dendritic tree and to the axon (although the axon may also originate from one of the dendrites) ([Thome et al., 2014](#)).

Along with the dendrites, the soma is the main neural segment which receives synaptic inputs from other cells ([Squire et al., 2012](#)). Although, the action potential in mammalian neurons is most frequently initiated at the axon initial segment, in some cases it is initiated at other sites: In the subpopulation of interneurons in the mammalian olfactory bulb, which do not have axon initial segment, action potentials are believed to initiate elsewhere, possibly in the soma ([Chand et al., 2015](#)). In these neurons, somatic recordings reveal a largely different shape of action potential (Fig 2.5, blue) when compared to neighbouring interneurons, where the action potential is known to be initiated in the axon initial segment (Fig 2.5, green).

In most of the mammalian neuron recordings, the somatic action potential is preceded

by a small depolarisation originating from the axonal spike, which invades the soma causing action potentials with bi-phasic phase plots and sharp onset (kink) (Coombs et al., 1957; Naundorf et al., 2006; Shu et al., 2007a). Those bi-phasic phase plots with a sharp onset at the initiation are characteristic of action potentials initiated at the axon initial segment. The first ‘phase’ corresponds to the current coming from the axon, while the second corresponds to the current flowing through the somatic sodium channels (Coombs et al., 1957). Although action potentials initiated in the AIS have a smooth initiation, in the soma this onset appears sharper; This is because the resistance between the large soma and the thin axon causes the voltage to rise much faster at AIS (a process which is explained in detail in Chapter 3). If the action potential was initiated in the soma, the gradual change of voltage would not allow for a fast enough opening of a sufficient number of sodium channels to cause the sharp rise of potential, as it was observed in many experiments (Figure 2.5B as compared to A). The rapid onset of action potentials make the single-compartment models with a sharp threshold (like integrate-and-fire model) better at reproducing the firing patterns of neurons with an axon initial segment initiation than single-compartment models, based on detailed channel kinetics (such as Hodgkin-Huxley model) (Brette, 2015).

### 2.3.2 Axon

Usually, the axon has its origin at the soma (Fig. 2.4) but it may also originate from the basal or (less frequently) apical dendrite, which strengthens its sensitivity to the inputs from this particular dendrite (Lorincz and Nusser, 2010; Thome et al., 2014). Like all morphological features of mammalian cells, the axon owes its formation and some of its function to a cytoskeleton made out of actin and microtubule (Kevenaar and Hoogenraad, 2015).

It consists of a wider axon hillock where dynein regulator NDEL1 forms a barrier, only allowing selected proteins and mitochondria to pass through (Kuijpers et al., 2016; Muth and Caplan, 2003). Due to this, axons have a distinct composition from other neuronal segments. When proteins, which are produced at the soma pass the barrier, their delivery is still a challenge because axons can extend for more than a meter (Debanne et al., 2011).

Following the hillock we find an axon initial segment and the main cylindrical axon which might be myelinated. The distal part of the AIS is not necessarily adjacent to myelin (Baranauskas et al., 2013). Myelin sheaths originate from Schwann cells or oligodendrocytes (in peripheral and central nervous system respectively) (Debanne et al., 2011). Myelin protects the axon and ensures electric insulation, enabling signal to traverse quickly and efficiently (100 m/s in large myelinated axons as opposite to 0.1 m/s in unmyelinated axons (Debanne et al., 2011)). Between the stretches of myelin there

are Nodes of Ranvier (NoR), where we can find a high density of sodium channels where the action potentials are reinforced. In some neurons (such as Purkinje cells) the first NoR may first act as an initiation area for the action potential (Clark et al., 2005). The axonal arbor branch ramifies to connect with several thousands (30,000 – 60,000 in the hippocampal CA3 pyramidal cell) of target cells via multiple terminals (boutons) (Major et al., 1994; Li et al., 1994; Ishizuka et al., 1990). The shape of axonal arbors might differ largely: Pyramidal cells in the hippocampus tend to have axons stretching far from the cell body whereas axonal trees of interneurons in the hippocampus and in the cortex tend to remain closer to the cell body, and are highly branched (e.g. Fig 2.6) (Debanne et al., 2011; Gulyas et al., 1993; Thomson and Destexhe, 1999).

Interestingly, a cut axon from cultured hippocampal neurons can be regenerated at its original position but only if the axon initial segment remains connected (i.e. site of the cut is more than  $35\mu\text{m}$  from the soma). Otherwise, it will regenerate from one of the dendrites (Gomis-Rüth et al., 2008).

Axons are not simply meant for propagation of the signal: Branch points are considered to be frequency filters, but there are more sophisticated ways in which axons do the

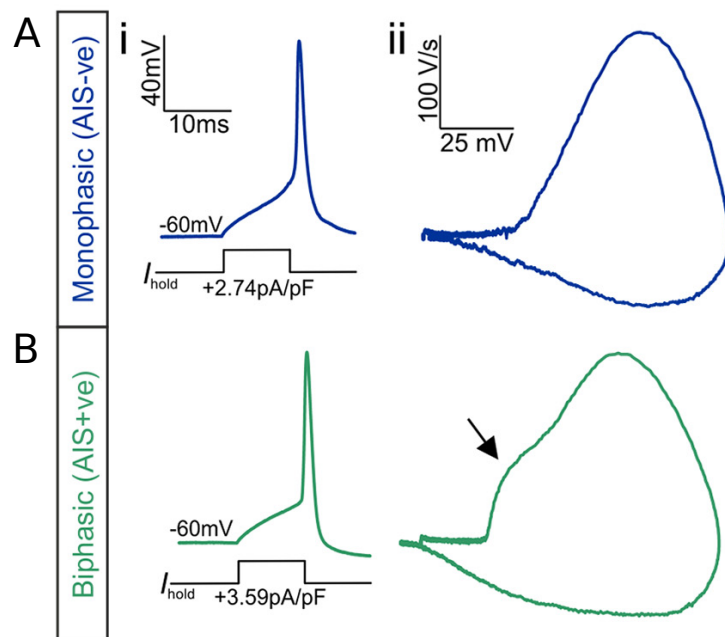


Figure 2.5: **Action potential shape depends on the initiation location.** Action potentials recorded from the interneurons in the mammalian olfactory bulb. **A.** The initiation of the action potential took place away from axon initial segment. Action potential (i) does not display a sharp onset which is even better visible in the phase plot (ii) which is monophasic. **B.** Initiation was distal from the soma and took place in the axon initial segment. Onset of the action potential is sharp (i) and the phase plot (ii) is biphasic. Adapted from Chand et al. (2015).

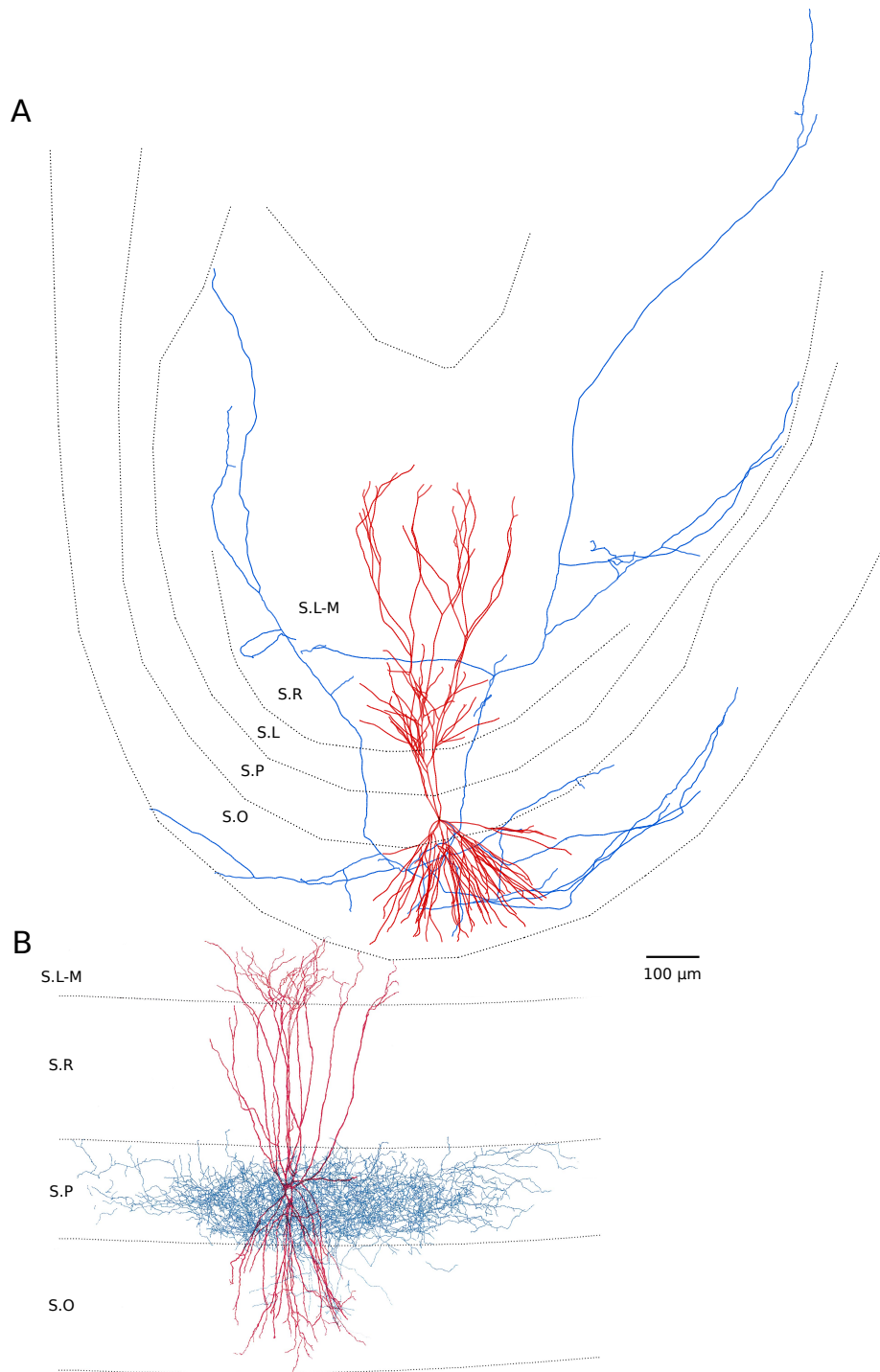


Figure 2.6: **Morphology of the hippocampal cells** with axons (blue) and dendrites (red). Hippocampal layers are indicated: lacunosum-moleculare (S.L-M), lucidum (S.L), radiatum (S.R); pyramidale (S.P) and oriens (S.O). **(A)** CA3 pyramidal cell extends its axon (note it is only partial reconstruction of the axon) far from the cell body. Adapted from [Ishizuka et al. \(1995\)](#), published as cell c12866 on [neuromorpho.org](#)), whereas **(B)** CA1 basket cell forms dense axonic tree in the proximity of the cell body. Adapted from [Thomson and Destexhe \(1999\)](#).

computation, for instance, by reflecting the impulse (Goldstein and Rall, 1974). They can also fail to conduct the action potential so that the selected signals are unable to reach other cells (Wall, 1995; Debanne et al., 1997; Meeks and Mennerick, 2004; Soleng et al., 2003).

It is also believed that axons are able to transmit both analog and digital signals by integrating subthreshold synaptic potentials and, depending on the activity, by increasing the width of action potentials (Cooper et al., 1998; Debanne et al., 2011).

For a long time the axon was inaccessible to record from because of its small diameter (between 0.08 and 0.4  $\mu\text{m}$ , unmyelinated axon) (Berbel and Innocenti, 1988; Debanne et al., 2011). Recently, some groups have reported patch-clamp recordings either from the axon directly or from the enlarged end of the axon that forms as a response to injury of the axon (called ‘bleb’, 3–6 $\mu\text{m}$  in diameter) (Atherton et al., 2008; Clark et al., 2005; Kole et al., 2007; Mathy et al., 2009; Meeks et al., 2005; Schmidt-Hieber et al., 2008; Shu et al., 2007a, 2006). Voltage-sensitive dyes (Foust et al., 2010; Palmer and Stuart, 2006; Palmer et al., 2010) and sodium imaging (Bender and Trussell, 2009; Fleidervish et al., 2010; Kole et al., 2008) are among other techniques which enable activity monitoring in the axon. The advances in these techniques allowed researchers to precisely identify the location of action potentials initiation and propagation.

It is also possible for two axons to communicate either through ephaptic connections, which allow them to synchronize the signal (Barr and Plonsey, 1992; Katz and Schmitt, 1940), chemical synapses (Chandelier cells contact selectively axon initial segment) (Inan and Anderson, 2014) or through gap junctions (also called electrical synapses) allowing for even tighter synchrony (Debanne et al., 2011).

### 2.3.3 Axon initial segment

In most mammalian neurons the action potential initiates in the distal part of the axon initial segment (AIS) which is located  $\sim 15\text{--}40\ \mu\text{m}$  from the soma (Fig 2.4) (Baranauskas et al., 2013; Colbert and Pan, 2002; Foust et al., 2010; Hu et al., 2009; Kole and Stuart, 2012; Khaliq and Raman, 2006; Mainen et al., 1995; Meeks and Mennerick, 2007; Palmer and Stuart, 2006; Shu et al., 2007a; Stuart et al., 1997b,a). But why does it take place there and not in the soma which receives direct input from the synapses and from the dendrites?

Until recently electrophysiologists and researchers performing immunostaining were trying to determine if it could be due to the higher density of sodium channels in the axon initial segment, as compared to the soma. Electrophysiologists claimed that the density is equal (Colbert and Johnston, 1996; Colbert and Pan, 2002), while theoretical (Mainen et al., 1995; Meeks and Mennerick, 2007; Moore et al., 1983; Rapp et al., 1996)

and immunostaining studies (Boiko et al., 2003; Catterall, 1981; Meeks and Mennerick, 2007; Inda et al., 2006; Wollner and Catterall, 1986) have shown a higher density in the distal part of the axon initial segment. Recently, Kole and colleagues resolved the issue by demonstrating that channel density might be underestimated as a result of tight channel anchoring to the intracellular cytoskeleton (Kole et al., 2008) and that the density of sodium channels is indeed higher in the AIS than in the soma. However, the overall density of sodium channels remains constant throughout the AIS (Hu et al., 2009).

Indeed, the AIS has the highest density of sodium channels (both transient and persistent) (Astman et al., 2006; Inda et al., 2006; Kole et al., 2008). Some groups report, that in the AIS sodium channels activate twice as fast than in the soma (Schmidt-Hieber and Bischofberger, 2010) and that it has tendency to generate persistent  $\text{Na}^+$  current (Astman et al., 2006; Fleidervish et al., 2010). The AIS is built out of Ankyrin G which directs sodium (Barry et al., 2014; Garrido et al., 2015; Zhou et al., 1998),  $\text{K}_v1.2$  (Sánchez-Ponce et al., 2012) and  $\text{K}_v7$  (KCNQ) (Pan et al., 2006) channels to concentrate in the AIS. Most of the mammalian pyramidal neurons have two types of sodium channels present in the AIS:  $\text{Na}_v1.6$  channels, which are located distally and have lower threshold for activation than the other type, the  $\text{Na}_v1.2$  channels, which are located more proximally. Sodium channel threshold is up to 15 mV higher in the soma than in AIS (Colbert and Pan, 2002; Hu et al., 2009). However, exact localisation of the different types of channels varies between cell types (e.g. localisation of four types of voltage-gated channels in AIS in different types of neurons, Fig 2.7). When the action potential initiates the influx of  $\text{Na}^+$ , current is the highest in the middle of the AIS and not at its distal end, where the initiation takes place (influx is up to 4 times lower at the initiation site than at the central location of AIS) (Baranauskas et al., 2013).

Furthermore, the small axon initial segment is electrically isolated from the soma and so less current is required to depolarize it. The current density is higher at this level, which allows the AIS to overcome their electric load (Mainen et al., 1995; Moore et al., 1983).

When the action potential is initiated in the axon initial segment, the current flows into the initial segment, then axially towards the somatodendritic compartment where it leaves the cell. The dipole then forms (we explain this process in detail in the Chapter 3).

During high frequency firing, the AIS is the most reliable to follow initiating full action potentials without attenuation (Clark et al., 2009; Debanne et al., 2011; Shu et al., 2007a). However, the function of the axon initial segment is not solely the initiation of action potentials. Together with the axon hillock it is responsible for the molecular separation between the rest of the axon and the somato-dendritic compartment (Leterrier

and Dargent, 2014; Leterrier, 2015; Rasband, 2010).

The AIS might have a different location depending on the cell type (Fried et al., 2009; Kuba et al., 2006). Its size and site might influence processing of the different frequency signalling. Some high-frequency processing neurons have short ( $\sim 10 \mu\text{m}$ ) and distal AIS ( $\sim 45 \mu\text{m}$  from the soma) while low-frequency processing neurons have longer ( $\sim 25 \mu\text{m}$ ) and more proximal AIS ( $\sim 10 \mu\text{m}$  from the soma) (Gulledge and Bravo, 2016; Kuba et al., 2006).

Surprisingly, despite its highly structured appearance, neuron might alter the size or exact site of the AIS, which is known to change as a response to elevated activity. In dissociated hippocampal cultures, excitatory neurons subjected to increased activity during long time periods (in scale of days) can shift their AIS away from the soma, leading to a decrease of excitability (Grubb and Burrone, 2010; Evans et al., 2013; Muir and Kittler, 2014). Dentate granule cells are able to quickly shorten their AIS, within 3 hrs, which dampens the excitability in multiple-spike firing (a process which can be neutralized by the modulation of  $\text{Na}_v$  channel properties) (Evans et al., 2015). On the other hand, in inhibitory olfactory bulb dopaminergic cells, elevated activity causes the opposite effect: a proximal shift and lengthening of AIS (Chand et al., 2015). These plasticity processes are reversible.

Depending on the cell type (e.g. cortical pyramidal neurons) the axon initial segment can be selectively contacted by chandelier (axo-axonic) interneurons (Kosaka, 1980; Fish et al., 2013; Howard et al., 2005). Chandelier cells are fast spiking GABA-ergic cells. Interestingly, they can have inhibitory or excitatory influence depending on the potential of postsynaptic cells (although most frequently they remain inhibitory). Depolarizing pyramidal cells to levels of reversal potential of GABA and beyond is sufficient to induce inhibitory and below - excitatory effect of the axo-axonic cell (Inan and Anderson, 2014; Khirug et al., 2008; Szabadics et al., 2006; Woodruff et al., 2009, 2011).

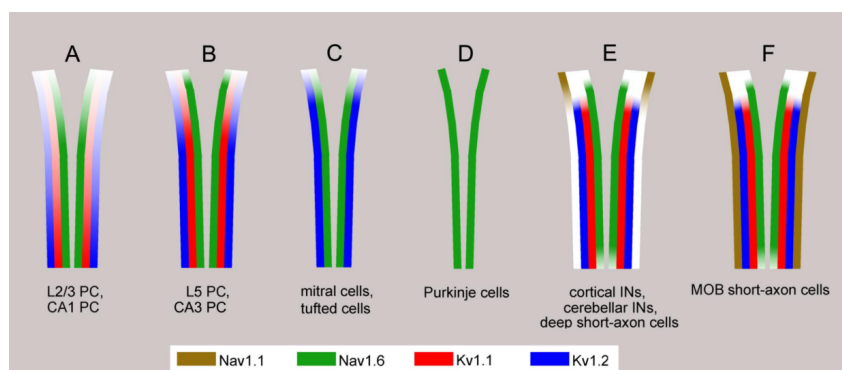


Figure 2.7: Localization of Nav1.1, Nav1.2, Kv1.1 and Kv1.2 in axon initial segment of different neuron types. Adapted from Trimmer (2015).

However, the importance of the AIS comes with risks as the axon initial segment is considered a ‘hot spot’ for various diseases such as inherited epilepsies (Wimmer et al., 2010) as well as neurological and psychiatric disorders (Buffington and Rasband, 2011).

### 2.3.4 Synapse

Axonal arbors are covered with multiple boutons of different size, which may form synapses with other neurons. When an action potential arrives at the synapse, voltage gated  $Ca_v$  channels open, causing neurotransmitter release. It then binds to a receptor of the target cells which leads to the opening of channels and to flow of current, inducing signal propagation. If different amount of transmitter is released, the signal received by the postsynaptic cell might change (Hille et al., 2001). Action potentials in the same neuron might display different amplitudes and width, for example during burst firing (Fig 2.8) (Williams and Stuart, 1999). As it traverses through the axon, the signal might also change; Earlier-mentioned branching points, synapses (especially of chandelier cells connecting AIS (Kosaka, 1980; Fish et al., 2013; Howard et al., 2005), availability of channels and ions are all factors that might impact the shape of the signal arriving at the terminals. Geiger and colleagues have shown that in repetitive stimulation, action potentials became broader in the axon terminal while they do not change in appearance in the soma (broadening is due to inactivation of  $K_v1$  family channels located in the terminal). A broader action potential enables more calcium influx and might double the amplitude of the excitatory postsynaptic current (EPSC) in the connecting cell (Geiger and Jonas, 2000).

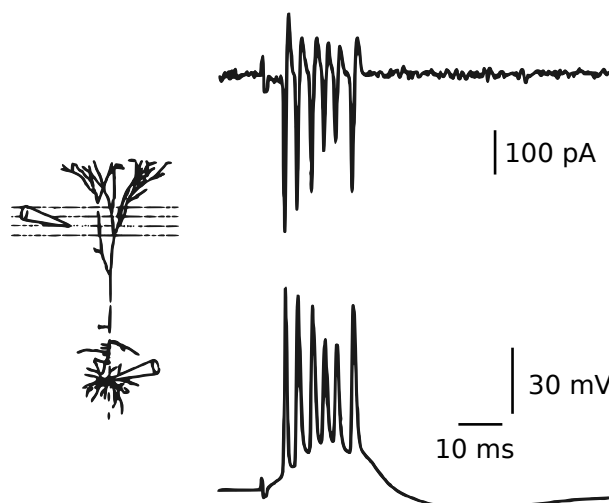


Figure 2.8: Extracellular and intracellular recordings from the bursting layer 5 pyramidal cell. Adapted from Williams and Stuart (1999).

### 2.3.5 Dendrite

The dendritic tree originates from the soma and might vary widely depending on the cell type and brain area (e.g. Fig 2.6). Its major functions include gathering and propagating synaptic inputs to the soma and backpropagating the action potential.

Synapses most commonly contact dendrites (although they can also contact soma or axon). When the action potential passes to the postsynaptic site it takes the form of postsynaptic potential. The dendrite forwards this signal, along with many other synaptic inputs, to the soma, performing computation on the way (which depend on the branching, state of the channels and received inputs) (Magee, 1998; Losonczy et al., 2008; Tran-Van-Minh et al., 2015). If the threshold is reached and action potential is initiated, it may backpropagate to the dendrites, which is essential for synaptic plasticity (backpropagating action potential causes  $\text{Ca}^{2+}$  channels to open which in spines induces some form of synaptic plasticity) (Stuart et al., 1997b). However, sometimes action potentials fail to backpropagate to the somatodendritic compartment (Williams and Stuart, 1999).

Furthermore, calcium and/or sodium action potentials might also be initiated in the dendrite (example of calcium mediated action potentials initiated in the dendrites is shown in the Fig 2.9) (Golding and Spruston, 1998; Milojkovic et al., 2005; Mainen and Sejnowski, 1996; Regehr et al., 1993; Schiller et al., 1997; Stuart et al., 1997a), but might also be initiated in the axon initial segment and then actively propagate to the dendrite (Stuart and Sakmann, 1994; Stuart et al., 1997b).

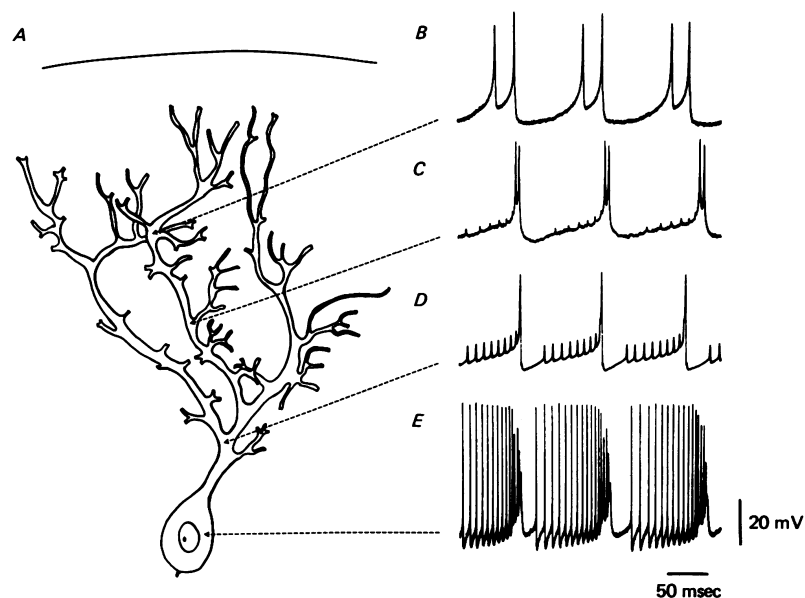


Figure 2.9: Bursts of action potentials backpropagating to the dendrite. In the furthest end of the dendrite, independent calcium action potentials are forming. Adapted from Llinás and Sugimori (1980).

### 2.3.6 Impact of morphology on the firing pattern

Neurons have varied morphologies. The most notable dendritic and axonal trees can have completely different appearance (e.g. Fig 2.6) with single (unipolar) or multiple (multipolar) processes extending from the soma (Ramon y Cajal, 1888). Additionally, soma size and shape also varies from cell to cell. For instance, the round cell bodies of interneurons tend to be smaller than those of pyramidal cells, whose somatic trans-section appears more triangular.

Because many types of neurons keep their firing properties even when the cell is dissociated from the network, the different firing patterns seem to be independent from the network activity (Chan et al., 2004; Do and Bean, 2003; Puopolo et al., 2007; Raman et al., 1997).

Given this, it would be surprising if the morphology of the neuron did not have an impact on the action potential. Indeed, Mainen and Sejnowski showed in their computational study that merely changing the morphology of a cell, while maintaining the ionic channel distribution was enough to trigger different types of firing patterns (Fig 2.9) (Mainen and Sejnowski, 1996).

Interestingly, it seems that morphology also impacts the location of the axon initial segment (AIS). Smaller neurons (such as dentate granule cells) tend to have an intermediate length of AIS, which is closer to the soma than in larger neurons (such as pyramidal cells), which have longer AIS (Gulledge and Bravo, 2016).

## 2.4 Kink at the initiation, experiments vs models

Action potentials are very distinct events where the membrane potential largely increases above the baseline level then falls back to its original value shortly after. The inflow of  $\text{Na}^+$  ions is responsible for the rising, and the outflow of  $\text{K}^+$  ions, largely for the falling phase of the action potential (the inactivation of sodium channels is also important).

Surprisingly, the onset of the action potential in the soma is much sharper than we could expect from the  $\text{Na}_v$  channel voltage-dependent opening, with its given voltage change (Angelino and Brenner, 2007; Brette, 2015). But what else, could impact action potential generation so strongly?

First, the initiation usually does not take place in the soma but in much smaller axon initial segment (AIS). Action potentials recorded from the AIS have a smoother onset, although most of the recordings have been done from the ‘bleb’ which forms when the axon is injured by cutting. Because of its nature, recordings from this site have been criticized (Öz et al., 2015). However, direct recordings from the AIS are of a similar, smooth appearance (Fig 2.10) (Kole et al., 2008; Palmer and Stuart, 2006; Shu et al.,

2007a; Stuart et al., 1997a). Recordings from the soma of the APs initiated either at the soma or in the dendrites (Fig 2.5) (Shu et al., 2007a) also reveal a smooth onset.

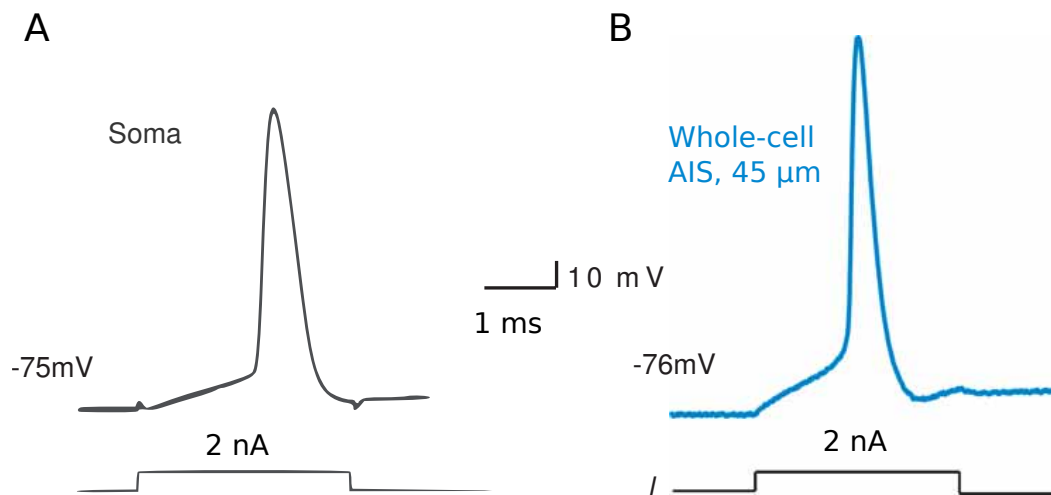


Figure 2.10: **Action potential recorded in the soma and AIS.** **A.** Action potential recorded in the soma with sharp onset. **B.** Action potential recorded in axon initial segment (AIS)  $45 \mu\text{m}$  away from soma reveals smooth onset. Adapted from Kole et al. (2008).

Before we go on to describe three hypotheses explaining the kink in the somatic spike, we will shortly discuss the significance of this phenomenon. It may seem that it is just a simple alternation in the shape of the action potential, but even minor modifications of the mechanism of action potential generation can qualitatively affect the neuronal encoding. Faster and more efficient initiation means that a neuron could fire at higher frequencies (Köndgen et al., 2008; Tchumatchenko et al., 2011). Interestingly, the firing frequencies observed experimentally (up to 200–300 Hz) could not be predicted by the isopotential HH model (Ilin et al., 2013; Fourcaud-trocme et al., 2003).

The action potential initiation in the AIS might be more energy efficient (Cooperativity and Critical Resistive Coupling Hypotheses propose mechanisms which take less metabolic cost than standard isopotential HH type models); When the action potential becomes an all-or-none event, as in the cooperativity or critical resistive coupling models, energy is conserved. This way, there is no unnecessary inflow of sodium, which would need to be reversed by energy-consuming ion pumps (Attwell and Laughlin, 2001).

### 2.4.1 Cooperativity Hypothesis

Naundorf and colleagues (Naundorf et al., 2006) proposed that the kink in somatic action potentials appears due to cooperativity between sodium channels. They claimed that the sharp onset of action potentials indicates that many sodium channels open simultaneously

– something which was shown to happen in other body parts and with other channels (Dekker and Yellen, 2006; Dixon et al., 2012; Marx et al., 1998; Molina et al., 2006; Undrovinas et al., 1992).

The cooperativity hypothesis was strongly criticised soon after (Naundorf et al., 2007; Yu et al., 2008), with one of the main arguments being that the model proposed by Naundorf and colleagues consisted only of a soma, and therefore lacked the axon initial segment where most of the action potentials are initiated.

The group responded to the criticism publishing several papers in support for their hypothesis (Baranauskas et al., 2010; Huang et al., 2012; Ilin et al., 2013; Öz et al., 2015). They proposed that cooperativity may still exist in the axon initial segment, leading to an action potential with a sharp onset in the soma (Öz et al., 2015). This hypothesis did not receive much support for several of reasons. Notably, recordings from the axon initial segment do not show a kink at the initiation of the action potential (Fig 2.10) (Kole et al., 2008). Moreover, experimental studies were unable to detect sodium cooperativity in the AIS (Hu et al., 2009).

## 2.4.2 Backpropagation Hypothesis

As a response to the Cooperativity Hypothesis, the McCormick group proposed a Backpropagation Hypothesis as a potential explanation for the kink (Naundorf et al., 2007; Yu et al., 2008). Here, the action potential follows standard Hodgkin-Huxley type model and the initiation of the action potential with a smooth onset is located at the AIS. As the action potential travels towards the soma, it sharpens with each further opening of sodium channels. When the AP reaches the soma it shows the kink. This explanation provides a simple account for the kink, which is unfortunately not completely correct (as we will argue in Chapter 3). The main flaw of this hypothesis is that the distance between the AIS and the soma is not long enough to account for the kink, as distance required would be  $\sim 2$  mm, as shown in the paper, opposite to the 30–50  $\mu\text{m}$  of actual biological distance from the soma to the AIS.

## 2.4.3 Critical Resistive Coupling Hypothesis

Finally, in 2013, Brette proposed the Critical Resistive Coupling (initially called Compartmentalization) Hypothesis (Brette, 2013). The Critical Resistive Coupling Hypothesis explains the kink based on two requirements: the distal initiation, and the large size difference between the soma and the axon initial segment, leading to a current sink formation in the soma. When the action potential is initiated in the AIS, a single current loop forms between the AIS and the soma (instead of small propagating current loops as

in the Backpropagation Hypothesis). Although the mechanism is very different, this hypothesis is mathematically very similar to the cooperativity hypothesis; In the Chapter 3, we will argue that this hypothesis indeed explains the kink correctly.

## 2.5 Signature of a single cell activity in the extracellular potential

The field potential is composed of the activity of multiple neurons, proximal and distal to the recording electrode (Katzner et al., 2009). It is believed to reflect transmembrane currents (Einevoll et al., 2013). To model this field, a dipole approximation is frequently used (Buzsáki et al., 2012).

The action potential (AP) of a single neuron is such a large signal that it can be detected in the extracellular medium, in the scale of microvolts (Henze et al., 2000). However, the extracellular field represents a much wider composition of signals related to other processes concomitant to, but not involved in the generation of the original AP, such as synaptic integration or network activity (Teleńczuk and Destexhe, 2013). An AP recorded at various sites around the cell might appear different, and an AP in the extracellular medium might show the action potential peak slightly sooner than in the soma (as we predict in the simulation described in Chapter 3).

In addition to the extracellular signature of AP, synaptic activity triggered by a single cell can also be recorded extracellularly. Spikes of thalamocortical neurons arriving at cortical synapses generate a unitary excitatory synaptic field in the cortex (Swadlow et al., 2002). Similarly, single hippocampal interneurons, such as basket cells, generate a local unitary inhibitory field (Bazeltot et al., 2010; Glickfeld et al., 2009). Interestingly, in these studies there is no record of excitatory postsynaptic potential (ePSP) in the extracellular field being generated by single pyramidal cells in the hippocampus. Others have argued that ePSPs are the main determinant of the LFP (Reimann et al., 2013) (but see Haider et al. (2015); Telenczuk et al. (2016)). Why then would we only see inhibitory PSP in the hippocampus?

The difference in the extracellular field evoked by interneurons and pyramidal neurons could be due to the distribution of their synaptic terminals. While most of the synapses of inhibitory cells are clustered proximally to the cell body of the hippocampal basket cell, and are most likely to contact the cell bodies of other neurons (which in the hippocampus are in the same layer), the synapses of pyramidal neurons are more widely distributed in space (Megias et al., 2001). Also, pyramidal cells tend to make contacts in all the layers, which will have signals more likely to cancel each other out in the extracellular medium

(Buzsáki et al., 2012).

Field potentials are relatively easy to record and they are often routinely used to measure neuronal population activities and to infer brain states (Cui et al., 2016; Destexhe et al., 1999).

## 2.6 Bursts of action potentials

Until now we only explained the process of the action potential (AP) initiation and propagation in different neuronal parts and the AP signature in the extracellular medium. However, a single AP is often directly followed by multiple other APs, forming a burst. Bursts of action potentials may play a different role than single APs and are worth mentioning. For instance, during the burst, interaction between soma and dendrite can be more complex. Multiple studies have showed that slow, calcium spikes or other active depolarizing events may take place in the dendrite and provide for the long depolarization driving the burst of action potentials in the soma (Helmchen et al., 1999; Kim and Connors, 1993; Larkum and Zhu, 2002; Larkum et al., 2001; Stuart et al., 1997a).

The soma is not always able to follow the burst initiated in the axon initial segment appropriately, thus bursts are easier to identify in the axon (Mathy et al., 2009). In the AIS, APs display a minimal decrease in amplitude during bursts (Shu et al., 2007a; Williams and Stuart, 1999).

In the hippocampus, when sodium channels are partly blocked, the amplitude of the first AP is not affected. This might suggest that there is an excess of sodium channels in the cell if only one action potential is fired. However, the next action potentials and the overall maximal discharge frequency will be affected by this change (Fig 2.11) (Madeja, 2000).

Firing patterns vary between different types of neurons. Since the distribution of ionic channels with divergent properties are particular for each cell type, it is more probable that the firing patterns stem from the properties of these different channels. Surprisingly, Mainen and colleagues (Mainen and Sejnowski, 1996) showed in their computational study that different morphologies of neurons are sufficient to produce variability of firing patterns (example, Fig 2.12).

## 2.7 Activity of single cell within population

A single cell can discharge a single action potential or bursts of action potentials to provide an input of information to other cells. But does the action of a single neuron really matter in the jungle of other cells and their activity? Some studies argue against this

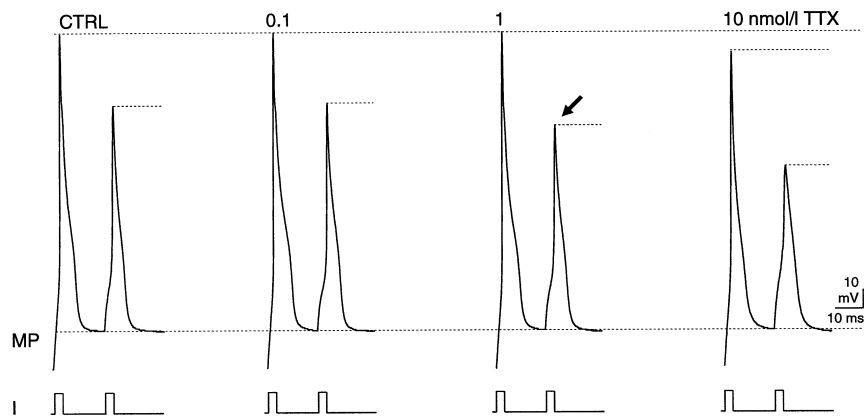


Figure 2.11: **Effects of TTX on recovery after activation of the action potential.** Recordings of pairs of action potentials at different concentration of TTX (no TTX on the left, 10 nmol/l TTX on the right). The amplitude of the first action potential is hardly affected, whereas amplitude of the second action potential changes with increasing TTX concentration (arrow) (I, amplitude 0.5 nA, duration 2ms, interpulse interval is 10 ms. Dissociated CA1 hippocampus neurons of guinea pig. Adapted from [Madeja \(2000\)](#).

([Shadlen and Newsome, 1998](#)) hypothesizing that it is rather the overall activity which makes an impact (so-called rate-coding). At this time, multiple studies have showed that a single action potential can have an impact on the overall network activity. For instance, stimulation of a single motor cortical neuron can evoke whisker movement ([Brecht et al., 2004](#)), and action potentials in a single somatosensory cortical neuron might induce behaviorally reportable effects ([Houweling and Brecht, 2008](#)). Also, single GABAergic cell might have an impact on population events in developing hippocampus ([Bonifazi et al., 2009](#)).

Furthermore, bursts of action potentials of a single cell can trigger a switch between brain states (slow wave and rapid-eye-movement sleep, and inversely) ([Li et al., 2009](#)). Finally, a single action potential in pyramidal neurons of the hippocampus can trigger the Sharp Wave Ripple (SPW-R) network activity (which we will discuss further in Chapter 5) ([Bazélot et al., 2016](#)).

## 2.8 Sharp Waves as example of network activity

In certain brain states neurons synchronize their activity, which can be recorded as different types of patterns in the extracellular medium and by electroencephalography (EEG) recordings. In the hippocampus there are two types of oscillations which can be found in

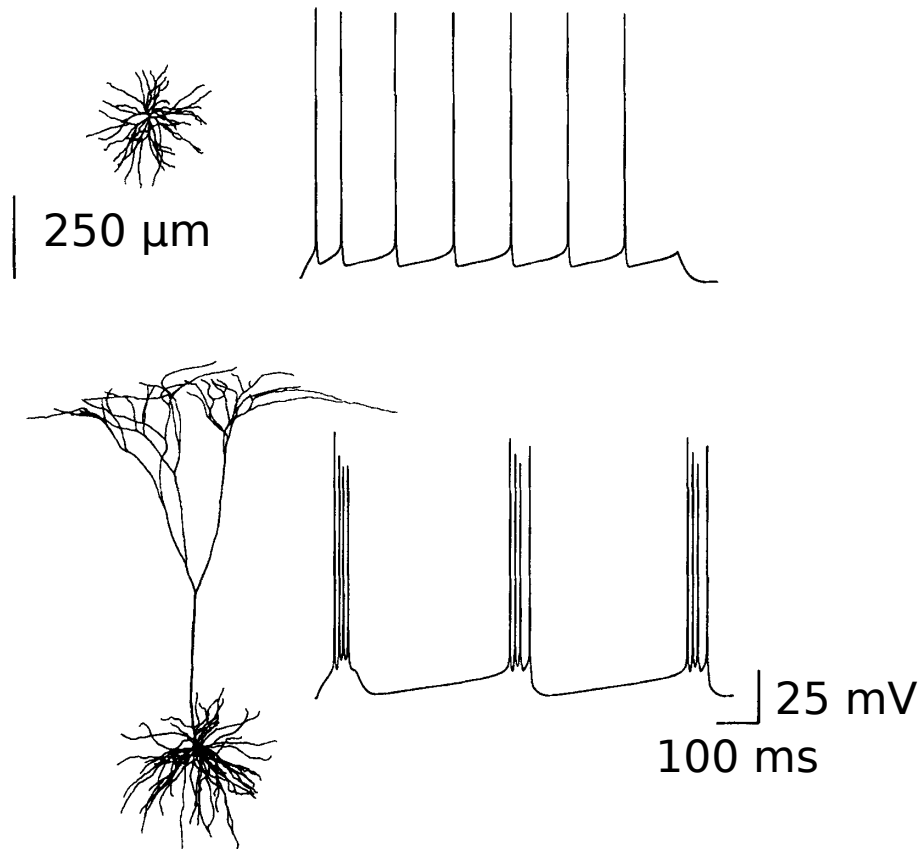


Figure 2.12: Two neurons with very different morphology but with the same channel compositions produce different firing patterns. Adapted from Mainen and Sejnowski (1996).

the healthy brain: First is the gamma wave (40–100 Hz), modulated by the slower theta wave (4–10 Hz) as recorded *in vivo* when the animal is awake (Fig 2.13 A). They are believed to be responsible for memory acquisition. Second, Sharp Wave-ripples (SPW-Rs) recorded during quiet immobility or during slow wave sleep are believed to be responsible for the consolidation of memory (Fig 2.13 A-B) (Buzsáki, 1996).

SPWs can be recorded *in vivo* and *in vitro* in the extracellular medium, and as input current to the recorded cell. These recordings are of 1–3 Hz with 100–200 Hz ripple oscillation imposed on the them.

It is still unclear how synchrony between multiple cells is achieved so quickly - when synaptic connections are blocked and much faster than synaptic activity would allow (Draguhn et al., 1998). Some studies conclude that this can be due to the electrical coupling through gap junctions (Traub et al., 2002) while others show the importance of excitatory (Maier et al., 2011) or inhibitory (Ho et al., 2009) recurrent circuits.

In Chapter 5, we will discuss an important milestone in understanding the mechanism

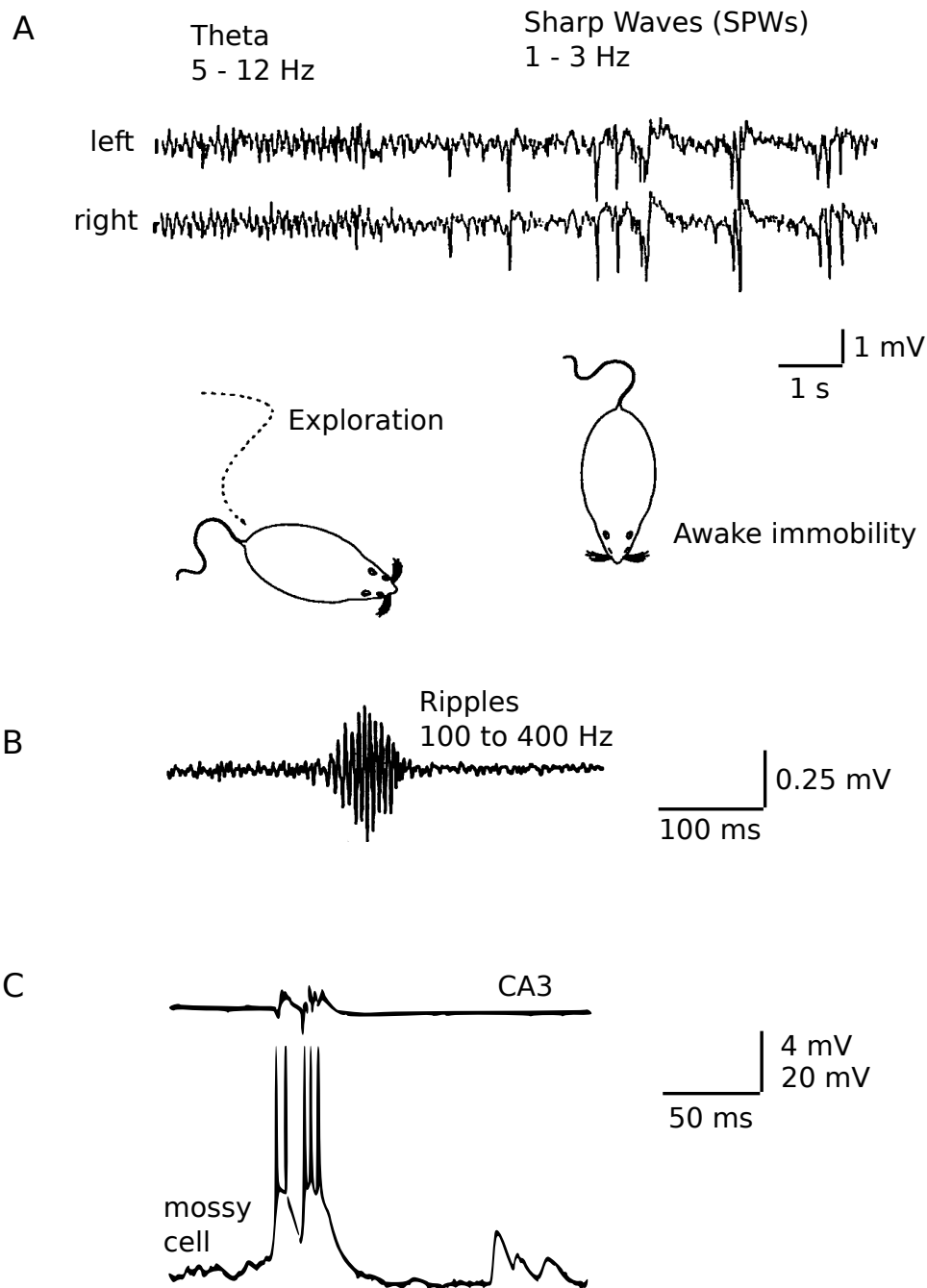


Figure 2.13: **Normal and pathological oscillations recorded in the hippocampus.** **A.** Recording of the hippocampus activity from the rat while it is exploring (left) shows theta activity. As soon as the rat changes its behaviour to awake immobility the field recordings follow to show slower but of higher amplitude Sharp Waves (adapted from Buzsáki (1996)). **B.** Sharp waves filtered to 100-400 Hz show very fast oscillatory pattern called 'ripples' (adapted from Buzsáki et al. (1992)). **C.** Epileptic discharges recorded from the CA3 area of the hippocampus (note the difference in scale from A and B) and simultaneous recording from mossy cell showing burst firing (Scharfman et al., 2001)

of the SPW-Rs, namely, that they can be triggered by the single action potential of a single pyramidal cell. It takes less than 5 ms (time needed for the synaptic transmission) after firing of the stimulated cell before the SPW-R is recorded extracellularly. In some cases only single inhibitory postsynaptic potential is generated as a response, whereas in others, the whole SPW-R can be recorded by multiple electrodes. Why this is the case, remains unclear.

Chandelier cells are an interesting type cells in the hippocampus. These inhibitory cells are normally silent, they fire more frequently if the overall cortical activity increases to suppress excessive excitation (Zhu et al., 2004). Between Sharp Waves the activity of the hippocampus is rather low and the decreased activity of chandelier cells could contribute to the generation of Sharp Waves (Klausberger et al., 2003; Viney et al., 2013).

## 2.9 Malfunction of action potential

What does it mean that an action potential has malfunctioned? Firstly, an action potential may not be generated at all in the condition when it should have been generated. This is the case in inhibitory neurons during epileptic seizures, which fail to generate enough action potentials and hence fail to provide sufficient inhibition to the network. But otherwise, these action potentials which are indeed generated appear normal in their shape and propagation.

Next, the sodium or potassium channels, which are crucial for the generation and functionality of action potentials may fail to function correctly. Indeed, ion channels are prone to genetic changes or over/sub-expression. This may also lead to different diseases, for example epilepsy (Nav1.1, Nav1.5, Kv8, Kv12) or episodic ataxia syndrome (Kv1),

A seemingly normal generation of action potentials is also recorded in the Charcot-Marie-Tooth disease, however they fail to propagate properly throughout the cell to reach synaptic connections.

Finally, it is the dysfunction of the brain itself (such as a stroke) which might alter the normal generation of action potentials.

### 2.9.1 Epilepsy

The hippocampus is a brain area prone to epilepsy. One of the factors might be the synchrony between excitatory cells, which can be easily achieved owing to the recurrent excitation found in this area (as described in details in Appendix A). Although both physiological sharp wave ripples and pathological epileptic discharges can be recorded

consequently in the same slices in vitro (Fig 2.13 C, note the difference in scale from A and B), the networks generating these events are very different. The overall firing rate is much higher in the epileptiform events while some of the inhibitory cells have completely stop firing (Karlocai et al., 2014).

Epilepsy is a disease with many subtypes which can be caused by different internal malfunction of sodium channels (Gastaldi et al., 1998; Meisler et al., 2010; Ogiwara et al., 2007; Papale et al., 2009; Whitaker et al., 2001b) or potassium channels (Villa and Combi, 2016) or even external states (e.g. head injuries) (Berkovic et al., 2006; Garga and Lowenstein, 2006). It is also surprisingly common, affecting up to 1% of the population (Bell and Sander, 2001).

Although, our understanding of the epilepsies has largely increased in recent years, we still lack the full picture of the ongoing processes and an understanding of the triggering conditions. Interestingly, some patients report that they can anticipate upcoming seizures, leading to the conclusion that in some types of epilepsy there might be an ongoing process and not a single triggering event (Schulze-Bonhage et al., 2006). But whatever the underlying cause is, it leads to excitatory cells producing an excessive number of action potentials, while some of the inhibitory cells stop firing, leading to lack of sufficient inhibition.

## 2.9.2 Stroke

Action potential (AP) generation might be altered after brain damage such as in stroke. A stroke causes a rapid and irreversible shortening of the cytoskeleton in the axon initial segment (AIS) in some neurons, which mostly leads to decreased expression of  $\text{Na}_v1.6$  channels, while it lengthens the AIS of other neurons, which exhibited initially short and immature AIS. This in turn, affects neuronal excitability (Hinman et al., 2012; Schafer et al., 2009). Hypothetically, damage to the AIS might increase the threshold for AP generation, suppress both AP backpropagation and spike timing-dependent plasticity (Stoler and Fleidervish, 2016). This in turn, could possibly explain the circuit dysfunction and neurological deficits in stroke and could potentially lead to other nervous system diseases (Leterrier, 2015).

## 2.9.3 Alzheimer's disease

Alzheimer's disease is common among the elderly and it leads to cognitive decline. Mutations in amyloid precursor protein are associated with Alzheimer disease. These changes cause increased expression of the  $\text{Na}_v1.6$  channels at the cell surface (Liu et al., 2015) and decreased expression of  $\text{Na}_v1.1$  channels in the parvalbumin cells (Verret et al., 2012),

leading to the dysfunction of the spiking activity of inhibitory cells, and possibly increasing synchrony between excitatory cells (Palop and Mucke, 2010).

### 2.9.4 Other Disease

There are multiple other known diseases which lead to the dysfunction of action potentials. One example is multiple sclerosis, where abnormal expression of ionic  $\text{Na}_v1.2$  or  $\text{Na}_v1.6$  channels leads to an aberrant action potential generation and propagation. In this disease, myelin degenerates, causing an impaired conduction of action potentials (Waxman, 2006).

Charcot-Marie-Tooth is an inherited disease which also causes decreased myelination. Action potentials cannot propagate efficiently, which in turn causes degeneration of the peripheral nerves (Suter and Scherer, 2003).

Finally, multiple diseases called collectively named “channelopathies” (e.g. episodic ataxia) are caused by the dysfunction of one of more ion channels and often lead to the malfunction of action potential (Kullmann, 2002).

---

## Bibliography

---

- Alle, H., Roth, A., and Geiger, J. R. P. (2009). Energy-Efficient Action Potentials in Hippocampal Mossy Fibers. *Science*, 49(September):1405–1408.
- Ames, A., Maynard, K. I., and Kaplan, S. (1995). Protection against CNS ischemia by temporary interruption of function-related processes of neurons. *Journal of cerebral blood flow and metabolism : official journal of the International Society of Cerebral Blood Flow and Metabolism*, 15(3):433–439.
- Angelino, E. and Brenner, M. P. (2007). Excitability Constraints on Voltage Gated Sodium Channels. *PLoS Computational Biology*, 3(9):1751–1760.
- Archer, S. L., Souil, E., Dinh-Xuan, a. T., Schremmer, B., Mercier, J. C., El Yaagoubi, a., Nguyen-Huu, L., Reeve, H. L., and Hampl, V. (1998). Molecular identification of the role of voltage-gated K<sup>+</sup> channels, Kv1.5 and Kv2.1, in hypoxic pulmonary vasoconstriction and control of resting membrane potential in rat pulmonary artery myocytes. *The Journal of clinical investigation*, 101(11):2319–2330.
- Astman, N., Gutnick, M. J., and Fleidervish, I. A. (2006). Persistent Sodium Current in Layer 5 Neocortical Neurons Is Primarily Generated in the Proximal Axon. *The Journal of Neuroscience*, 26(13):3465–3473.
- Atalar, F., Acuner, T. T., Cine, N., Oncu, F., Yesilbursa, D., Ozbek, U., and Turkcan, S. (2010). Two four-marker haplotypes on 7q36.1 region indicate that the potassium channel gene HERG1 (KCNH2, Kv11.1) is related to schizophrenia: a case control study. *Behavioral and brain functions*, 6:27.
- Atherton, J. F., Wokosin, D. L., Ramanathan, S., and Bevan, M. D. (2008). Autonomous initiation and propagation of action potentials in neurons of the subthalamic nucleus. *The Journal of physiology*, 586(Pt 23):5679–700.
- Attwell, D. and Iadecola, C. (2002). The neural basis of functional brain imaging signals. *Trends in Neurosciences*, 25(12):621–625.
- Attwell, D. and Laughlin, S. B. (2001). An energy budget for signaling in the grey matter of the brain. *Journal of cerebral blood flow and metabolism*, 21(10):1133–1145.

- Baranauskas, G., David, Y., and Fleidervish, I. A. (2013). Spatial mismatch between the Na<sup>+</sup> flux and spike initiation in axon initial segment. *Proceedings of the National Academy of Sciences*, 110(10):4051–6.
- Baranauskas, G., Mukovskiy, A., Wolf, F., and Volgushev, M. (2010). The determinants of the onset dynamics of action potentials in a computational model. *Neuroscience*, 167(4):1070–1090.
- Barr, R. C. and Plonsey, R. (1992). Electrophysiological interaction through the interstitial space between adjacent unmyelinated parallel fibers. *Biophysical journal*, 61(5):1164–1175.
- Barry, J., Gu, Y., Jukkola, P., O’Neill, B., Gu, H., Mohler, P., Rajamani, K. T., and Gu, C. (2014). Ankyrin-G Directly Binds to Kinesin-1 to Transport Voltage-Gated Na<sup>+</sup> Channels into Axons. *Developmental Cell*, 28(2):117–131.
- Barthó, P., Hirase, H., Monconduit, L., Zugaro, M., Harris, K. D., and Buzsáki, G. (2004). Characterization of neocortical principal cells and interneurons by network interactions and extracellular features. *Journal of Neurophysiology*, 92(1):600–608.
- Bazelot, M., Dinocourt, C., Cohen, I., and Miles, R. (2010). Unitary inhibitory field potentials in the CA3 region of rat hippocampus. *The Journal of physiology*, 588(Pt 12):2077–90.
- Bazelot, M., Teleńczuk, M. T., and Miles, R. (2016). Single CA3 pyramidal cells trigger sharp waves in vitro by exciting interneurons. *Journal of Physiology*, 0:1–13.
- Bean, B. P. (2007). The action potential in mammalian central neurons. *Nature reviews Neuroscience*, 8(6):451–65.
- Beckh, S., Noda, M., Lübbert, H., and Numa, S. (1989). Differential regulation of three sodium channel messenger RNAs in the rat central nervous system during development. *The EMBO journal*, 8(12):3611–6.
- Bell, G. S. and Sander, J. W. (2001). CPD - Education and self-assessment. The epidemiology of epilepsy: The size of the problem. *Seizure*, 10(4):306–316.
- Bender, K. J. and Trussell, L. O. (2009). Axon Initial Segment Ca<sup>2+</sup> Channels Influence Action Potential Generation and Timing. *Neuron*, 61(2):259–271.
- Berbel, P. and Innocenti, G. (1988). The Development of the Corpus Callosum in Cats: A Light- and Electron-Microscopic Study. *The Journal of comparative neurology*, 27699:132–156.
- Berkovic, S. F., Mulley, J. C., Scheffer, I. E., and Petrou, S. (2006). Human epilepsies: interaction of genetic and acquired factors. *Trends in Neurosciences*, 29(7):391–397.
- Bocksteins, E. (2016). Kv5, Kv6, Kv8, and Kv9 subunits: No simple silent bystanders. *The Journal of General Physiology*, 147(2):105–125.
- Boiko, T., Rasband, M. N., Levinson, S. R., Caldwell, J. H., Mandel, G., Trimmer, J. S., and Matthews, G. (2001). Compact myelin dictates the differential targeting of two sodium channel isoforms in the same axon. *Neuron*, 30(1):91–104.

- Boiko, T., Wart, A. V., Caldwell, J. H., Levinson, S. R., Trimmer, J. S., and Matthews, G. (2003). Functional Specialization of the Axon Initial Segment by Isoform-Specific Sodium Channel Targeting. *The Journal of Neuroscience*, 23(6):2306–2313.
- Bonifazi, P., Goldin, M., Picardo, M. A., Jorquera, I., Cattani, A., Bianconi, G., Represa, A., Ben-Ari, Y., and Cossart, R. (2009). GABAergic hub neurons orchestrate synchrony in developing hippocampal networks. *Science*, 326(5958):1419–1424.
- Brecht, M., Schneider, M., Sakmann, B., and Margrie, T. W. (2004). Whisker movements evoked by stimulation of single pyramidal cells in rat motor cortex. *Nature*, 427(6976):704–710.
- Brette, R. (2013). Sharpness of Spike Initiation in Neurons Explained by Compartmentalization. *PLoS Computational Biology*, 9(12):e1003338.
- Brette, R. (2015). What Is the Most Realistic Single-Compartment Model of Spike Initiation? *PLoS Computational Biology*, 11(4):1–13.
- Brown, D. A. and Adams, P. R. (1980). Muscarinic suppression of a novel voltage-sensitive K<sup>+</sup> current in a vertebrate neurone. *Nature*, 283(5748):673–676.
- Browne, D. L., Gancher, S. T., Nutt, J. G., Brunt, E. R. P., Smith, E. A., Kramer, P., and Litt, M. (1994). Episodic ataxia/myokymia syndrome is associated with point mutations in the human potassium channel gene, KCNA1. *Nature genetics*, 8(2):136–40.
- Buffington, S. A. and Rasband, M. N. (2011). The axon initial segment in nervous system disease and injury. *European Journal of Neuroscience*, 34(10):1609–1619.
- Buzsáki, G. (1996). The Hippocampo-Neocortical Dialogue. *Cerebral Cortex*, 6:81–92.
- Buzsáki, G., Anastassiou, C. a., and Koch, C. (2012). The origin of extracellular fields and currents—EEG, ECoG, LFP and spikes. *Nature reviews. Neuroscience*, 13(6):407–20.
- Buzsáki, G., Horváth, Z., Urioste, R., Hetke, J., and Wise, K. (1992). High-frequency network oscillation in the hippocampus. *Science*, 256(5059):1025.
- Carter, B. C. and Bean, B. P. (2009). Sodium Entry during Action Potentials of Mammalian Neurons: Incomplete Inactivation and Reduced Metabolic Efficiency in Fast-Spiking Neurons. *Neuron*, 64(6):898–909.
- Catterall, W. A. (1980). Neurotoxins taht act on voltage-sensitive sodium channels in excitable membranes. *Annual Review of Pharamacology and Toxicology*, 20:15–43.
- Catterall, W. A. (1981). Localization of sodium channels in cultured neural cells. *The Journal of neuroscience*, 1(7):777–83.
- Catterall, W. A. (2000). From Ionic Currents to Molecular Mechanisms: The Structure and Function of Voltage-Gated Sodium Channels. *Neuron*, 26(1):13–25.
- Catterall, W. A., Goldin, A. L., and Waxman, S. G. (2005a). International Union of Pharmacology. XLVII. Nomenclature and structure-function relationships of voltage-gated sodium channels. *Pharmacological reviews*, 57(4):397–409.

- Catterall, W. A., Perez-Reyes, E., Snutch, T. P., and Striessnig, J. (2005b). International Union of Pharmacology. XLVIII. Nomenclature and structure-function relationships of voltage-gated calcium channels. *Pharmacological Reviews*, 57(4):411–425.
- Chan, C. S., Shigemoto, R., Mercer, J. N., and Surmeier, D. J. (2004). HCN2 and HCN1 Channels Govern the Regularity of Autonomous Pacemaking and Synaptic Resetting in Globus Pallidus Neurons. *The Journal of Neuroscience*, 24(44):9921–9932.
- Chand, A. N., Galliano, E., Chesters, R. A., and Grubb, M. S. (2015). A Distinct Subtype of Dopaminergic Interneuron Displays Inverted Structural Plasticity at the Axon Initial Segment. *Journal of Neuroscience*, 35(4):1573–1590.
- Clancy, S. M., Chen, B., Bertaso, F., Mamet, J., and Jegla, T. (2009). KCNE1 and KCNE3  $\gamma$ -subunits regulate membrane surface expression of Kv12.2 K<sup>+</sup> channels in vitro and form a tripartite complex in vivo. *PLoS ONE*, 4(7):19–23.
- Clark, B. A., Monsivais, P., Branco, T., London, M., and Häusser, M. (2005). The site of action potential initiation in cerebellar Purkinje neurons. *Nat Neurosci*, 8(2):137–139.
- Clark, B. D., Goldberg, E. M., and Rudy, B. (2009). Electrogenic tuning of the axon initial segment. *The Neuroscientist*, 15(6):651–68.
- Colbert, C. M. and Johnston, D. (1996). Axonal Action-Potential Initiation and Na<sup>+</sup> Channel Densities in the Soma and Axon Initial Segment of Subicular Pyramidal Neurons. *The Journal of Neuroscience*, 16(21):6676–6686.
- Colbert, C. M. and Pan, E. (2002). Ion channel properties underlying axonal action potential initiation in pyramidal neurons. *Nature neuroscience*, 5(6):533–538.
- Connors, B. W. and Gutnick, M. J. (1990). Intrinsic firing patterns of diverse neocortical neurons. *Trends in Neurosciences*, 13(3):99–104.
- Constantinople, C. M., Disney, A. A., Maffie, J., Rudy, B., and Hawken, M. J. (2009). Quantitative analysis of neurons with Kv3 potassium channel subunits, Kv3.1b and Kv3.2 in macaque primary visual cortex. *Journal of Comparative Neurology*, 516(4):291–311.
- Coombs, J. S., Curtis, D. R., and Eccles, J. C. (1957). The interpretation of spike potentials of motoneurons. *The Journal of physiology*, 139(2):198–231.
- Cooper, E. C. (2011). Made for "anchorin" Kv7.2/7.3 (KCNQ2/KCNQ3) channels and the modulation of neuronal excitability in vertebrate axons. *Seminars in Cell and Developmental Biology*, 22(2):185–192.
- Cooper, E. C., Milroy, A., Jan, Y. N., Jan, L. Y., and Lowenstein, D. H. (1998). Presynaptic localization of Kv1.4-containing A-type potassium channels near excitatory synapses in the hippocampus. *The Journal of neuroscience*, 18(3):965–974.
- Crill, W. E. (1996). Persistent sodium current in mammalian central neurons. *Annual review of physiology*, 58(31):349–362.

- Cruz, J. S., Silva, D. F., Ribeiro, L. A., Araújo, I. G. A., Magalhães, N., Medeiros, A., Freitas, C., Araujo, I. C., and Oliveira, F. A. (2011). Resurgent Na<sup>+</sup> current: A new avenue to neuronal excitability control. *Life Sciences*, 89(15-16):564–569.
- Cui, Y., Liu, L. D., McFarland, J. M., Pack, C. C., and Butts, D. A. (2016). Inferring Cortical Variability from Local Field Potentials. *The Journal of Neuroscience*, 36(14):4121–4135.
- Dayan, P. and Abbott, L. F. (2001). *Theoretical neuroscience*, volume 806. Cambridge, MA: MIT Press.
- Debanne, D., Campanac, E., Bialowas, A., Carlier, E., and Alcaraz, G. (2011). Axon physiology. *Physiological Reviews*, 91(2):555–602.
- Debanne, D., Guérineau, N. C., Gähwiler, B. H., and Thompson, S. M. (1997). Action-potential propagation gated by an axonal I(A)-like K<sup>+</sup> conductance in hippocampus. *Nature*, 389(6648):286–289.
- Dekker, J. P. and Yellen, G. (2006). Cooperative gating between single HCN pacemaker channels. *The Journal of general physiology*, 128(5):561–7.
- Destexhe, A., Contreras, D., and Steriade, M. (1999). Spatiotemporal Analysis of Local Field Potentials and Unit Discharges in Cat Cerebral Cortex during Natural Wake and Sleep States. *The Journal of Neuroscience*, 19(11):4595–4608.
- Devaux, J., Alcaraz, G., Grinspan, J., Bennett, V., Joho, R., Crest, M., and Scherer, S. S. (2003). Kv3.1b is a novel component of CNS nodes. *The Journal of neuroscience*, 23(11):4509–4518.
- Devaux, J. J., Kleopa, K. A., Cooper, E. C., and Scherer, S. S. (2004). KCNQ2 Is a Nodal K<sup>+</sup> Channel. *The Journal of Neuroscience*, 24(5):1236–1244.
- Dixon, R. E., Yuan, C., Cheng, E. P., Navedo, M. F., and Santana, L. F. (2012). Ca<sup>2+</sup> signaling amplification by oligomerization of L-type Cav1.2 channels. *PNAS*, 109(5):1749–1754.
- Do, M. T. H. and Bean, B. P. (2003). Subthreshold sodium currents and pacemaking of subthalamic neurons: Modulation by slow inactivation. *Neuron*, 39(1):109–120.
- Donahue, L. M., Coates, P. W., Lee, V. H., Ippensen, D. C., Arze, S. E., and Poduslo, S. E. (2000). The cardiac sodium channel mRNA is expressed in the developing and adult rat and human brain. *Brain research*, 887(2):335–343.
- Draguhn, A., Traub, R. D., Schmitz, D., and Jefferys, J. G. (1998). Electrical coupling underlies high-frequency oscillations in the hippocampus in vitro. *Nature*, 394(6689):189–92.
- Du, J., Tao-Cheng, J. H., Zerfas, P., and McBain, C. J. (1998). The K<sup>+</sup> channel, Kv2.1, is apposed to astrocytic processes and is associated with inhibitory postsynaptic membranes in hippocampal and cortical principal neurons and inhibitory interneurons. *Neuroscience*, 84(1):37–48.
- Einevoll, G. T., Kayser, C., Logothetis, N. K., and Panzeri, S. (2013). Modelling and analysis of local field potentials for studying the function of cortical circuits. *Nature Reviews Neuroscience*, 14(11):770–785.
- Elliott, A. A. and Elliott, J. R. (1993). Characterization of TTX-sensitive and TTX-resistant sodium currents in small cells from adult rat dorsal root ganglia. *Journal of Physiology*, 1350:39–56.

- Engeland, B., Neu, A., Ludwig, J., Roeper, J., and Pongs, O. (1998). Cloning and functional expression of rat ether-a-go-go-like K<sup>+</sup> channel genes. *Journal of Physiology*, 513(3):647–654.
- Epsztein, J., Lee, A. K., Chorev, E., and Brecht, M. (2010). Impact of Spikelets on Hippocampal. *Science*, 327(January):474–477.
- Evans, M. D., Dumitrescu, A. S., Kruijssen, D. L. H., Taylor, S. E., and Grubb, M. S. (2015). Rapid Modulation of Axon Initial Segment Length Influences Repetitive Spike Firing. *Cell Reports*, 13(6):1233–1245.
- Evans, M. D., Sammons, R. P., Lebron, S., Dumitrescu, A. S., Watkins, T. B. K., Uebele, V., Renger, J. J., and Grubb, M. S. (2013). Calcineurin signaling mediates activity-dependent relocation of the axon initial segment. *The Journal of Neuroscience*, 33(16):6950–6963.
- Faber, E. S. L. and Sah, P. (2002). Physiological role of calcium-activated potassium currents in the rat lateral amygdala. *The Journal of neuroscience*, 22(5):1618–1628.
- Farias, L. M. B., Ocana, D. B., Diaz, L., Larrea, F., Avila-Chavez, E., Cadena, A., Hinojosa, L. M., Lara, Gerardo and Villanueva, L. A., Vargas, C., Hernandez-Gallegos, E., Camacho-Arroyo, I., Duenas-Gonzalez, A., Perez-Cardenas, E., Pardo, L. A., Moreles, A., Taja-Chayeb, L., Escamilla, J., Sanchez-Pena, C., and Camacho, J. (2004). Ether a go-go Potassium Channels as Human Cervical Cancer Markers. *Cancer Research*, 64(19):6996–7001.
- Fatt, P. and Ginsborg, B. (1958). The ionic requirements for the initiation of action potentials in insect muscle fibers. *The Journal of Physiology*, 142:516–543.
- Fish, K. N., Hoftman, G. D., Sheikh, W., Kitchens, M., and Lewis, D. A. (2013). Parvalbumin-containing chandelier and basket cell boutons have distinctive modes of maturation in monkey prefrontal cortex. *The Journal of Neuroscience*, 33(19):8352–8358.
- Fleidervish, I. a., Lasser-Ross, N., Gutnick, M. J., and Ross, W. N. (2010). Na<sup>+</sup> imaging reveals little difference in action potential-evoked Na<sup>+</sup> influx between axon and soma. *Nature neuroscience*, 13(7):852–860.
- Fohlmeister, J. F. (2009). A nerve model of greatly increased energy-efficiency and encoding flexibility over the Hodgkin-Huxley model. *Brain Research*, 1296:225–233.
- Fourcaud-trocme, N., Hansel, D., Vreeswijk, C. V., and Brunel, N. (2003). How Spike Generation Mechanisms Determine the Neuronal Response to Fluctuating Inputs. *The Journal of Neuroscience*, 23(37):11628–11640.
- Foust, A., Popovic, M., Zecevic, D., and McCormick, D. A. (2010). Action Potentials Initiated In the Axon Initial Segment and Propagate through Axon Collaterals Reliably in Cerebellar Purkinje Neurons. *The Journal of Neuroscience*, 30(20):6891–6902.
- Fried, S. I., Lasker, A. C. W., Desai, N. J., Eddington, D. K., and Rizzo, J. F. (2009). Axonal sodium-channel bands shape the response to electric stimulation in retinal ganglion cells. *Journal of neurophysiology*, 101:1972–1987.

- Garga, N. and Lowenstein, D. H. (2006). Posttraumatic Epilepsy: A Major Problem in Desperate Need of Major Advances. *Epilepsy Currents*, 6(1):1–5.
- Garrido, J. J., Giraud, P., Carlier, E., Fernandes, F., Moussif, A., Fache, M.-p., Debanne, D., and Dargent, B. (2015). A Targeting Motif Involved in Sodium Channel Clustering at the Axonal Initial Segment. *Science*, 300(5628):2091–2094.
- Gastaldi, M., Robaglia-Schlupp, A., Massacrier, A., Planells, R., and Cau, P. (1998). mRNA coding for voltage-gated sodium channel beta2 subunit in rat central nervous system: cellular distribution and changes following kainate-induced seizures. *Neuroscience letters*, 249(1):53–6.
- Geiger, J. R. P. and Jonas, P. (2000). Dynamic control of presynaptic Ca<sup>2+</sup> inflow by fast-inactivating K<sup>+</sup> channels in hippocampal mossy fiber boutons. *Neuron*, 28(3):927–939.
- Glickfeld, L. L., Roberts, David, J., Somogyi, P., and Scanziani, M. (2009). Interneurons hyperpolarize pyramidal cells along their entire somatodendritic axis. *Nature Neuroscience*, 12(1):21–23.
- Goldin, A. L., Barchi, R. L., Caldwell, J. H., Hofmann, F., Howe, J. R., Hunter, J. C., Kallen, R. G., Mandel, G., Meisler, M. H., Netter, Y. B., Noda, M., Tamkun, M. M., Waxman, S. G., Wood, J. N., and Catterall, W. A. (2000). Nomenclature of Voltage-Gated Sodium Channels. *Neuron*, 28:365–368.
- Golding, N. L. and Spruston, N. (1998). Dendritic sodium spikes are variable triggers of axonal action potentials in hippocampal CA1 pyramidal neurons. *Neuron*, 21(5):1189–1200.
- Goldstein, S. S. and Rall, W. (1974). Changes of action potential shape and velocity for changing core conductor geometry. *Biophysical journal*, 14(10):731–757.
- Gomis-Rüth, S., Wierenga, C. J., and Bradke, F. (2008). Plasticity of Polarization: Changing Dendrites into Axons in Neurons Integrated in Neuronal Circuits. *Current Biology*, 18(13):992–1000.
- Gong, B., Rhodes, K. J., Bekele-Arcuri, Z., and Trimmer, J. S. (1999). Type I and type II Na(+) channel alpha-subunit polypeptides exhibit distinct spatial and temporal patterning, and association with auxiliary subunits in rat brain. *The Journal of comparative neurology*, 412(2):342–352.
- Grubb, M. S. and Burrone, J. (2010). Activity-dependent relocation of the axon initial segment fine-tunes neuronal excitability. *Nature*, 465(7301):1070–4.
- Gulledge, A. T. and Bravo, J. J. (2016). Neuron morphology influences axon initial segment plasticity. *eNeuro*, 10.1523/EN.
- Gulyas, A. I., Miles, R., Hajos, N., and Freund, T. F. (1993). Precision and variability in postsynaptic target selection of inhibitory cells in the hippocampal CA3 region. *European Journal of Neuroscience*, 5(12):1729–1751.
- Gutman, G. A., Chandy, K. G., Grissmer, S., Lazdunski, M., McKinnon, D., Pardo, L. A., Robertson, G. A., Rudy, B., Sanguinetti, M. C., Stühmer, W., and Wang, X. (2005). International Union of Pharmacology. LIII. Nomenclature and molecular relationships of voltage-gated potassium channels. *Pharmacological reviews*, 57(4):473–508.

- Haider, B., Schulz, D. P. A., Häusser, M., and Carandini, M. (2015). Millisecond Coupling of Local Field Potentials to Synaptic Currents in the Awake Visual Cortex. *Neuron*, pages 35–42.
- Hallermann, S., de Kock, C. P. J., Stuart, G. J., and Kole, M. H. P. (2012). State and location dependence of action potential metabolic cost in cortical pyramidal neurons. *Nature neuroscience*, 15(7):1007–1014.
- Hartmann, H. A., Colom, L. V., Sutherland, M. L., and Noebels, J. L. (1999). Selective localization of cardiac SCN5A sodium channels in limbic regions of rat brain. *Nature neuroscience*, 2(7):593–595.
- Helmchen, F., Svoboda, K., Denk, W., and Tank, D. W. (1999). In vivo dendritic calcium dynamics in deep-layer neocortical pyramidal neurons. *Nature*, 2:989–996.
- Henze, D. A., Borhegyi, Z., Csicsvari, J., Mamiya, A., Harris, K. D., and Buzsáki, G. (2000). Intracellular features predicted by extracellular recordings in the hippocampus in vivo. *Journal of neurophysiology*, 84(1):390–400.
- Herculano-Houzel, S. (2009). The human brain in numbers: a linearly scaled-up primate brain. *Frontiers in human neuroscience*, 3(November):31.
- Hille, B. et al. (2001). *Ion channels of excitable membranes*, volume 507. Sinauer Sunderland, MA.
- Hinman, J. D., Rasband, M. N., and Carmichael, S. T. (2012). Remodeling of the axon initial segment after focal cortical and white matter stroke. *Stroke*, 44(1):182–189.
- Hiyama, T. Y., Watanabe, E., Ono, K., Inenaga, K., Tamkun, M. M., Yoshida, S., and Noda, M. (2002). Na<sub>x</sub> channel involved in CNS sodium-level sensing. *Nature neuroscience*, 5(6):511–512.
- Ho, E. C. Y., Zhang, L., and Skinner, F. K. (2009). Inhibition dominates in shaping spontaneous CA3 hippocampal network activities in vitro. *Hippocampus*, 19(2):152–165.
- Hodgkin, A. L. and Huxley, A. F. (1939). Action Potentials Recorded from Inside a Nerve Fibre. *Nature*, 144(3651):710–711.
- Hodgkin, A. L. and Huxley, A. F. (1952). A quantitative description of membrane current and its application to conduction and excitation in nerve. *Journal of Physiology*, 117:500–544.
- Houweling, A. R. and Brecht, M. (2008). Behavioural report of single neuron stimulation in somatosensory cortex. *Nature*, 451(7174):65–8.
- Howard, A., Tamas, G., and Soltesz, I. (2005). Lighting the chandelier: New vistas for axo-axonic cells. *Trends in Neurosciences*, 28(6 SPEC. ISS.):310–316.
- Howarth, C., Gleeson, P., and Attwell, D. (2012). Updated energy budgets for neural computation in the neocortex and cerebellum. *Journal of cerebral blood flow and metabolism*, 32(7):1222–32.
- Hu, W., Tian, C., Li, T., Yang, M., Hou, H., and Shu, Y. (2009). Distinct contributions of Na(v)1.6 and Na(v)1.2 in action potential initiation and backpropagation. *Nature neuroscience*, 12(8):996–1002.

- Huang, J., Han, C., Estacion, M., Vasylyev, D., Hoeijmakers, J. G. J., Gerrits, M. M., Tyrrell, L., Lauria, G., Faber, C. G., Dib-Hajj, S. D., Merkies, I. S. J., and Waxman, S. G. (2014). Gain-of-function mutations in sodium channel NaV1.9 in painful neuropathy. *Brain*, 137(6):1627–1642.
- Huang, M., Volgushev, M., and Wolf, F. (2012). A small fraction of strongly cooperative sodium channels boosts neuronal encoding of high frequencies. *PLoS one*, 7(5):e37629.
- Hugnot, J.-P., Salinas, M., Lesage, F., Guillemare, E., de Weille, J., Heurteaux, C., Mattéi, M.-G., and Lazdunski, M. (1996). Kv8.1, a new neuronal potassium channel subunit with specific inhibitory properties towards Shab and Shaw channels. *The EMBO journal*, 15(13):3322–31.
- Ilin, V., Malyshev, A., Wolf, F., and Volgushev, M. (2013). Fast Computations in Cortical Ensembles Require Rapid Initiation of Action Potentials. *The Journal of Neuroscience*, 33(6):2281–2292.
- Inan, M. and Anderson, S. A. (2014). The chandelier cell, form and function. *Current Opinion in Neurobiology*, 26:142–148.
- Inda, M. C., DeFelipe, J., and Muñoz, A. (2006). Voltage-gated ion channels in the axon initial segment of human cortical pyramidal cells and their relationship with chandelier cells. *PNAS*, 103(8):2920–2925.
- Ishikawa, T., Nakamura, Y., Saitoh, N., Li, W.-B., Iwasaki, S., and Takahashi, T. (2003). Distinct roles of Kv1 and Kv3 potassium channels at the calyx of Held presynaptic terminal. *The Journal of neuroscience*, 23(32):10445–10453.
- Ishizuka, N., Cowan, W. M., and Amaral, D. G. (1995). A quantitative analysis of the dendritic organization of pyramidal cells in the rat hippocampus. *Journal of Comparative Neurology*, 362(1):17–45.
- Ishizuka, N., Weber, J., and Amaral, D. G. (1990). Organization of intrahippocampal projections originating from CA3 pyramidal cells in the rat. *Journal of Comparative Neurology*, 295(4):580–623.
- Jan, L. Y. and Jan, Y. N. (2012). Voltage-gated potassium channels and the diversity of electrical signalling. *The Journal of physiology*, 590(Pt 11):2591–9.
- Jeong, S.-Y., Goto, J., Hashida, H., Suzuki, T., Ogata, K., Masuda, N., Hirai, M., Isahara, K., Uchiyama, Y., and Kanazawa, I. (2000). Identification of a novel human voltage-gated sodium channel alpha subunit gene, SCN12A. *Biochemical and biophysical research communications*, 267(1):262–70.
- Jerng, H. H., Pfaffinger, P. J., and Covarrubias, M. (2004). Molecular physiology and modulation of somatodendritic A-type potassium channels. *Molecular and Cellular Neuroscience*, 27(4):343–369.
- Johnston, D., Wu, S. M.-S., and Gray, R. (1995). *Foundations of cellular neurophysiology*. Number 577.25 JOH. MIT press Cambridge, MA.
- Jorge, B. S., Campbell, C. M., Miller, A. R., Rutter, E. D., Gurnett, C. a., Vanoye, C. G., George, A. L., and Kearney, J. a. (2011). Voltage-gated potassium channel KCNV2 (Kv8.2) contributes to epilepsy susceptibility. *PNAS*, 108(13):5443–8.
- Kandel, E. R., Schwartz, J. H., Jessell, T. M., et al. (2000). *Principles of neural science*, volume 4. McGraw-hill New York.

- Kaplan, M. R., Cho, M. H., Ullian, E. M., Isom, L. L., Levinson, S. R., and Barres, B. A. (2001). Differential control of clustering of the sodium channels Nav1.2 and Nav1.6 at developing CNS nodes of Ranvier. *Neuron*, 30(1):105–119.
- Karlocai, M. R., Kohus, Z., Kali, S., Ulbert, I., Szabo, G., Mate, Z., Freund, T. F., and Gulyas, A. I. (2014). Physiological sharp wave-ripples and interictal events in vitro: What’s the difference? *Brain*, 137(2):463–485.
- Katz, B. Y. B. and Schmitt, O. H. (1940). Electric interaction between two adjacent nerve fibres. *Journal of Physiology*, 97:471–488.
- Katzner, S., Nauhaus, I., Benucci, A., Bonin, V., Ringach, D. L., and Carandini, M. (2009). Local Origin of Field Potentials in Visual Cortex. *Neuron*, 61(1):35–41.
- Kevenaar, J. T. and Hoogenraad, C. C. (2015). The axonal cytoskeleton: from organization to function. *Frontiers in molecular neuroscience*, 8(August):44.
- Khaliq, Z. M. and Raman, I. M. (2006). Relative Contributions of Axonal and Somatic Na Channels to Action Potential Initiation in Cerebellar Purkinje Neurons. *The Journal of Neuroscience*, 26(7):1935–1944.
- Khirug, S., Yamada, J., Afzalov, R., Voipio, J., Khiroug, L., and Kaila, K. (2008). GABAergic depolarization of the axon initial segment in cortical principal neurons is caused by the Na-K-2Cl cotransporter NKCC1. *The Journal of neuroscience*, 28(18):4635–4639.
- Kim, H. G. and Connors, B. W. (1993). Apical dendrites of the neocortex: correlation between sodium- and calcium-dependent spiking and pyramidal cell morphology. *The Journal of neuroscience*, 13(12):5301–5311.
- Klausberger, T., Magill, P. J., Márton, L. F., Roberts, J. D. B., Cobden, P. M., Buzsáki, G., and Somogyi, P. (2003). Brain-state- and cell-type-specific firing of hippocampal interneurons in vivo. *Nature*, 421(February):844–848.
- Kole, M. H. P., Ilshner, S. U., Kampa, B. M., Williams, S. R., Ruben, P. C., and Stuart, G. J. (2008). Action potential generation requires a high sodium channel density in the axon initial segment. *Nature neuroscience*, 11(2):178–86.
- Kole, M. H. P., Letzkus, J. J., and Stuart, G. J. (2007). Axon Initial Segment Kv1 Channels Control Axonal Action Potential Waveform and Synaptic Efficacy. *Neuron*, 55(4):633–647.
- Kole, M. H. P. and Stuart, G. J. (2012). Signal Processing in the Axon Initial Segment. *Neuron*, 73(2):235–247.
- Köndgen, H., Geisler, C., Fusi, S., Wang, X. J., Lüscher, H. R., and Giugliano, M. (2008). The dynamical response properties of neocortical neurons to temporally modulated noisy inputs in vitro. *Cerebral Cortex*, 18(9):2086–2097.
- Kosaka, T. (1980). The axon initial segment as a synaptic site: Ultrastructure and synaptology of the initial segment of the pyramidal cell in the rat hippocampus (CA3 region). *Journal of Neurocytology*, 9(6):861–882.

- Kuba, H., Ishii, T. M., and Ohmori, H. (2006). Axonal site of spike initiation enhances auditory coincidence detection. *Nature*, 444(7122):1069–1072.
- Kuijpers, M., vandeWillige, D., Freal, A., Chazeau, A., Franker, M., Hofenk, J., Rodrigues, R., Kapitein, L., Akhmanova, A., Jaarsma, D., and Hoogenraad, C. (2016). Dynein Regulator NDEL1 Controls Polarized Cargo Transport at the Axon Initial Segment. *Neuron*, 89(3):461–471.
- Kullmann, D. M. (2002). The neuronal channelopathies. *Brain*, 125(6):1177–1195.
- Lai, H. C. and Jan, L. Y. (2006). The distribution and targeting of neuronal voltage-gated ion channels. *Nature reviews. Neuroscience*, 7(7):548–562.
- Larkum, M. E. and Zhu, J. J. (2002). Signaling of layer 1 and whisker-evoked Ca<sup>2+</sup> and Na<sup>+</sup> action potentials in distal and terminal dendrites of rat neocortical pyramidal neurons in vitro and in vivo. *The Journal of neuroscience*, 22(16):6991–7005.
- Larkum, M. E., Zhu, J. J., and Sakmann, B. (2001). Dendritic mechanisms underlying the coupling of the dendritic with the axonal action potential initiation zone of adult rat layer 5 pyramidal neurons. *Journal of Physiology*, 533(2):447–466.
- Lennie, P. (2003). The Cost of Cortical Computation. *Current Biology*, 13:493–497.
- Leterrier, C. (2015). *The Axon Initial Segment, 50Years Later: A Nexus forNeuronal Organization and Function*, volume 77. Elsevier Ltd.
- Leterrier, C. and Dargent, B. (2014). No Pasaran! Role of the axon initial segment in the regulation of protein transport and the maintenance of axonal identity. *Seminars in Cell and Developmental Biology*, 27:44–51.
- Li, C.-Y. T., Poo, M.-M., and Dan, Y. (2009). Burst spiking of a single cortical neuron modifies global brain state. *Science*, 324(5927):643–6.
- Li, X.-G., Somogyi, P., Ylinen, a., and Buzsaki, G. (1994). The hippocampal CA3 network: an in vivo intracellularly labeling study. *Journal of Comparative Neurology*, 339(2):181–208.
- Liu, C., Tan, F. C. K., Xiao, Z.-C., and Dawe, G. S. (2015). Amyloid precursor protein enhances Nav1.6 sodium channel cell surface expression. *The Journal of Biological Chemistry*, 290(19):12048–12057.
- Llinás, R. and Sugimori, M. (1980). Electrophysiological properties of in vitro Purkinje cell dendrites in mammalian cerebellar slices. *The Journal of physiology*, 305:197–213.
- London, M., Roth, A., Beeren, L., Häusser, M., and Latham, P. E. (2010). Sensitivity to perturbations in vivo implies high noise and suggests rate coding in cortex. *Nature*, 466(7302):123–7.
- Lorincz, A. and Nusser, Z. (2008). Cell-type-dependent molecular composition of the axon initial segment. *The Journal of neuroscience*, 28(53):14329–40.
- Lorincz, A. and Nusser, Z. (2010). Molecular Identity of Dendritic Voltage-Gated Sodium Channels. *Science*, 328(5980):906–909.

- Losonczy, A., Makara, J. K., and Magee, J. C. (2008). Compartmentalized dendritic plasticity and input feature storage in neurons. *Nature*, 452(7186):436–441.
- Lujan, R. (2010). Organisation of potassium channels on the neuronal surface. *Journal of Chemical Neuroanatomy*, 40(1):1–20.
- Lüthi, A. and McCormick, D. A. (1998). H-current: Properties of a neuronal and network pacemaker. *Neuron*, 21(1):9–12.
- Madeja, M. (2000). Do neurons have a reserve of sodium channels for the generation of action potentials? A study on acutely isolated CA1 neurons from the guinea-pig hippocampus. *European Journal of Neuroscience*, 12(1):1–7.
- Magee, J. C. (1998). Dendritic hyperpolarization-activated currents modify the integrative properties of hippocampal CA1 pyramidal neurons. *The Journal of neuroscience*, 18(19):7613–7624.
- Maier, N., Tejero-Cantero, Á., Dornn, A. L., Winterer, J., Beed, P. S., Morris, G., Kempter, R., Poulet, J. F. A., Leibold, C., and Schmitz, D. (2011). Coherent Phasic Excitation during Hippocampal Ripples. *Neuron*, 72(1):137–152.
- Mainen, Z. and Sejnowski, T. (1996). Influence of dendritic structure on firing pattern in model neocortical neurons.
- Mainen, Z. F., Joerges, J., Huguenard, J. R., and Sejnowski, T. J. (1995). A model of spike initiation in neocortical pyramidal neurons. *Neuron*, 15(6):1427–1439.
- Major, G., Larkman, A. U., Jonas, P., Sakmann, B., and Jack, J. J. (1994). Detailed passive cable models of whole-cell recorded CA3 pyramidal neurons in rat hippocampal slices. *The Journal of neuroscience*, 14(8):4613–4638.
- Marx, S. O., Ondrias, K., and Marks, A. R. (1998). Coupled gating between individual skeletal muscle Ca<sup>2+</sup> release channels (ryanodine receptors). *Science*, 281(5378):818–821.
- Massengill, J. L., Smith, M. A., Son, D. I., and O’Dowd, D. K. (1997). Differential Expression of K4-AP Currents and Kv3.1 Potassium Channel Transcripts in Cortical Neurons that Develop Distinct Firing Phenotypes. *The Journal of Neuroscience*, 17(9):3136–3147.
- Mathy, A., Ho, S. S. N., Davie, J. T., Duguid, I. C., Clark, B. A., and Häusser, M. (2009). Encoding of Oscillations by Axonal Bursts in Inferior Olive Neurons. *Neuron*, 62(3):388–399.
- McCormick, D. A., Connors, B. W., Lighthall, J. W., and Prince, D. a. (1985). Comparative electrophysiology of pyramidal and sparsely spiny stellate neurons of the neocortex. *Journal of neurophysiology*, 54(4):782–806.
- Meeks, J. P., Jiang, X., and Mennerick, S. (2005). Action potential fidelity during normal and epileptiform activity in paired soma-axon recordings from rat hippocampus. *The Journal of physiology*, 566(Pt 2):425–441.
- Meeks, J. P. and Mennerick, S. (2004). The selective effects of potassium elevation on glutamate signaling and action potential conduction in hippocampus. *The Journal of Neuroscience*, 24(1):197–206.

- Meeks, J. P. and Mennerick, S. (2007). Action potential initiation and propagation in CA3 pyramidal axons. *Journal of neurophysiology*, 97(5):3460–3472.
- Megias, M., Emri, Z., Freud, T., and Gulyás, A. I. (2001). Total number and distribution of inhibitory and excitatory synapses on hippocampal CA1 pyramidal cells. *Neuroscience*, 102(3):527–540.
- Meisler, M. H., O’Brien, J. E., and Sharkey, L. M. (2010). Sodium channel gene family: epilepsy mutations, gene interactions and modifier effects. *The Journal of physiology*, 588(Pt 11):1841–1848.
- Milojkovic, B. A., Wuskell, J. P., Loew, L. M., and Antic, S. D. (2005). Initiation of sodium spikelets in basal dendrites of neocortical pyramidal neurons. *Journal of Membrane Biology*, 208(2):155–169.
- Molina, M. L., Barrera, F. N., Fernandez, A. M., Poveda, J. A., Renart, M. L., Encinar, J. A., Riquelme, G., and Gonzalez-Ros, J. M. (2006). Clustering and coupled gating modulate the activity in KcsA, a potassium channel model. *Journal of Biological Chemistry*, 281(27):18837–18848.
- Moore, J. W., Stockbridge, N., and Westerfield, M. (1983). On the site of impulse initiation in a neurone. *The Journal of physiology*, 336:301–311.
- Morinville, A., Fundin, B., Meury, L., Jureus, A., Sandberg, K., Krupp, J., Ahmed, S., and O’Donnell, D. (2007). Distribution of the Voltage-Gated Sodium Channel Nav1.7 in the Rat: Expressed in the Autonomic and Endocrine Systems. *The Journal of comparative neurology*, 504(680-689):680–689.
- Muir, J. and Kittler, J. T. (2014). Plasticity of GABAA receptor diffusion dynamics at the axon initial segment. *Frontiers in cellular neuroscience*, 8(June):151.
- Murakoshi, H. and Trimmer, J. S. (1999). Identification of the Kv2.1 K<sup>+</sup> channel as a major component of the delayed rectifier K<sup>+</sup> current in rat hippocampal neurons. *The Journal of neuroscience*, 19(5):1728–35.
- Muth, T. R. and Caplan, M. J. (2003). Transport protein trafficking in polarized cells. *Annual review of cell and developmental biology*, 19(1):333–66.
- Naundorf, B., Wolf, F., and Volgushev, M. (2006). Unique features of action potential initiation in cortical neurons. *Nature*, 440(7087):1060–3.
- Naundorf, B., Wolf, F., and Volgushev, M. (2007). Neurophysiology: Hodgkin and Huxley model - still standing? *Nature*, 445(7123):E2–E3.
- Nowak, L. G., Azouz, R., Sanchez-Vivew, M. V., Gray, C. M., and McCormick, D. A. (2003). Electrophysiological Classes of Cat Primary Visual Cortical Neurons In Vivo as Revealed by Quantitative Analyses. *Journal of Neurophysiology*, 89(3):1541–1566.
- Nusser, Z. (2012). Differential subcellular distribution of ion channels and the diversity of neuronal function. *Current Opinion in Neurobiology*, 22(3):366–371.
- Ogiwara, I., Miyamoto, H., Morita, N., Atapour, N., Mazaki, E., Inoue, I., Takeuchi, T., Itoharu, S., Yanagawa, Y., Obata, K., Furuichi, T., Hensch, T. K., and Yamakawa, K. (2007). Nav1.1 Localizes to Axons of Parvalbumin-Positive Inhibitory Interneurons: A Circuit Basis for Epileptic Seizures in Mice Carrying an Scn1a Gene Mutation. *The Journal of Neuroscience*, 27(22):5903–5914.

- Ottshytsch, N., Raes, A., Van Hoorick, D., and Snyders, D. J. (2002). Obligatory heterotetramerization of three previously uncharacterized Kv channel alpha-subunits identified in the human genome. *PNAS*, 99(12):7986–7991.
- Öz, P., Huang, M., and Wolf, F. (2015). Action potential initiation in a multi-compartmental model with cooperatively gating Na channels in the axon initial segment. *Journal of Computational Neuroscience*, 39(1):63–75.
- Palmer, L. M., Clark, B. A., Gründemann, J., Roth, A., Stuart, G. J., and Häusser, M. (2010). Initiation of simple and complex spikes in cerebellar Purkinje cells. *The Journal of physiology*, 588(Pt 10):1709–17.
- Palmer, L. M. and Stuart, G. J. (2006). Site of action potential initiation in layer 5 pyramidal neurons. *The Journal of Neuroscience*, 26(6):1854–1863.
- Palop, J. J. and Mucke, L. (2010). Amyloid- $\beta$ -induced neuronal dysfunction in Alzheimer’s disease: from synapses toward neural networks. *Nature neuroscience*, 13(7):812–818.
- Pan, Z., Kao, T., Horvath, Z., Lemos, J., Sul, J.-Y., Cranstoun, S. D., Bennett, V., Scherer, S. S., and Cooper, E. C. (2006). A Common Ankyrin-G-Based Mechanism Retains KCNQ and NaV Channels at Electrically Active Domains of the Axon. *The Journal of Neuroscience*, 26(10):2599–2613.
- Papale, L. A., Beyer, B., Jones, J. M., Sharkey, L. M., Tufik, S., Epstein, M., Letts, V. A., Meisler, M. H., Frankel, W. N., and Escayg, A. (2009). Heterozygous mutations of the voltage-gated sodium channel SCN8A are associated with spike-wave discharges and absence epilepsy in mice. *Human Molecular Genetics*, 18(9):1633–1641.
- Post, M. A., Kirsch, G. E., and Brown, A. M. (1996). Kv2.1 and electrically silent Kv6.1 potassium channel subunits combine and express a novel current. *FEBS Letters*, 399(1-2):177–182.
- Puopolo, M., Raviola, E., and Bean, B. P. (2007). Roles of Subthreshold Calcium Current and Sodium Current in Spontaneous Firing of Mouse Midbrain Dopamine Neurons. *The Journal of Neuroscience*, 27(3):645–656.
- Raman, I. M. and Bean, B. P. (1997). Resurgent sodium current and action potential formation in dissociated cerebellar Purkinje neurons. *The Journal of Neuroscience*, 17(12):4517–4526.
- Raman, I. M., Sprunger, L. K., Meisler, M. H., and Bean, B. P. (1997). Altered subthreshold sodium currents and disrupted firing patterns in Purkinje neurons of Scn8a mutant mice. *Neuron*, 19(4):881–891.
- Ramon y Cajal, S. (1888). Revista trimestral de histología normal y patológica. *Revista trimestral de histología normal y patológica*, 2(May):33–41.
- Rapp, M., Yarom, Y., and Segev, I. (1996). Modeling back propagating action potential in weakly excitable dendrites of neocortical pyramidal cells. *PNAS*, 93(21):11985–11990.
- Rasband, M. N. (2010). The axon initial segment and the maintenance of neuronal polarity. *Nature reviews. Neuroscience*, 11(8):552–562.

- Regehr, W., Kehoe, J., Ascher, P., and Armstrong, C. (1993). Synaptically triggered action potentials in dendrites. *Neuron*, 11(1):145–151.
- Reimann, M. W., Anastassiou, C. a., Perin, R., Hill, S. L., Markram, H., and Koch, C. (2013). A biophysically detailed model of neocortical local field potentials predicts the critical role of active membrane currents. *Neuron*, 79(2):375–90.
- Ren, C. T., Li, D. M., Ou, S. W., Wang, Y. J., Lin, Y., Zong, Z. H., Kameyama, M., and Kameyama, A. (2012). Cloning and expression of the two new variants of Nav1.5/SCN5A in rat brain. *Molecular and Cellular Biochemistry*, 365(1-2):139–148.
- Rhodes, K. J., Strassle, B. W., Monaghan, M. M., Bekele-Arcuri, Z., Matos, M. F., and Trimmer, J. S. (1997). Association and colocalization of the Kvbeta1 and Kvbeta2 beta-subunits with Kv1 alpha-subunits in mammalian brain K+ channel complexes. *The Journal of neuroscience*, 17(21):8246–8258.
- Rowan, M. J. M., Tranquil, E., and Christie, J. M. (2014). Distinct Kv Channel Subtypes Contribute to Differences in Spike Signaling Properties in the Axon Initial Segment and Presynaptic Boutons of Cerebellar Interneurons. *The Journal of Neuroscience*, 34(19):6611–6623.
- Royeck, M., Horstmann, M.-T., Remy, S., Reitze, M., Yaari, Y., and Beck, H. (2008). Role of axonal Nav1.6 sodium channels in action potential initiation of CA1 pyramidal neurons. *Journal of neurophysiology*, 100(4):2361–80.
- Rudy, B., Chow, A., Lau, D., Amarillo, Y., Ozaita, A., Saganich, M., Moreno, H., Nadal, M. S., Hernandez-Pineda, R., Hernandez-Cruz, A., Erisir, A., Leonard, C., and Vega-Saenz De Miera, E. (1999). Contributions of Kv3 channels to neuronal excitability. *Annals of the New York Academy of Sciences*, 868:304–343.
- Rush, A. M., Dib-Hajj, S. D., and Waxman, S. G. (2005). Electrophysiological properties of two axonal sodium channels, Nav1.2 and Nav1.6, expressed in mouse spinal sensory neurones. *The Journal of physiology*, 564(Pt 3):803–15.
- Sah, P. (1996). Ca<sup>2+</sup> activated K<sup>+</sup> currents in neurons: types, physiological roles and modulation. *Trends in neurosciences*, 19:150–154.
- Sah, P. and Louise Faber, E. S. (2002). Channels underlying neuronal calcium-activated potassium currents. *Progress in Neurobiology*, 66(5):345–353.
- Sánchez-Ponce, D., DeFelipe, J., Garrido, J. J., and Muñoz, A. (2012). Developmental Expression of Kv Potassium Channels at the Axon Initial Segment of Cultured Hippocampal Neurons. *PLoS ONE*, 7(10).
- Schafer, D. P., Jha, S., Liu, F., Akella, T., McCullough, L. D., and Rasband, M. N. (2009). Disruption of the axon initial segment cytoskeleton is a new mechanism for neuronal injury. *The Journal of neuroscience*, 29(42):13242–13254.
- Scharfman, H. E., Smith, K., Goodman, J. H., and Sollas, A. L. (2001). Survival of Dentate Hilar Mossy Cells after Pilocarpine-Induced Seizures and their Synchronized Burst Discharges with Area CA3 Pyramidal Cells. *Neuroscience*, 104(3):741–759.

- Schiller, J., Schiller, Y., Stuart, G., and Sakmann, B. (1997). Calcium action-potentials restricted to distal apical dendrites of rat neocortical pyramidal neurons. *Journal of Physiology*, 505:605–616.
- Schmidt-Hieber, C. and Bischofberger, J. (2010). Fast Sodium Channel Gating Supports Localized and Efficient Axonal Action Potential Initiation. *The Journal of Neuroscience*, 30(30):10233–10242.
- Schmidt-Hieber, C., Jonas, P., and Bischofberger, J. (2008). Action potential initiation and propagation in hippocampal mossy fibre axons. *Journal of physiology*, 586(7):1849–57.
- Schulze-Bonhage, A., Kurth, C., Carius, A., Steinhoff, B. J., and Mayer, T. (2006). Seizure anticipation by patients with focal and generalized epilepsy: A multicentre assessment of premonitory symptoms. *Epilepsy Research*, 70(1):83–88.
- Serôdio, P. and Rudy, B. (1998). Differential expression of Kv4 K<sup>+</sup> channel subunits mediating sub-threshold transient K<sup>+</sup> (A-type) currents in rat brain. *Journal of neurophysiology*, 79(2):1081–1091.
- Shadlen, M. N. and Newsome, W. T. (1998). The variable discharge of cortical neurons: implications for connectivity, computation, and information coding. *The Journal of Neuroscience*, 18(10):3870–3896.
- Shah, B. S., Stevens, E. B., Pinnock, R. D., Dixon, A. K., and Lee, K. (2001). Developmental expression of the novel voltage-gated sodium channel auxiliary subunit  $\beta 3$ , in rat CNS. *Journal of Physiology*, 534(3):763–776.
- Shah, M. M., Migliore, M., Valencia, I., Cooper, E. C., and Brown, D. A. (2008). Functional significance of axonal Kv7 channels in hippocampal pyramidal neurons. *PNAS*, 105(22):7869–7874.
- Shao, L.-R., Halvorsrud, R., Borg-Graham, L., and Storm, J. F. (1999). The role of BK-type Ca<sup>2+</sup>-dependent K<sup>+</sup> channels in spike broadening during repetitive firing in rat hippocampal pyramidal cells. *Journal of Physiology*, 521.1:135–146.
- Shepard, P. D. and Trudeau, M. C. (2008). Emerging roles for ether-a-go-go-related gene potassium channels in the brain. *Journal of Physiology*, 586(Pt 20):4785–4786.
- Shi, W., Wang, H. S., Pan, Z., Wymore, R. S., Cohen, I. S., McKinnon, D., and Dixon, J. E. (1998). Cloning of a mammalian elk potassium channel gene and EAG mRNA distribution in rat sympathetic ganglia. *Journal of Physiology*, 511(3):675–682.
- Shoukimas, J. J. and French, R. J. (1980). Incomplete inactivation of sodium currents in nonperfused squid axon. *Biophysical journal*, 32(2):857–862.
- Shu, Y., Duque, A., Yu, Y., Haider, B., and McCormick, D. A. (2007a). Properties of action potential initiation in neocortical pyramidal cells: evidence from whole cell axon recordings. *Journal of Neurophysiology*, 97(1):746–760.
- Shu, Y., Hasenstaub, A., Duque, A., Yu, Y., and McCormick, D. A. (2006). Modulation of intracortical synaptic potentials by presynaptic somatic membrane potential. *Nature*, 441(7094):761–765.
- Shu, Y., Yu, Y., Yang, J., and McCormick, D. A. (2007b). Selective control of cortical axonal spikes by a slowly inactivating K<sup>+</sup> current. *PNAS*, 104(27):11453–11458.

- Softky, W. R. and Koch, C. (1993). The highly irregular firing of cortical cells is inconsistent with temporal integration of random EPSPs. *The Journal of neuroscience*, 13(1):334–50.
- Soleng, A. F., Chiu, K., and Raastad, M. (2003). Unmyelinated axons in the rat hippocampus hyperpolarize and activate an H current when spike frequency exceeds 1 Hz. *The Journal of physiology*, 552(2):459–470.
- Squire, L., Berg, D., Bloom, F. E., Du Lac, S., Ghosh, A., and Spitzer, N. C. (2012). *Fundamental neuroscience*. Academic Press.
- Stoler, O. and Fleidervish, I. A. (2016). Functional implications of axon initial segment cytoskeletal disruption in stroke. *Acta Pharmacologica Sinica*, 37(1):75–81.
- Stuart, G., Schiller, J., and Sakmann, B. (1997a). Action potential initiation and propagation in rat neocortical pyramidal neurons. *Journal of Physiology*, 505(3):617–632.
- Stuart, G., Spruston, N., Sakmann, B., and Hausser, M. (1997b). Action potential initiation and back propagation in neurons of the mammalian central nervous system. *Trends in Neurosciences*, 20(3):125–131.
- Stuart, G. J. and Sakmann, B. (1994). Active propagation of somatic action potentials into neocortical pyramidal cell dendrites. *Nature*, 367:69–72.
- Suter, U. and Scherer, S. S. (2003). Disease mechanisms in inherited neuropathies. *Nature reviews. Neuroscience*, 4(9):714–726.
- Swadlow, H. A., Gusev, A. G., and Bezdudnaya, T. (2002). Activation of a Cortical Column by a Thalamocortical Impulse. *The Journal of Neuroscience*, 22(17):7766–7773.
- Szabadies, J., Varga, C., Molnar, G., Olah, S., Barzo, P., and Tamas, G. (2006). Excitatory Effect of GABAergic Axo-Axonic Cells in Cortical Microcircuits. *Science*, 311(January):233–235.
- Tchumatchenko, T., Malyshev, A., Wolf, F., and Volgushev, M. (2011). Ultrafast Population Encoding by Cortical Neurons. *The Journal of neuroscience*, 31(34):12171–12179.
- Telenczuk, B., Dehghani, N., Le Van Quyen, M., Cash, S. S., Halgren, E., Hatsopoulos, N. G., and Destexhe, A. (2016). Local field potentials primarily reflect inhibitory neuron activity in human and monkey cortex. *bioRxiv*.
- Teleńczuk, B. and Destexhe, A. (2013). *Local Field Potential, Relationship to Unit Activity*, pages 1–6. Springer New York, New York, NY.
- Thome, C., Kelly, T., Yanez, A., Schultz, C., Engelhardt, M., Cambridge, S. B., Both, M., Draguhn, A., Beck, H., and Egorov, A. V. (2014). Axon-carrying dendrites convey privileged synaptic input in hippocampal neurons. *Neuron*, 83(6):1418–1430.
- Thomson, A. M. and Destexhe, A. (1999). Dual intracellular recordings and computational models of slow inhibitory postsynaptic potentials in rat neocortical and hippocampal slices. *Neuroscience*, 92(4):1193–1215.

- Tian, C., Wang, K., Ke, W., Guo, H., and Shu, Y. (2014). Molecular identity of axonal sodium channels in human cortical pyramidal cells. *Frontiers in cellular neuroscience*, 8(September):297.
- Tran-Van-Minh, A., Cazé, R. D., Abrahamsson, T., Cathala, L., Gutkin, B. S., and DiGregorio, D. A. (2015). Contribution of sublinear and supralinear dendritic integration to neuronal computations. *Frontiers in cellular neuroscience*, 9(March):67.
- Traub, R. D., Draguhn, A., Whittington, M. a., Baldeweg, T., Bibbig, A., Buhl, E. H., and Schmitz, D. (2002). Axonal gap junctions between principal neurons: a novel source of network oscillations, and perhaps epileptogenesis. *Reviews in the neurosciences*, 13(1):1–30.
- Trimmer, J. S. (2015). Subcellular localization of K<sup>+</sup> channels in mammalian brain neurons: Remarkable precision in the midst of extraordinary complexity. *Neuron*, 85(2):238–256.
- Trimmer, J. S. and Rhodes, K. J. (2004). Localization of voltage-gated ion channels in mammalian brain. *Annual review of physiology*, 66(1):477–519.
- Undrovinas, A. I., Fleidervish, I. a., and Makielski, J. C. (1992). Inward sodium current at resting potentials in single cardiac myocytes induced by the ischemic metabolite lysophosphatidylcholine. *Circulation research*, 71(5):1231–1241.
- Vacher, H., Mohapatra, D. P., and Trimmer, J. S. (2008). Localization and targeting of voltage-dependent ion channels in mammalian central neurons. *Physiological reviews*, 88(4):1407–47.
- Van Wart, A., Trimmer, J. S., and Matthews, G. (2007). Polarized Distribution of Ion Channels within Microdomains of the Axon Initial Segment. *The Journal of comparative neurology*, 500:339–352.
- Verret, L., Mann, E. O., Hang, G. B., Barth, A. M. I., Cobos, I., Ho, K., Devidze, N., Masliah, E., Kreitzer, A. C., Mody, I., Mucke, L., and Palop, J. J. (2012). Inhibitory interneuron deficit links altered network activity and cognitive dysfunction in Alzheimer model. *Cell*, 149(3):708–721.
- Villa, C. and Combi, R. (2016). Potassium Channels and Human Epileptic Phenotypes: An Updated Overview. *Frontiers in Cellular Neuroscience*, 10(March):1–14.
- Viney, T. J., Lasztocki, B., Katona, L., Crump, M. G., Tukker, J. J., Klausberger, T., and Somogyi, P. (2013). Network state-dependent inhibition of identified hippocampal CA3 axo-axonic cells in vivo. *Nature neuroscience*, 16(12):1802–1811.
- Wall, P. D. (1995). Do nerve impulses penetrate terminal arborizations? A pre-presynaptic control mechanism. *Trends in Neurosciences*, 18(2):99–103.
- Wang, D. T., Hill, A. P., Mann, S. a., Tan, P. S., and Vandenberg, J. I. (2011). Mapping the sequence of conformational changes underlying selectivity filter gating in the Kv11.1 potassium channel. *Nature structural & molecular biology*, 18(1):35–41.
- Wang, H., Kunkel, D. D., Martin, T. M., Schwartzkroin, P. A., and Tempel, B. L. (1993). Heteromultimeric K<sup>+</sup> channels in terminal and juxtaparanodal regions of neurons. *Nature*, 365(6441):75–9.

- Wang, H., Kunkel, D. D., Schwartzkroin, P. A., and Tempel, B. L. (1994). Localization of Kv1.1 and Kv1.2, two K channel proteins, to synaptic terminals, somata, and dendrites in the mouse brain. *The Journal of neuroscience*, 14(8):4588–4599.
- Watanabe, E., Fujikawa, A., Matsunaga, H., Yasoshima, Y., Sako, N., Yamamoto, T., Saegusa, C., and Noda, M. (2000). Nav2/NaG channel is involved in control of salt-intake behavior in the CNS. *The Journal of neuroscience*, 20(20):7743–7751.
- Waxman, S. G. (2006). Axonal conduction and injury in multiple sclerosis: the role of sodium channels. *Nature reviews. Neuroscience*, 7(12):932–941.
- Westenbroek, R. E., Merrick, D. K., and Catterall, W. A. (1989). Differential subcellular localization of the RI and RII Na<sup>+</sup> channel subtypes in central neurons. *Neuron*, 3(6):695–704.
- Westenbroek, R. E., Noebels, J. L., and Catterall, W. A. (1992). Elevated Expression of Type II Na<sup>+</sup> Channels Axons of shiverer Mouse Brain in Hypomyelinated. *The Journal of Neuroscience*, 72(June):2259–2267.
- Whitaker, W. R., Faull, R. L., Waldvogel, H. J., Plumpton, C. J., Emson, P. C., and Clare, J. J. (2001a). Comparative distribution of voltage-gated sodium channel proteins in human brain. *Brain research. Molecular brain research*, 88(1-2):37–53.
- Whitaker, W. R. J., Faull, R. L. M., Dragunow, M., Mee, E. W., Emson, P. C., and Clare, J. J. (2001b). Changes in the mRNAs encoding voltage-gated sodium channel types II and III in human epileptic hippocampus. *Neuroscience*, 106(2):275–285.
- Williams, S. R. and Stuart, G. J. (1999). Mechanisms and consequences of action potential burst firing in rat neocortical pyramidal neurons. *The Journal of physiology*, 521 Pt 2:467–482.
- Wimmer, V. C., Reid, C. A., So, E. Y.-W., Berkovic, S. F., and Petrou, S. (2010). Axon initial segment dysfunction in epilepsy. *The Journal of physiology*, 588(Pt 11):1829–40.
- Wollner, D. A. and Catterall, W. A. (1986). Localization of sodium channels in axon hillocks and initial segments of retinal ganglion cells. *PNAS*, 83(21):8424–8428.
- Woodruff, A., Xu, Q., Anderson, S. A., and Yuste, R. (2009). Depolarizing effect of neocortical chandelier neurons. *Frontiers in neural circuits*, 3(October):15.
- Woodruff, A. R., McGarry, L. M., Vogels, T. P., Inan, M., Anderson, S. A., and Yuste, R. (2011). State-Dependent Function of Neocortical Chandelier Cells. *The Journal of Neuroscience*, 31(49):17872–17886.
- Wu, L., Nishiyama, K., Hollyfield, J. G., and Wang, Q. (2002). Localization of Nav1.5 sodium channel protein in the mouse brain. *Neuroreport*, 13(18):2547–51.
- Wu, W., Dong, M. Q., Wu, X. G., Sun, H. Y., Tse, H. F., Lau, C. P., and Li, G. R. (2012). Human ether-a-go-go gene potassium channels are regulated by EGFR tyrosine kinase. *Biochimica et Biophysica Acta - Molecular Cell Research*, 1823(2):282–289.

- Yan, Z., Xu, Y., Liang, M., and Ren, X. (2015). Expression and functional role of Nav1.9 sodium channel in cartwheel cells of the dorsal cochlear nucleus. *Molecular Medicine Reports*, 11(3):1833–1836.
- Yu, F. H. and Catterall, W. a. (2003). Overview of the voltage-gated sodium channel family. *Genome biology*, 4(3):207.
- Yu, F. H. and Catterall, W. A. (2004). The VGL-Chanome : A Protein Superfamily Specialized for Electrical Signaling and Ionic Homeostasis. *Science Signaling*, pages 1–17.
- Yu, Y., Shu, Y., and McCormick, D. A. (2008). Cortical action potential backpropagation explains spike threshold variability and rapid-onset kinetics. *The Journal of neuroscience*, 28(29):7260–72.
- Yue, C. and Yaari, Y. (2006). Axo-Somatic and Apical Dendritic Kv7 / M Channels Differentially Regulate the Intrinsic Excitability of Adult Rat CA1 Pyramidal Cells. *Journal of Neurophysiology*, 95:3480–3495.
- Zhang, X., Bertaso, F., Yoo, J. W., Baumgärtel, K., Clancy, S. M., Lee, V., Cienfuegos, C., Wilmot, C., Avis, J., Hunyh, T., Daguia, C., Schmedt, C., Noebels, J., and Jegla, T. (2010). Deletion of the potassium channel Kv12.2 causes hippocampal hyperexcitability and epilepsy. *Nature neuroscience*, 13(9):1056–8.
- Zhang, Y., Jiang, X., Snutch, T. P., and Tao, J. (2013). Modulation of low-voltage-activated T-type Ca<sup>2+</sup> channels. *Biochimica et Biophysica Acta - Biomembranes*, 1828(7):1550–1559.
- Zhou, D., Lambert, S., Malen, P. L., Carpenter, S., Boland, L. M., and Bennett, V. (1998). Ankyrin(G) is required for clustering of voltage-gated Na channels at axon initial segments and for normal action potential firing. *Journal of Cell Biology*, 143(5):1295–1304.
- Zhu, Y., Stornetta, R. L., and Zhu, J. J. (2004). Chandelier Cells Control Excessive Cortical Excitation : Characteristics of Whisker-Evoked Synaptic Responses of Layer 2 / 3 Nonpyramidal and Pyramidal Neurons. *The Journal of Neuroscience*, 24(22):5101–8.



---

## The basis of sharp spike onset in standard biophysical models

---

In this chapter, we present the work which has been done under the supervision of Romain Brette and in the collaboration with Bertrand Fontaine. At the moment of writing this thesis, it is under the peer-revision in the PLOS Computational Biology and it has been published in bioRxiv (Teleńczuk et al., 2016).

### 3.1 Abstract

In most vertebrate neurons, spikes initiate in the axonal initial segment (AIS). When recorded in the soma, they have a surprisingly sharp onset, as if sodium (Na) channels opened abruptly. The main view stipulates that spikes initiate in a conventional manner at the distal end of the AIS, then progressively sharpen as they backpropagate to the soma. We examined the biophysical models used to substantiate this view, and we found that spikes do not initiate through a local axonal current loop that propagates along the axon, but through a global current loop encompassing the AIS and soma, which forms an electrical dipole. Therefore, the phenomenon is not adequately modeled as the backpropagation of an electrical wave along the axon, since the wavelength would be as large as the entire system. Instead, in these models, we found that spike initiation rather follows the critical resistive coupling model proposed recently, where the Na current entering the AIS is matched by the axial resistive current flowing to the soma. Besides demonstrating it by examining the balance of currents at spike initiation, we show that the observed increase in spike sharpness along the axon is artifactual and disappears when an appropriate measure of rapidness is used; instead, somatic onset rapidness can be predicted from spike shape at initiation site. Finally, we reproduce the phenomenon in a two-compartment model, showing that it does not rely on propagation. In these

models, the sharp onset of somatic spikes is therefore not an artifact of observing spikes at the incorrect location, but rather the signature that spikes are initiated through a global soma-AIS current loop forming an electrical dipole.

## 3.2 Author summary

In most vertebrate neurons, spikes are initiated in the axonal initial segment, next to the soma. When recorded at the soma, action potentials appear to suddenly rise as if all sodium channels opened at once. This has been previously attributed to the backpropagation of spikes from the initial segment to the soma. Here we demonstrate with biophysical models that backpropagation does not contribute to the sharpness of spike onset. Instead, we show that the phenomenon is due to the resistive coupling between the large somatodendritic compartment and the small axonal compartment, a geometrical discontinuity that leads to an abrupt variation in voltage.

## 3.3 Introduction

In most vertebrate neurons, action potentials are generated by the opening of sodium (Na) channels in the axon initial segment (AIS) (Debanne et al., 2011). According to the standard textbook account, spikes initiate through the interplay between two local transmembrane currents, when the inward Na current exceeds the outward leak current, carried mostly by potassium (K) (Fig. 3.1A). Because macroscopically Na channels open gradually with depolarization (Boltzmann slope factor:  $k_a \approx 6$  mV (Kole et al., 2008)), spike onset appears smooth in standard isopotential neuron models (Fig. 3.1B, top left). In contrast, the onset of spikes recorded at the soma of cortical neurons appears very sharp: in a voltage trace, spikes appear to suddenly rise from resting potential (Naundorf et al., 2006) (Fig. 3.1B, bottom, human cortical pyramidal neuron from Testa-Silva et al. (2014)), as if all Na channels opened at once.

It has been proposed that Na channels in the AIS cooperate, so that they actually open all at once instead of gradually as a function of local voltage (Naundorf et al., 2006; Öz et al., 2015). However, this phenomenon has not been observed in the AIS (see Discussion). In addition, detailed multicompartmental models with standard biophysics can exhibit sharp somatic spikes (McCormick et al., 2007; Yu et al., 2008), when Na channel density is high enough (Baranauskas et al., 2010). According to the backpropagation hypothesis, this phenomenon is due to the progressive sharpening of spike onset between the axonal initiation site and the soma, partly due to the Na channels placed between the two sites (Fig. 3.1C; Yu et al. (2008)). In this view, spike initiation follows the standard

account: a spike initiates at a distal point of the AIS through a local current loop, and the electrical wave progressively propagates along the axon towards the soma, while its shape becomes sharper. In this view, the somatic kink does not bear any significance for excitability, since it only appears after spike initiation. This point is disputed because input-output properties and other features of excitability do not empirically match the predictions of standard accounts of spike initiation (Brette, 2015; Ilin et al., 2013).

A theoretical study proposed a different view, which we will call critical resistive coupling (Brette, 2013). The soma acts as a current sink for the initiation site because of the size difference and the short distance between the two sites. It follows that the Na current at spike initiation is not opposed by local transmembrane currents (the leak current), but by the resistive axial current flowing to the soma (Fig. 3.1D). Consequently, spikes initiate through a global current loop that encloses the AIS and soma, rather than a local axonal current loop: Na current through the AIS, resistive current between soma and AIS, capacitive current through the soma, and resistive current in the extracellular space to close the loop. Thus the soma and AIS form an electrical dipole at spike initiation, and it is therefore not appropriate to speak of wave propagation (the wavelength would enclose both the soma and AIS). When the product of axial resistance and Na conductance is greater than a critical value, Na channels open as a discontinuous function of somatic voltage, with consequences not only on somatic spike shape but also on input-output properties of neurons (Brette, 2015). This explanation attributes no role to active backpropagation or to the somatodendritic capacitance, beyond the requirement that the capacitance must be large enough for the soma to act as a current sink. Which of the critical resistive coupling and backpropagation hypotheses applies has not been determined in detailed biophysical models.

We therefore examined multicompartmental models of spike initiation, including models that were previously used to substantiate the backpropagation hypothesis, to determine which of the critical resistive coupling and backpropagation hypotheses actually applies. We found that: 1) the soma and AIS form an electrical dipole at spike initiation; 2) Na channels open as a discontinuous function of somatic voltage; 3) at spike initiation, the main current opposing the Na current is the axial resistive current; 4) excitability increases with intracellular resistivity; 5) active backpropagation is neither sufficient nor necessary for sharp spike initiation; 6) provided the somatodendritic compartment is large enough, its size has no quantitative impact on somatic onset rapidness; 7) the apparent sharpening of spikes as they backpropagate to the soma is an artifact of the measure of rapidness; in contrast, somatic onset rapidness can be predicted from spike shape at the initiation site. Finally, we show that the phenomenon can be reproduced by a model with only two resistively coupled compartments and standard channel properties. We conclude

that in standard biophysical models, the biophysical basis of sharp somatic spikes is not backpropagation but critical resistive coupling, where spikes initiate through a global current loop encompassing the soma and AIS, rather than local current loops propagating towards the soma. This implies that in these models the sharpness of spike initiation is not an artifact, but a feature of normal (i.e., not ectopic) spike initiation through the soma-AIS dipole.

## 3.4 Results

### 3.4.1 Intracellular and extracellular features of sharp spike initiation in multicompartmental models

We examined two multicompartmental Hodgkin-Huxley models that display somatic spikes with sharp onset (Yu et al. (2008); see Methods): one with an idealized morphology consisting of a uniform cylindrical axon (diameter  $1\ \mu\text{m}$ , length  $50\ \mu\text{m}$ ) and a larger cylindrical soma (Fig. 3.2, left column), and one with the reconstructed morphology of a cortical pyramidal cell (Fig. 3.2, middle column). Action potentials are initiated in the axon, which has a high density of Na channels ( $8000\ \text{pS}/\mu\text{m}^2$ ), and regenerated in the soma, which has a lower density of Na channels ( $800\ \text{pS}/\mu\text{m}^2$ ). In both models, voltage traces show a distinct ‘kink’ at the onset of somatic spikes (Fig. 3.2A, top, orange), which appears also when somatic Na channels are blocked (dotted orange). This kink is not present in the axonal spike (blue). Phase plots of  $dV/dt$  versus membrane potential  $V$  are biphasic (Fig. 3.2A, bottom), with a first component corresponding to the axonal Na current and a second component due to the somatic Na current. The sharpness of spike onset appears as a steep slope at threshold in the phase plots, called ‘initial phase slope’ or ‘onset rapidness’ (Na channels in the soma:  $52.5\ \text{ms}^{-1}$  and  $52\ \text{ms}^{-1}$  in the simple and detailed model, respectively; no Na channels in the soma:  $55.6\ \text{ms}^{-1}$  and  $54\ \text{ms}^{-1}$ ; compare with Fig. 3.1 B:  $5.6\ \text{ms}^{-1}$ ; see Methods). We also examined spike initiation in the same way in another multicompartmental model of rat cortical pyramidal cell, where the models of Na and K currents were fitted to patch-clamp measurements in those neurons, separately in soma and AIS (Hallermann et al., 2012). The same qualitative features were observed (Fig. 3.2, right column).

### 3.4.2 Extracellular field at spike initiation

We then examined the extracellular field at spike initiation in the simple model (Fig. 3.3 and Movie S1). At the very beginning of the spike (Fig. 3.3A), the current injected at

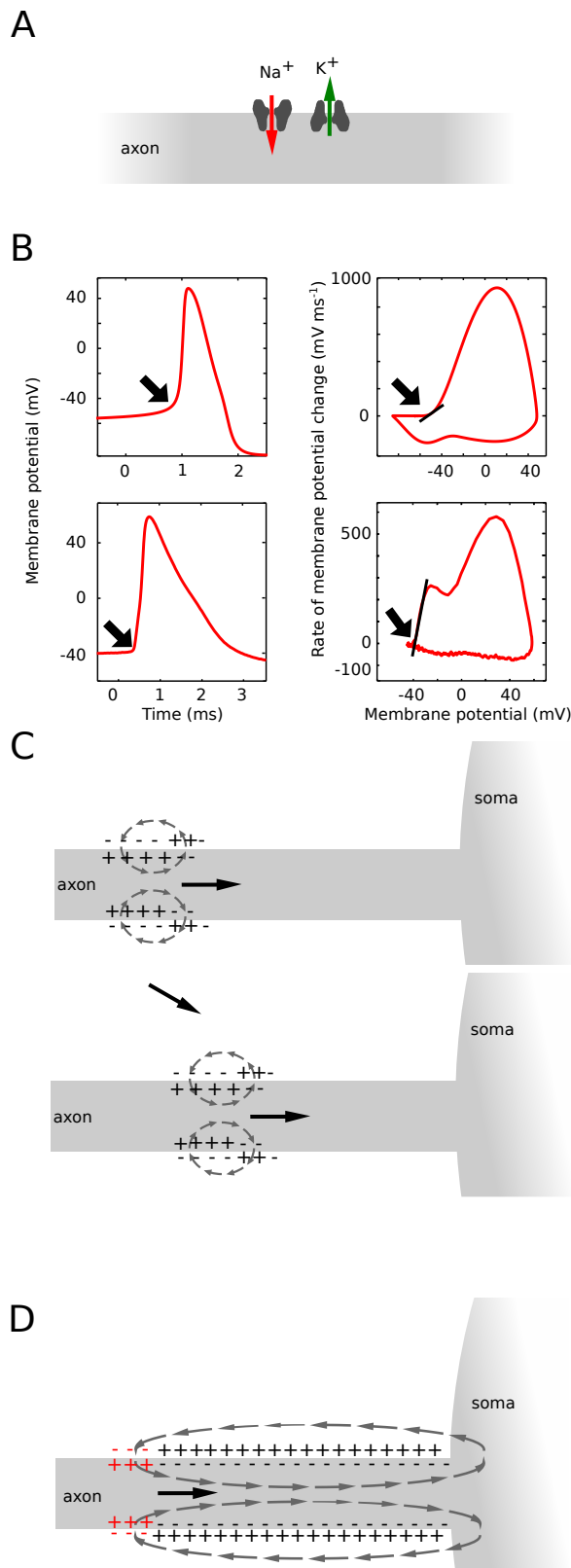


Figure 3.1: **Theories of spike initiation.** **A.** Standard account of spike initiation: spike initiation results from the interplay between Na current and K current (mostly leak) flowing through the membrane at the initiation site. **B.** Top: The isopotential Hodgkin-Huxley model produces spikes with smooth onset (left), exhibiting a gradual increase in  $dV/dt$  as a function of membrane potential  $V$  (right: onset rapidness measured as the slope at  $20 \text{ mV/ms} = 5.6 \text{ ms}^{-1}$ ). Bottom: cortical neurons have somatic spikes with sharp onsets (left), with step increase in  $dV/dt$  as a function of  $V$  (onset rapidness:  $28.8 \text{ ms}^{-1}$ ; human cortical data from [Testa-Silva et al. \(2014\)](#)). **C.** Backpropagation hypothesis: spikes are initiated according to the conventional account, with a local axonal current loop propagating towards the soma. **D.** Critical resistive coupling hypothesis: owing to the strong resistive coupling between the two sites and the soma acting as a current sink, spike initiation results from the interplay between Na current and axial current. Spikes then initiate through a global current loop encompassing AIS and soma, which behaves as an electrical dipole.

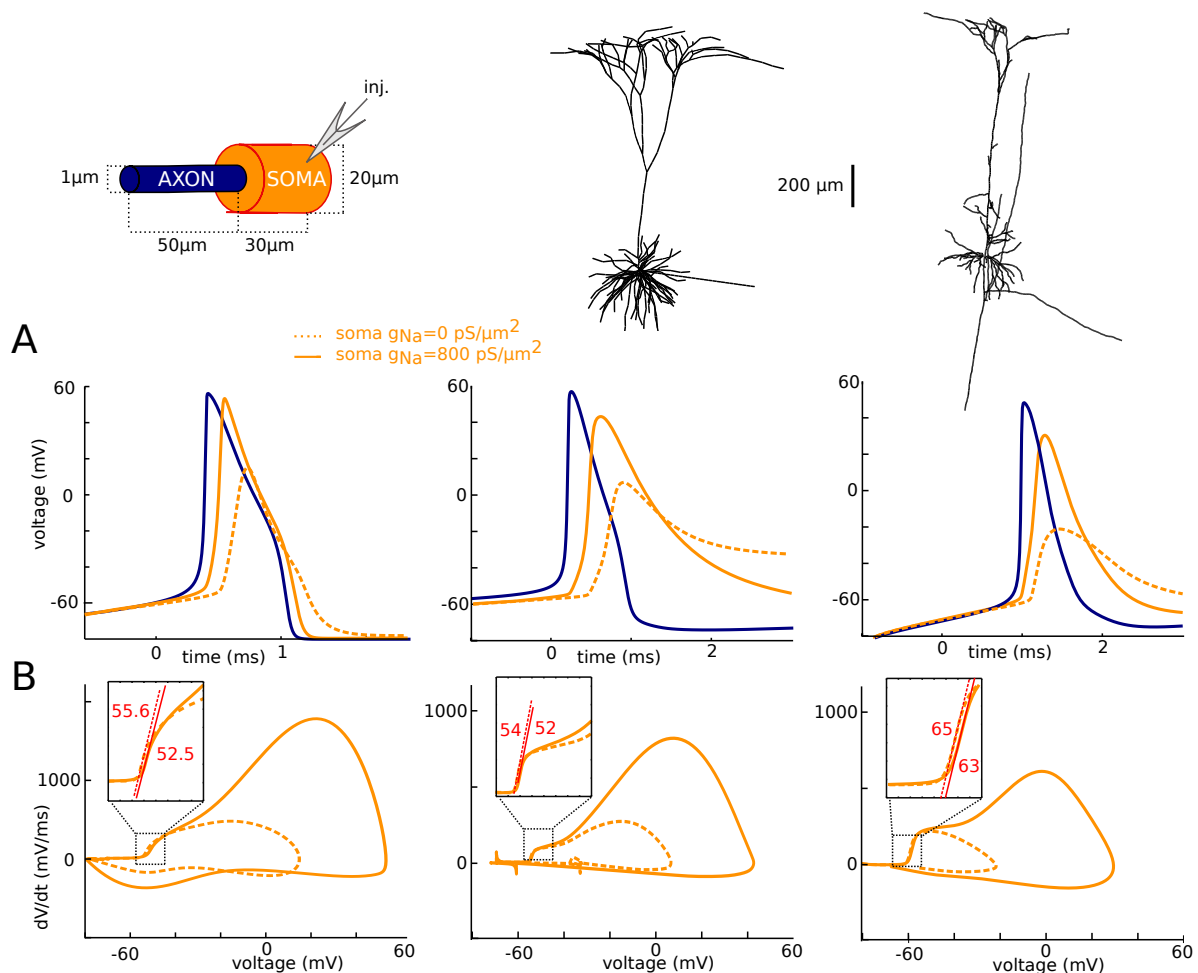


Figure 3.2: **Intracellular features of sharp spike initiation in multicompartmental models.** Left: model with simplified soma-axon geometry. Middle: cortical pyramidal cell model with morphological reconstruction from Yu et al. (2008). Right: pyramidal cell model from Hallermann et al. (2012). **A.** Somatic voltage trace of a spike, with (solid orange) and without (dotted orange) somatic Na channels, and axonal spike (blue). **B.** Phase plot of the same trace, showing  $dV/dt$  versus membrane potential  $V$ .

the soma is seen to exit the soma and part of it enters the distal end of the AIS. At the peak of the distal axonal spike (Fig. 3.3B), which corresponds to the knee of the somatic spike, the electrical field clearly shows that the soma and AIS form an electrical dipole, with current entering the AIS, flowing to the soma, exiting at the soma and returning through the extracellular space. During repolarization (Fig. 3.3C), the soma-AIS dipole is inverted, with current flowing intracellularly from soma to AIS, and extracellularly from AIS to soma.

It is important to notice that even though the intracellular spike appears at the soma after a substantial delay following the axonal spike (Fig. 3.3D), the electrical dipole forms very quickly over the entire system (Fig. 3.3E). This discrepancy is due to the fact that the soma has a large capacitance and therefore a large charging time. Thus, the delay between the axonal and somatic spikes is better understood as a charging time (as an electrode charging a cell) rather than a propagation time.

The formation of the soma-AIS dipole at spike initiation manifests itself as negative extracellular potential near the AIS (current entering the AIS) and positive extracellular potential near the soma (current leaving the soma), as seen in Fig. 3.3E. Near the soma, this is followed by a negative peak corresponding to the somatic spike, and a smaller positive peak corresponding to the repolarization. Near the AIS, the negative peak is followed by a positive potential corresponding to the somatic spike (inversion of the dipole) and the axonal repolarization. Fig. 3.3F-G show extracellular recordings next to the soma and AIS, recorded experimentally in two different neurons. There are clearly quantitative differences with Fig. 3.3E, which depend both on the particular model and the position of the extracellular electrodes, but the same extracellular features of a dipole are seen. However, the precise temporal relationship between the extracellular waveforms of the two sites would be necessary to draw firm conclusions.

### 3.4.3 Currents at spike initiation

The sharpness of spike initiation is not only seen in the initial shape of action potentials. It also appears in voltage-clamp (Fig. 3.4). In the same 3 models used in Fig. 3.2, we recorded currents in somatic voltage-clamp, with an ideal configuration (access resistance  $R_s = 0.1 \text{ M}\Omega$ ), varying the command potential from 1 mV below spike threshold to 5 mV above it (Fig. 3.3A). This type of recording can be challenging in practice because the pipette resistance introduces artifacts when passing large currents (see Discussion), but this was not the case in these simulations. We notice that recorded currents do not increase gradually with voltage, as when recording an isopotential patch of membrane, but instead have all-or-none characteristics: there is no current 1 mV below threshold (black), and a very large current (10-20 nA) just above threshold (red). Current amplitude

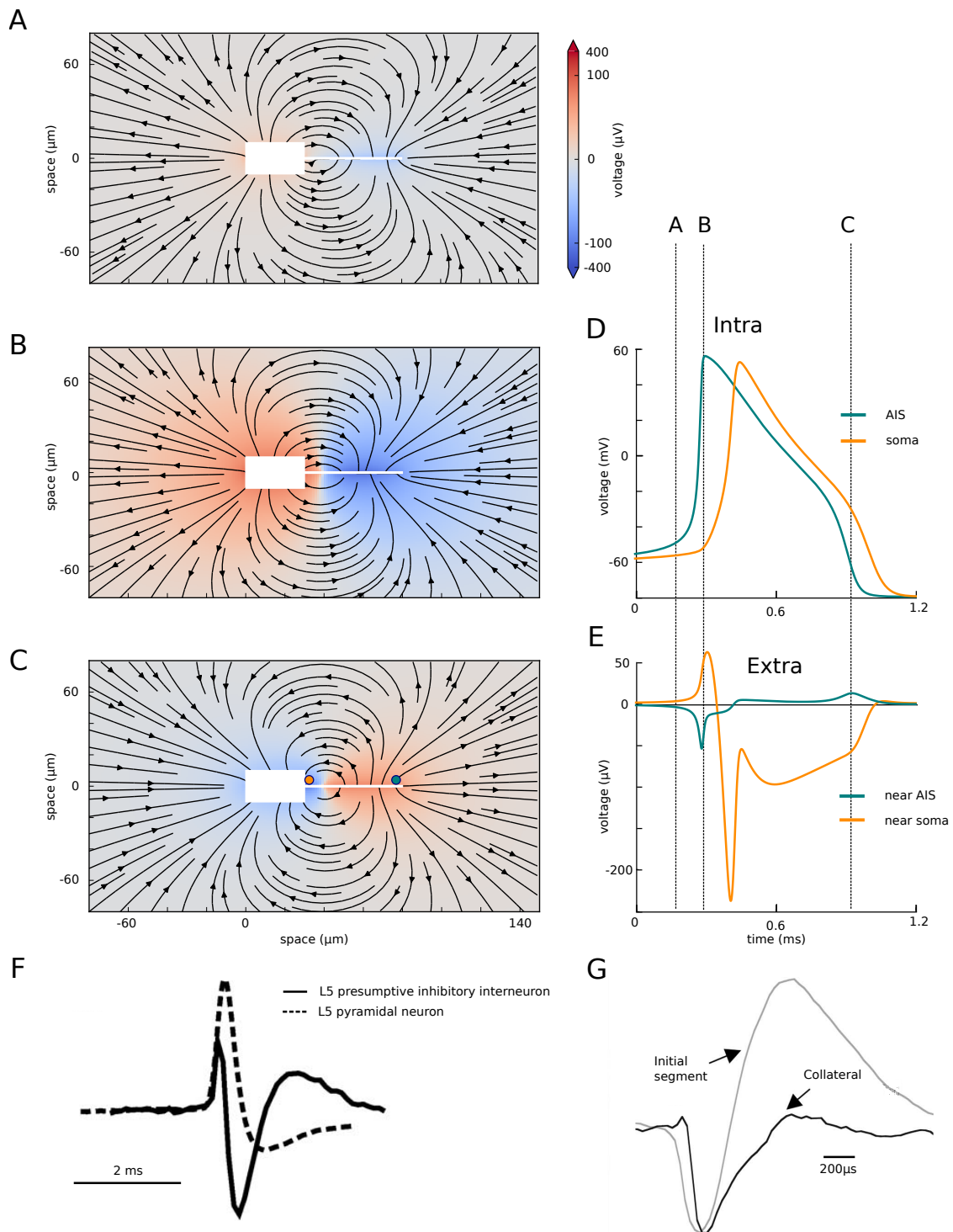


Figure 3.3: **Extracellular field at spike initiation.** **A-C.** Extracellular potential (color coded) and electrical field (arrows) around the simplified neuron (white box and line), at three different times indicated in D and E. **D.** Intracellular voltage trace at the soma and AIS distal end. **E.** Extracellular potential near the soma and AIS distal end. **F.** Extracellular recording near the soma of two cortical neurons (adapted from Joshi and Hawken (2006)). **G.** Extracellular AP recording near the AIS (grey) of a cortical pyramidal cell (adapted from Palmer and Stuart (2006)).

varies little, but latency decreases when command potential is increased. We can see that this current mirrors the membrane potential in the distal AIS, where a spike is produced (Fig. 3.4A, bottom). Thus these currents recorded in somatic voltage-clamp correspond to axial currents coming from the AIS.

Plotting the peak current as a function of command potential shows that the peak current increases discontinuously when the voltage command exceeds a threshold value (Fig. 3.4B, top), which is close to the voltage at spike onset measured in current-clamp (-60 mV, -58.2 mV and -62.2 mV in voltage-clamp vs. -59.7 mV, -56 mV and -65.3 mV in current-clamp, when  $dV/dt = 5$  mV/ms).

Blocking the somatic Na channels has no effect on this discontinuity (dotted orange). This discontinuity in the current-voltage relationship corresponds to a discontinuity in the proportion of open Na channels in the initiation site (distal end of the axon) as a function of somatic voltage (Fig. 3.4B, bottom), even though the activation curve of Na channels is smooth: effectively, Na channels open simultaneously as a function of somatic (but not axonal) voltage.

At first sight, it might seem trivial that a spike is produced when the somatic voltage exceeds a threshold. Yet, this is not the case in case in isopotential models, spatially extended models with somatic initiation (Koch et al., 1995), or axonal models (Jack et al., 1975), where a charge or a voltage threshold may apply depending on cases. A voltage threshold is a defining feature of integrate-and-fire models and a property of models with distal axonal initiation (Brette, 2015), but only when the axial resistance between soma and axonal initiation site is large enough (hence the name critical resistive coupling) (Brette, 2013). Therefore, the phenomenon of sharp initiation is not only about spike shape, but also about the way the axonal current changes with somatic voltage. Specifically, a very small change in somatic voltage can produce a very large change in axonal current. This phenomenon is the basic feature of the critical resistive coupling model (Brette, 2013), which also predicts the inverse relation between latency and distance to threshold characteristic of a saddle-node bifurcation. It can be reproduced by a two-compartment model (Milescu et al. (2010), Fig. 3.3A).

Empirically, this phenomenon has been observed in motoneurons (Barrett and Crill, 1980), cortical pyramidal cells and inferior olivary neurons (Milescu et al., 2010). An example is shown on Fig. 3.4C in a raphé neuron (from (Milescu et al., 2010)). Peak current shows a discontinuity when command potential is increased (right, red), except when axonal Na channels are inactivated with a prepulse (black). Note that the somatic contribution to the current (depolarized range) is smaller than in our simulations because TTX was applied to reduce the current so as to ensure proper voltage control. Fig. 3.4D shows similar data, but obtained with a two-electrode voltage-clamp and no TTX in a

cat motoneuron (Barrett and Crill, 1980).

We then examined the balance of currents near threshold at the axonal initiation site (Fig. 3.5). In all three models, the main current opposing the Na current (red) is the axial current flowing to the soma (black), while the K current (green) becomes significant only near the peak of the axonal spike. In this figure, transmembrane currents are summed over the AIS membrane, and the axial current is measured at the soma-axon junction. Thus, at spike initiation, the initial dynamics of the spike is determined by the interaction between the axial and Na current, rather than between the K (mainly leak) and Na current. This reflects the fact that current flows intracellularly between the two poles of the soma-AIS dipole (Fig. 3.3). It follows in particular that axial resistance rather than membrane resistance should determine excitability.

### 3.4.4 Excitability increases with intracellular resistivity

A consequence of this unconventional balance of currents is that the axial resistance between the soma and initiation site has a direct and possibly counter-intuitive impact on excitability: if axial resistance is increased, the neuron should become more excitable, despite the fact that the electrotonic distance of the initiation site increases. Axial resistance is proportional to the resistivity  $R_i$  of the intracellular medium. We therefore tested this prediction by manipulating the intracellular resistivity  $R_i$  in the model (Fig. 3.6A). When  $R_i$  is increased to 250  $\Omega\cdot\text{cm}$  (orange) compared to 150  $\Omega\cdot\text{cm}$  originally (green), spikes are initiated at a lower voltage. Conversely, when  $R_i$  is decreased to 30  $\Omega\cdot\text{cm}$ , spikes are initiated at a higher voltage (light blue). When  $R_i$  is decreased further to 1  $\Omega\cdot\text{cm}$ , the kink at spike onset disappears (dark blue). In all these cases except when  $R_i = 1 \Omega\cdot\text{cm}$  where the cell is essentially isopotential, spikes initiate in the axon.

The same effect is seen in somatic voltage-clamp (Fig.3.6B): the discontinuity in current is seen at increasingly higher voltages as resistivity decreases. These curves also demonstrate another feature of resistive coupling: as resistivity decreases, the peak current increases. This occurs because the resistive current is inversely proportional to resistance, by Ohms law. Thus, as resistivity increases, the neuron becomes less excitable (higher threshold) but the axon transmits a larger current at initiation.

Finally, when intracellular resistivity is decreased further (Fig. 3.6B, dark blue), the phenomenon disappears, as predicted by the critical resistive coupling hypothesis: axonal current and proportion of open Na channels vary gradually with somatic voltage. In summary, excitability depends on the resistance between soma and AIS, and not only on local membrane properties of the initiation site.

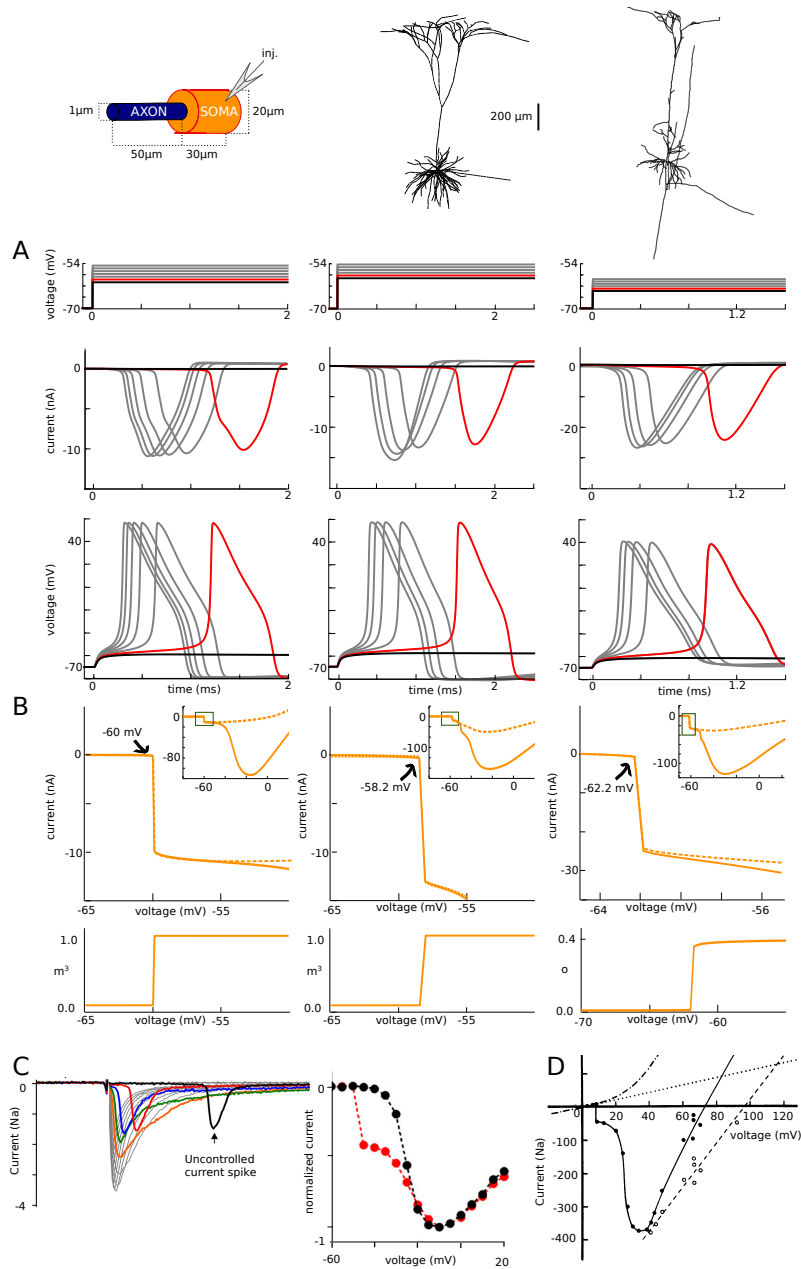


Figure 3.4: **Currents at spike initiation.** **A.** Somatic voltage-clamp recordings. Top: somatic membrane potential, spaced by 1 mV increments from threshold (red), with one trace just below threshold. Middle: recorded currents. Bottom: membrane potential at the AIS end. **B.** Top: peak current measured in somatic voltage-clamp versus holding voltage, with and without somatic Na channels, showing a discontinuity. Bottom: peak proportion of open Na channels at the distal axonal end versus holding voltage (variable  $m^3$  representing activation is shown for the first two models; variable  $o$  representing current-passing state is shown for the third model). **C.** Left, Current traces experimentally measured in somatic voltage-clamp in raph neuron (from (Milescu et al., 2010)). Right, Peak current vs. command voltage (red; the black curve is obtained when axonal Na channels are inactivated with a prepulse). **D.** Same as C, but in a two-electrode somatic voltage-clamp of a cat motoneuron (Barrett and Crill, 1980). Voltage is relative to the resting potential.

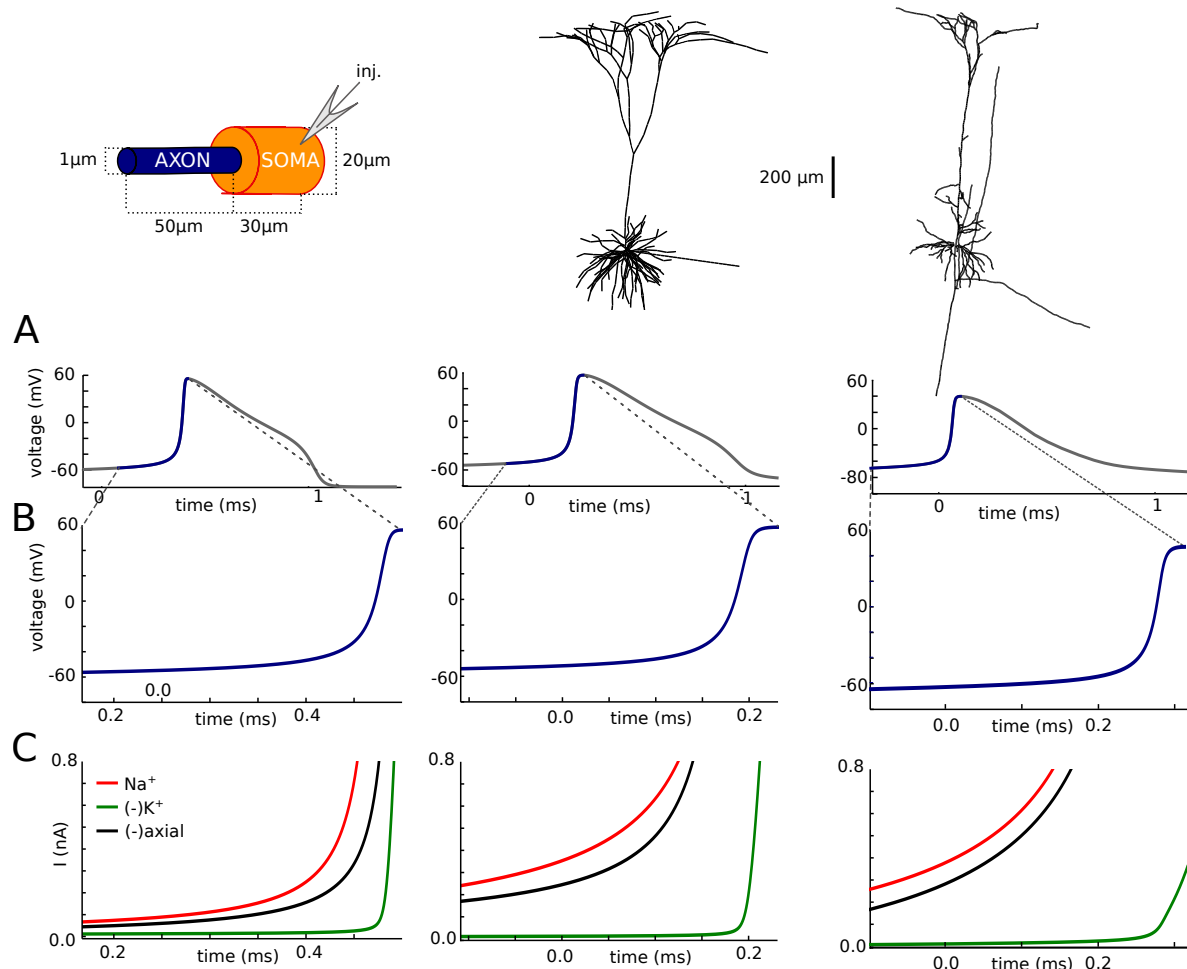


Figure 3.5: **Balance of currents at spike initiation.** **A.** Axonal spike. **B.** Rising phase of the spike. **C.** Na (red), K (green) and axial (green) current traces at the axonal initiation site. Na and K currents are summed over the AIS membrane; axial current is measured at the soma-axon junction. potential.

### 3.4.5 Sharp spike initiation requires a large enough somatodendritic compartment

A requirement of critical resistive coupling is that the soma effectively clamps the voltage at the beginning of the axon at spike initiation, which can occur if the somatodendritic compartment is large enough (Brette, 2013). We therefore show how spike initiation is affected by changing soma size in the simple model (Fig. 3.7). As was previously noted (Yu et al., 2008), the kink at spike onset entirely disappears when the soma has the same diameter as the axon (Fig. 3.7A, left; phase slope at 20 mV/ms:  $5 \text{ ms}^{-1}$ ) and only appears when the soma is large enough (Fig. 3.7A, middle and right; phase slope at 20 mV/ms: 12 and  $31 \text{ ms}^{-1}$ ; maximum phase slope of first component: 50 and  $42 \text{ ms}^{-1}$ ), or when a

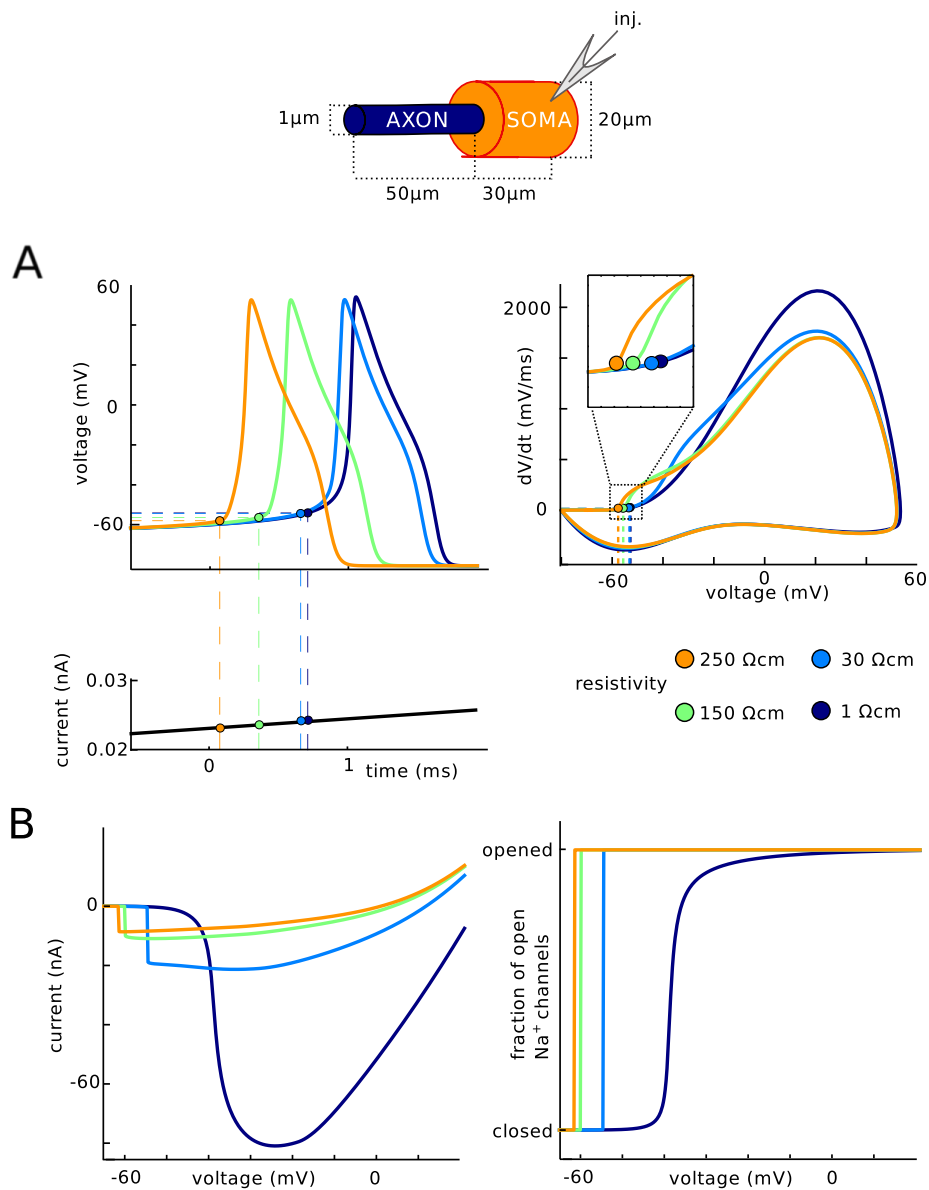


Figure 3.6: **Impact of intracellular resistivity  $R_i$  on excitability.** **A.** Spikes are triggered by a slow current ramp, for different values of  $R_i$  between 1  $\Omega\text{.cm}$  and 250  $\Omega\text{.cm}$  (green: original value). The neuron is more excitable for larger values of  $R_i$ . **B.** Current vs. somatic voltage in somatic voltage-clamp (as in Fig. 3.2B) and fraction of open  $\text{Na}^+$  channels vs. somatic voltage, for different values of  $R_i$ .

dendrite is added (Yu et al., 2008). Yet in all cases, when the soma is voltage-clamped, both the Na current and the proportion of open Na channels change abruptly when the somatic voltage exceeds a threshold (Fig. 3.7). This phenomenon is not explained by backpropagation.

Why does the discontinuity in somatic voltage-clamp result in sharp spike onsets when the soma is large but not when it is small? On Fig. 3.7C, we show the voltage along the axon at different moments of the spike upstroke, when somatic voltage is -58, -54, -40 and 30 mV (corresponding to the colored disks on Fig. 3.7A). In the case of the uniform axon (left), the neuron is essentially isopotential: the entire axon is depolarized synchronously. The situation is different when the soma is large (middle and right): at spike initiation, the soma almost clamps the proximal end of the axon while the voltage at the distal end rises with the Na influx. That is, the somatic current-clamp configuration corresponds, from the viewpoint of the axon, to a voltage-clamp of the start of the axon at the time scale of spike initiation. Thus the current discontinuity seen in somatic voltage-clamp (Fig. 3.7B) also appears in current-clamp near spike initiation, resulting in the sharp onset of spikes (Fig. 3.7A). Accordingly, the axial current is the main current opposing the Na current at the initiation site, meaning that the soma is a current sink for the initiation site, which is not the case with the uniform axon, where the axial current is small (Fig. 3.7D).

### 3.4.6 Backpropagation does not sharpen spikes

Next, we show that the spike does not actually sharpen as it travels to the soma, and furthermore onset rapidness does not depend on somatodendritic capacitance, once the basic phenomenon is present. The sharp somatic spike onset is not a sharpened axonal spike onset, but rather reflects the maximum rapidness of the axonal spike, observed at a higher voltage.

We first make a methodological point. The standard way of measuring onset rapidness is to calculate the slope of the phase plot ( $dV/dt$  vs.  $V$ ) at an arbitrary value of  $dV/dt$  (typically 5–20 mV/ms). In real somatic recordings, the phase plot is approximately linear over a wide enough range of  $dV/dt$  values, so that the exact choice is not critical (Baranauskas et al., 2010) (see Fig. 2F therein), all the more than it generally corresponds to only a few data points. However, in models where morphological parameters are varied over several orders of magnitude, this choice of  $dV/dt$  can be important. Fig. 3.8A (left) shows the phase plot of a spike in the simple model, for a somatic area of  $3,000 \mu^2$  (grey) and  $10,000 \mu$  (orange). It appears that the phase plot is linear around different values of  $dV/dt$  in the two cases (25 mV/ms and 60 mV/ms). When measured in the linear region of the phase plot, phase slope is similar in the two cases (40 and  $50 \text{ ms}^{-1}$ ). But

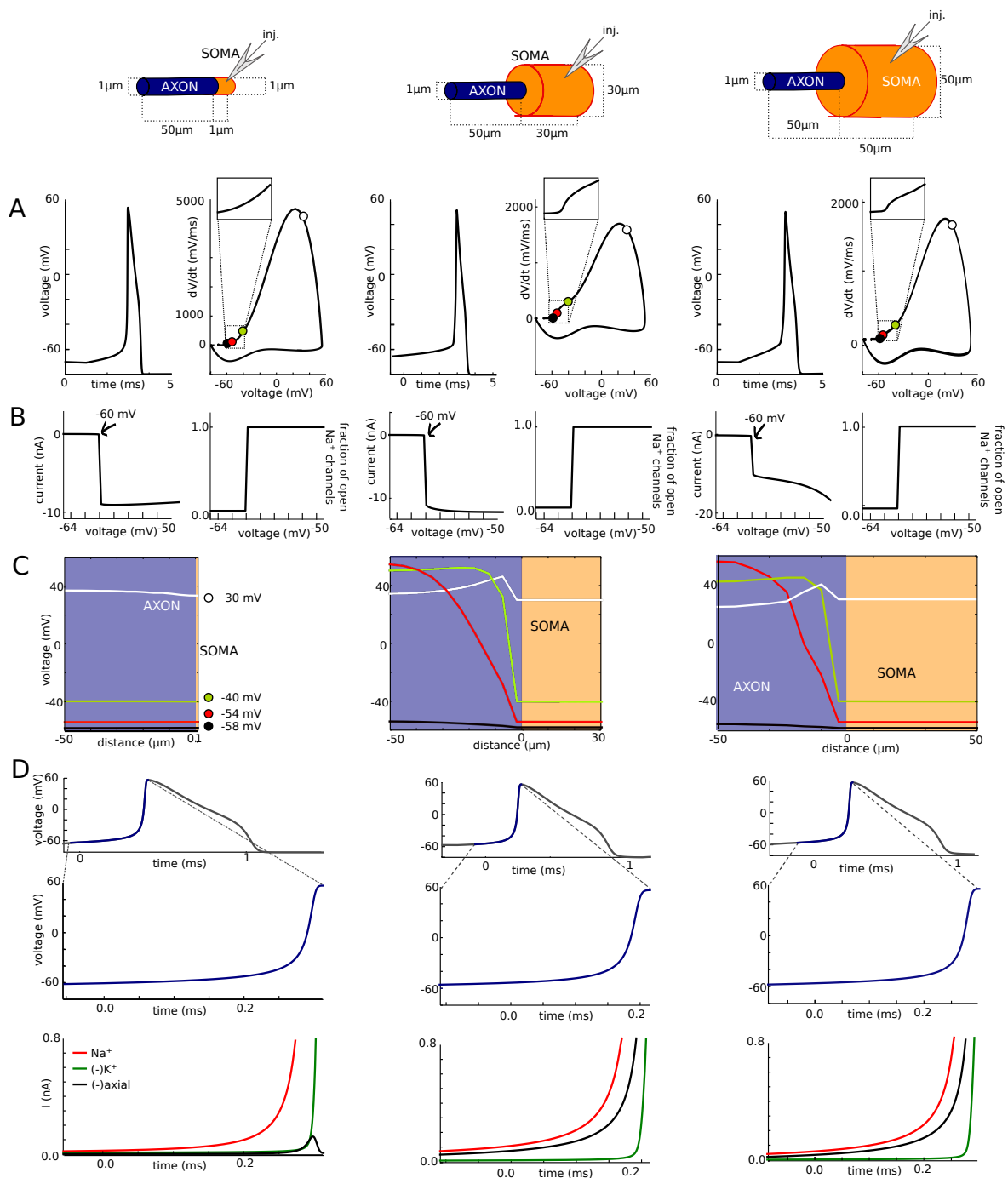


Figure 3.7: **Influence of soma size on spike initiation.** **A.** Somatic voltage trace and phase plot. **B.** Peak Na current (left) and proportion of open axonal Na channels (right) versus holding potential in somatic voltage-clamp. **C.** Membrane potential across the neuron at different instants near spike initiation. **D.** Balance of currents at initiation site (bottom) near spike initiation (top and middle: voltage trace)

when measured at the same value of  $dV/dt$ , phase slope can be very different in the two cases: at 20 mV/ms, it is about 3 times larger with the larger soma than with the smaller soma (Fig. 3.8A, right). This is artifactual because the measurements are done in different parts of the spike. Therefore, we defined onset rapidness as the phase slope in the linear part of the phase plot, which corresponds to the maximum phase slope of the first component of the phase plot.

To isolate the contribution to onset rapidness due to the axonal current, in the following analysis we removed somatic Na channels from the models. As is shown on Fig. 3.8B for a somatic area of 10,000  $\mu\text{m}^2$  (left), the presence of somatic Na channels makes a small but significant difference in onset rapidness (39  $\text{ms}^{-1}$  with and 53  $\text{ms}^{-1}$  without). Fig. 3.8B (right) shows the axonal spike at the distal initiation site (dark blue) and at different places along the axon (light blue), when somatic Na channels are removed. It appears that the maximum  $dV/dt$  decreases approximately linearly as it travels to the soma, which can be directly explained by a resistive effect. In the critical resistive coupling hypothesis, the soma is driven at spike initiation by an axonal current that is essentially resistive, so that somatic onset rapidness should be determined by properties of the axonal spike at the initiation site. Specifically, somatic onset rapidness should equal the slope of a tangent to the axonal phase plot passing through spike threshold (see Methods), a value of the same magnitude as the maximum phase slope. As is shown on Fig. 3.8B (red), this theoretical prediction is satisfied in this model (50  $\text{ms}^{-1}$  vs. 53  $\text{ms}^{-1}$ ). In addition, the theory predicts that the same should hold at all axonal points between initiation site and soma, which is also approximately the case here (the red line is also almost tangent to all light blue curves). Thus, spikes do not sharpen as they travel to the soma; rather, the maximum phase slope is reached at lower and lower voltages.

This theoretical prediction matches somatic onset rapidness when somatic area is varied over several orders of magnitude (Fig. 3.8C, left). In fact, it can be seen that, as soon as somatic area is larger than a few hundred  $\mu\text{m}^2$ , somatic onset rapidness (orange) does not depend much on somatic area. For comparison, Fig. 3.8C (right) shows the change in total somatic capacitance over the same variation in somatic area. It may appear so only when onset rapidness is measured at a fixed value of  $dV/dt$  (grey), for the reasons explained above, as also observed by Eyal et al. (2014) in a model with a dendrite of varying size. Note that the high values of onset rapidness for small soma are somewhat artifactual because they correspond to a case when the somatic phase plot is monophasic and maximum onset rapidness is reached at very high voltages (Fig. 3.7, left column).

We examined the simultaneous recordings of a spike in the soma and AIS bleb shown in Yu et al. (2008) so as to test the theoretical prediction. Fig. 3.8D shows the digitized

phase plots of the spike measured at the two sites. In the soma (orange), onset rapidness was about  $25 \text{ ms}^{-1}$ . In the AIS (blue), the phase plot was nearly linear in the rising phase, with a slope of  $23 \text{ ms}^{-1}$  (note the different vertical scale). This match supports the resistive coupling hypothesis.

Thus, neither active backpropagation nor capacitive effects of the somatodendritic compartment sharpen spikes. Rather, the same value of maximum rapidness is reached at a lower voltage in the soma than in the axon. In fact, not only are spikes not sharpened by propagation, but their maximum slope ( $dV/dt$ ) is in fact scaled down as they approach the soma (Fig. 3.8B, right), in agreement with the resistive coupling theory and with direct axonal measurements (Kole et al. 2008; Fig. 5 therein).

### 3.4.7 Active backpropagation is not necessary for sharp spike initiation

We have seen that active backpropagation is not sufficient for sharp spike initiation. We next show that it is also not necessary (Fig. 3.9), both in the simple model (left column) and the morphologically detailed model (right column). We move all axonal Na channels to the same compartment, thereby suppressing active backpropagation. The exact result depends on the location of that compartment, in agreement with theoretical predictions (Brette, 2013), but in all cases, phase plots are biphasic, with initial onset rapidness between  $46$  and  $71 \text{ ms}^{-1}$  for the simple model and between  $56$  and  $76 \text{ ms}^{-1}$  for the detailed model (Fig. 3.9A). In detail, the voltage at spike onset decreases with increasing distance of the Na channels, and so does the maximum  $dV/dt$  in the first component of the phase plot. These features appear more clearly in somatic voltage-clamp (Fig. 3.9B). In all cases, Na channels open as a step function of somatic voltage. The spike threshold, corresponding to the discontinuity point in the current-voltage relationship, decreases when Na channels are placed further away, and peak axonal Na current also decreases with increasing distance. Thus the neuron is more excitable when Na channels are placed further away, but the axonal current transmitted to the soma is smaller. These two features are predicted by critical resistive coupling because the resistive axo-somatic current is smaller when Na channels are further away, so that a smaller Na current is required to trigger a spike, and a smaller resistive current is transmitted to the soma (Brette, 2013). Despite these quantitative variations with the distance of the initiation site, the sharpness of spike initiation is unaffected by the exact distance: except when Na channels are very close to the soma, somatic onset rapidness is essentially independent of Na channel distance, around  $70 \text{ ms}^{-1}$  (Fig. 3.9C). This value is also close (in fact slightly higher) to the value obtained when Na channels are distributed across the AIS (about

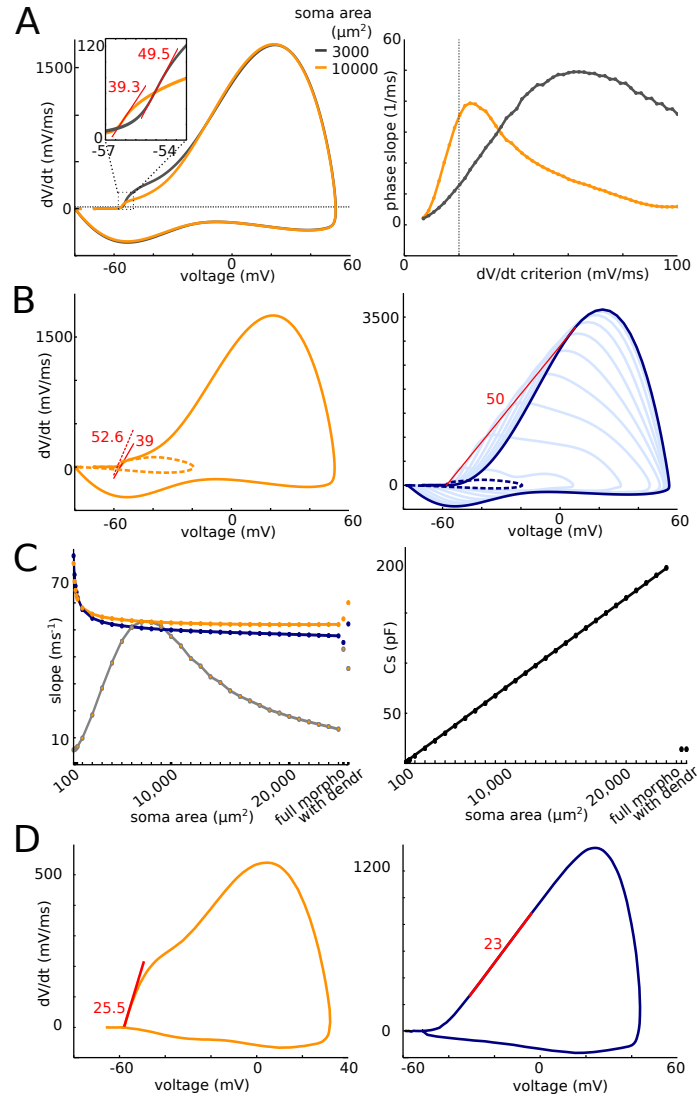


Figure 3.8: **Somatic onset rapidness.** **A.** Phase plot of a somatic spike with a large soma (orange,  $10,000 \mu\text{m}^2$ ) and a small soma (gray,  $3,000 \mu\text{m}^2$ ). The phase plot is linear (corresponding to locally constant phase slope) around  $dV/dt = 25 \text{ mV/ms}$  in the former case and around  $60 \text{ mV/ms}$  in the latter case. Maximum phase slope is similar in both cases ( $39.3$  and  $49.5 \text{ ms}^{-1}$ ). **B.** Left: phase plot for a large soma ( $10,000 \mu\text{m}^2$ ). The presence of somatic Na channels slightly decreases onset rapidness (orange, slope:  $39 \text{ ms}^{-1}$ ). Without them, onset rapidness is  $52.6 \text{ ms}^{-1}$ . Right: phase plots at different points along the axon (dotted blue: soma; dark blue: distal end; light blue: intermediate axonal positions). The prediction of somatic onset rapidness based on resistive coupling is the maximum slope of a tangent to the phase plot intersecting the spike initiation point, which gives  $50 \text{ ms}^{-1}$  at the distal end (red line). **C.** Left: Somatic onset rapidness (orange) and prediction from axonal phase plots (blue) as a function of soma area for the simple model. The morphologically detailed model and the simple model with a dendrite are also shown on the right. Grey: somatic phase slope at  $20 \text{ mV/ms}$ . Right: For comparison, total somatic capacitance is shown as a function of soma area. **D.** Somatic (left) and axonal (right) phase plots of a spike digitized from Yu et al. (2008). Maximum phase slopes are similar.

50 ms<sup>-1</sup>). Therefore active backpropagation is not necessary to produce sharp spikes, and in fact does not contribute in making spikes sharper.

### 3.4.8 Sharp somatic onset is reproduced by a model with two resistively coupled compartments

Finally, we designed a minimal two-compartment model that displays these features (Fig. 3.10A). The model included only Na and K channels with voluntarily highly simplified kinetics, with single gates and voltage-independent time constants, so as to show that the phenomenon is due to critical resistive coupling and not to specificities of channel kinetics (equilibrium values of gating variables shown in Fig. 3.10A). The maximum somatic Na conductance determines the threshold for spike regeneration in the soma (second component of the phase plots) (Platkiewicz and Brette, 2010); it was set at  $g_{\text{Na}_{\text{soma}}} = 800$  nS. For a somatic area of  $2000 \mu\text{m}^2$  (corresponding to a  $30 \mu\text{m}$  by  $20 \mu\text{m}$  cylinder), this value corresponds to a conductance density of  $400 \text{ pS}/\mu\text{m}^2$ . The somatodendritic compartment is connected to the AIS compartment by a resistance  $R_a$ . As shown in Fig. 3.9, this value determines the maximum  $dV/dt$  in the first component of the somatic phase plot (by Ohms law, it is inversely proportional to  $R_a$ ), and we chose  $R_a = 4.5 \text{ M}\Omega$ . This value corresponds to the onset of the AIS, close to the soma (rather than the distal initiation site), that is, the closest location where we expect to see a full spike at spike initiation. Finally, spike threshold is determined by the product  $g_{\text{Na}_{\text{axon}}}\cdot R_a$  (Brette, 2013), and we chose  $g_{\text{Na}_{\text{axon}}} = 1200$  nS accordingly. For an AIS area of  $50 \mu\text{m}^2$ , this corresponds to a conductance density of about  $7500 \text{ pS}/\mu\text{m}^2$ . Again, this value should be considered as an effective value and an overestimation of true conductance density, because distal channels have a greater impact on spike threshold and therefore require less conductance ( $R_a$  is greater at the distal end).

With these parameter values, which are all within reasonable physiological ranges, we can see on Fig. 3.10B that the model exhibits sharp somatic spikes (onset rapidness:  $17 \text{ ms}^{-1}$ ) and a biphasic somatic phase plot, while in the AIS (Fig. 3.10C) spikes are smooth. The model also has a discontinuous current-voltage relationship measured in somatic voltage-clamp (Fig. 3.10D, left), as experimentally observed (Milescu et al., 2010). Finally, despite the order of magnitude difference between somatic and axonal Na conductance densities, total Na influxes in the AIS and in the soma are comparable (50% larger in AIS; Fig. 3.10D, right), as experimentally observed (Fleidervish et al., 2010). This occurs because the total conductances over each of the two compartments are in fact comparable. In detail, spike shape is not identical to measurements and this is expected given the simplicity of the model, but all features of sharp spike initiation are

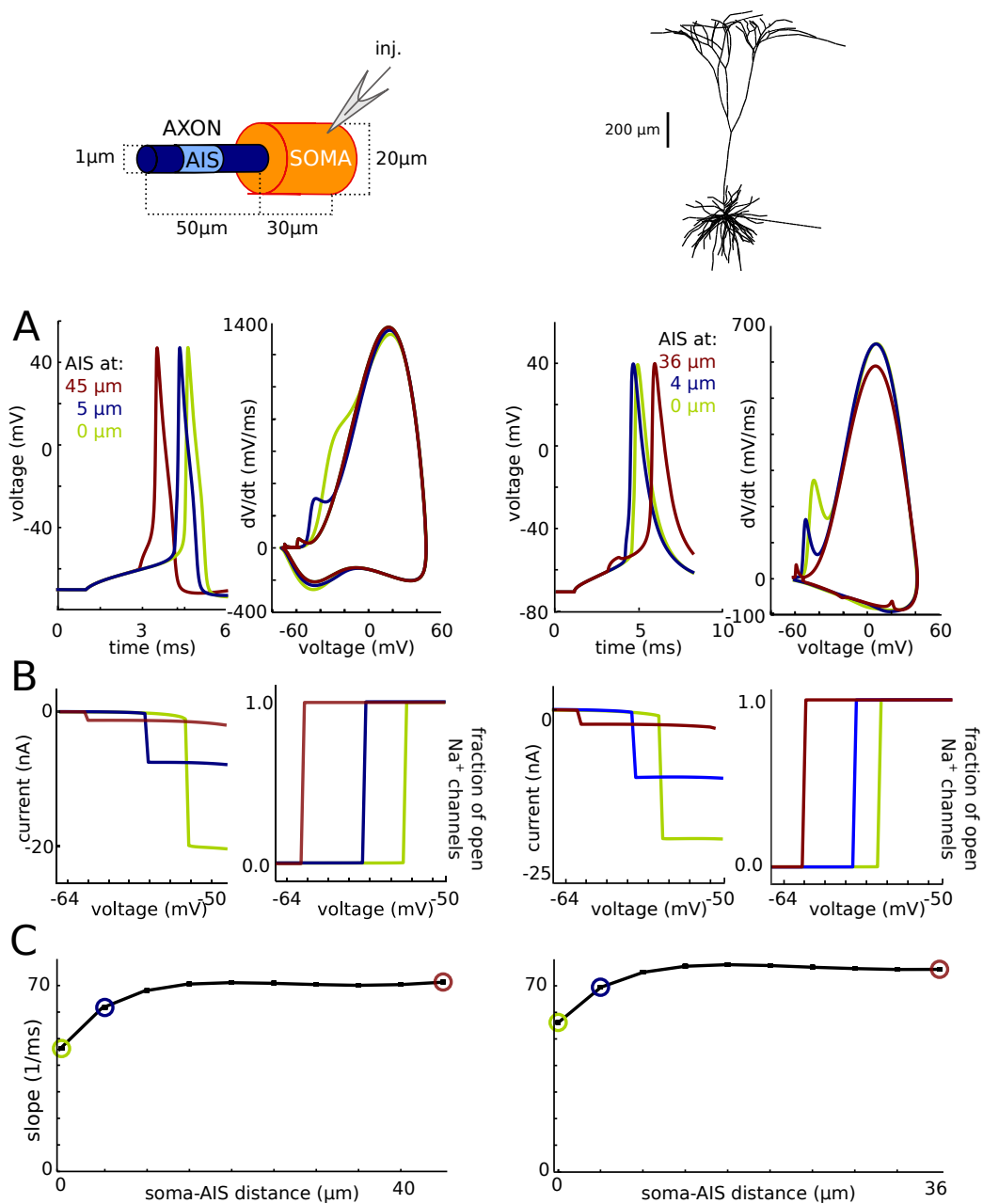


Figure 3.9: **Active backpropagation is not necessary for sharp initiation.** Left: model with simplified soma-axon geometry. Right: cortical pyramidal cell model with morphological reconstruction. **A.** Axonal Na channels are moved to a single axonal location (3 different locations shown). Left: voltage traces; right: phase plots. **B.** Peak Na current (left) and proportion of open axonal Na channels (right) versus holding potential in somatic voltage-clamp. **C.** Onset rapidness as a function of AIS position.

present even though the transmission of the axonal spike to the soma is purely resistive.

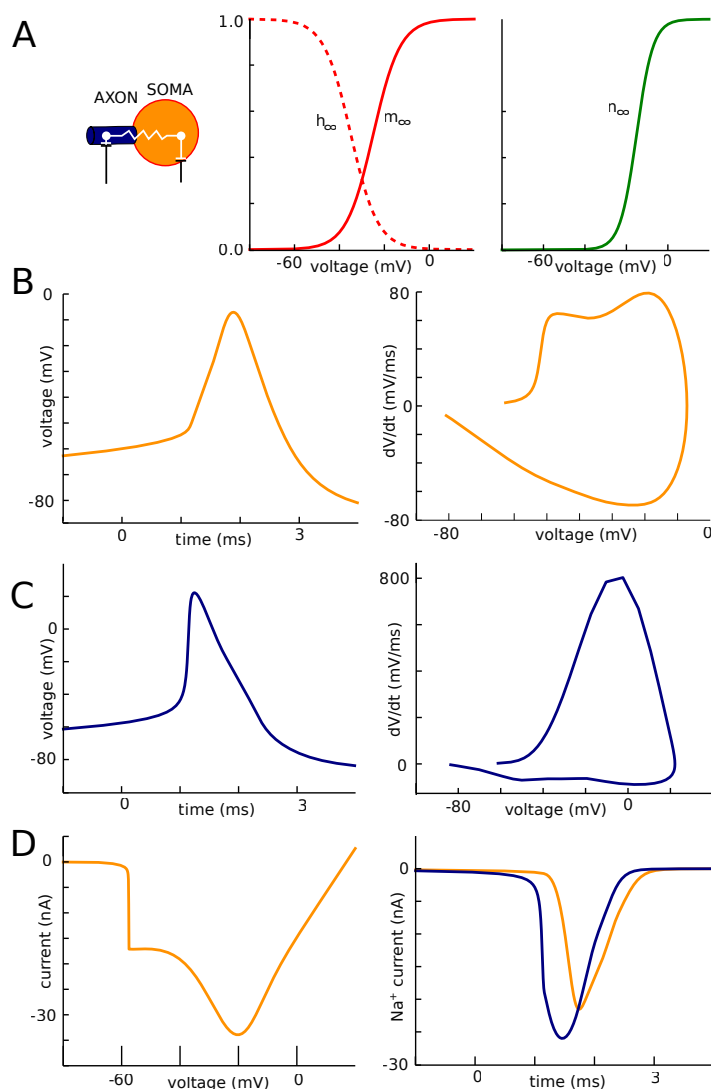


Figure 3.10: **Two-compartment model.** **A.** Equilibrium values of the gating variables for the Na (left) and K (right) channels. **B.** Voltage trace (left) and phase plot (right) of a somatic spike. **C.** Voltage trace (left) and phase plot (right) of an AIS spike. **D.** Left: Peak current recorded in somatic voltage-clamp as a function of holding voltage. Right: Na current in the AIS (blue) and soma (orange) during a spike in current-clamp.

## 3.5 Discussion

By examining multicompartmental Hodgkin-Huxley models of spike initiation that reproduce the sharp onset of somatic spikes, we have found that active backpropagation

and capacitive currents have no role in this phenomenon. Previous studies proposed that active channels between the initiation site and the soma increase spike onset rapidness. We have shown that entirely suppressing those currents has no effect on somatic onset rapidness. It has also been proposed that spike onset rapidness is further increased by the capacitance of the somatodendritic compartment (Eyal et al., 2014; Yu et al., 2008). We have shown that the increased somatic onset rapidness with larger capacitances observed in models is an artifact resulting from measuring phase slope at a fixed arbitrary value of  $dV/dt$ . When defined as the phase slope in the linear part of the phase plot, somatic onset rapidness does not change when capacitance is increased beyond a critical value. Finally, somatic onset rapidness can be directly predicted from spike shape at the distal initiation site (as maximum phase slope). Therefore, the sharpness of somatic spike onset in these models does not result from the properties of spike propagation, but rather of spike initiation.

The biophysical models examined in this study were precisely those used in a previous study to support the backpropagation hypothesis (Yu et al., 2008), as well as an independent biophysical model, more tightly constrained by experimental data (Hallermann et al., 2012). Thus, no known biophysical model currently supports the backpropagation account of spike initiation sharpness. Instead, our analysis supports a biophysical explanation based on resistive coupling between the soma and the initiation site, where the soma effectively clamps the voltage at the start of the axon at spike initiation. According to this account, and as we have shown in these models, the main current opposing the Na current at spike initiation is not the transmembrane K current (i.e., mostly the leak), but the axial resistive current between the soma and initiation site. As a result, spikes initiate by the soma and AIS forming an electrical dipole, with current flowing between the two poles and charging the soma. Therefore, the phenomenon is not well modeled by the propagation of an electrical wave, with a dipole travelling from AIS to soma, since the size of the dipole (wavelength) is the entire distance to be travelled. The observed delay between axonal and somatic spikes is thus better understood as a charging time than a propagation delay. One implication is that spike initiation is not a local axonal event, and therefore its characteristics are determined by the properties of the soma-AIS system, in particular its geometry. Specifically, the sharpness of spike initiation arises from the geometrical heterogeneity of that system. It could be opposed that small neurons would then be expected to display smooth spike initiation. For example, cerebellar granule cells have a capacitance of just 3–4 pF (Diwakar et al., 2009) (corresponding to about  $300 \mu\text{m}^2$  of membrane). However, these cells also have very thin axons, with a diameter of about 0.2–0.3  $\mu\text{m}$  (Perge et al., 2012; Wyatt et al., 2005), and therefore the somatodendritic area is still relatively large in comparison. Figure 3.11 shows indeed

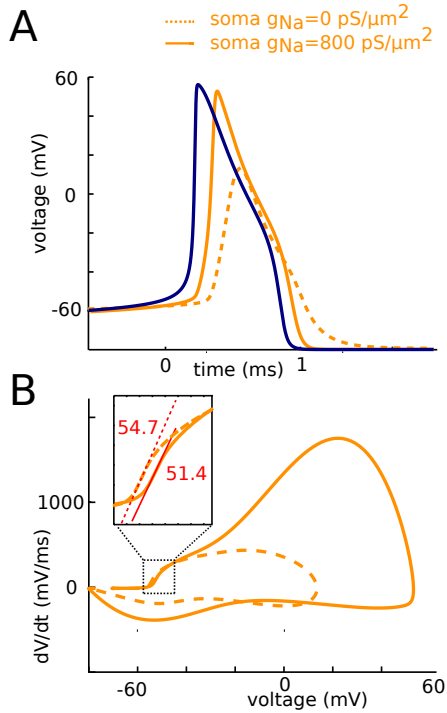
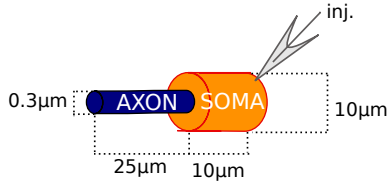


Figure 3.11: **Sharpness of spike initiation in a small simulated neuron (axon diameter: 0.3  $\mu\text{m}$ ).** **A.** Action potential in the axon (blue) and distal AIS (orange; dotted: with no somatic Na channels). **B.** Corresponding phase plot of the action potential, showing onset rapidness greater than  $50 \text{ ms}^{-1}$  (inset).

that with this geometry, the model still displays sharp spike initiation. Experimentally, hippocampal dentate granule cells, another type of granule cell, have a distinct kink at spike onset (Schmidt-Hieber et al., 2008).

In a simplified two-compartment model representing the soma-AIS dipole, it was previously shown that spikes are initiated abruptly if the product of axial resistance and maximum Na conductance exceeds a critical value (Brette, 2013). Phenomenologically (but not biophysically), the corresponding model is mathematically quasi-equivalent to the cooperative gating model of spike initiation (Naundorf et al., 2006) and therefore shares all its functional properties. A major common feature between these two models, supported by our analysis of the biophysical models and by experiments (Milescu et al., 2010), is that peak axonal current varies abruptly with somatic voltage, while current latency is inversely related to the difference between somatic voltage and threshold. A specific feature of the resistive model, also observed in the biophysically detailed models, is that increasing axial resistance, and therefore reducing axial currents, makes the neuron more excitable. This feature has been previously suggested to underlie structural

tuning of the AIS (Kuba, 2012).

As we have mentioned, an alternative hypothesis is that Na channels in the AIS cooperate, so that they effectively open all at once when the axonal voltage exceeds a threshold (Naundorf et al., 2006). Cooperative activation has been demonstrated in calcium (Marx et al., 2001, 1998), potassium (Molina et al., 2006) and HCN channels (Dekker and Yellen, 2006), and in pharmacologically altered Na channels of cardiac myocytes (Undrovinas et al., 1992). It should appear in AIS phase plots as a very large increase in  $dV/dt$  at spike initiation (Öz et al., 2015), with a biphasic phase plot if only part of the channels (e.g. the Nav1.6 subtype) cooperate (Huang et al., 2012). However, phase plots of spikes recorded in axonal blebs near the AIS are monophasic, with a gradual increase with voltage as expected with non-cooperative channels (McCormick et al., 2007; Yu et al., 2008). In isolated blebs, TTX has no effect on half-activation voltage of Na channels, whereas cooperativity predicts an increase (Hu et al., 2009). It has been opposed that cooperativity may depend on the intact cytoskeleton of the AIS, which might be disrupted in axonal blebs (Naundorf et al., 2007), but the axonal bleb recordings were performed simultaneously with somatic recordings, which did exhibit a distinct kink at spike onset. Finally, voltage traces recorded in whole cell patch clamp in intact axons appear very similar to axonal bleb recordings and show no sign of cooperativity, with a smooth spike onset at the AIS (Kole and Stuart, 2008). We conclude that at this date there is no evidence of cooperativity of Na channels in the AIS.

The cooperativity hypothesis was also motivated by the observation of input-output properties of cortical neurons that are not well accounted for by the standard account of spike initiation (Brette, 2015), in particular the fact that cortical neurons can transmit very high input frequencies (Ilin et al., 2013). The backpropagation account only addresses somatic spike shape, but not spike initiation per se. The critical resistive coupling model addresses both aspects because it is mathematically almost equivalent to the cooperativity model, although it has a different biophysical basis (axial resistance in the resistive model corresponds to channel coupling in the cooperativity model) and makes different predictions in the axonal initiation site.

We now discuss experimental evidence regarding the critical resistive coupling hypothesis, starting with the notion that the somatodendritic compartment is a current sink for the initiation site. First, the initiation site is very close to the soma, as previously noted, and axonal diameter is small compared to the soma, especially if the conductance load of the dendritic tree is considered (Hay et al., 2013). Thus, biophysical theory predicts that the soma is a current sink for the initiation site (Brette, 2013), i.e., that most Na current entering the AIS flows to the soma, producing a voltage gradient between the two sites. This prediction is backed up by several lines of evidence. First, there is generally

no voltage gradient across the two sites between spikes, but this gradient rises to about 7 mV near spike initiation due to the opening of Na channels (Kole and Stuart, 2008), a value close to the theoretical prediction of  $k_a$  (Boltzmann slope factor of Na channel activation) (Brette, 2013). Second, axonal outside-out patch-clamp recordings show that there is little K current flowing during the rising phase of the AIS spike (Hallermann et al., 2012). Third, Na imaging experiments show that the peak of Na influx during a spike occurs at an axonal position closer to the soma than the initiation site (Baranauskas et al., 2013). This is indeed expected if most Na current flows to the soma, because voltage then increases monotonously with distance from the soma (spatial gradient of voltage is proportional to axial current), so that spikes are initiated at the distal end of the AIS even though Na channel density may be lower.

Thus, there is convincing experimental evidence that the soma acts as a current sink for the initiation site, with most Na current flowing directly to the soma. Evidence that the product of axial resistance and Na conductance is large enough to produce an abrupt opening of Na channels is most directly provided by somatic voltage-clamp experiments, which show a discontinuity in the measured current-voltage relationship (Barrett and Crill, 1980; Milescu et al., 2010), although a finer resolution in the voltage commands would be desirable (voltage resolution is generally 5 mV). In practice, somatic voltage-clamp recordings are complicated by the fact that currents can be very large, and the precision of voltage clamping is limited to the product of current and uncompensated series resistance. Electrode artifacts could produce a discontinuity in observed current-voltage relationships when there is actually none. This cannot be the case in the data of (Barrett and Crill, 1980), since they used different electrodes for current passing and voltage measurement (two-electrode voltage-clamp). This was also not the case in Milescu et al. (2010) because continuous currents of the same magnitude were observed when axonal channels were inactivated with a prepulse. In that study, currents were reduced by applying a small dose of TTX. Indirect evidence about the discontinuous opening of Na channels, including somatic spike onset and input-output properties, is reviewed in Brette (2015). Finally, the comparison of somatic onset rapidness and axonal phase slope also matches theoretical predictions (Fig. 3.5D), although more experimental recordings would be required to test these predictions.

To test the critical resistive coupling theory more directly, one would need to manipulate the axial resistance between soma and initiation site. The neuron should be more excitable when axial resistance is increased, but the current transmitted to the soma should decrease. If the resistance were decreased very substantially, spike initiation should become smooth instead of sharp. We list here several experimental possibilities, chemical and mechanical, although none is particularly easy to perform. Intracellular

resistivity could be changed by manipulating the ionic composition of the intracellular medium. This is difficult because it must be compensated by corresponding changes in the extracellular medium to preserve osmotic equilibrium, without disturbing reversal potentials, but the extracellular and intracellular media cannot be modified simultaneously. In a similar way, extracellular resistance could be manipulated: although typically neglected in models, it has the effect of increasing the total axial resistance. For example, Hodgkin demonstrated that conduction velocity decreased when the axon was immersed in oil, which reduces the water volume around the axon to a thin layer (Hodgkin and Huxley, 1939). A similar experiment could be done to test changes in excitability. Another idea is to use osmotic pressure to change the diameter of the axon, thereby changing total axial resistance. However, it is possible that the dense cytoskeleton of the AIS provides rigidity so that changes in shape might be limited to the soma. Finally, pinching the base of the axon with two glass pipettes would increase axial resistance, and it has been done with dendrites (Bekkers and Häusser, 2007). All of these experimental ideas are challenging, but not impossible in principle.

In conclusion, biophysical modeling and experimental evidence support the notion that, in neurons with an AIS, normal spike initiation results from the interplay between the Na current and the resistive axial current flowing between the AIS and soma, rather than between local transmembrane Na and K (leak) currents as in somatic and ectopic initiation (in an axon far from the soma). This means that the mechanism of spike initiation is not local to the axon, but rather occurs through the formation of a resistively coupled soma-AIS dipole. This situation occurs because of the large variation in geometry and biophysical properties over a small spatial scale. Accordingly, at least in the biophysical models that we have examined, the kink at somatic spike onset results from strong coupling of the soma-AIS system, rather than from an artifact of somatic recording.

## 3.6 Materials and methods

### 3.6.1 Detailed neuron models

We used two spatially extended neuron models described in Yu et al. (2008), a simple model of a cylindrical soma and a cylindrical 50  $\mu\text{m}$  long axon (diameter 1  $\mu\text{m}$ ) available on ModelDB (Hines et al., 2004) and a morphologically detailed model based on a reconstruction of a cortical pyramidal cell (personal communication of Prof. Yuguo Yu). We also used a multicompartmental model of a pyramidal cell described in Hallermann et al. (2012), also available on ModelDB. These models were implemented in Neuron

7.4 (Hines and Carnevale, 1997) with time step  $1 \mu\text{s}$  and analyzed in Python. In Fig. 3.3, the extracellular field was computed with the standard line source method (Einevoll et al., 2013; Holt and Koch, 1999), with extracellular conductivity  $\sigma = 0.3 \text{ S}\cdot\text{m}^{-1}$ , and simulated with the NeuronEAP Python library (Telenczuk and Telenczuk, 2016).

### 3.6.1.1 Morphology

The simple model consists of an axon modeled as a cylinder of length  $50 \mu\text{m}$  and diameter  $1 \mu\text{m}$ , and a soma modeled as a cylinder of variable length and diameter (the bleb and dendrite were not included unless stated otherwise). In Fig. 3.2 and 3.6, the soma has diameter  $20 \mu\text{m}$  and length  $30 \mu\text{m}$ . In Fig. 3.4 and 3.5, soma size was varied with equal length and diameter. In one case (Fig. 3.4C-D), we kept the dendrite of length  $3000 \mu\text{m}$  and diameter  $5 \mu\text{m}$  (60 segments). The first morphologically detailed model (Yu et al., 2008) is based on a reconstructed layer 5 cortical pyramidal cell. The axon consists of a  $10 \mu\text{m}$  long axon hillock, with diameter tapering from  $4.8 \mu\text{m}$  to  $1.2 \mu\text{m}$ , connected to an initial segment of diameter  $1.2 \mu\text{m}$  and length  $40 \mu\text{m}$ , followed by a  $500 \mu\text{m}$  myelinated axon with 5 nodes of Ranvier separated by  $100 \mu\text{m}$ . The second morphologically detailed model (Hallermann et al., 2012) is also based on a reconstructed layer 5 cortical pyramidal cell, and we used the model as described in that reference.

### 3.6.1.2 Channel properties

Passive properties were set as in Yu et al. (2008): specific membrane capacitance  $C_m = 0.75 \text{ pS}/\mu\text{m}^2$ , intracellular resistivity  $R_i = 150 \Omega\cdot\text{cm}$ , specific membrane resistance  $R_m = 30,000 \Omega\cdot\text{cm}^2$ , leak reversal potential  $E_L = -70 \text{ mV}$ , membrane time constant  $\tau = 22.5 \text{ ms}$ . In the simple model, Na conductance densities were  $8000 \text{ pS}/\mu\text{m}^2$  in the axon, 0 or  $800 \text{ pS}/\mu\text{m}^2$  in the soma and  $20 \text{ pS}/\mu\text{m}^2$  in the dendrite. In the morphologically detailed model, Na conductance densities were  $8000 \text{ pS}/\mu\text{m}^2$  in the hillock and in the axon initial segment,  $800 \text{ pS}/\mu\text{m}^2$  in the soma and  $100 \text{ pS}/\mu\text{m}^2$  in dendrites. In the simple model, we only included Na and potassium channels; in the morphologically detailed model, we used all the channels present in the original model. Detailed channel kinetics and properties of other channels are described in Yu et al. (2008)

In Fig. 3.9 we moved all channels involved in spike generation (Na and potassium) to a single compartment while maintaining the same total conductance. As the initial segment consists of 10 compartments, this corresponds to multiplying conductance densities by 10 in the target compartment and setting them to 0 in all other compartments.

## 3.6.2 Two-compartment model

The two-compartment model represents the soma and the axon initiation site, coupled by axial resistance  $R_a = 4.5 \text{ M}\Omega$ . Capacitances are  $C_s = 250 \text{ pF}$  for the soma, in the range of values measured in layer 5 pyramidal neurons of rats (Arsiero et al., 2007), and  $C_a = 5 \text{ pF}$  for the axon. The axonal value was chosen empirically, as in reality axon impedance is highly frequency-dependent. Leak conductance is  $12 \text{ nS}$  (corresponding to a  $20 \text{ ms}$  membrane time constant) and leak reversal potential is  $-80 \text{ mV}$ .

For ionic channels, we deliberately used the simplest possible models so as to show that the sharpness of spikes does not result from subtle aspects of their detailed properties (Fig. 3.10A). Na channel activation is modeled with first-order kinetics, half-activation  $-25 \text{ mV}$ , Boltzmann slope  $6 \text{ mV}$ , time constant  $100 \mu\text{s}$  (voltage-independent). Na channel inactivation is considered independent with time constant  $0.5 \text{ ms}$ , half-inactivation voltage  $-35 \text{ mV}$ , Boltzmann slope  $6 \text{ mV}$ . K channels are also modeled with first-order kinetics, half-activation  $-15 \text{ mV}$ , Boltzmann slope  $4 \text{ mV}$ , time constant  $2 \text{ ms}$ . Total Na conductance is  $800 \text{ nS}$  in the soma and  $1200 \text{ nS}$  in the axon; total K conductance is  $2200 \text{ nS}$  in the soma and  $1200 \text{ nS}$  in the axon.

The model was simulated with the Brian simulator 2.0 (Stimberg et al., 2014).

## 3.6.3 Analysis

### 3.6.3.1 Voltage-clamp

In voltage-clamp measurements, the soma was clamped to a holding potential and the current was measured and corrected for the leak current with the P/n protocol, as in Bezanilla and Armstrong (1977); Miles et al. (2010). The peak current is shown as a function of holding potential.

### 3.6.3.2 Phase slope

The standard way of measuring onset rapidness is to calculate the slope of the phase plot ( $dV/dt$  vs  $V$ ) at a certain value of  $dV/dt$  (typically  $5\text{-}20 \text{ mV/ms}$ ). In real somatic recordings, the phase plot is approximately linear over a wide enough range of  $dV/dt$  values, so that the exact choice is not critical (Baranauskas et al., 2010) (see Fig. 2F therein). However, in models where morphological parameters are varied over several orders of magnitude, the phase plot can be linear around different values of  $dV/dt$  (Fig. 3.8). Therefore, we defined onset rapidness as the phase slope in the linear part of the phase plot, which corresponds to the maximum phase slope. When the spike is regenerated at the soma (somatic Na channels), there are two local maxima and we choose the smaller

one (closer to spike onset).

### 3.6.4 Theoretical prediction of onset rapidness

From the resistive coupling hypothesis, we can derive a theoretical prediction about somatic onset rapidness. We first assume that the major somatic current at spike initiation is the axonal current, so that the membrane equation reads:

$$C \frac{dV}{dt} = I$$

where  $C$  is membrane capacitance. Phase slope is then:

$$\frac{\frac{d^2V}{dt^2}/dV}{dt} = \frac{dI}{dt}/I$$

The resistive coupling hypothesis postulates that the axonal current is a resistive current:

$$I = \frac{V_a - V}{R_a}$$

where  $V_a$  is axonal voltage and  $R_a$  is axial resistance between the two sites. It follows that:

$$\text{somatic phase slope} = \frac{dV_a}{dt} / (V_a - V)$$

Assuming further that the axonal spike develops before the somatic spike, we consider that  $V$  is close to spike threshold. Onset rapidness is defined as the maximum phase slope (for the first component), as discussed above, and therefore should correspond to the maximum value of the formula above. Graphically, this maximum corresponds to the slope of a tangent to the axonal phase slope, starting from threshold (Fig. 3.8B, right). This value is in fact close to the maximum axonal phase slope. A simplified theoretical prediction is thus that somatic onset rapidness (or initial phase slope) approximately equals maximum axonal phase slope.

## 3.7 Acknowledgments

We thank Yuguo Yu for sharing the code of his morphologically detailed model.

---

## Bibliography

---

- Arsiero, M., Lüscher, H.-R., Lundstrom, B. N., and Giugliano, M. (2007). The impact of input fluctuations on the frequency–current relationships of layer 5 pyramidal neurons in the rat medial prefrontal cortex. *The Journal of neuroscience*, 27(12):3274–3284.
- Baranauskas, G., David, Y., and Fleidervish, I. A. (2013). Spatial mismatch between the Na<sup>+</sup> flux and spike initiation in axon initial segment. *Proceedings of the National Academy of Sciences*, 110(10):4051–6.
- Baranauskas, G., Mukovskiy, A., Wolf, F., and Volgushev, M. (2010). The determinants of the onset dynamics of action potentials in a computational model. *Neuroscience*, 167(4):1070–1090.
- Barrett, J. N. and Crill, W. E. (1980). Voltage clamp of cat motoneurone somata: properties of the fast inward current. *The Journal of physiology*, 304:231–249.
- Bekkers, J. M. and Häusser, M. (2007). Targeted dendrotomy reveals active and passive contributions of the dendritic tree to synaptic integration and neuronal output. *Proceedings of the National Academy of Sciences of the United States of America*, 104(27):11447–11452.
- Bezánilla, F. and Armstrong, C. M. (1977). Inactivation of the sodium channel. I. Sodium current experiments. *The Journal of general physiology*, 70(5):549–66.
- Brette, R. (2013). Sharpness of Spike Initiation in Neurons Explained by Compartmentalization. *PLoS Computational Biology*, 9(12):e1003338.
- Brette, R. (2015). What Is the Most Realistic Single-Compartment Model of Spike Initiation? *PLoS Computational Biology*, 11(4):1–13.
- Debanne, D., Campanac, E., Bialowas, A., Carlier, E., and Alcaraz, G. (2011). Axon physiology. *Physiological Reviews*, 91(2):555–602.
- Dekker, J. P. and Yellen, G. (2006). Cooperative gating between single HCN pacemaker channels. *The Journal of general physiology*, 128(5):561–7.

- Diwakar, S., Magistretti, J., Goldfarb, M., Naldi, G., and D'Angelo, E. (2009). Axonal Na<sup>+</sup> Channels Ensure Fast Spike Activation and Back-Propagation in Cerebellar Granule Cells. *J Neurophysiol*, 101:519–532.
- Einevoll, G. T., Kayser, C., Logothetis, N. K., and Panzeri, S. (2013). Modelling and analysis of local field potentials for studying the function of cortical circuits. *Nature Reviews Neuroscience*, 14(11):770–785.
- Eyal, G., Mansvelder, H. D., de Kock, C. P. J., and Segev, I. (2014). Dendrites impact the encoding capabilities of the axon. *The Journal of neuroscience*, 34(24):8063–71.
- Fleidervish, I. a., Lasser-Ross, N., Gutnick, M. J., and Ross, W. N. (2010). Na<sup>+</sup> imaging reveals little difference in action potential-evoked Na<sup>+</sup> influx between axon and soma. *Nature neuroscience*, 13(7):852–860.
- Hallermann, S., de Kock, C. P. J., Stuart, G. J., and Kole, M. H. P. (2012). State and location dependence of action potential metabolic cost in cortical pyramidal neurons. *Nature neuroscience*, 15(7):1007–1014.
- Hay, E., Schürmann, F., Markram, H., and Segev, I. (2013). Preserving axosomatic spiking features despite diverse dendritic morphology. *Journal of neurophysiology*, 109(12):2972–2981.
- Hines, M. L. and Carnevale, N. T. (1997). The NEURON simulation environment. *Neural computation*, 9(6):1179–1209.
- Hines, M. L., Morse, T., Migliore, M., Carnevale, N. T., and Gordon, S. M. (2004). ModelDB : a Database to Support Computational Neuroscience. *Journal of computational neuroscience*, 17(1):7–11.
- Hodgkin, A. L. and Huxley, A. F. (1939). Action Potentials Recorded from Inside a Nerve Fibre. *Nature*, 144(3651):710–711.
- Holt, G. R. and Koch, C. (1999). Electrical interactions via the extracellular potential near cell bodies. *Journal of Computational Neuroscience*, 6(2):169–184.
- Hu, W., Tian, C., Li, T., Yang, M., Hou, H., and Shu, Y. (2009). Distinct contributions of Na(v)1.6 and Na(v)1.2 in action potential initiation and backpropagation. *Nature neuroscience*, 12(8):996–1002.
- Huang, M., Volgushev, M., and Wolf, F. (2012). A small fraction of strongly cooperative sodium channels boosts neuronal encoding of high frequencies. *PloS one*, 7(5):e37629.
- Ilin, V., Malyshev, A., Wolf, F., and Volgushev, M. (2013). Fast Computations in Cortical Ensembles Require Rapid Initiation of Action Potentials. *The Journal of Neuroscience*, 33(6):2281–2292.
- Jack, J. J. B., Noble, D., and Tsien, R. W. (1975). *Electric current flow in excitable cells*. Clarendon Press Oxford.
- Joshi, S. and Hawken, M. J. (2006). Loose-patch-juxtacellular recording in vivo—A method for functional characterization and labeling of neurons in macaque V1. *Journal of Neuroscience Methods*, 156(1-2):37–49.

- Koch, C., Bernander, Ö., and Douglas, R. J. (1995). Do neurons have a voltage or a current threshold for action potential initiation? *Journal of Computational Neuroscience*, 2(1):63–82.
- Kole, M. H. P., Ilschner, S. U., Kampa, B. M., Williams, S. R., Ruben, P. C., and Stuart, G. J. (2008). Action potential generation requires a high sodium channel density in the axon initial segment. *Nature neuroscience*, 11(2):178–86.
- Kole, M. H. P. and Stuart, G. J. (2008). Is action potential threshold lowest in the axon? *Nature neuroscience*, 11(11):1253–1255.
- Kuba, H. (2012). Structural tuning and plasticity of the axon initial segment in auditory neurons. *The Journal of physiology*, 590(Pt 22):5571–9.
- Marx, S. O., Gaburjakova, J., Gaburjakova, M., Henrikson, C., Ondrias, K., and Marks, A. R. (2001). Coupled gating between cardiac calcium release channels (ryanodine receptors). *Circulation research*, 88(11):1151–1158.
- Marx, S. O., Ondrias, K., and Marks, A. R. (1998). Coupled gating between individual skeletal muscle Ca<sup>2+</sup> release channels (ryanodine receptors). *Science*, 281(5378):818–821.
- McCormick, D. A., Shu, Y., and Yu, Y. (2007). Neurophysiology: Hodgkin and Huxley model still standing? *Nature*, 445(7123):E1—E2.
- Milescu, L. S., Bean, B. P., and Smith, J. C. (2010). Isolation of somatic Na<sup>+</sup> currents by selective inactivation of axonal channels with a voltage prepulse. *The Journal of neuroscience : the official journal of the Society for Neuroscience*, 30(22):7740–8.
- Molina, M. L., Barrera, F. N., Fernandez, A. M., Poveda, J. A., Renart, M. L., Encinar, J. A., Riquelme, G., and Gonzalez-Ros, J. M. (2006). Clustering and coupled gating modulate the activity in KcsA, a potassium channel model. *Journal of Biological Chemistry*, 281(27):18837–18848.
- Naundorf, B., Wolf, F., and Volgushev, M. (2006). Unique features of action potential initiation in cortical neurons. *Nature*, 440(7087):1060–3.
- Naundorf, B., Wolf, F., and Volgushev, M. (2007). Neurophysiology: Hodgkin and Huxley model - still standing? *Nature*, 445(7123):E2–E3.
- Öz, P., Huang, M., and Wolf, F. (2015). Action potential initiation in a multi-compartmental model with cooperatively gating Na channels in the axon initial segment. *Journal of Computational Neuroscience*, 39(1):63–75.
- Palmer, L. M. and Stuart, G. J. (2006). Site of action potential initiation in layer 5 pyramidal neurons. *The Journal of Neuroscience*, 26(6):1854–1863.
- Perge, J. a., Niven, J. E., Mugnaini, E., Balasubramanian, V., and Sterling, P. (2012). Why Do Axons Differ in Caliber? *The Journal of Neuroscience*, 32(2):626–638.
- Platkiewicz, J. and Brette, R. (2010). A threshold equation for action potential initiation. *PLoS computational biology*, 6(7):e1000850.

- Schmidt-Hieber, C., Jonas, P., and Bischofberger, J. (2008). Action potential initiation and propagation in hippocampal mossy fibre axons. *Journal of physiology*, 586(7):1849–57.
- Stimberg, M., Goodman, D. F. M., Benichoux, V., and Brette, R. (2014). Equation-oriented specification of neural models for simulations. *Frontiers in neuroinformatics*, 8.
- Telenczuk, B. and Telenczuk, M. (2016). NeuronEAP library. *Zenodo*, 10.5281/zenodo.49560.
- Teleńczuk, M., Fontaine, B., and Brette, R. (2016). The basis of sharp spike onset in standard biophysical models. *bioRxiv*.
- Testa-Silva, G., Verhoog, M. B., Linaro, D., De Kock, C. P. J., Baayen, J. C., Meredith, R. M., De Zeeuw, C. I., Giugliano, M., and Mansvelder, H. D. (2014). High bandwidth synaptic communication and frequency tracking in human neocortex. *PLoS biology*, 12(11):1–13.
- Undrovinas, A. I., Fleidervish, I. a., and Makielski, J. C. (1992). Inward sodium current at resting potentials in single cardiac myocytes induced by the ischemic metabolite lysophosphatidylcholine. *Circulation research*, 71(5):1231–1241.
- Wyatt, K. D., Tanapat, P., and Wang, S. S. H. (2005). Speed limits in the cerebellum: Constraints from myelinated and unmyelinated parallel fibers. *European Journal of Neuroscience*, 21(8):2285–2290.
- Yu, Y., Shu, Y., and McCormick, D. A. (2008). Cortical action potential backpropagation explains spike threshold variability and rapid-onset kinetics. *The Journal of neuroscience*, 28(29):7260–72.



---

## Local field potential generated by neurons with different localisation of axon initial segment

---

Here, we present unpublished results based on ongoing work of Maria Teleńczuk, Bartosz Teleńczuk and Romain Brette. In the previous chapter, we showed a simulation of the local field potential during action potentials. In the following section, we would like to explore the impact of the location of axon initial segment (AIS) on this field. Different neurons tend to have an AIS of different length and situated at different distances from the soma (Fried et al., 2009; Kuba et al., 2006). Furthermore, the AIS is plastic and its length and position can change as a result of elevated activity (Chand et al., 2015; Evans et al., 2013; Grubb and Burrone, 2010; Muir and Kittler, 2014) or as a consequence of a diseased state such as a stroke (Hinman et al., 2013; Schafer et al., 2009). We investigated whether the difference in position might be reflected in extracellular recordings of the action potential (AP). This might be of importance because in extracellular recordings, the amplitude and shape of the action potential often changes (for example in a burst, action potentials tend to decrease in amplitude and increase in duration) (Williams and Stuart, 1999), but the reasons are not always understood.

We will investigate whether the AP amplitude might be modulated by the shift in the AIS position, which could occur due to plastic changes in a time scale of hours (Evans et al., 2015) to days (Grubb and Burrone, 2010; Evans et al., 2013; Muir and Kittler, 2014). We compare the amplitude of the extracellular AP generated by models considering different AIS positions. Below we explain our results based on the calculations of extracellular potentials around electrical models of neurons. We have calculated the extracellular potential of a dipole in the near field and its far-field approximations and

compared it with field generated by a soma-axon calculated numerically using linear source approximation (LSA). We found that the AP amplitude varies in the near field with the position of AIS. We conclude that far-field dipole approximation is not sufficient to explain the field potential around the soma and the AIS. Although the differences between action potentials initiated at different distances from the soma should be visible experimentally, the exact location might be difficult to determine from the extracellular action potential without additional information, such as how far the electrode was placed from the soma. We might however be able to monitor the change of the AIS position over time in a single neuron by looking at the change in AP amplitude.

## 4.1 Results

### 4.1.1 Soma-axon model

In the simple neuron model consisting of a soma and an axon we shifted the  $\text{Na}^+$  and  $\text{K}^+$  channels in the axon to a single chosen location (5- $\mu\text{m}$ -long segment of the axon) which we will here call the axon initial segment (AIS), as it is where the action potential (AP) initiates. We then calculated the electric potential at different locations of the extracellular space to see if the shift of AIS is reflected extracellularly.

First, we recorded extracellular potential at various locations in the vertical axis from the soma (Fig. 4.1). Indeed, the location of the AIS has a pronounced effect on the amplitude of the extracellular action potential (Fig. 4.1B). At 20  $\mu\text{m}$  from soma (Fig. 4.1Ca), the extracellular potential initiated by the model with the AIS closest to soma (0  $\mu\text{m}$ , blue trace) has the smallest amplitude (measured from peak to valley) when compared with the other models with different AIS positions (7.8  $\mu\text{V}$  as compared to 10  $\mu\text{V}$  and 9.3  $\mu\text{V}$  for the models with AIS located 20  $\mu\text{m}$ , green trace, and 45  $\mu\text{m}$ , orange trace, from the soma). Since the extracellular potential decays proportionally with distance from the soma, in distant recordings the AIS location showed less influence on the extracellular AP amplitude than in the recordings done close to the cell. However, for all recordings points  $> 20 \mu\text{m}$  from the soma the extracellular potential is highest when the AIS is most distal from the soma and decreases when the AIS is moved closer to soma (Fig. 4.1Cc).

In addition to the amplitude, the shape of the action potential recorded extracellularly also changes proportionally with distance between soma and AIS (Figs. 4.1C and 4.2B, inset), while the intracellular waveforms remain similar (Fig. 4.2A, insets).

To study the effect of the AIS position on the extracellular action potential width, we calculated the extracellular potential generated by models with the AIS placed at ten

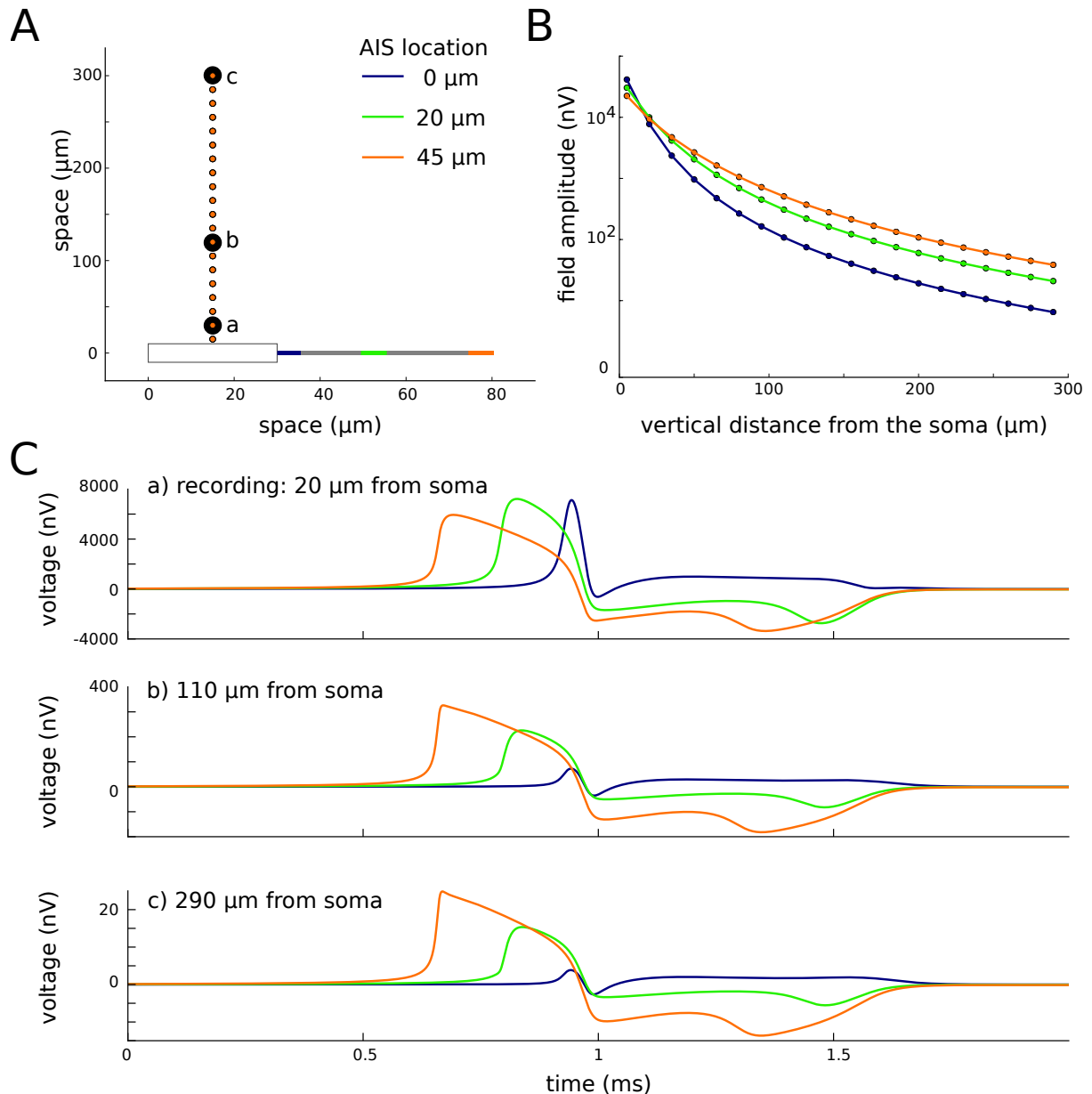


Figure 4.1: Extracellular potential calculated from the soma-axon model with the AIS at three different positions: 0  $\mu\text{m}$  from the soma (blue), 20  $\mu\text{m}$  from the soma (green) and 45  $\mu\text{m}$  from the soma (orange). **A**. Each dot represents the location of the measurement vertically from the soma. Black circles correspond to the locations of recordings shown in C. Schematics shows the cell body (left) and the axon (grey) with the AIS at different locations (color-coded). **B**. Double logarithmic plot of the peak-to-peak amplitude of the extracellular potential vs the distance of the recording site from the soma. Color lines correspond to different positions of the AIS (see color code in A). **C**. Example traces of extracellular fields recorded at different distances from the soma-axon axis (panels a-c, recording positions correspond to black circles in A) and different AIS positions (color lines). The traces are aligned such that 1 ms represents the peak of the action potential in the soma.

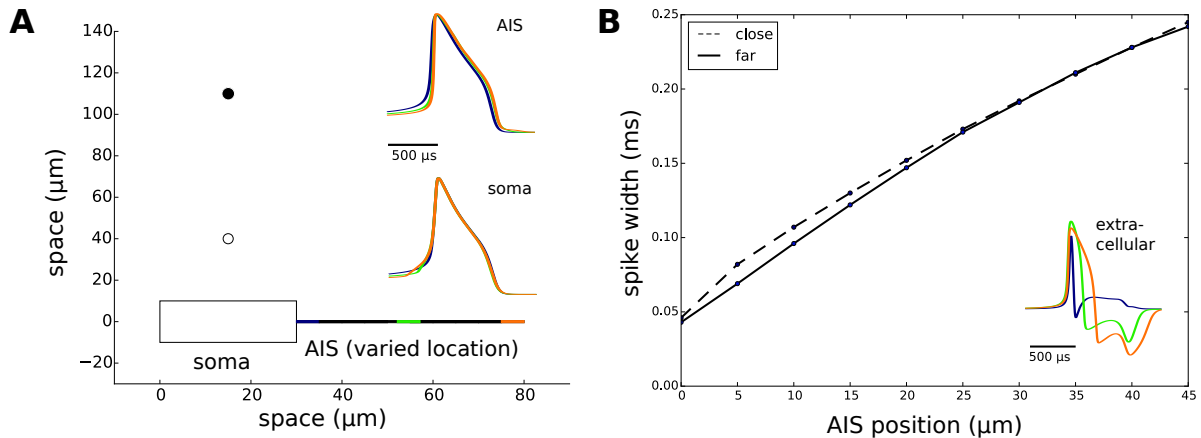


Figure 4.2: Width of the extracellular AP as the function of the soma-AIS separation. **A.** Schematic representation of the soma-axon model (bottom) and their relation to the recording points (dots above soma). The AIS position was systematically varied from 0 (directly attached to the soma) to 45  $\mu\text{m}$ . Insets: Waveforms of action potentials recorded intracellularly in the AIS (top inset) and the soma (bottom). **B.** Action potential width measured at half amplitude as a function of the AIS position for two different recording locations (close: 30  $\mu\text{m}$  from soma, far: 100  $\mu\text{m}$  from soma). Inset: Examples of extracellular AP wavershapes for 3 different locations of AIS (recorded 40  $\mu\text{m}$  above the soma, cf. Figure 4.1C).

different positions from the end of the soma, up to 45  $\mu\text{m}$  distally. We observed that the extracellular action potentials become gradually wider with increasing distance between the soma and the AIS (Fig. 4.2B). The functional form of this dependence changes only slightly with the location of the recording site (Fig. 4.2B, dashed vs. solid line).

This dependence of the amplitude and width of extracellular action potential on the AIS position could be due to two factors: (1) the distance of the measuring electrode from the extracellular potential generators, current sinks and sources, and (2) the change of magnitude and time course of these currents due to a change in AIS position. To isolate these two factors, we recorded the extracellular potential along a vertical axis passing through the middle point between the centers of the soma and AIS; this means that the horizontal position of the recording site changed when we moved the AIS along the axon. In this case the distances from the recording electrode to the current sink (AIS) and to the current source (soma) would remain equal independently of the position of the AIS. Even with this approach (Fig. 4.3) we found differences between the extracellular potential amplitude from neuron models with an AIS at different positions. The differences were even larger when compared to the former situation: the recordings performed in proximity to the axon (20  $\mu\text{m}$  away, Fig. 4.3C, top) showed amplitudes of 7.9  $\mu\text{V}$ , 2.6  $\mu\text{V}$  and 3.8  $\mu\text{V}$ , with distances of 0  $\mu\text{m}$ , 20  $\mu\text{m}$  and 45  $\mu\text{m}$ , respectively between the AIS and the soma.

The amplitude of the action potential was the highest for all probed distances of

recording electrodes from the axon, when the AIS was closest to the soma (Fig. 4.3C, blue trace in all panels). Note that for all distances above 100  $\mu\text{m}$  the change of the field with increasing AIS distance from the soma is reversed when compared to the recording over the soma, meaning that at a fixed position of the recording electrode, the action potential amplitude decreases with the increasing distance of the AIS (Fig. 4.3B).

Importantly, for two AIS locations (0 and 20  $\mu\text{m}$  from soma) the extracellular action potentials recorded at the midpoint between the soma and the AIS are of opposite polarity compared to the recordings over the soma (compare blue/green traces in Figure 4.1C with same traces in Figure 4.3C). To find the exact position of this polarity reversal we calculated the difference between the peak and trough amplitude of the extracellular AP recorded at different sites along a horizontal line parallel to the soma-AIS axis (Fig. 4.4). We found that the position at which the potential changes its polarity moves with the AIS location. However, the exact position of the polarity reversal did not always coincide with the midpoint between the soma and the AIS centers (Fig. 4.4, triangles).

### 4.1.2 Far-field dipole approximation

In a resistive, homogeneous medium the contribution of a single current source of intensity  $I$  (current monopole) to the extracellular potential is given by:

$$V_{mon} = \frac{1}{4\pi\sigma} \frac{I}{r} \quad (4.1)$$

where  $\sigma$  is the conductance of extracellular medium and  $r$  is the distance between the location of the recording electrode and the monopole.

A current dipole consists of two point-like sources of currents of equal intensities, but opposite directions (current sink and source) separated by a fixed distance. We can calculate its field by the superposition of two monopoles:

$$V_{dip} = V_{mon^+} + V_{mon^-} = \frac{I}{4\pi\sigma} \left( \frac{1}{r^+} - \frac{1}{r^-} \right) \quad (4.2)$$

where  $r^-$  and  $r^+$  are the distances of the recording site from the current sink and source, respectively.

When the distance between the two monopoles is small compared to the distance between the recording electrode and the midpoint between the two sources (far field), we can approximate this formula by:

$$V_{dip} \approx \frac{1}{4\pi\sigma} \frac{Id}{r^2} \cos(\theta) \quad (4.3)$$

where  $\theta$  is the angle between dipole axis (vector connecting source and sink) and position

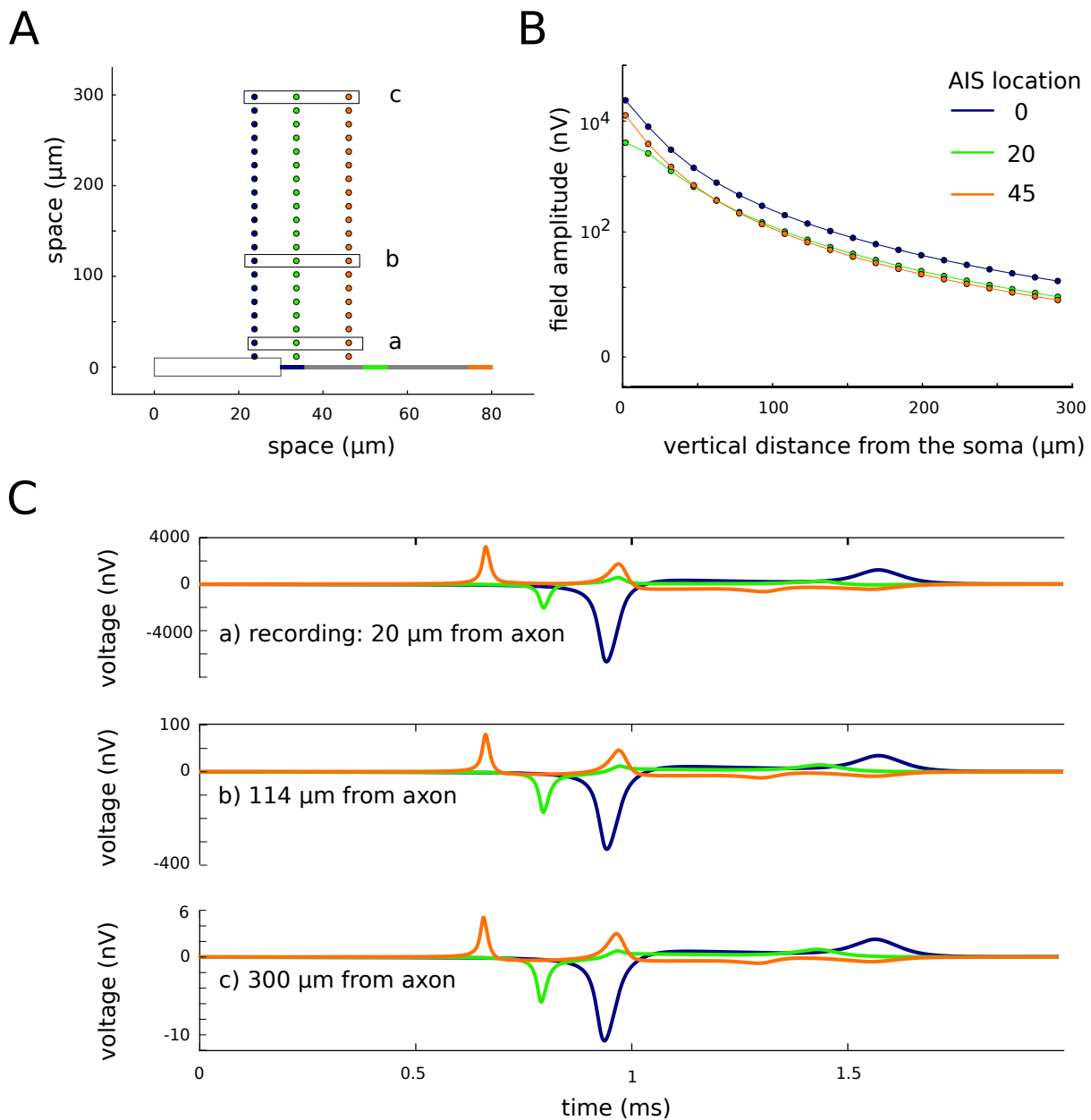


Figure 4.3: Extracellular AP measured along the midline between soma and AIS. **A**. The recording site lays in the middle between centers of soma and AIS. Colors correspond to the AIS position in the axon: 0  $\mu\text{m}$  (blue), 20  $\mu\text{m}$  (green) and 45  $\mu\text{m}$  from the soma (orange). The three vertical lines represent different midline positions for each of the AIS positions. **B**. The absolute peak-to-peak amplitude of the extracellular potential (on a log-scale) vs distance of the recording site from the soma-AIS midpoint. There is a large difference very close to the neuron which decays with the distance. **C**. Sample traces recorded at three locations (represented in A by the rectangles) for each of the AIS position. Note different voltage scales. For more details see caption of Figure 4.1.

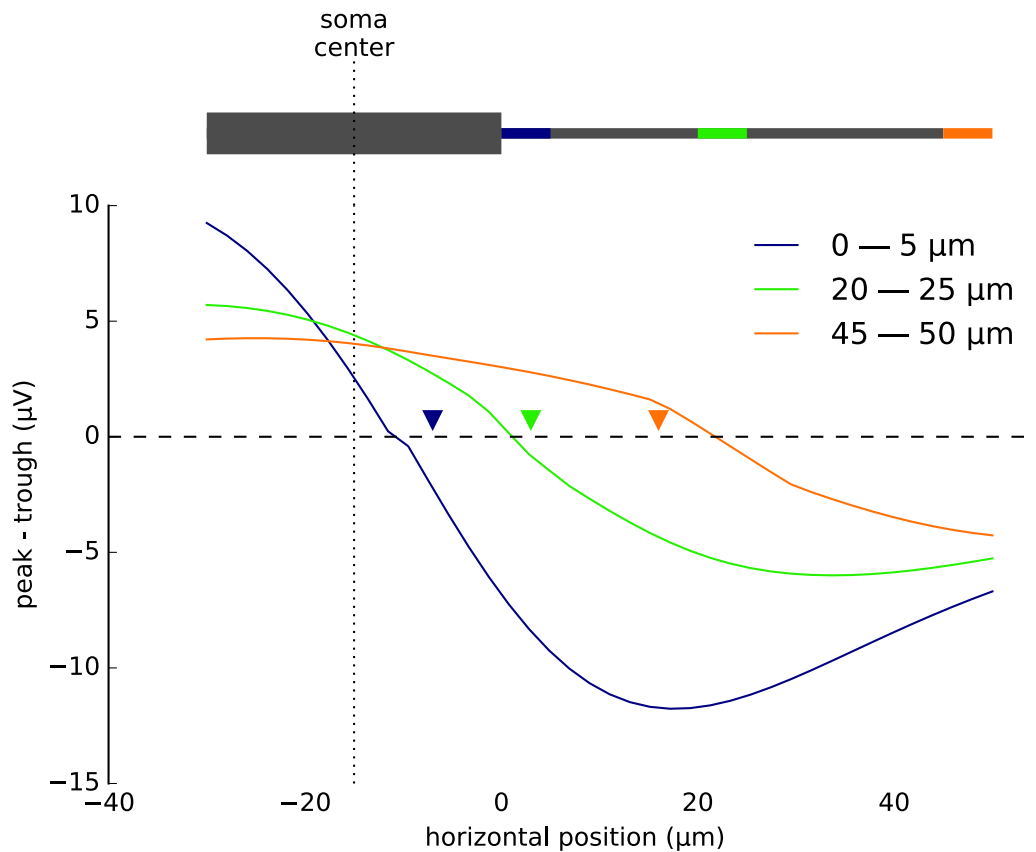


Figure 4.4: Profile of extracellular potential along soma and axon. Extracellular potential associated with an action potential was calculated along a horizontal line  $40 \mu\text{m}$  above the axon and extending from the proximal end of the soma towards the distal end of the axon for three different positions of AIS (see top drawing for a model schematics, scale on the x-axis is given relative to the distal end of the soma). For each recording and AIS position, we calculated the amplitude of the highest peak minus the amplitude of deepest trough (shown on y-axis) in a short window ( $0.3 \text{ ms}$  wide). The triangles on the x-axis show the midpoint between the centers of soma and AIS for each of the models. The vertical dotted line marks the position of soma's center.

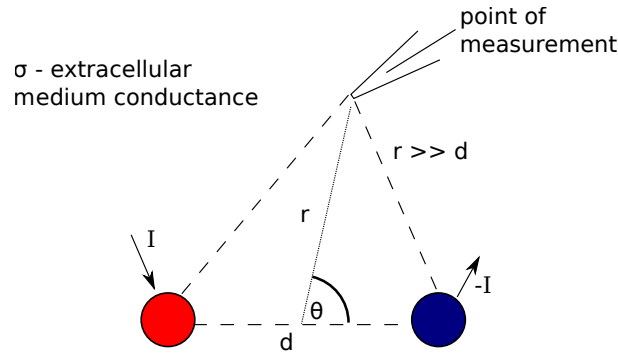


Figure 4.5: Dipole model consisting of a current sink (red) and a current source (blue) separated by  $d$ . Point of measurement represents a possible recording location. For the far-field approximation to hold, the distance between the sink and source should be much smaller than the distance to the recording point. See text for more detail.

vector (vector connecting the center of the dipole and the recording position),  $d$  is the distance between sink and source and  $r$  is the distance between the location of recording to dipole center (Fig. 4.5).

To investigate the effect of the AIS position on the current intensity  $I$ , we measured the axial current during the action potential for varying positions of the AIS. We found that the amplitude of the axial current decreased with the inverse of the distance between the AIS and the soma (Fig. 4.6A). Indeed, the same figure (Fig. 4.6B) shows that it is possible to fit a straight line of slope  $a = -1$  through the points representing the logarithm of the maximum axial current versus the logarithm of the soma-AIS distance. This linear relation confirms that the amplitude of the axial current is inversely proportional to the distance between the soma and the AIS,  $I \sim 1/d$ . Since the far-field model of the extracellular potential predicts that the potential increases with the distance between source and sink, this trend should compensate for the drop of current magnitude shown in Figure 4.6. Therefore, the far-field approximation of the dipole model would predict no difference in the amplitude of the extracellular potential due to the AIS position.

Taken together, the dependence of the extracellular action potential amplitude on the AIS positions presented in Figures 4.3 and 4.6 can arise only in the close neighbourhood of the neuron (its near field).

### 4.1.3 Dipole model – near field

To study the effect of the soma-AIS distance on their near-field potential, we constructed an electrical model of the axon consisting of a pair of current source and sink, representing the soma and the AIS, respectively (Fig. 4.7). We set the dipole moment  $Q = Id$  to the value obtained from the simulation of the soma-axon model (Fig. 4.6) and varied the

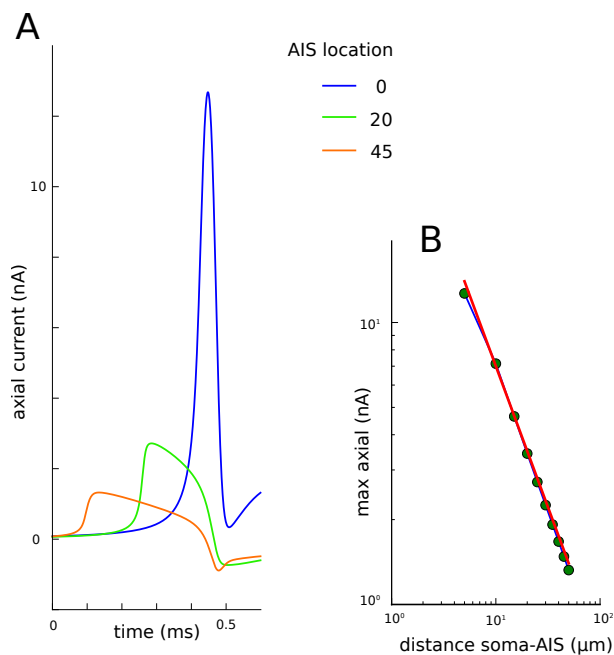


Figure 4.6: Dependence of axial current amplitude on the distance between the soma and the AIS in soma-axon model. **A**. The axial current passing from axon to the soma during the action potential, shifted to the peak of somatic spike, **B**. The maximum of axial current vs the distance of the AIS end proximal to the soma in double-logarithmic scale. Red line shows the fitted function  $I = (70 \text{ nA} \cdot \mu\text{m})/d$  (which is a linear function in double-logarithmic scale).

separation between the current source and sink modifying the current intensity  $I$ , so that the dipole moment is conserved. The extracellular field was then calculated as an exact superposition of contributions from the two current monopoles (source and sink, equation (4.2)). We found that this simplified model could capture the dependence between the AIS position and the extracellular field observed in the soma-axon model (compare Figure 4.1B and 4.7B). In particular, the extracellular potential was largest when the AIS was at the most distant point from the soma (soma/AIS separation of 45  $\mu\text{m}$ ).

These results show that the dependence of the extracellular potential on the AIS position are only noticeable in the immediate neighbourhood of the neuron (near field). If the distance of the recording electrode from the neuron is much larger than the separation between the current source and sink (far field), as it is the case in EEG recordings, the equation (4.3) offers a good approximation of the total field. As discussed above, this equation predicts that in the far field the amplitude of the extracellular action potential is not affected by the AIS position. Indeed, using the exact dipole calculation, we find that the absolute differences in the extracellular field for different AIS positions diminish when recording away from the neuron. However, in logarithmic scale the differences remain constant for distances above 200  $\mu\text{m}$  from the axon (Fig. 4.1B and 4.7B) meaning that

the ratios between the respective amplitudes of extracellular fields remain constant (as a consequence of the relation:  $\log(V_1/V_2) = \text{const} = \log(V_1) - \log(V_2)$ ).

We conclude that the amplitude of the extracellular action potential recorded close to the neuron depends on the position of the AIS.

#### 4.1.4 Two cylinder model

One deviation of the simulated extracellular potential from the dipole model is that the field at the axis going through the middle between the centers of the AIS and the soma is not zero (Fig. 4.3). Both the dipole model and its far-field approximation predict that the field between the current sink and source should be exactly zero (cf. Fig. 4.7C), which can be observed when we set  $r^+ = r^-$  in the equation (4.2) or  $\theta = \pi$  in the equation (4.3). Therefore we built another model, which could account for these results. The main contribution of this model is based on the fact that the soma and the AIS are spatially-extended compartments (cylinders) and their sizes are not equal – the soma and the AIS have the same dimensions as in our soma-axon model (soma:  $30 \times 20 \mu\text{m}$ , AIS:  $5 \times 1 \mu\text{m}$ , Fig. 4.8 A).

For the potential calculated along a vertical axis above the soma the results are similar to the ones obtained using the dipole model (compare Figures 4.7B and 4.8B). However, when we calculated the potential above the midpoint between the centers of the two cylinders, we found that the potential was larger than 0, but that it decreased rapidly with diminishing distances from the axon (Fig. 4.8C). Due to the asymmetry of the cylinder sizes the potential crossed the zero value proximally to soma (Fig. 4.8D) and not at the center between the compartments, as predicted by the dipole models (Fig. 4.7C). Interestingly, the offset between the zero-crossing and the center becomes smaller with decreasing distance from the axon and an increasing separation between the soma and the AIS, which explains the sudden drop of the potential at very short distances and when positioning the AIS at a large distance, as shown in Figure 4.8C (orange and green curves).

Similarly to the soma-axon model we also observed a reversal in the relation between the extracellular AP amplitude and the AIS distance from the soma when the recording was shifted from above the soma to the midpoint between the AIS and the soma centers. For recordings above the soma ( $20 \mu\text{m}$  and more), the extracellular potential increased with separation between the soma and the AIS (Fig. 4.1B and 4.8B), whereas it decreased when recorded above the midpoint (Fig. 4.3B and 4.8C).

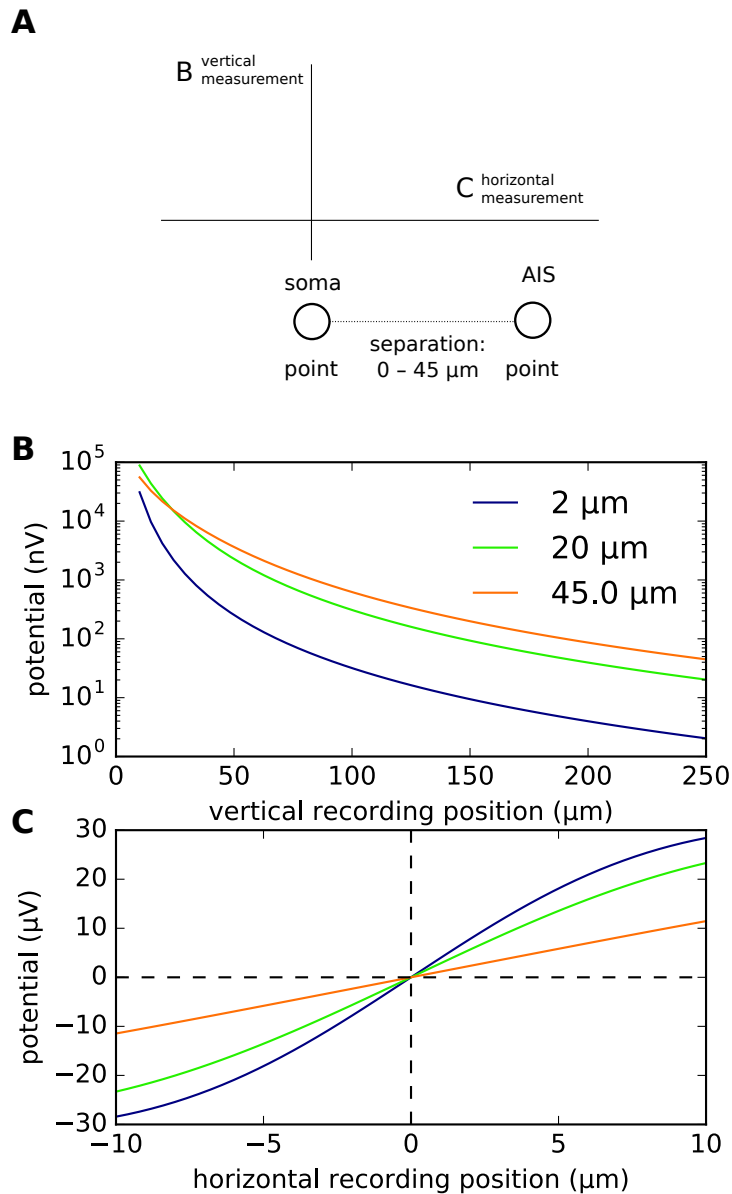


Figure 4.7: Dipole model of AIS and soma. **A**. Somatic and AIS compartments are modeled by a pair of point current source and sink (here represented as circles). Distance between the source and sink is varied ( $2 \mu\text{m}$ ,  $20 \mu\text{m}$ ,  $45 \mu\text{m}$ , color lines in B and C), but the dipole moment remains constant  $Q = 70 \text{ nA}\cdot\mu\text{m}$ . **B**. The change of extracellular potential along a line above the soma perpendicular to the dipole's axis for three different separations between soma and AIS (line B in panel (A)). **C**. Extracellular potential along a line parallel to the dipole's axis at the distance of  $20 \mu\text{m}$  from the axon (line C in panel (A)). In both directions the potential depends on the distance between the AIS and soma (color lines).

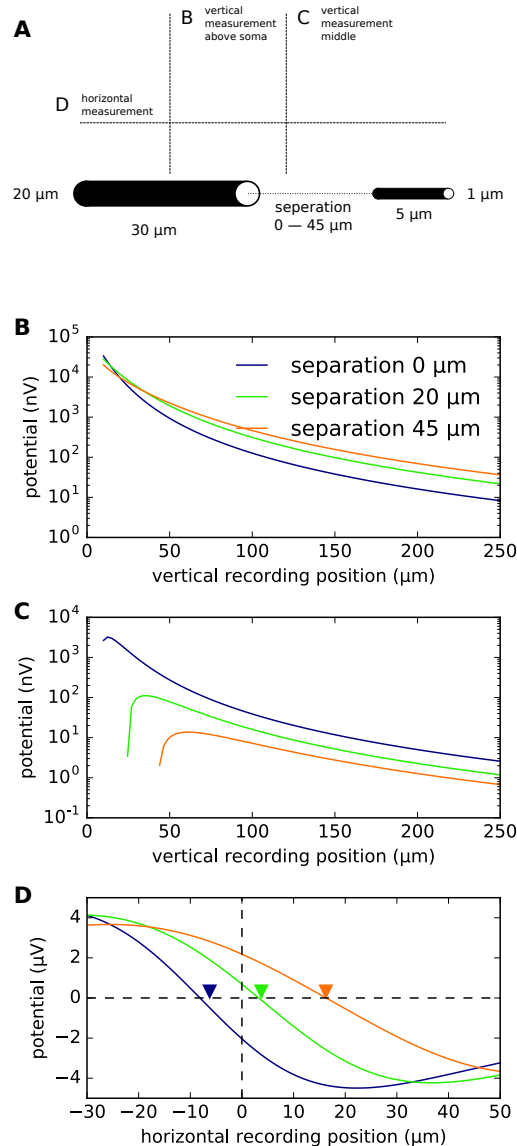


Figure 4.8: Two cylinder model of the AIS/soma dipole. **A**. Schematics of the two cylinder model with soma (cylinder on the left) and AIS (smaller cylinder on the right). The dipole moment is equal to  $70 \text{ nA} \cdot \mu\text{m}$  and the current is calculated as  $I = Q/d$  where  $d$  is the distance between the centers of cylinders. The vertical and horizontal lines show the axis of measurement of extracellular potential shown in panels (B-D). **B**. Extracellular potential measured for three different AIS separations (color lines) above the soma center. **C**. Extracellular potential along a vertical axis in the middle between soma and AIS centers. In both cases the potential is sensitive to the separation between the cylinders, but the relation is reversed (increase in potential with increasing soma/AIS separation in B, and decrease in potential in C). **D**. Extracellular potentials measured along a horizontal axis 40 μm from the axon. Zero crossing is shifted towards soma with respect to the midpoint between soma and AIS centers (shown with triangles). The shift is largest for AIS directly attached to the the soma (blue curve). Note that potential in C was reversed in sign.

## 4.2 Discussion

Using linear source approximation (LSA) and Neuron simulations (soma-axon model) we have shown that the extracellular action potential can be recorded at different locations close to the spiking neuron and that its amplitude varies with the distance between the soma and the action potential initiation site.

We argued that at large distances compared to the separation between the soma and the AIS, the dipole contribution to the extracellular field does not depend on the separation between the AIS and the soma (far-field approximation). However, simulations of the near-field extracellular field using LSA reveal the dependence of the extracellular action potential on the localisation of the AIS. We demonstrated that this dependence can be reproduced in simple models consisting of two monopoles or two cylinders (with sizes matched to the dimensions of the soma and the AIS). Furthermore, we found that for a cylindrical soma and AIS, the position of reversal of the extracellular AP polarity along the soma and axon axis can be offset with respect to the midpoint between their centers. This phenomenon occurs due to the asymmetric field generated by cylinders and might disappear if we considered a spherical soma instead.

Our results provide an important insight into the understanding of extracellular action potentials. It is known that the shape and the amplitude of the extracellular action potentials vary depending on the location of the recordings (Gold et al., 2006). Also, different types of neurons display extracellular action potentials of different width, such as excitatory cells, which tend to have broader extracellular action potentials when compared with interneurons (Barthó et al., 2004; McCormick et al., 1985), although there are exceptions (Vigneswaran et al., 2011). To separate action potentials of multiple neurons recorded extracellularly, it is common to use the waveform features of an extracellular action potential, such as the half-widths of the positive and negative peaks, the interval between them and the difference of their amplitudes (Lewicki, 1998; Einevoll et al., 2012). In addition, these and other waveform features sometimes allow the identification of neurons of different types (Peyrache et al., 2012; Dehghani et al., 2016). However, the significance of such features and their biophysical underpinnings are not completely understood. Numerical simulations of extracellular field around reconstructed morphology of CA1 pyramidal neurons showed that the width of the extracellular action potential increases proportionally with the distance between the soma and the recording electrode (Gold et al., 2006). In addition, in this study the shape and amplitude of the extracellular potential was strongly affected by the channel densities in the dendrites and in the axon initial segment. In our work we show that the extracellular features of action potentials depend also on the exact location of the their initiation site.

At the population level, the contribution of neurons to the local field potential (LFP) depends critically on the presence of voltage-dependent channels and neuronal morphology. For example, during the up state the LFP contains larger contributions from the active potassium and sodium currents than from synaptic currents (Reimann et al., 2013); similarly active conductances in the dendrites were shown to have major impact on the spectrum of the field potential (Ness et al., 2016). The structure of the dendritic tree has also been identified as a plausible factor influencing the LFP signals (Lindén et al., 2010). Results in the present work suggest that the biophysics of the axon and the site of the action potential initiation may also be an important factor determining the amplitude and spectrum of the extracellular potential. The effects of the AIS position on LFP generated from a network of multi-compartmental model neurons is an interesting outlook of the present work.

Finally, our results show that it should be possible, and of great interest, to follow experimentally the dynamic change of the AIS position by means of extracellular recordings.

## 4.3 Methods

### 4.3.1 Soma-axon model

We used a simple neuron consisting of a soma ( $20 \times 30 \mu\text{m}$ , 6 segments) and an axon ( $1 \times 50 \mu\text{m}$ , 10 segments). Adapted from Yu et al. (2008). Figures 4.1 (top left) and 4.3 (top left) show the sample schematics of the shape of the neuron. The simulation was controlled from Python using the Neuron-Python interface (Hines et al., 2009).

### 4.3.2 Linear Source Approximation

To estimate the extracellular potential, we used the Linear Source Approximation (LSA) method, which calculates the summed potential generated by currents originating from line sources with known sizes and positions. This method is known to be more precise than approximating the currents by point sink and sources (Holt, 1997; Wilson and Bower, 1992). We then applied the LSA estimation to cylinders obtained from the segmentation by Neuron simulator (in total 16 cylinders, see above) (Hines and Carnevale, 1997). The field was calculated using the LSA implementation of NeuronEAP Python library (Telenczuk and Telenczuk, 2016) which uses Linear Source Approximation to calculate the field generated by a neuron simulated in Neuron simulator. In all calculations we used an extracellular conductivity of  $0.3 \text{ Sm}^{-1}$ .

In Figures 4.1 and 4.3 we removed the baseline by calculating an average potential in a window of 2 to 1 ms before the peak of the action potential. This baseline shift arises because of the current injected in the soma, which effectively creates a monopole moment in the extracellular potential.

### 4.3.3 Two cylinders model

To study the effect of the soma and AIS sizes on the action potential we modelled them by two cylinders of  $30 \mu\text{m}$  (length)  $\times$   $20 \mu\text{m}$  (diameter) and  $5 \mu\text{m} \times 1 \mu\text{m}$ , respectively. To calculate the extracellular potential we added the total contribution of each cylinder to the extracellular field given by the formula:

$$V_{\text{cylinder}} = \frac{i_m R}{2\sigma} \log \left| \frac{\sqrt{h^2 + r^2} - h}{\sqrt{(h + L)^2 + r^2} - h + L} \right| \quad (4.4)$$

where  $i_m$  is the current per membrane surface,  $\sigma$  is the extracellular conductance,  $R$  and  $L$  are the cylinder radius and length,  $r$  is the radial distance from the cylinder,  $h$  is the longitudinal distance from one of cylinder's ends.

The current density was chosen such that the total current of the AIS and the soma are of the same magnitude (but of opposite signs).

---

## Bibliography

---

- Barthó, P., Hirase, H., Monconduit, L., Zugaro, M., Harris, K. D., and Buzsáki, G. (2004). Characterization of neocortical principal cells and interneurons by network interactions and extracellular features. *Journal of Neurophysiology*, 92(1):600–608.
- Chand, A. N., Galliano, E., Chesters, R. A., and Grubb, M. S. (2015). A Distinct subtype of dopaminergic interneuron displays inverted structural plasticity at the axon initial segment. *Journal of Neuroscience*, 35(4):1573–1590.
- Dehghani, N., Peyrache, A., Telenczuk, B., Van Quyen, M. L., Halgren, E., Cash, S. S., Hatsopoulos, N. G., and Destexhe, A. (2016). Dynamic balance of excitation and inhibition in human and monkey neocortex. *Scientific Reports*, 6(23176):1–12.
- Einevoll, G. T., Franke, F., Hagen, E., Pouzat, C., and Harris, K. D. (2012). Towards reliable spike-train recordings from thousands of neurons with multielectrodes. *Current Opinion in Neurobiology*, 22(1):11–17.
- Evans, M. D., Dumitrescu, A. S., Kruijssen, D. L. H., Taylor, S. E., and Grubb, M. S. (2015). Rapid modulation of axon initial segment length influences repetitive spike firing. *Cell Reports*, 13(6):1233–1245.
- Evans, M. D., Sammons, R. P., Lebron, S., Dumitrescu, A. S., Watkins, T. B., Uebele, V. N., Renger, J. J., and Grubb, M. S. (2013). Calcineurin signaling mediates activity-dependent relocation of the axon initial segment. *Journal of Neuroscience*, 33(16):6950–6963.
- Fried, S. I., Lasker, A. C. W., Desai, N. J., Eddington, D. K., and Rizzo, J. F. (2009). Axonal sodium-channel bands shape the response to electric stimulation in retinal ganglion cells. *Journal of neurophysiology*, 101:1972–1987.
- Gold, C., Henze, D. A., Koch, C., and Buzsáki, G. (2006). On the origin of the extracellular action potential waveform: A modeling study. *Journal of neurophysiology*, 95(5):3113–28.
- Grubb, M. S. and Burrone, J. (2010). Activity-dependent relocation of the axon initial segment fine-tunes neuronal excitability. *Nature*, 465(7301):1070–4.

- Hines, M. L. and Carnevale, N. T. (1997). The neuron simulation environment. *Neural computation*, 9(6):1179–1209.
- Hines, M. L., Davison, A. P., and Muller, E. (2009). NEURON and Python. *Frontiers in Neuroinformatics*, 3:1.
- Hinman, J. D., Rasband, M. N., and Carmichael, S. T. (2013). Remodeling of the axon initial segment after focal cortical and white matter stroke. *Stroke*, 44(1):182–189.
- Holt, G. R. (1997). *A critical reexamination of some assumptions and implications of cable theory in neurobiology*. PhD thesis, California Institute of Technology.
- Kuba, H., Ishii, T. M., and Ohmori, H. (2006). Axonal site of spike initiation enhances auditory coincidence detection. *Nature*, 444(7122):1069–1072.
- Lewicki, M. S. (1998). A review of methods for spike sorting: the detection and classification of neural action potentials. *Network*, 9(4):R53–78.
- Lindén, H., Pettersen, K. H., and Einevoll, G. T. (2010). Intrinsic dendritic filtering gives low-pass power spectra of local field potentials. *Journal of Computational Neuroscience*, 29(3):423–444.
- McCormick, D. A., Connors, B. W., Lighthall, J. W., and Prince, D. a. (1985). Comparative electrophysiology of pyramidal and sparsely spiny stellate neurons of the neocortex. *Journal of neurophysiology*, 54(4):782–806.
- Muir, J. and Kittler, J. T. (2014). Plasticity of GABAA receptor diffusion dynamics at the axon initial segment. *Frontiers in cellular neuroscience*, 8(June):151.
- Ness, T. V., Remme, M. W. H., and Einevoll, G. T. (2016). Active subthreshold dendritic conductances shape the local field potential. *Journal of Physiology*, 0(1):1–31.
- Peyrache, A., Dehghani, N., Eskandar, E. N., Madsen, J. R., Anderson, W. S., Donoghue, J. A., Hochberg, L. R., Halgren, E., Cash, S. S., and Destexhe, A. (2012). Spatiotemporal dynamics of neocortical excitation and inhibition during human sleep. *PNAS*, 109(5):1731–1736.
- Reimann, M. W., Anastassiou, C. a., Perin, R., Hill, S. L., Markram, H., and Koch, C. (2013). A biophysically detailed model of neocortical local field potentials predicts the critical role of active membrane currents. *Neuron*, 79(2):375–90.
- Schafer, D. P., Jha, S., Liu, F., Akella, T., McCullough, L. D., and Rasband, M. N. (2009). Disruption of the axon initial segment cytoskeleton is a new mechanism for neuronal injury. *Journal of neuroscience*, 29(42):13242–13254.
- Telenczuk, B. and Telenczuk, M. (2016). NeuronEAP library. *Zenodo*, 10.5281/zenodo.49560.
- Vigneswaran, G., Kraskov, A., and Lemon, R. N. (2011). Large Identified Pyramidal Cells in Macaque Motor and Premotor Cortex Exhibit ”Thin Spikes”: Implications for Cell Type Classification. *Journal of Neuroscience*, 31(40):14235–14242.

- Williams, S. R. and Stuart, G. J. (1999). Mechanisms and consequences of action potential burst firing in rat neocortical pyramidal neurons. *The Journal of physiology*, 521 Pt 2:467–482.
- Wilson, M. and Bower, J. M. (1992). Cortical oscillations and temporal interactions in a computer simulation of piriform cortex. *Journal of Neurophysiology*, 67(4):981–995.
- Yu, Y., Shu, Y., and McCormick, D. A. (2008). Cortical action potential backpropagation explains spike threshold variability and rapid-onset kinetics. *The Journal of neuroscience*, 28(29):7260–72.

---

## Single CA3 pyramidal cells trigger sharp waves *in vitro* by exciting interneurons

---

This paper was born thanks to the collaboration between Michaël Bazelot, Richard Miles and Maria Teleńczuk. It has been published in the Journal of Physiology in year 2016 (Bazelot et al., 2016).

### 5.1 Abstract

Sharp waves (SPWs) are a hippocampal population activity that has been linked to neuronal representations. We show that SPWs in the CA3 region of rat hippocampal slices can be triggered by the firing of single pyramidal cells. Single action potentials in almost one-third of pyramidal cells initiated SPWs at latencies of 2–5 ms with probabilities of 0.07–0.76. Initiating pyramidal cells evoked field IPSPs (fIPSPs) at similar latencies when SPWs were not initiated. Similar spatial profiles for fIPSPs and middle components of SPWs suggested that SPW fields reflect repeated fIPSPs. Multiple extracellular records showed that the initiated SPWs tended to start near the stimulated pyramidal cell, whereas spontaneous SPWs could emerge at multiple sites. Single pyramidal cells could initiate two to six field IPSPs with distinct amplitude distributions, typically preceded by a short-duration extracellular action potential. Comparison of these initiated fields with spontaneously occurring inhibitory field motifs allowed us to identify firing in different interneurons during the spread of SPWs. Propagation away from an initiating pyramidal cell was typically associated with the recruitment of interneurons and field IPSPs that were not activated by the stimulated pyramidal cell. SPW fields initiated by

single cells were less variable than spontaneous events, suggesting that more stereotyped neuronal ensembles were activated, although neither the spatial profiles of fields, nor the identities of interneurone firing were identical for initiated events. The effects of single pyramidal cell on network events are thus mediated by different sequences of interneurone firing.

## 5.2 Introduction

Single mammalian pyramidal cells are not considered to have major effects on the cortical networks to which they belong (Shadlen and Newsome, 1998). Even so, single pyramidal cells of layers 5 and 6 of the motor cortex can induce or affect whisker movements (Brecht et al., 2004), whereas stimulation of single layer 5 somatosensory pyramidal cells modifies behavioural responses during a detection task (Houweling and Brecht, 2007). Single neurones can also modify the collective activities of cortical neuronal populations. In the somatosensory or visual cortex, single cells can induce transitions between cortical up and down states (Cheng-yu et al., 2009). The firing of a single GABAergic inhibitory cell can alter the timing of population events in the immature hippocampus (Bonifazi et al., 2009), whereas some pyramidal cells entrain or initiate epileptiform population events in the adult hippocampus (de la Prida et al., 2006; Miles and Wong, 1983). Sharp waves (SPWs) are hippocampal EEG events with a duration of 30–60 ms (Buzsáki et al., 1983; O’keefe and Nadel, 1978) that occur during behaviours including awake immobility and slow wave sleep. Buzsaki et al. (Buzsaki et al., 1992) showed that SPWs are accompanied by high frequency interneurone firing. They are initiated in CA3, spread into the CA1 region of the hippocampus, and pyramidal cell and GABAergic interneurones fire during SPWs of both regions (Csicsvari et al., 2000; Klausberger et al., 2003). SPWs are suggested to involve various forms of replay of previous sequences of spike discharge and so they have been associated with the consolidation of neuronal representations (Ji and Wilson, 2007; Girardeau et al., 2009; Jadhav et al., 2012). SPW-like events occur spontaneously in vitro (Kubota et al., 2003) and the mechanisms responsible for their generation have mostly been examined in slices. These mechanisms remain controversial and may differ for SPWs of the CA3 and CA1 regions. SPWs have been ascribed to electrotonic junctions between pyramidal cells (Draguhn et al., 1998; Böhner et al., 2011) or to interactions within recurrent circuits (Ellender et al., 2010) with predominant excitatory (Maier et al., 2011) or inhibitory synaptic signals (Ho et al., 2009; Aivar et al., 2014). Data on how single neurones affect the timing or initiation of SPWs could help discriminate between these possible mechanisms. Ellender et al. (Ellender et al., 2010) showed that stimulation of single interneurones increased the probability of SPW occurrence in slices with long ( $\sim 1$  s)

latencies, whereas stimulation of single pyramidal cells had no effect. In the present study, we show, *in vitro*, that firing in single CA3 pyramidal cells could initiate SPW with latencies of 2 – 6 ms. This latency is similar to that between pyramidal cell firing and the discharge of post-synaptic interneurons (Miles, 1990; Csicsvari et al., 1998). Extracellular records suggested that repeated firing of the same or different interneurons contributed to SPWs. SPWs induced by single cells were more stereotyped than SPWs that occurred spontaneously without stimulation. However, the identities and the timing of interneurone firing varied between successive initiated SPWs.

## 5.3 Methods

### 5.3.1 Slice preparation

Hippocampal slices were prepared from rats, aged 7–10 weeks and weighing 150–300 g, in accordance with EC Directive 08/120/EC and local INSERM guidelines. Protocols were approved by the Comité d’Ethique Darwin, Ministère de l’Enseignement Supérieur et de la Recherche; Paris. Twenty-two animals were used to obtain the data reported in the present study. Rats were anaesthetized I.P. with ketamine (80 mg kg<sup>-1</sup>) and xylazine (12 mg kg<sup>-1</sup>) and perfused intracardially with a solution containing (in mM) 62 NaCl, 26 NaHCO<sub>3</sub>, 1 KCl, 10 MgCl<sub>2</sub>, 1 CaCl<sub>2</sub>, 122 sucrose and 10 D-glucose and equilibrated with 5% CO<sub>2</sub> in 95% O<sub>2</sub> at 3 – 5 °C. Both hippocampi were dissected free and transverse slices (thickness 500 μm) were cut with a vibratome (HM650V; Microm International GmbH, Walldorf, Germany) from their ventral portion. Slices were transferred to an interface recording chamber, where they were equilibrated with 5% CO<sub>2</sub> in 95% O<sub>2</sub>, heated to 35 – 37 °C and perfused with a solution containing (in mM) 124 NaCl, 26 NaHCO<sub>3</sub>, 3–5 KCl, 2 MgCl<sub>2</sub>, 2 CaCl<sub>2</sub> and 10 glucose.

### 5.3.2 Drugs

In some experiments, GABA<sub>A</sub> receptor mediated signalling was suppressed by picrotoxin (100 μM). We also used the μ-opioid receptor agonist (D-Ala<sup>2</sup>, N-MePhe<sup>4</sup>, Gly-ol)-enkephalin (20 μM ; DAMGO), which is suggested to hyperpolarize perisomatic targeting interneurons and reduce release from inhibitory terminals (Svoboda et al., 1999; Gulyás et al., 2010). Drugs were obtained from Tocris Neuramin (Bristol, UK) or Ascent Scientific (Cambridge, UK).

### 5.3.3 Recordings

Intracellular records were made with glass electrodes filled with 4 M KAc (resistance 50–80 M $\Omega$ ). Signals were amplified with an Axoclamp 2B amplifier (Molecular Devices, Sunnyvale, CA, USA) operated in current-clamp mode. Intracellular records from neurons with over-shooting action potentials, an input resistance larger than 20 M and a time constant longer than 10 ms were retained. Extracellular records were made with arrays of eight to 12 nichrome electrodes (diameter 50  $\mu$ m) positioned to contact slices from above (Bazelon et al., 2010). In some experiments, linear arrays with a separation of  $\sim$ 100  $\mu$ m between electrodes were placed along the CA3 pyramidal cell somatodendritic axis, orthogonal to the stratum pyramidale. In other experiments, curved arrays of separation  $\sim$ 200  $\mu$ m between electrodes were used to record from sites along the CA3 stratum pyramidale. Signals were amplified and filtered (pass-band 0.1 Hz to 20 kHz) with a 16 channel amplifier (Dr F. Dubois; Dipsi, Châtillon, France). Intracellular and extracellular voltage signals were digitized using a 12 bit, 16 channel analog-to-digital converter (Digidata 1200A; Molecular Devices) and visualized on a PC (Axoscope; Molecular Devices).

### 5.3.4 Signal analysis

Intracellular and multiple (8–12) extracellular records were analysed with laboratory-written routines (Matlab, MathWorks Inc., Natick, MA, USA; Python, <https://www.python.org>). The amplitude of SPWs and unitary inhibitory synaptic fields (fIPSPs) was measured at their peak on any recording site. Extracellular spikes were detected from signals filtered above 600 Hz using a threshold of 5\* the SD of baseline fluctuations. Field IPSPs (fIPSPs) were detected from low pass-filtered (80 Hz) signals as single positive-going waves of amplitude exceeding 5 SDs. SPWs were detected (Fig. 5.1) from low pass-filtered (80 Hz) signals obtained from eight sites of the CA3 stratum pyramidale. An amplitude threshold was adjusted to detect events similar to user-identified SPWs defined as fields generated at three or more sites, with at least three waves (Fig. 5.1 A). Wave components of SPWs (Fig. 5.1B) were detected from zero-crossings of the second derivative of voltage in low-pass filtered records (80 Hz). Spikes associated with SPWs (Fig. 5.1B) were detected from high-pass filtered traces (600 Hz). The start of an SPW was defined as the shortest latency spikes and/or waves across all recording sites in the stratum pyramidale (Fig. 5.1C). Sequential wave components of SPWs were defined from their start and peak, as well as the timing of firing, in comparisons of records from all sites in the CA3 stratum pyramidale. An index of the spatial coherence of SPWs, their similarity at different recording sites, was

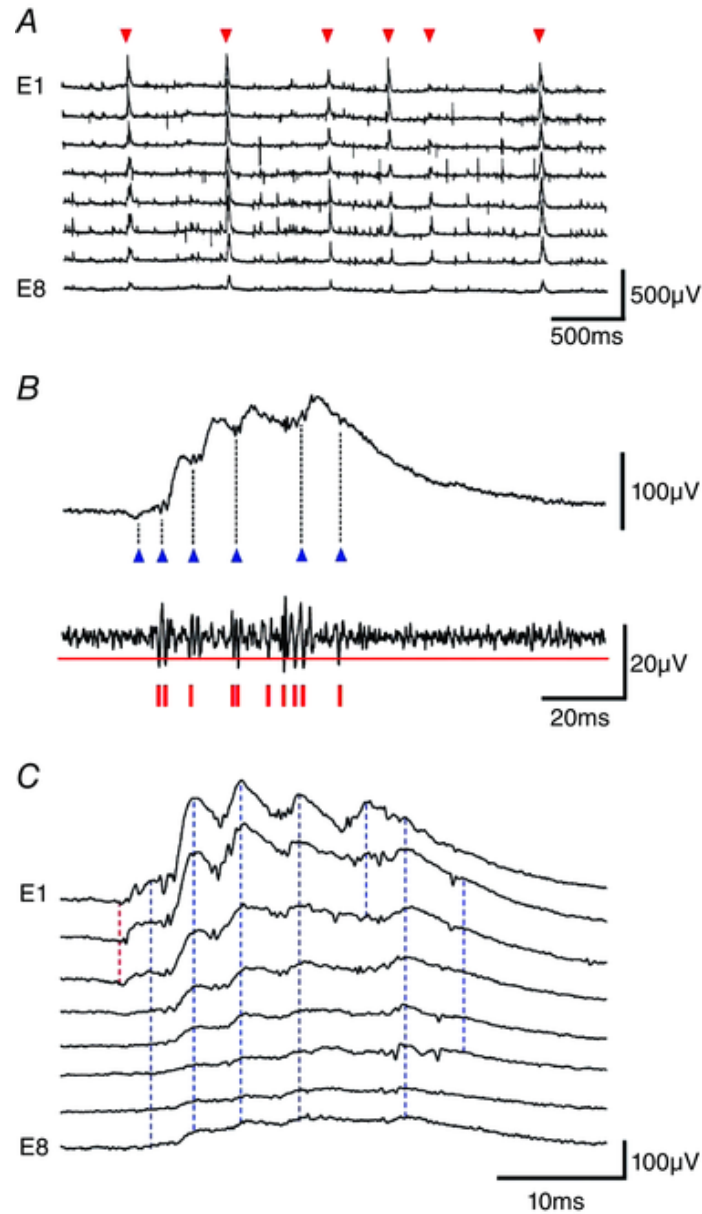


Figure 5.1: **Detection and measurement of SPWs.** **A**, SPWs (red triangles) were recorded extracellularly from the CA3 stratum pyramidale with eight electrodes, E1–E8 separated by  $\sim 200 \mu\text{m}$  in a curved array. SPWs were defined as events recorded from at least three electrodes, comprising three or more waves, and exceeding a user-defined amplitude threshold. **B**, multi-unit and wave components of SPW fields. Upper trace, SPW field (band pass filtered, 1–80 Hz); lower trace, unit activity (high-pass filtered, 600 Hz). Blue triangles indicate the start of six detected waves and red vertical lines indicate 10 detected spikes. **C**, SPW recorded by eight extracellular electrodes (E1–E8) from the CA3 stratum pyramidale. The onset of the SPW was detected on electrodes E1–E3 (red dotted line). Seven waves were detected (blue dotted lines). The first, fifth and seventh waves were recorded by some (but not all) electrodes. An index of spatial coherence was used to define the spatial variability of SPWs: (summed number of waves detected from all sites)/(the number of recording sites  $\times$  number of waves). The index has a value of 1 for an SPW where each wave is detected at each site. For this event, it was  $0.77 = (3 + 8 + 8 + 8 + 3 + 8 + 5)/(8 \times 7)$ .

derived as: (summed number of waves detected from all sites)/(the number of recording sites \* number of waves). Spontaneously occurring and induced fIPSPs and associated spikes were sorted by unsupervised clustering of extracellular signals ( $n = 8$ ) recorded from the stratum pyramidale. Events with overlaps of spikes or fIPSPs were excluded. Traces were measured at multiple time points chosen to provide a good discrimination of extracellular spikes and fIPSPs. The time points, with respect to the peak of the largest extracellular spike, were typically at -1.0, -0.5, -0.1, 0 (spike peak), 0.1 and 2.0 ms. Subtracting values for each trace from the value at -1.0 ms gave five parameters per trace and with eight channels a string of 40 numbers. Strings were analysed using k-mean clustering procedures as described previously (Bazelot et al., 2010). Reliability of the clustering was confirmed by visual matching of the form of spikes and fIPSPs at all recording sites on sets of eight traces aligned to the peak of the largest extracellular spike. Current source densities were estimated from eight to 12 extracellular records made along the CA3 pyramidal cell somatodendritic axis as described previously (Bazelot et al., 2010) using the approximation of Nicholson and Freeman (1975). Initiated and spontaneous SPWs were selected from all events detected in records with a duration of 10–45 min. SPWs occurring with latencies  $< 5$  ms after a pyramidal cell action potential induced by current injection were classed as evoked events. Other SPWs were considered to occur spontaneously. The initiation of spontaneous and evoked SPWs was compared for events aligned at their start, defined from both waves and unit spikes. Extracellular firing at SPW initiation was compared for all spikes detected from all electrodes within 1 ms of the start of the SPW. A cumulative sum procedure was used to compare the variability of spontaneous and single-cell initiated SPWs. A running sum was made from each point, of root-mean-square differences between the voltage trajectory of each event on each electrode, and the mean event from that electrode for all spontaneous or initiated SPWs. Cumulative variability from all electrodes was then added to derive summed values for spontaneous and initiated events. The significance of differences was explored using a bootstrap test, which compared sums of the squared differences from the means of either spontaneous or triggered events with values derived identically from 1000 randomized groups. The amplitude of fIPSPs and SPWs were compared using the peak amplitude detected at any site.

### 5.3.5 Statistical analysis

Values are reported as the mean  $\pm$  SD. Statistical analyses were conducted using Student's t test in SigmaStat, version 3.0 (Systat Software Inc., Chicago, IL, USA).  $P < 0.05$  was considered statistically significant.

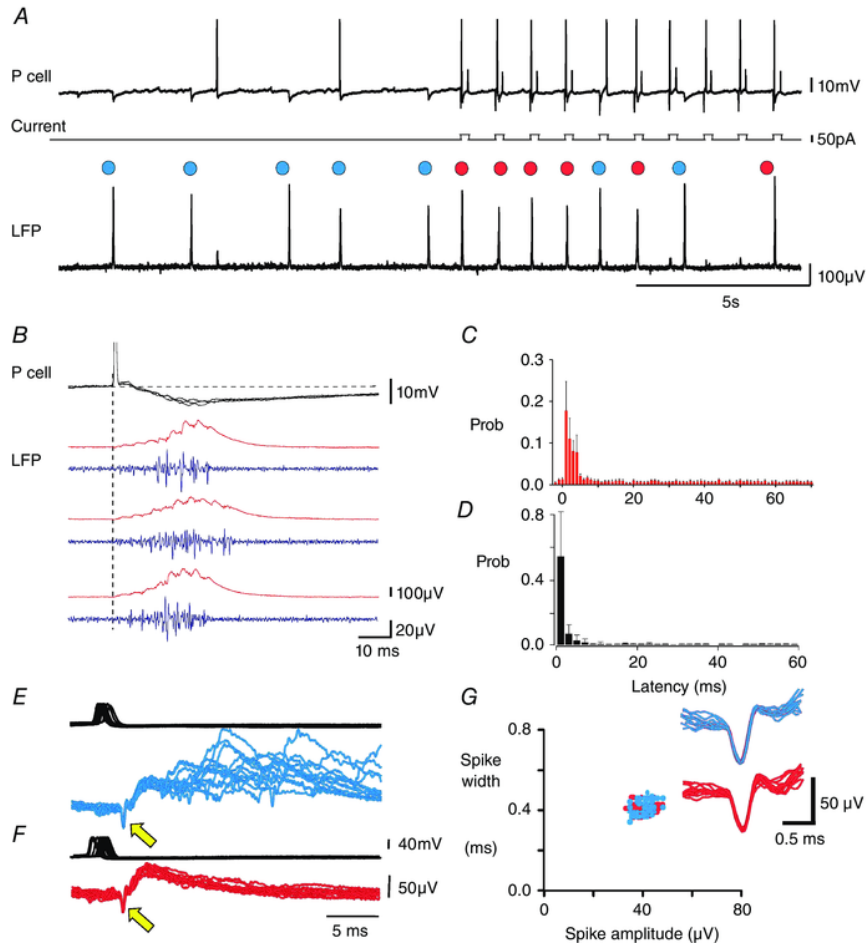


Figure 5.2: **Single CA3 pyramidal cells trigger SPWs.** **A**, traces are CA3 pyramidal cell membrane potential, injected current and local field potential (LFP). Blue circles indicate spontaneously occurring SPWs at intervals of 1.5–3.0 s. Current pulses (50 pA, duration 200 ms, interval 1000 ms) were injected to induce single pyramidal cell action potentials almost half-way along the traces. Red circles indicate six of 10 action potentials followed at short latency by a SPW. Overall, 172 of 626 spikes induced in this pyramidal cell were followed by a SPW at a latency shorter than 5 ms. In total, 99 spikes elicited no response, 128 spikes evoked a single fIPSP and 227 spikes elicited events intermediate between a single fIPSP and an SPW. **B**, three SPWs initiated by pyramidal cell firing. Intracellular potential, field (red) and multi-unit firing (blue, 0.5–5 kHz band-pass filtered). **C**, interval distribution between the intracellular action potential and the start of detected SPWs ( $n = 10$  experiments, 1145 SPWs, mean  $\pm$  SD of probabilities). **D**, normalized probability distribution of latencies from single pyramidal action potentials to extracellular spikes associated with the next SPW (mean  $\pm$  SD of probabilities,  $n = 1726$  action potentials from 10 pyramidal cells). **E–G**, SPWs, fIPSPs and unit firing. **E**, overlay of 20 SPWs (blue) initiated by single pyramidal cell action potentials (upper trace) and preceded by an extracellular spike (yellow arrow). **F**, overlay of 20 fIPSPs (red), initiated by single pyramidal cell spikes (upper trace) and preceded by an extracellular spike (yellow arrow). Traces of (**E**) and (**F**) triggered on the extracellular spike. **G**, plot of width against amplitude for spikes preceding fIPSPs (red) and SPWs (blue). The inset shows overlays of extracellular spikes preceding SPWs ( $n = 20$ , blue) and fIPSPs ( $n = 20$ , red).

## 5.4 Results

### 5.4.1 Single pyramidal cells initiate SPWs and field IPSPs

We observed action potentials in some CA3 pyramidal cells affected the timing of SPWs (Fig. 5.2). Pyramidal cells were made to fire single action potentials by current injection at intervals of 1–5 s. In 10 of 30 CA3b–c pyramidal cells tested, SPWs followed action potentials with latencies of  $\leq 5$  ms (Fig. 2A–C) and a probability of 0.07–0.76 (from 250 or more trials). The probability of SPW occurrence by chance was estimated to be in the range 0.002–0.012, as a result of dividing the latency of 5 ms by the mean interval between SPWs for each slice (de la Prida et al., 2006). The mean delay from the pyramidal cell spike to the first wave of the SPW was  $2.7 \pm 0.5$  ms (20% of peak;  $n = 10$ ) (Fig. 5.2B and C). Initiated SPWs were accompanied by an increase in multi-unit activity. The duration and pattern of this firing is shown in Fig. 5.2D, which plots all the extracellular spikes from SPWs initiated by single pyramidal cells ( $n = 10$  cells; 38–252 SPWs per cell). A delay of 2–3 ms is similar to that between pyramidal cell firing and discharge of a post-synaptic interneurone (Miles, 1990; Csicsvari et al., 1998). Field IPSPs are an extracellular sign of the activation of all the inhibitory synapses established by a single interneurone (Glickfeld et al., 2009; Bazelot et al., 2010). We found the same pyramidal cells induced either SPWs (Fig. 5.2E) or fIPSPs (Fig. 5.2F) with similar latency. Both fIPSPs and SPWs could be preceded by an extracellular action potential typically of short duration (0.3–0.6 ms;  $n = 10$ ) as associated with interneurone firing (Henze et al., 2000). The probability of inducing a fIPSP was 0.08–0.42 ( $n = 10$  cells; 250 or more trials). The observation that a single pyramidal cell could initiate either a fIPSP or a SPW suggested that the same circuits might be involved. Similar latencies (Fig. 5.2E and F) and spike shapes (Fig. 5.2G) suggest that the same extracellular unit may have fired when a single pyramidal cell initiated a fIPSP or a SPW.

### 5.4.2 fIPSPs from perisomatic interneurons are repeated in SPW fields

We therefore examined the role of interneurons and inhibitory synaptic circuits in SPW generation. Most recorded pyramidal cells were inhibited both during spontaneous SPWs and those that they initiated (24 of 30 neurons) (Figs 5.2B and 5.3A). Three were depolarized and three others received mixed excitatory–inhibitory synaptic events (not shown). Inhibitory events occurring during a SPW were correlated in time and in amplitude with fields recorded from the stratum pyramidale. By contrast, all ( $n = 4$ ) fast-spiking interneurons recorded close to the stratum pyramidale received depolarizing events cor-

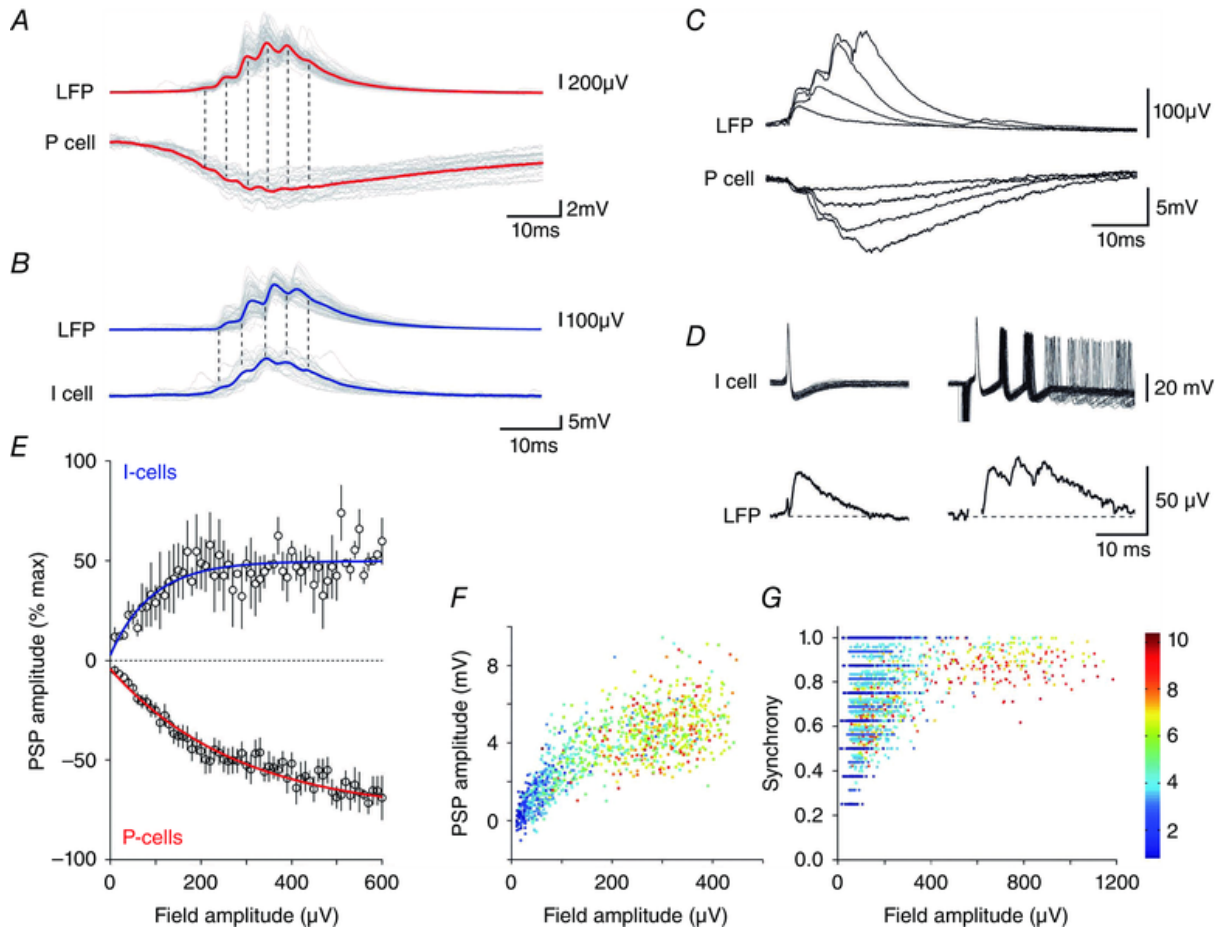


Figure 5.3: **Synaptic events corresponding to SPWs and fIPSPs.** Correlates of SPWs in pyramidal cells (red) (**A**) and in interneurons (blue) (**B**) showing the averaged local field and intracellular membrane potential with overlays of 20 traces (grey). **C**, overlaid field and pyramidal cell membrane potentials for a fIPSP and for SPWs of up to four waves; same records as in (**A**). **D**, field potentials (average of 30) induced by single and multiple action potentials in an interneuron. **E**, peak SPW field amplitude plotted against membrane potential changes in interneurons (blue,  $n = 4$ ,  $r^2 = 0.22$ ) and pyramidal cells (red,  $n = 16$ ,  $r^2 = 0.96$ ). **F**, hyperpolarizing change in pyramidal cell membrane potential ( $n = 16$ ) plotted against the amplitude of fields associated with events from single fIPSPs (blue) to eight to 10 wave SPWs (red). **G**, spatial coherence for fIPSPs (blue) through to eight to 10 wave SPWs (red) plotted against field potential amplitude (all events from 10 slices).

related with successive waves of SPWs (Fig. 5.3B). There was a continuum between single inhibitory events and multicomponent SPWs in field records and intracellular traces from pyramidal cells. Each wave of a SPW field was similar in form to a fIPSP of time to peak 2–5 ms (Glickfeld et al., 2009; Bazelot et al., 2010). Typically, three to 10 waves were repeated at intervals of 4–10 ms. Figure 5.3C shows a superimposition of field and pyramidal cell membrane potential records for an isolated fIPSP and SPWs of up to four waves. Figure 5.3D shows that, although one interneurone action potential evoked a fIPSP, repeated firing elicited field events similar to those at the start of a SPW. Relationships between peak field amplitude and the amplitude of depolarizations in interneurons ( $n = 4$ ) or hyperpolarizations in pyramidal cells ( $n = 8$ ) are summarized in Fig. 5.3E ( $n = 300 - 800$  events at resting potential). Peak SPW field amplitude and membrane hyperpolarizations in pyramidal cells increased together with the number of waves in a SPW (Fig. 5.3F). Figure 5.3G shows how the spatial coherence of SPWs (see Methods) recorded from multiple electrodes also co-varied with field amplitude and the number of waves. These data suggest that a continuum exists between fIPSPs consisting of a single wave and SPWs of up to eight to 10 waves. We next attempted to compare the identity of inhibitory synapses contributing to fIPSPs and to SPWs using current source density analysis. Fields were recorded with multiple electrodes ( $n = 12$ ) from sites along the somatodendritic axis of CA3 pyramidal cells ( $n = 5$  slices).

Comparisons of the spatial profiles of fIPSPs (Fig. 5.4A) and an intermediate wave of SPWs (Fig. 5.4B) revealed a current source in the stratum pyramidale. These data suggest that pyramidal cells initiating SPWs also excite interneurons (Csicsvari et al., 1998). Repeated firing in the same or different interneurons is associated with succeeding waves of the SPW field. Confirmation that interneurons are involved in SPW generation was obtained by showing that SPWs were suppressed by the GABA A receptor antagonist picrotoxin ( $20 \mu\text{M}$ ;  $n = 5$ , data not shown). The opiate DAMGO, which hyperpolarizes and reduces transmitter release from perisomatic interneurons (Svoboda et al., 1999; Gulyás et al., 2010), also suppressed SPWs ( $20 \mu\text{M}$ ,  $n = 4$ ) (Fig. 5.4 C and D). Together with the current profile data (Fig. 5.4 A and B), these data suggest that interneurons forming perisomatic synapses contribute to SPW fields. Pyramidal cell initiation of SPWs involves the excitation of one or several perisomatic interneurons.

### 5.4.3 Excitation of interneurons by single pyramidal cells

We estimated the number and spatial distribution of interneurons discharged by single pyramidal cells by making multiple extracellular records of fIPSPs from sites along the CA3 stratum pyramidale with eight electrodes separated by  $\sim 200 \mu\text{m}$  (Fig. 5.5). Inhibitory fields were typically recorded from three to six of these electrodes (Fig. 5.5 A–D),

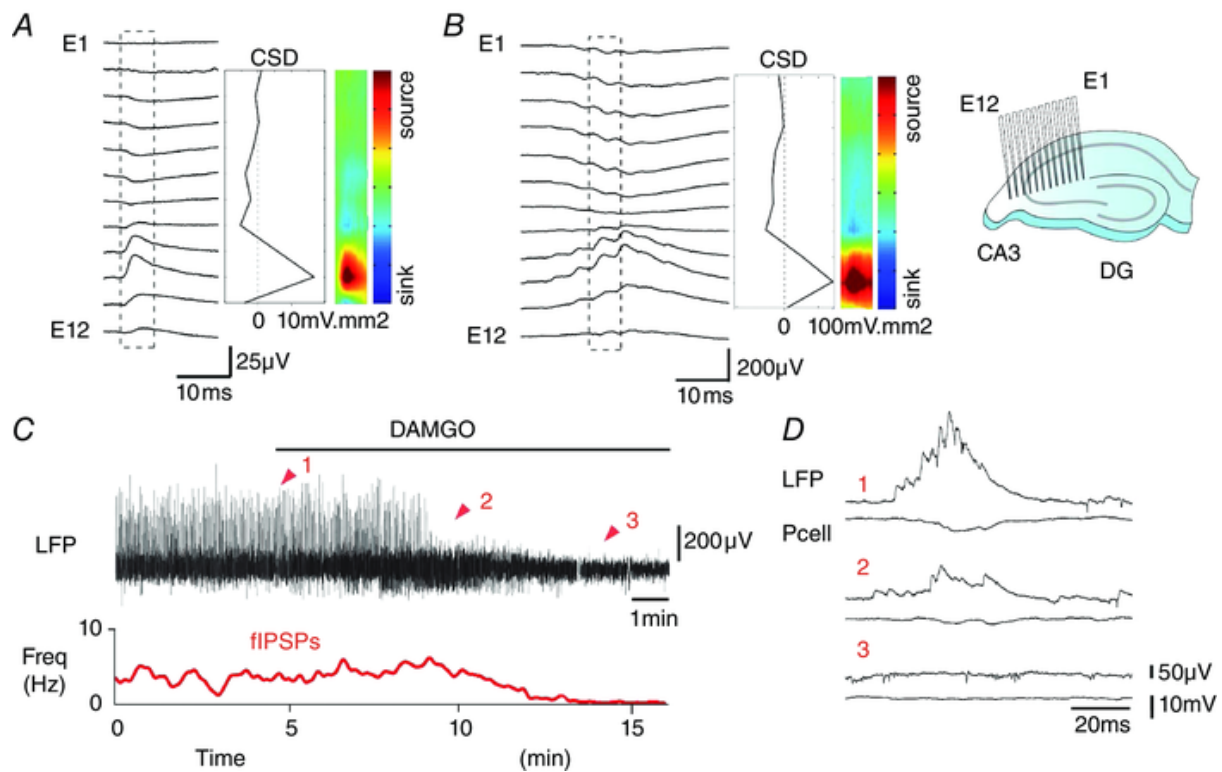


Figure 5.4: **Evidence for activation of perisomatic inhibitory synapses during SPWs** Comparison of CSD profiles for a fIPSP (A) and an intermediate wave of a SPW (B) recorded with 12 electrodes (E1–E12, separation  $\sim 100 \mu\text{m}$ ) placed along the CA3 pyramidal cell somatodendritic axis (inset). A current source (red) was apparent near the stratum pyramidale for both fIPSPs ( $n = 200$ ) and SPWs ( $n = 200$ ). C and D, DAMGO ( $20 \mu\text{M}$ ) suppressed both SPWs and fIPSPs. Traces are the LFP (upper) and fIPSP frequency (red, lower). D, field and pyramidal cell potentials during DAMGO application as indicated by red arrows (1–3).

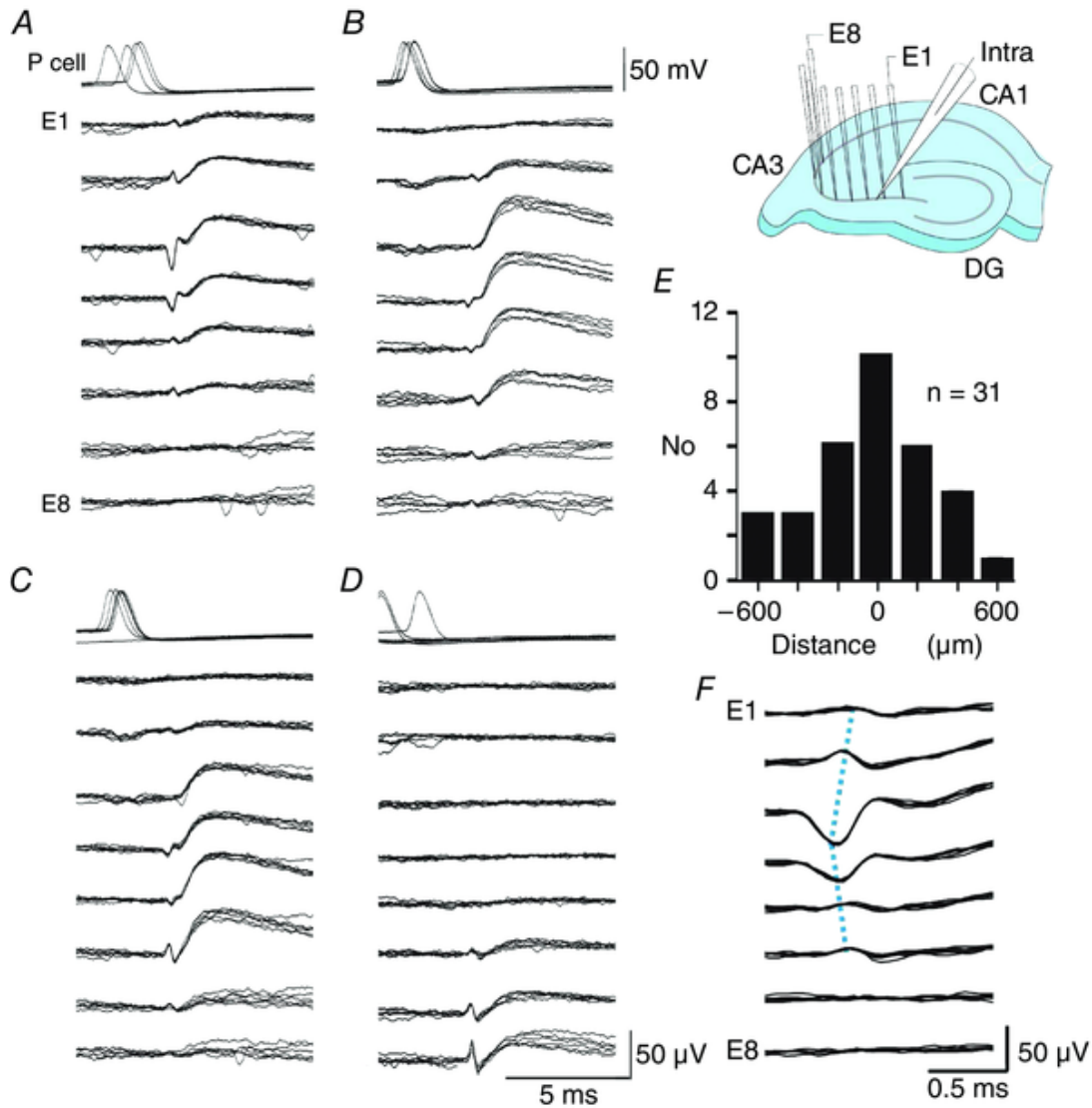


Figure 5.5: **Single pyramidal cells induce firing in multiple interneurons.** **A** to **D**, single action potentials of the same CA3 pyramidal cell initiated four spatially distinct combinations of an extracellular spike followed by a field IPSP. Overlays of six traces for pyramidal cell potential and extracellular potentials at eight sites in the stratum pyramidale (inset, E1–E8, electrode separation  $200\ \mu\text{m}$ ). All sets of traces are aligned on the largest extracellular spike. Spikes were detected at three to six sites and fIPSPs were recorded by three to seven electrodes. In total, 436 action potentials of this pyramidal cell triggered 90 fIPSPs, 130 events intermediate between fIPSPs and SPWs, and 178 SPWs, and 38 spikes elicited no response. **A**, the largest spike amplitude was  $\sim 55\ \text{V}$  on E3 (13 of 90 initiated fIPSPs). **B**, the largest spike was  $\sim 25\ \text{V}$  on E4 (18 of 90 fIPSPs). **C**, the largest spike was  $\sim 40\ \mu\text{V}$  on E6 (43 of 90 fIPSPs). **D**, the largest spike amplitude was  $\sim 55\ \mu\text{V}$  on E8, (16 of 90 fIPSPs). **E**, distance between the initiating pyramidal cell and the site of the maximal extracellular spike ( $n = 31$  spikes of amplitude  $> 20\ \mu\text{V}$ ; duration  $< 0.6\ \text{ms}$ , initiated by 10 pyramidal cells). **F**, enlarged extracellular spikes from (**A**), detected over distances of  $4\text{--}800\ \mu\text{m}$ , suggest that interneurone axonal action potentials may propagate at  $\sim 1\ \text{mm ms}^{-1}$  (blue dotted lines aligned to spike peaks).

which is consistent with the dimensions of axonal arbors of perisomatically-terminating inhibitory cells in this region (Gulyás et al., 2010). fIPSPs were often preceded, at two to four recording sites, by a short-duration extracellular spike (Figs 5.2 E and F and 5.5A-D). These two features, a local spike, presumably generated by an interneurone, and a more widespread fIPSP of distinct amplitude distribution across different sites, could define multiple, spatially different inhibitory field motifs. Pyramidal cells that initiated SPWs also activated multiple distinct fIPSP motifs. Overlays of traces selected after clustering and template matching show (Fig. 5.5A-D) that a single pyramidal cell initiated distinct fIPSPs with maximal amplitude at different recording sites preceded by a short-duration extracellular spike. Nine of 10 single pyramidal cells that initiated SPWs (Fig. 5.2) initiated at least two (2–6) spatially distinct fIPSP motifs. The other initiating cell evoked fIPSPs, although no extracellular spike was reliably detected. Plotting distances between stimulated pyramidal cells ( $n = 10$ ) and all detected spikes (31 spikes of amplitude larger than  $20 \mu\text{V}$ ) revealed a distribution clustered around the initiating neurone (Fig. 5.5E). Extracellular spikes preceding fIPSPs were typically recorded on several electrodes (Fig. 5.5F). This is unexpected because the amplitude of extracellular spikes generated by pyramidal cells decays to undetectable levels at distances of  $\sim 100 \mu\text{m}$  (Cohen and Miles, 2000; Henze et al., 2000). The extracellular spike shown in Fig. 5.5F, propagated at  $\sim 1 \text{ mm ms}^{-1}$ , which is similar to the speed of action potential conduction in interneurone axons (Hu and Jonas, 2014).

#### 5.4.4 Comparison of spontaneous SPWs and SPWs initiated by single cells

If pyramidal cells tend to discharge nearby interneurons, then evoked SPWs might also be initiated at sites clustered around a stimulated pyramidal cell. We examined this by comparing initiation sites for initiated and spontaneously occurring SPW field potentials in the stratum pyramidale. The initial wave of initiated SPW fields always began close to the initiating cell (Fig. 5.6A and C). By contrast, spontaneous SPWs were typically initiated at multiple sites in CA3 (Fig. 5.6B and C). Thus, although SPWs appear to be initiated via the firing of interneurons near the stimulated pyramidal cell, spontaneous SPWs may depend on similar processes at multiple, distinct sites. We compared several characteristics of spontaneous SPWs and those initiated by single pyramidal cells. The duration of SPWs was measured as the delay between the start of the first and the last detected fIPSP. For initiated events, the mean duration was  $23.8 \pm 5.3 \text{ ms}$  and, for spontaneous events, it was  $21.6 \pm 4.0 \text{ ms}$  (paired t test,  $P = 0.15$ ,  $n = 1233$  initiated and 1233 spontaneous events from 10 different slices). The mean number of waves or

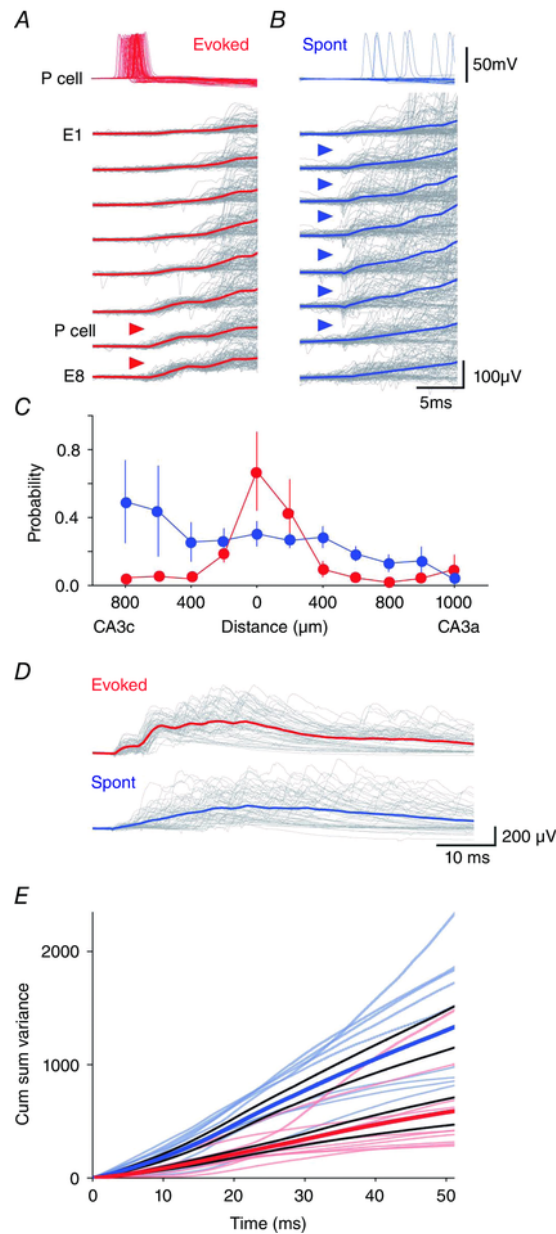


Figure 5.6: **Differences between initiated and spontaneous SPW fields.** The site of initiation for evoked SPWs (red triangles) (A) varied less than that of spontaneous SPWs (blue triangles) (B). Overlay (grey) and averages of 100 initiated (red) and 100 spontaneous SPWs recorded over the same period from electrodes E1–E8 in the CA3 stratum pyramidale. SPWs were aligned at their initiation site defined from spikes and field. The stimulated pyramidal cell was situated between E6 and E7. C, the spatial distribution of extracellular unit activity at the start of initiated SPWs (red) was more restricted than that preceding spontaneous events (blue). Data from 10 slices, with distance 0  $\mu\text{m}$  corresponding to the extracellular electrode closest to the initiating cell. D, cumulative variability of SPW fields was less for initiated than spontaneous events ( $P = 0.016$ , bootstrap). Above: overlays of 50 evoked SPWs (grey, mean shown in red) and 50 spontaneous SPWs (grey, mean in blue). E, time course of cumulative variability for initiated (red,  $n = 10$  slices) and spontaneous SPWs (blue;  $n = 10$ ), with mean  $\pm$  SE (bold lines). A lower variability at initiation was maintained through SPW time course.

fIPSPs was counted across eight recording sites, with events simultaneous at multiple sites counted as one event. There were  $6.7 \pm 1.4$  waves for initiated events and  $6.3 \pm 1.2$  waves for spontaneous events (paired t test,  $P = 0.29$ ,  $n = 2466$ ). The mean interval between fIPSPs, from all electrodes, was  $6.7 \pm 1.4$  for initiated events and  $7.1 \pm 1.0$  for spontaneous events (paired t test,  $P = 0.17$ ,  $n = 2466$ ). On the basis of these criteria, initiated events did not differ from spontaneously occurring SPWs. Finally, we investigated whether later phases of initiated SPW fields followed a more stereotyped time course than spontaneous SPW fields (Fig. 5.6D). As an index of field variability, we used a cumulative sum of root-mean-square differences between each field potential and the mean field from each electrode (see Methods). Identical numbers of initiated and spontaneous SPWs from the same time period for each recording were analysed ( $n = 10$ ). This index of cumulative field variability was always lower near the start of initiated SPWs, as expected, because the initiation site tended to be more stereotyped. Figure 5.6D and E shows that the lower variability for initiated SPWs was maintained throughout their time course. If SPW fields in the stratum pyramidale largely reflect fIPSPs, then the set of interneurons firing during evoked SPWs may be more stereotyped than those active during spontaneous SPWs.

#### 5.4.5 Patterns of SPW spread and the activity of identified interneurons

We attempted to identify interneurons that fired during SPWs from the involvement of distinct spike and fIPSP motifs in SPW fields. We searched for spatially distinct events involving large extracellular spikes ( $> 20 \mu\text{V}$ ) as shown in Fig. 5.5. In seven of 10 records, we could distinguish (1) a motif triggered by a pyramidal cell that initiated SPWs and (2) a second inhibitory motif not evoked by that pyramidal cell. Figure 5.7A shows an example where the initiated motif consisted of a maximal spike on electrode E3 and a fIPSP on electrodes E1–E6. By contrast, the inhibitory motif shown in Fig. 5.5B, consisting of a maximal spike on electrode E6 and a fIPSP on electrodes E3–E8, was not initiated by the recorded pyramidal cell. Both extracellular units (Fig. 5.7A and C) appeared to participate in initiated SPWs (Fig. 5.7C–E). Isolated motifs and those embedded in SPWs were compared on the basis of spike amplitude and shape, as well as on the amplitude and form of fIPSPs recorded from all electrodes. In this way, the initiated motif of Fig. 5.7A appeared to be involved in 81 of 118 (69%) and the non-initiated fIPSP motif of Fig. 5.7B in 37 of 118 (31%) of triggered SPWs. FIPSP motifs triggered by initiating pyramidal cells were detected in SPWs with probabilities of 38–82% ( $n = 7$ ). Identified fIPSP motifs that were not elicited by pyramidal cell firing were

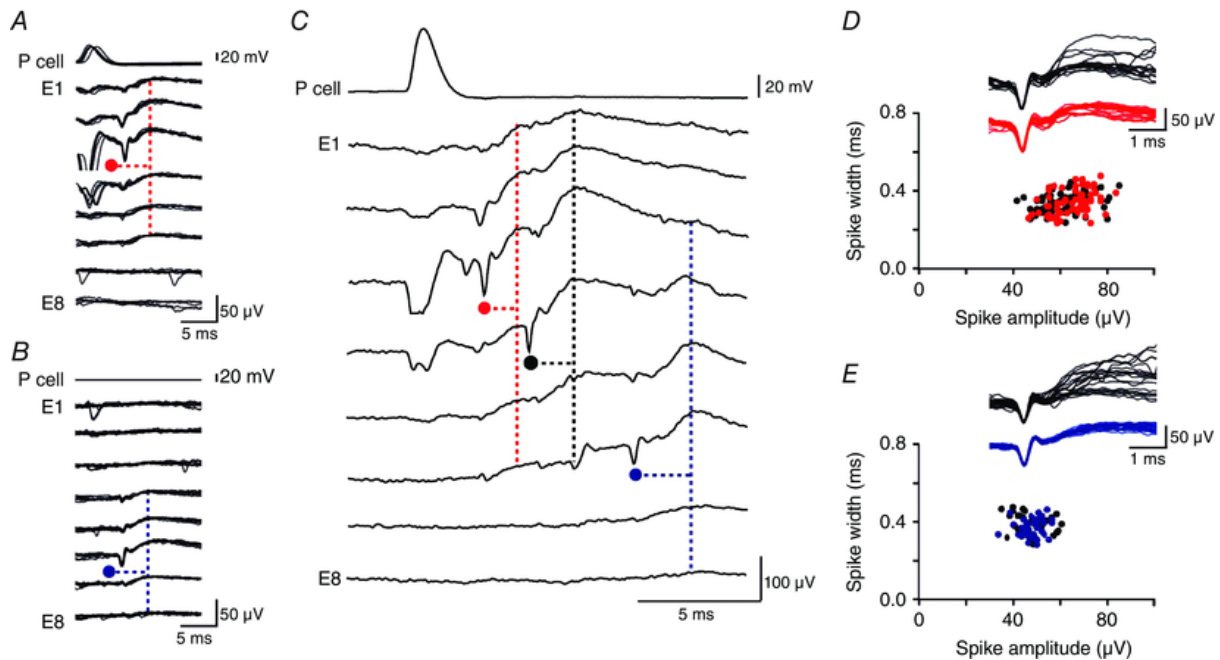


Figure 5.7: **Field inhibitory motifs during SPWs.** **A**, pyramidal cell spikes induce a presumed interneurone spike (red, maximum on electrode E3) and associated fIPSP. In total, 377 pyramidal cell action potentials initiated 130 single fIPSPs and 118 SPWs. Traces aligned on the extracellular spike. **B**, a spatially distinct interneurone spike (blue, maximum on E6) and fIPSP was never initiated by pyramidal cell firing. **A** and **B**, pyramidal cell and eight extracellular records from the stratum pyramidale. **C**, spike and fIPSP motifs were evident during SPWs initiated by the stimulated pyramidal cell. One interneurone spike (red, E3; A) occurs at  $\sim 2$  ms and the other (blue, E6; B) at  $\sim 10$  ms after pyramidal cell firing in this example. Another putative interneurone spike of amplitude  $> 20 \mu\text{V}$  (black, maximum on E4) occurs at a latency of  $\sim 5$  ms. **D**, amplitude plotted against width of spikes initiated by the pyramidal cell and recorded by electrode E3 before fIPSPs (red) or SPWs (black). Examples are overlain in the inset (fIPSPs,  $n = 20$ , red; SPWs,  $n = 20$ , black). **E**, amplitude plotted against width for spikes not directly initiated by the pyramidal cell and recorded on electrode E6 before fIPSPs (blue) or SPWs (black). Overlaid examples in the insets (fIPSPs,  $n = 20$ , blue; SPWs,  $n = 20$ , black).

detected with probability of 16–62% ( $n = 7$ ). These data suggest that, as SPWs spread, previously silent interneurons were recruited at longer latencies than directly excited interneurons. The occurrence and the timing of firing in identified interneurons during SPWs initiated by the same pyramidal cell varied between trials (Fig. 5.6).

## 5.5 Discussion

Single identified neurones of invertebrates and fish can initiate motor behaviours (Ikeda and Wiersma, 1964; Getting and Dekin, 1985; Eaton et al., 1977). Single mammalian pyramidal cells can affect movement (Brecht et al., 2004), sensory perception (Houweling and Brecht, 2007), volition (Fried et al., 2011), entrain or initiate population activities (Miles and Wong, 1983; de la Prida et al., 2006; Bonifazi et al., 2009), and alter EEG activities between patterns associated with different brain states (Cheng-yu et al., 2009). These effects depend on the identity and numbers of neurones driven to discharge by firing in the single initiating cell (Kwan and Dan, 2012). Data are reported in the present study showing that  $\sim 30\%$  of CA3 pyramidal cells triggered SPW-like events in vitro. We further show that these pyramidal cells evoked firing at similar latencies in several (2–6) perisomatic interneurons. Comparison of inhibitory fields and SPW fields suggested that, during a SPW, different interneurons fire repeatedly at intervals of 3–8 ms.

### 5.5.1 Advantages of an in vitro study

The work in the present study was facilitated by employing an in vitro approach. Accurate placement of linear electrode arrays orthogonal to the CA3 stratum pyramidale permitted field profile analyses of current profiles associated with SPWs and fIPSPs. Curved arrays placed along the stratum pyramidale allowed us to discriminate between the firing of different interneurons and the fIPSPs that they generated, revealing distinct fIPSP motifs. SPW-like fields in vitro have a form and duration similar to those recorded in the intact animal. Equally, single pyramidal cells discharge post-synaptic interneurons at comparable latencies and probabilities in vivo (Csicsvari et al., 1998), as well as in slices kept in an interface chamber (Miles, 1990). Inhibitory field motifs consisting of an interneurone spike followed mono-synaptically by a spatially extended fIPSP have not yet been detected in vivo, possibly as a result of higher levels of background field fluctuations. Lower levels of fluctuation in fields in slices may have facilitated attempts to follow the firing of specific interneurons during SPWs. We used a clustering approach to sort inhibitory motifs identified by measurements of spike and inhibitory field waveforms, followed by visual comparison of aligned traces. To validate this approach, multiple field

records from stratum pyramidale could be compared with responses to single action potentials of intracellularly recorded, anatomically identified interneurons (Bazelot et al., 2010). This would provide data on the variability and spatial distribution of extracellular spikes and inhibitory fields initiated by an identified interneuron and also permit comparison with other extracellularly recorded motifs. Population activities involving interneurons may be detected more easily when slices are maintained at a liquid–gas interface or when precautions are taken to enhance oxygenation of submerged slices (Hajos et al., 2009). The amplitude of field IPSPs recorded from slices in interface chambers is several times larger than similar events recorded from submerged slices (Glickfeld et al., 2009; Bazelot et al., 2010). These factors may have contributed to the data reported by Ellender et al. (Ellender et al., 2010) suggesting that single pyramidal cell firing does not influence SPWs in submerged slices.

### **5.5.2 Initiating pyramidal cells excite perisomatic interneurons**

Evidence suggesting that SPW initiation involves pyramidal cell excitation of interneurons (Figs 5.5 and 5.7) is based on the latency of initiated events and signs of interneurone firing at the start of SPWs (Hajos et al., 2013; Sasaki et al., 2014; Schlingloff et al., 2014). The intervals between pyramidal cell firing and SPW initiation are comparable to the delays between pyramidal cell firing and spikes discharged by a post-synaptic interneurone. By contrast, transmission of firing between mono-synaptically coupled pyramidal cells requires multiple pre-synaptic action potentials and occurs at latencies of 10–15 ms or more (Miles and Wong, 1987; Kwan and Dan, 2012; Ikegaya et al., 2013). Extracellular spikes detected at SPW initiation possessed characteristics of interneurone spikes (Henze et al., 2000). When SPWs were not triggered, these spikes could be followed by unitary extracellular inhibitory fields (Glickfeld et al., 2009; Bazelot et al., 2010). Recorded from the stratum pyramidale, SPW fields apparently correspond to repeated, summed fIPSPs at intervals of 3–8 ms, as first suggested by Buzsaki et al. (Buzsaki et al., 1992). Our comparison of current sources for fIPSPs and SPWs, as well as the suppression of SPWs by the opiate DAMGO, suggests that the interneurons involved synapse with pyramidal cells at perisynaptic sites as inferred from studies performed *in vitro* (Hajos et al., 2013; Aivar et al., 2014) and *in vivo* (Klausberger et al., 2003).

### **5.5.3 Continuation, spread and cellular components of SPWs**

Although our data suggest that interneurone firing, which may be induced by pyramidal cells, should precede SPWs, they do not clarify the mechanisms ensuring repeated

firing of the same or different interneurons as SPWs continue. Records from interneurons (Fig. 5.3B) show repeated, fast depolarizations aligned with each wave of a SPW. Possibly, these events reflect excitatory synaptic inputs from pyramidal cells. However, few pyramidal cells fired during SPW-like events and the second EPSP in interneurons appears to occur too soon (at 5–10 ms after SPW initiation) for it to depend on synaptically induced firing in pyramidal cells recruited by the initiating cell. Figure 5.5 shows that single initiating pyramidal cells can induce firing in multiple interneurons. Firing is probabilistic. Not all innervated interneurons fire in response to the same pyramidal cell action potential, and we found no evidence for a delayed firing by different interneurons that could sculpt successive waves of a SPW (Sasaki et al., 2014). Possibly, interactions between interneurons (Fukuda and Kosaka, 2000) ensure that SPWs continue after their initiation. If so, such interactions should be able to generate the repeated depolarizations recorded from interneurons during a SPW (Fig. 5.3B). Alternatively repeated events emerging from supralinear dendritic electrogenesis may ensure that SPWs continue (Memmesheimer, 2010). Records with electrodes placed along the CA3 stratum pyramidale demonstrate how SPW-like events spread in a slice. SPWs are known to propagate from CA3 into the CA1 region (Csicsvari et al., 2000; Maier et al., 2003) and macroscopic array records show that some SPWs are spatially restricted in the intact animal, whereas others spread longitudinally throughout the CA3 region (Patel et al., 2013). At the smaller scale of a transverse slice, our data suggest that previously silent, distant interneurons fire as later waves of a SPW field spread to new sites. Because these interneurons are not excited by the initiating pyramidal cell (Fig. 5.7), they must be recruited in another way. Their activity generates a spatially distinct fIPSP and so underlies, in part, propagation of the SWP field. Field potentials of SPWs initiated by single pyramidal cells are more stereotyped than those associated with spontaneous SPWs (Fig. 5.6A and D). However, even if only some participating neurons were recognized, our data show variation with respect to the occurrence and identity of directly triggered interneuron firing and those of interneurons indirectly recruited during the later stages of SPWs (Figs 5.2, 5.5 and 5.7). Presumably, more complex mechanisms control the apparently precise time sequences of pyramidal cell firing replay during SPWs in the intact animal (Lee and Wilson, 2002; Diba and Buzsáki, 2007; Stark et al., 2014). In summary, the results of the present study reveal a continuum between single fIPSPs and SPWs. Both events were triggered by some (~30%) recorded pyramidal cells. Latencies were consistent with those for the transmission of firing at synapses that excite interneurons. Multiple extracellular records allow us to separate spatially distinct spikes of interneurons and the resulting inhibitory fields. In this way, pyramidal cells that initiate SPWs were shown to excite several interneurons. The identification of different interneurons

and the fields that they produced revealed (1) fluctuations in the composition of SPWs initiated by the same pyramidal cell and (2) the recruitment of previously silent inhibitory cells as SPWs spread through the CA3 region.

---

## Bibliography

---

- Aivar, P., Valero, M., Bellistri, E., and de la Prida, L. M. (2014). Extracellular calcium controls the expression of two different forms of ripple-like hippocampal oscillations. *The Journal of Neuroscience*, 34(8):2989–3004.
- Bähner, F., Weiss, E. K., Birke, G., Maier, N., Schmitz, D., Rudolph, U., Frotscher, M., Traub, R. D., Both, M., and Draguhn, A. (2011). Cellular correlate of assembly formation in oscillating hippocampal networks in vitro. *Proceedings of the National Academy of Sciences*, 108(35):E607–E616.
- Bazelot, M., Dinocourt, C., Cohen, I., and Miles, R. (2010). Unitary inhibitory field potentials in the ca3 region of rat hippocampus. *The Journal of physiology*, 588(12):2077–2090.
- Bazelot, M., Teleńczuk, M. T., and Miles, R. (2016). Single CA3 pyramidal cells trigger sharp waves in vitro by exciting interneurons. *Journal of Physiology*, 0:1–13.
- Bonifazi, P., Goldin, M., Picardo, M. A., Jorquera, I., Cattani, A., Bianconi, G., Represa, A., Ben-Ari, Y., and Cossart, R. (2009). Gabaergic hub neurons orchestrate synchrony in developing hippocampal networks. *Science*, 326(5958):1419–1424.
- Brecht, M., Schneider, M., Sakmann, B., and Margrie, T. W. (2004). Whisker movements evoked by stimulation of single pyramidal cells in rat motor cortex. *Nature*, 427(6976):704–710.
- Buzsáki, G., Vanderwolf, C. H., et al. (1983). Cellular bases of hippocampal eeg in the behaving rat. *Brain Research Reviews*, 6(2):139–171.
- Buzsaki, G., Wise, K., et al. (1992). High-frequency network oscillation in the hippocampus. *Science*, 256(5059):1025.
- Cheng-yu, T. L., Poo, M.-m., and Dan, Y. (2009). Burst spiking of a single cortical neuron modifies global brain state. *Science*, 324(5927):643–646.
- Cohen, I. and Miles, R. (2000). Contributions of intrinsic and synaptic activities to the generation of neuronal discharges in in vitro hippocampus. *The Journal of physiology*, 524(2):485–502.

- Csicsvari, J., Hirase, H., Czurko, A., and Buzsáki, G. (1998). Reliability and state dependence of pyramidal cell–interneuron synapses in the hippocampus: an ensemble approach in the behaving rat. *Neuron*, 21(1):179–189.
- Csicsvari, J., Hirase, H., Mamiya, A., and Buzsáki, G. (2000). Ensemble patterns of hippocampal ca3-cal neurons during sharp wave–associated population events. *Neuron*, 28(2):585–594.
- de la Prida, L. M., Huberfeld, G., Cohen, I., and Miles, R. (2006). Threshold behavior in the initiation of hippocampal population bursts. *Neuron*, 49(1):131–142.
- Diba, K. and Buzsáki, G. (2007). Forward and reverse hippocampal place-cell sequences during ripples. *Nature neuroscience*, 10(10):1241–1242.
- Draguhn, A., Traub, R., Schmitz, D., and Jefferys, J. (1998). Electrical coupling underlies high-frequency oscillations in the hippocampus in vitro. *Nature*, 394(6689):189–192.
- Eaton, R. C., Bombardieri, R. A., and Meyer, D. L. (1977). The mauthner-initiated startle response in teleost fish. *Journal of Experimental Biology*, 66(1):65–81.
- Ellender, T. J., Nissen, W., Colgin, L. L., Mann, E. O., and Paulsen, O. (2010). Priming of hippocampal population bursts by individual perisomatic-targeting interneurons. *The Journal of neuroscience*, 30(17):5979–5991.
- Fried, I., Mukamel, R., and Kreiman, G. (2011). Internally generated preactivation of single neurons in human medial frontal cortex predicts volition. *Neuron*, 69(3):548–562.
- Fukuda, T. and Kosaka, T. (2000). Gap junctions linking the dendritic network of gabaergic interneurons in the hippocampus. *The Journal of Neuroscience*, 20(4):1519–1528.
- Getting, P. and Dekin, M. (1985). Mechanisms of pattern generation underlying swimming in tritonia. iv. gating of central pattern generator. *Journal of Neurophysiology*, 53(2):466–480.
- Girardeau, G., Benchenane, K., Wiener, S. I., Buzsáki, G., and Zugaro, M. B. (2009). Selective suppression of hippocampal ripples impairs spatial memory. *Nature neuroscience*, 12(10):1222–1223.
- Glickfeld, L. L., Roberts, J. D., Somogyi, P., and Scanziani, M. (2009). Interneurons hyperpolarize pyramidal cells along their entire somatodendritic axis. *Nature neuroscience*, 12(1):21–23.
- Gulyás, A. I., Szabó, G. G., Ulbert, I., Holderith, N., Monyer, H., Erdélyi, F., Szabó, G., Freund, T. F., and Hájos, N. (2010). Parvalbumin-containing fast-spiking basket cells generate the field potential oscillations induced by cholinergic receptor activation in the hippocampus. *The Journal of neuroscience*, 30(45):15134–15145.
- Hajos, N., Ellender, T. J., Zemankovics, R., Mann, E. O., Exley, R., Cragg, S. J., Freund, T. F., and Paulsen, O. (2009). Maintaining network activity in submerged hippocampal slices: importance of oxygen supply. *European Journal of Neuroscience*, 29(2):319–327.
- Hájos, N., Karlócai, M. R., Németh, B., Ulbert, I., Monyer, H., Szabó, G., Erdélyi, F., Freund, T. F., and Gulyás, A. I. (2013). Input-output features of anatomically identified ca3 neurons during hippocampal sharp wave/ripple oscillation in vitro. *The Journal of Neuroscience*, 33(28):11677–11691.

- Henze, D. A., Borhegyi, Z., Csicsvari, J., Mamiya, A., Harris, K. D., and Buzsáki, G. (2000). Intracellular features predicted by extracellular recordings in the hippocampus in vivo. *Journal of neurophysiology*, 84(1):390–400.
- Ho, E. C., Zhang, L., and Skinner, F. K. (2009). Inhibition dominates in shaping spontaneous ca3 hippocampal network activities in vitro. *Hippocampus*, 19(2):152–165.
- Houweling, A. R. and Brecht, M. (2007). Behavioural report of single neuron stimulation in somatosensory cortex. *Nature*, 450(7172).
- Hu, H. and Jonas, P. (2014). A supercritical density of na+ channels ensures fast signaling in gabaergic interneuron axons. *Nature neuroscience*, 17(5):686–693.
- Ikeda, K. and Wiersma, C. (1964). Autogenic rhythmicity in the abdominal ganglia of the crayfish: the control of swimmeret movements. *Comparative biochemistry and physiology*, 12(1):107–115.
- Ikegaya, Y., Sasaki, T., Ishikawa, D., Honma, N., Tao, K., Takahashi, N., Minamisawa, G., Ujita, S., and Matsuki, N. (2013). Interpyramid spike transmission stabilizes the sparseness of recurrent network activity. *Cerebral Cortex*, 23(2):293–304.
- Jadhav, S. P., Kemere, C., German, P. W., and Frank, L. M. (2012). Awake hippocampal sharp-wave ripples support spatial memory. *Science*, 336(6087):1454–1458.
- Ji, D. and Wilson, M. A. (2007). Coordinated memory replay in the visual cortex and hippocampus during sleep. *Nature neuroscience*, 10(1):100–107.
- Klausberger, T., Magill, P. J., Márton, L. F., Roberts, J. D. B., Cobden, P. M., Buzsáki, G., and Somogyi, P. (2003). Brain-state-and cell-type-specific firing of hippocampal interneurons in vivo. *Nature*, 421(6925):844–848.
- Kubota, D., Colgin, L. L., Casale, M., Brucher, F. A., and Lynch, G. (2003). Endogenous waves in hippocampal slices. *Journal of neurophysiology*, 89(1):81–89.
- Kwan, A. C. and Dan, Y. (2012). Dissection of cortical microcircuits by single-neuron stimulation in vivo. *Current Biology*, 22(16):1459–1467.
- Lee, A. K. and Wilson, M. A. (2002). Memory of sequential experience in the hippocampus during slow wave sleep. *Neuron*, 36(6):1183–1194.
- Maier, N., Nimrich, V., and Draguhn, A. (2003). Cellular and network mechanisms underlying spontaneous sharp wave–ripple complexes in mouse hippocampal slices. *The Journal of physiology*, 550(3):873–887.
- Maier, N., Tejero-Cantero, Á., Dorn, A. L., Winterer, J., Beed, P. S., Morris, G., Kempter, R., Poulet, J. F., Leibold, C., and Schmitz, D. (2011). Coherent phasic excitation during hippocampal ripples. *Neuron*, 72(1):137–152.
- Memmesheimer, R.-M. (2010). Quantitative prediction of intermittent high-frequency oscillations in neural networks with supralinear dendritic interactions. *Proceedings of the National Academy of Sciences*, 107(24):11092–11097.

- Miles, R. (1990). Synaptic excitation of inhibitory cells by single ca3 hippocampal pyramidal cells of the guinea-pig in vitro. *The Journal of physiology*, 428(1):61–77.
- Miles, R. and Wong, R. (1987). Inhibitory control of local excitatory circuits in the guinea-pig hippocampus. *The Journal of Physiology*, 388(1):611–629.
- Miles, R. and Wong, R. K. (1983). Single neurones can initiate synchronized population discharge in the hippocampus. *Nature*, 306(5941):371–3.
- Nicholson, C. and Freeman, J. A. (1975). Theory of current source-density analysis and determination of conductivity tensor for anuran cerebellum. *Journal of Neurophysiology*, 38(2):356–368.
- O’keefe, J. and Nadel, L. (1978). *The hippocampus as a cognitive map*, volume 3. Clarendon Press Oxford.
- Patel, J., Schomburg, E. W., Berényi, A., Fujisawa, S., and Buzsáki, G. (2013). Local generation and propagation of ripples along the septotemporal axis of the hippocampus. *The Journal of Neuroscience*, 33(43):17029–17041.
- Sasaki, T., Matsuki, N., and Ikegaya, Y. (2014). Interneuron firing precedes sequential activation of neuronal ensembles in hippocampal slices. *European Journal of Neuroscience*, 39(12):2027–2036.
- Schlingloff, D., Káli, S., Freund, T. F., Hájos, N., and Gulyás, A. I. (2014). Mechanisms of sharp wave initiation and ripple generation. *The Journal of Neuroscience*, 34(34):11385–11398.
- Shadlen, M. N. and Newsome, W. T. (1998). The variable discharge of cortical neurons: implications for connectivity, computation, and information coding. *The Journal of neuroscience*, 18(10):3870–3896.
- Stark, E., Roux, L., Eichler, R., Senzai, Y., Royer, S., and Buzsáki, G. (2014). Pyramidal cell-interneuron interactions underlie hippocampal ripple oscillations. *Neuron*, 83(2):467–480.
- Svoboda, K. R., Adams, C. E., and Lupica, C. R. (1999). Opioid receptor subtype expression defines morphologically distinct classes of hippocampal interneurons. *The Journal of neuroscience*, 19(1):85–95.

---

## Conclusions

---

The action potential (AP) is a signal generated in the nerve cell used for the transmission of messages. This short (compared to other changes in potential in the cell) but relatively large rise in potential is easy to record intra- and extracellularly with the technologies available at the present time. Multiple analytical and computational models efficiently reproduce the general shape of the action potential (e.g. [Hodgkin and Huxley \(1952\)](#) and [Mainen and Sejnowski \(1996\)](#)).

The present work aims to investigate the generation of the action potential, and its impact on the extracellular field and on the local network. Our study reveals that the action potential is a complex event whose intra- and extracellular characteristics depend on the type, density and location of active ion channels. Furthermore, the location of the axon initial segment has an impact on the extracellular field. Finally, we suggest that single action potentials might play a significant role in the triggering of network activity.

The generation of action potentials depends on multiple variables such as density and location of ion channels, as well as on the morphology of the cell; We explored some of these factors. Most importantly, we contribute to the long-standing debate on the origin of the ‘kink’ of the action potentials recorded in the soma of mammalian neurons and on the initiation process of the action potential in those cells (Chapter 3). Furthermore, we highlighted the importance of the exact location of the initiation site, which is affected by the localisation of active ion channels, in the study of the shape of extracellular action potential recordings (Chapter 4). Finally we have shown that single action potentials of the pyramidal cells in the hippocampus can trigger network events that involve the activity of many interneurons (Chapter 5).

In the following sections we will discuss how these findings relate to the broader questions regarding the axon and action potential physiology, namely: Is each action

potential a unique signature of the activity or rather an all-or-none event? What is the role of the axon in neural coding?

## 6.1 Uniqueness of Action Potential

The action potential is a well described signal with a particular shape, defined mostly by the activation of sodium and potassium channels. Surprisingly, even within one cell type along different development stages, a neuron might display action potentials of various shapes and firing patterns; changes reflecting the development stage and properties of ionic channels (Dufour et al., 2014). The location of active ion channels might also have an impact on the action potential. In our study we show that the location of the ion channels forming the axon initial segment plays a role in the action potential initiation (Chapter 3) as well as in the amplitude and shape of action potentials recorded extracellularly (Chapter 4). Even with the same active ion channel composition, neurons of variable morphologies are found to produce different firing patterns (Mainen and Sejnowski, 1996). All of these underlying differences act on the action potential, each of which is unique in its initiation, propagation and impact on the extracellular field.

Does it mean that each of the action potentials should be considered and studied separately and only in its own unique environment given by the cell structure and channel distribution? Some studies argue that single action potentials are not very significant in the context of the population activity and that only the total number of APs in the population matters; This hypothesis is called rate coding (Softky and Koch, 1993). As an argument for rate coding, London and colleagues proposed that the timing of single action potentials responding to the signal received from its presynaptic connections is offset by noise and so does not carry information in a busy *in vivo* environment (London et al., 2010). However, even in *in vitro* preparations we noticed a high variability in the shape of the network activity (Sharp-Wave ripple) triggered by action potentials of the same pyramidal cell (Chapter 5). These responses were nevertheless more uniform than spontaneous Sharp-Wave ripple activity. Furthermore, it was clear that the first cell triggered by the action potential of the pyramidal cell was not always the same from one time to the next. This could potentially depend on the excitable state of the pyramidal cell, the current stage of its postsynaptic connections, or it could reflect the plasticity state of the synapses; perhaps eventually leading to rather complex information being transmitted by single action potential to other cells. Strikingly, some studies showed that the information content of single action potentials is higher than simple binary information. They suggest that not only is the action potential transmitted to post-synaptic targets, but that the presynaptic membrane potential also influences AP amplitude (Clark and

Hausser, 2006; Debanne et al., 2013). From an evolutionary perspective, what could be the purpose for the brain to shape neurons with different types and densities of active ion channels if they all eventually led to the same - initiation and propagation of the action potential carrying binary information?

If a single action potential carries significant information, to which extent does its timing matter? The hypothesis that brain information is encoded in the precise timing of AP from individual neurons is termed temporal coding. Multiple studies have shown that such temporal data may contain a significant amount of information about the stimuli (Panzeri et al., 2001). This view treats the neurons as information channels (Bialek et al., 1991). However, other researchers dismiss the idea on epistemological grounds and suggest that the real question regards the causal role of a single AP on the neural activity. From this point of view it only seems justifiable to consider a spike-timing based model (Brette, 2015). The results of our experiments in hippocampal slices described above appear to be consistent with this hypothesis.

In this study, we do not solve the ongoing debate between spike- and rate-based approaches as neural coding question, but we do show that single action potentials are unique in their initiation, which is also reflected extracellularly, and that they may be significant enough to trigger events in the scale of the network.

## 6.2 Role of the axon in neuronal coding

With ever-advancing techniques it is now possible to measure the electric potential even from structures as thin as the mammalian axon (Kole et al., 2007). However, even with multiple available possibilities to studying AP, it is not always straightforward to answer some of the fundamental questions regarding the axon's role in coding. We know that the axonal tree plays an important role in information transmission between the nerve cells and that the type and distribution of ionic channels in the axon may lead to differences, such as in the number of generated single action potentials or bursts, in the plasticity of the synaptic connections or that it can cause axonal transmission delays.

Aspects as fundamental as the plasticity of the location and the length of the axon initial segment have been revealed only recently (Grubb and Burrone, 2010). We show that location of the axon initial segment is significant for the 'kink' in the soma (Chapter 3). This sharpness has consequences in the energy efficiency of AP initiation and for neurons to respond faster to changes in its inputs (Brette, 2013). Our work also highlights the differences in the extracellular potentials which are influenced by the shift in the axon initial segment (Chapter 4). However, besides the visible effects of the location of axon initial segment within the axon, an answer to the crucial question of how this plasticity affects

the message received by other cells remains elusive (although Grubb and Burrone (2010) hypothesize that together with synaptic homeostatic scaling it could help the neuron to stabilize its excitability and maximize its information processing capabilities).

In the present work we put major emphasis on the active ion channels expressed in the axon initial segment. However, after its initiation, action potential propagates along the axonal tree, which might vary in its morphology, number and distribution of synapses, and whether or not it is myelinated. The location and purpose of each part of the axon seems to be well designed to efficiently carry its function. For instance, the dynamics of sodium and potassium channels in axons is optimized to provide maximum energy efficiency (Alle et al., 2009). The axon may act on the signal by failing, delaying or succeeding to propagate the action potential (Goldstein and Rall, 1974). Furthermore, the shape of the action potential might be altered within the axon before it reaches the synapses. Depending on the frequency of stimulation, action potentials might vary in duration when they arrive at the hippocampal mossy fiber boutons, leading to a different signal transmission to the postsynaptic cell (Geiger and Jonas, 2000).

Furthermore, the axon may also be involved in the synchronisation of neurons at a precision unattainable by chemical synapse connections. This, for example might be the case in the Sharp-Wave ripple complexes. In the Chapter 5 we show that Sharp-Wave ripple rests on the activity of multiple of interneurons firing in tight synchrony, but it is not understood how they manage to synchronize quickly enough to form such large network events (Bazelot et al., 2016). Recurrent connections in the hippocampus are believed to have some responsibility in the perpetration of Sharp-Waves (Chapter A), however they could not fully explain the presence of this phenomenon. Multiple hypotheses propose different solutions. For instance, gap junctions between the axons could potentially help to quickly synchronize cells (Traub and Bibbig, 2000), although some studies argue that Sharp-Waves persist (although with reduced strength) even when the genes responsible for the formation of gap junctions are silenced (Pais et al., 2011).

On another note, gap junctions between two axons are an interesting alternative to chemical synapses for the generation of different events. Draguhn and colleagues show that gap junctions might be necessary for fast synchronisations in the hippocampus (Draguhn et al., 1998), and in the fly, gap junctions between visual interneurons are proposed to be responsible for encoding quickly-varying visual information (Cuntz et al., 2007).

In summary, in spite of the fact that the Hodgkin-Huxley model is over 60 years old, and that action potentials and axons are some of the most investigated topics in biophysics, there are still many unexplored aspects of their physiology. We hope that this work advances our knowledge about the action potential at network, cell and ionic levels.

---

## Bibliography

---

- Alle, H., Roth, A., and Geiger, J. R. P. (2009). Energy-Efficient Action Potentials in Hippocampal Mossy Fibers. *Science*, 49(September):1405–1408.
- Bazelot, M., Teleńczuk, M. T., and Miles, R. (2016). Single CA3 pyramidal cells trigger sharp waves in vitro by exciting interneurons. *Journal of Physiology*, 0:1–13.
- Bialek, W., Rieke, F., de Ruyter van Steveninck, R. R., and David, W. (1991). Reading a Neural Code. *Science*, 252:1854–1857.
- Brette, R. (2013). Sharpness of Spike Initiation in Neurons Explained by Compartmentalization. *PLoS Computational Biology*, 9(12):e1003338.
- Brette, R. (2015). Philosophy of the spike: rate-based vs. spike-based theories of the brain. *Frontiers in systems neuroscience*, 9(November):1–14.
- Clark, B. and Hausser, M. (2006). Neural Coding: Hybrid Analog and Digital Signalling in Axons. *Current Biology*, 16(15):R585–R589.
- Cuntz, H., Haag, J., Forstner, F., Segev, I., and Borst, A. (2007). Robust coding of flow-field parameters by axo-axonal gap junctions between fly visual interneurons. *PNAS*, 104(24):10229–10233.
- Debanne, D., Bialowas, A., and Rama, S. (2013). What are the mechanisms for analogue and digital signalling in the brain? *Nature reviews. Neuroscience*, 14(1):63–9.
- Draguhn, A., Traub, R. D., Schmitz, D., and Jefferys, J. G. (1998). Electrical coupling underlies high-frequency oscillations in the hippocampus in vitro. *Nature*, 394(6689):189–92.
- Dufour, M. A., Woodhouse, A., Amendola, J., and Goillard, J.-M. (2014). Non-linear developmental trajectory of electrical phenotype in rat substantia nigra pars compacta dopaminergic neurons. *eLife*, 3:1–28.
- Geiger, J. R. P. and Jonas, P. (2000). Dynamic control of presynaptic Ca<sup>2+</sup> inflow by fast-inactivating K<sup>+</sup> channels in hippocampal mossy fiber boutons. *Neuron*, 28(3):927–939.

- Goldstein, S. S. and Rall, W. (1974). Changes of action potential shape and velocity for changing core conductor geometry. *Biophysical journal*, 14(10):731–757.
- Grubb, M. S. and Burrone, J. (2010). Activity-dependent relocation of the axon initial segment fine-tunes neuronal excitability. *Nature*, 465(7301):1070–4.
- Hodgkin, A. L. and Huxley, A. F. (1952). A quantitative description of membrane current and its application to conduction and excitation in nerve. *Journal of Physiology*, 117:500–544.
- Kole, M. H. P., Letzkus, J. J., and Stuart, G. J. (2007). Axon Initial Segment Kv1 Channels Control Axonal Action Potential Waveform and Synaptic Efficacy. *Neuron*, 55(4):633–647.
- London, M., Roth, A., Beeren, L., Häusser, M., and Latham, P. E. (2010). Sensitivity to perturbations in vivo implies high noise and suggests rate coding in cortex. *Nature*, 466(7302):123–7.
- Mainen, Z. and Sejnowski, T. (1996). Influence of dendritic structure on firing pattern in model neocortical neurons.
- Pais, I., Hormuzdi, S. G., Monyer, H., Traub, R. D., Wood, I. C., Buhl, E. H., Whittington, M. A., and LeBeau, F. E. N. (2011). Sharp Wave-Like Activity in the Hippocampus In Vitro in Mice Lacking the Gap Junction Protein Connexin 36. *Journal of Neurophysiology*, 89(December 2002):2046–2054.
- Panzeri, S., Petersen, R. S., Schultz, S. R., Lebedev, M., and Diamond, M. E. (2001). The Role of Spike Timing in the Coding of Stimulus Location in Rat Somatosensory Cortex. *Neuron*, 44-46:573–578.
- Softky, W. R. and Koch, C. (1993). The highly irregular firing of cortical cells is inconsistent with temporal integration of random EPSPs. *The Journal of neuroscience*, 13(1):334–50.
- Traub, R. D. and Bibbig, A. (2000). A model of high-frequency ripples in the hippocampus based on synaptic coupling plus axon-axon gap junctions between pyramidal neurons. *The Journal of neuroscience : the official journal of the Society for Neuroscience*, 20(6):2086–2093.

---

## Recurrent synapses and circuits in the CA3 region of the hippocampus: an associative network

---

This chapter is the revision written together by Caroline Le Duigou, Jean Simonnet, Desdemona Fricker, Richard Miles and Maria Teleńczuk. It has been published in *Frontiers in Cellular Neuroscience* in 2014 (Le Duigou et al., 2014).

### A.1 Abstract

In the CA3 region of the hippocampus, pyramidal cells excite other pyramidal cells and interneurons. The axons of CA3 pyramidal cells spread throughout most of the region to form an associative network. These connections were first drawn by Cajal and Lorente de No. Their physiological properties were explored to understand epileptiform discharges generated in the region. Synapses between pairs of pyramidal cells involve one or few release sites and are weaker than connections made by mossy fibers on CA3 pyramidal cells. Synapses with interneurons are rather effective, as needed to control unchecked excitation. We examine contributions of recurrent synapses to epileptiform synchrony, to the genesis of sharp waves in the CA3 region and to population oscillations at theta and gamma frequencies. Recurrent connections in CA3, as other associative cortices, have a lower connectivity spread over a larger area than in primary sensory cortices. This sparse, but wide-ranging connectivity serves the functions of an associative network, including acquisition of neuronal representations as activity in groups of CA3 cells and completion involving the recall from partial cues of these ensemble firing patterns.

## A.2 Recurrent excitatory synapses between CA3 cells: emergence

Recurrent connections between CA3 cells in the hippocampus can be seen in early drawings of Golgi stained neurons. Schaffer (1892) and Ramón y Cajal (1899) drew pyramidal cell processes that ramify extensively in the CA3 region as well as projecting into CA1 (Schaffer, 1892; Ramón y Cajal, 1899). Later, but still before cellular physiology, Lorente de N (1934) drew axonal terminals of a CA3 cell contacting mid-apical dendrites of a nearby pyramidal cell and a basket cell ((Lorente de Nó, 1934), Figure A.1). So a basis for recurrent excitation existed before synaptic operations were fully accepted. The absence of this detail did not impede speculation. Recurrent connections between cells of the same region were linked to feedback in chains of connected neurons. Lorente de No (1938) and later Hebb (1949) proposed they might generate reverberating neuronal discharges as an immediate electrical memory (Lorente de Nó, 1934; Hebb, 1949).

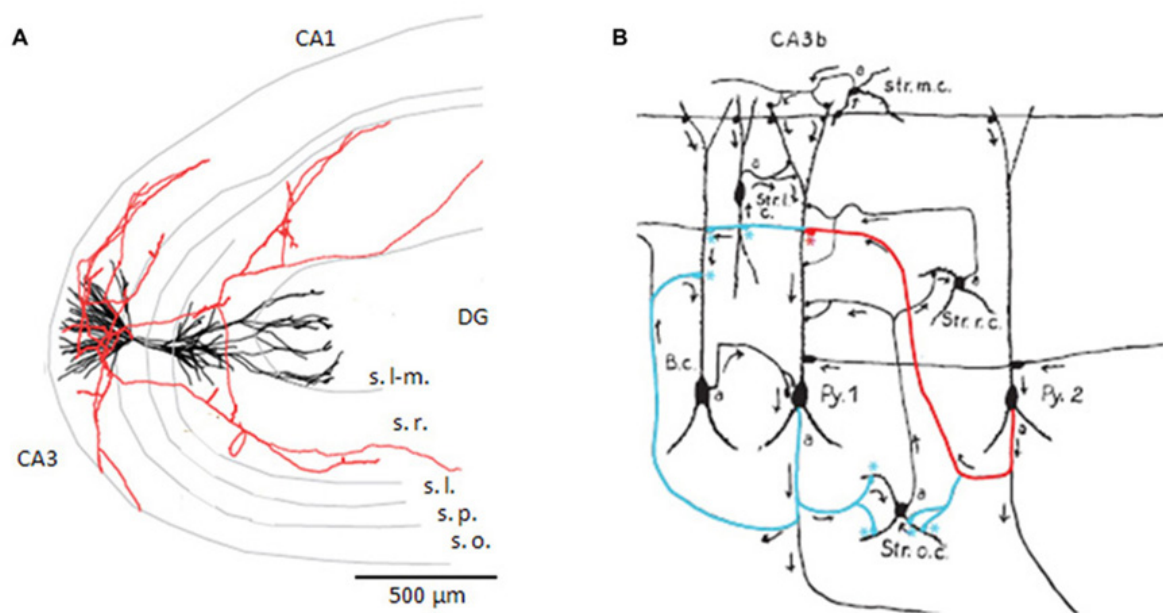


Figure A.1: **CA3 pyramidal cell axon and targets.** **A.** Reconstruction of a CA3 pyramidal cell dendrites, in black, and partial reconstruction of the axon, in red. Adapted from a cell filled by Ishizuka et al. ((Ishizuka et al., 1995), published as cell c12866 on neuromorpho.org). The CA3, CA1, and dentate gyrus (DG) regions are indicated as are the layers lacunosum-moleculare (s. l-m.), radiatum (s. r.), lucidum (s.l.), pyramidale (s.p.), and oriens (s.o.). **B.** Drawing of putative axo-dendritic connexions between pyramidal cells (Py. 1 and 2) and interneurons with somata in different layers (B.c., Str. o.c., Str. r.c., Str. l.c., Str. m.c.). The axon of Py. 2 may contact the dendrites of Py. 1, in red, and the interneuron of stratum oriens, in blue. The axon of Py. 1 is drawn contacting the basket cell, in blue (drawing adapted from Lorente de Nó (1934)).

Intracellular electrophysiology began for the hippocampus with the work of Spencer and Kandel. Initial results dampened the excitation somewhat. They showed that stimulating CA3 cell axons induced dominant inhibitory actions mediated by pyramidal cell excitation of interneurons (Spencer and Kandel, 1961). However recurrent actions were soon linked to reverberation and epileptic synchrony (Kandel and Spencer, 1961). This link was later strengthened by work on epileptiform synchrony induced by penicillin an early antagonist of inhibitory synaptic actions (Lebovitz et al., 1971). Explicitly combining computer simulations and in vitro physiology, Traub and Wong (1982) and Wong and Traub (1983) showed how recurrent excitatory synapses might underly delayed all-or-nothing population bursts induced by disinhibition (Traub and Wong, 1982; Wong and Traub, 1983). Physiological support for recurrent synaptic actions came from records of synaptic interactions between CA3 pyramidal cells in slices (Miles and Wong, 1986). Recurrent synapses together with the modeling work could explain the unexpected finding that stimulating a single cell could initiate interictal-like bursts of much larger neuronal populations (Miles and Wong, 1983).

### A.3 Axonal distributions of CA3 pyramidal cells

Axons of single CA3 pyramidal cells of the rat (Figure A.1) and guinea-pig have been traced from neurons filled with biocytin or horseradish peroxidase (Ishizuka et al., 1990; Sik et al., 1993; Li et al., 1994; Wittner et al., 2007; Wittner and Miles, 2007). Before projecting out of the region, axons ramify in stratum oriens and radiatum of CA3 contacting apical and basilar dendrites of other pyramidal cells as well as interneurons. Typically they divide into 5–10 collaterals projecting in different directions but rarely returning towards their parent neuron. Longitudinal projections of single axons (Lorente de Nó, 1934) can extend for ~70% of the dorso-ventral extent of rodent hippocampus (Sik et al., 1993; Li et al., 1994). A significant proportion of synapses made by a CA3 pyramidal cell may contact other CA3 cells. The Li et al. (1994) estimated 30–70%. Other connections are made onto CA1 neurons, while there is also a strong commissural projection (Li et al., 1994).

The total axonal length of well-filled CA3 pyramidal cell arbors is estimated as 150–300 mm in the rat with about 30% of the ramification within CA3 (Ishizuka et al., 1990; Li et al., 1994). Terminals are present along all of this distance and a single pyramidal cell is estimated to form 30,000 to 60,000 terminals. Terminals have been thought to target pyramidal cells and interneurons with a frequency similar to the presence of these neuronal types. Recent data suggest some interneuron subtypes may be selectively innervated (Wittner et al., 2007). Intra-regional differences exist: CA3b pyramidal cells tend to

innervate targets in stratum oriens and radiatum about equally, while CA3a pyramidal cell axons target stratum oriens targets more than those in stratum radiatum (Wittner and Miles, 2007).

## A.4 CA3 pyramidal cell axon physiology

Axon collaterals of CA3 pyramidal cells are un-myelinated. They include Schaffer collaterals that project to CA1 as well as those that ramify within the CA3 region. Action potentials are initiated at  $\sim 30\text{--}40\ \mu\text{m}$  from the soma, where sodium (Na) channel density reaches a peak according to physiology and immunostaining (Meeks and Mennerick, 2007). In regions beyond the action potential initiation site, recurrent axons of CA3 pyramidal cells conduct at velocities of  $0.2\text{--}0.4\ \text{mm/ms}$  (Soleng et al., 2003b; Meeks and Mennerick, 2007).

The Na channels expressed by CA3 recurrent collaterals seem likely to be  $\text{Na}_v1.2$  and  $\text{Na}_v1.6$  (Royeck et al., 2008; Debanne et al., 2011). These axons express multiple voltage-gated potassium (K) channels including  $\text{K}_v1.1$ ,  $\text{K}_v1.2$ , and  $\text{K}_v1.4$  (Lorincz and Nusser, 2008), ID (Saviane et al., 2003), the M-channel ( $\text{K}_v7/\text{KCNQ}$  (Vervaeke et al., 2006)), and the hyperpolarization activated h-current (Soleng et al., 2003a). This diversity of channel expression provides multiple means to modulate action potential shape and so control transmitter release (Bischofberger et al., 2006). Action potential modulation by axonal K-channels may become a total suppression of transmission when an IA-like K-current is fully activated (Debanne et al., 1997; Kopysova and Debanne, 1998).

## A.5 CA3 pyramidal cell terminals: numbers, form, contents, channels and release

Varicosities are formed at distances of  $2\text{--}5\ \mu\text{m}$  all along CA3 recurrent axons. They often have an ovoid form of diameter  $\sim 0.4\ \mu\text{m}$  compared to an axonal diameter of  $\sim 0.2\ \mu\text{m}$  (Sik et al., 1993; Li et al., 1994; Wittner and Miles, 2007)). Electron microscopy (EM; Figure A.2) indicates they possess attributes of pre-synaptic boutons with active zones and synaptic vesicles and they face densities at post-synaptic sites ((Schikorski and Stevens, 1997; Shepherd and Harris, 1998; Holderith et al., 2012)). While varicosities may contain up to three to four active sites, typically they have just one. Synaptic vesicles in recurrent terminals have diameters of  $20\text{--}40\ \text{nm}$ . A terminal may contain up to 800 vesicles with a mean number of  $150\text{--}270$  vesicles.

A small proportion of vesicles are so close ( $\sim 5\ \text{nm}$ ) to pre-synaptic membrane that

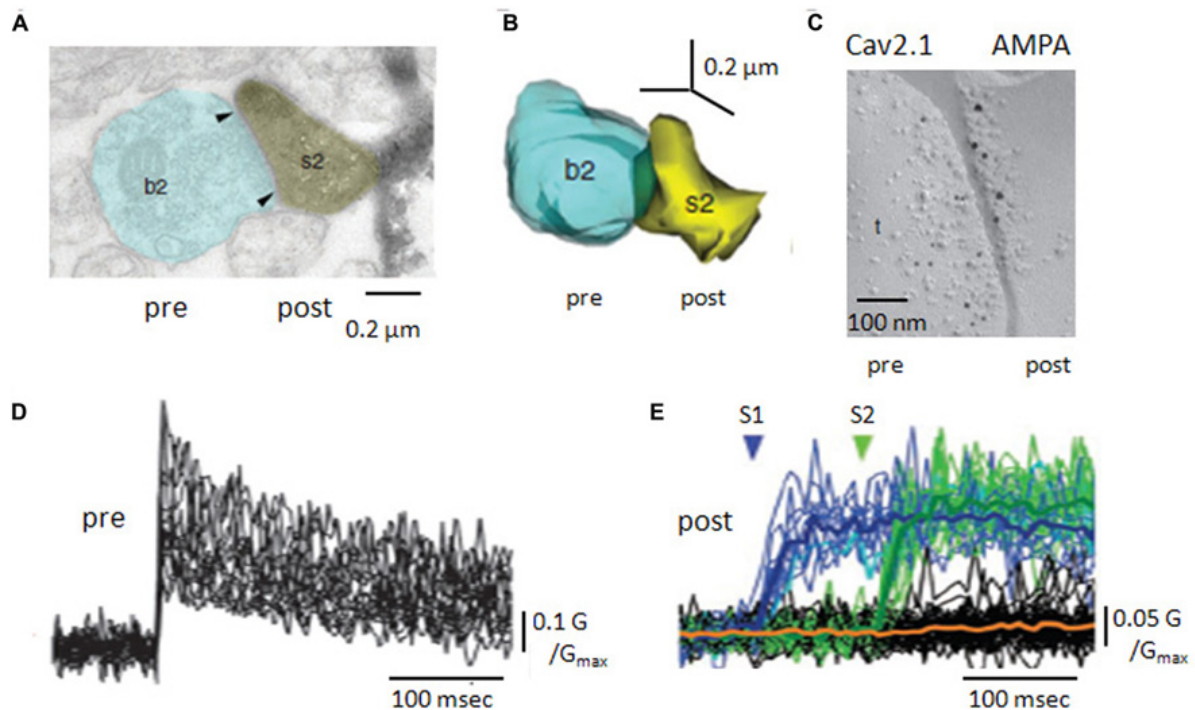


Figure A.2: **Anatomy and Ca handling at recurrent synapses between CA3 pyramidal cells.** **A.** Electron microscopy of a recurrent terminal, b2, apposed to a CA3 pyramidal cell dendritic spine, s2. **B.** Three-dimensional reconstruction of the contact. The area of the active zone [arrows in (A)] was  $0.10 \mu\text{m}^2$ . **C.** Double immuno-staining of SDS-digested freeze fracture replica of a recurrent synapse. The smaller gold particles label  $\text{Ca}_v2.1$  molecules (pre) and the larger gold particles recognize a pan-AMPA antibody (post). **D.** Pre-synaptic Ca transients, measured as changes in fluorescent intensity, for 25 axon terminals of a CA3 pyramidal cell. **E.** Post-synaptic Ca transients, in response to two pre-synaptic stimuli. Note the occurrence of failures in both post-synaptic responses but their absence from pre-synaptic signals (adapted with permission from Holderith et al. (2012)).

they are considered to be docked or available for release. The number of docked vesicles is estimated at 1–15 per terminal (Schikorski and Stevens, 1997; Shepherd and Harris, 1998; Holderith et al., 2012). Vesicles in terminals of CA3 pyramidal cell axons express the transporters, VGLUT1 and 2, and so presumably contain glutamate (Herzog et al., 2006). EM studies on CA3 axon terminals have not revealed a distinct population of large dense-core vesicles, which might contain peptides or other co-transmitters. About half of recurrent terminals contain one mitochondrion (Shepherd and Harris, 1998) and smooth endoplasmic reticulum is typically present: both organelles contribute to calcium (Ca) homeostasis (Sheng and Cai, 2012).

Ca entry into presynaptic terminals triggers transmitter release. CA3 axonal terminals express multiple Ca channel subtypes including  $\text{Ca}_v2.1$ ,  $\text{Ca}_v2.2$ ,  $\text{Ca}_v2.3$  (Holderith

et al., 2012), as do the mossy fiber terminals that also terminate on CA3 pyramidal cells (Li et al., 2007). Freeze-fracture replica gold immuno-labeling (Figure A.2) suggests a single terminal expresses several tens of  $Ca_v2.1$  channels (Holderith et al., 2012). This is more, but not many more, than estimates of the number of Ca-channels needed to trigger release from hippocampal inhibitory terminals (Bucurenciu et al., 2010). Possibly, an elevated Na channel density in terminals enhances Ca entry by boosting depolarization due to axonal spikes (Engel and Jonas, 2005). Certainly, recurrent terminals express various types of K channel which control transmitter release by limiting terminal depolarization. They may include the delayed rectifier type channels  $K_v1.1$  and  $K_v1.2$ , the fast-inactivating A-type channel  $K_v1.4$  (Debanne et al., 1997; Kopysova and Debanne, 1998; Lorincz and Nusser, 2008; Palani et al., 2010) as well as K-channels sensitive to both Ca and voltage (Saviane et al., 2003; Raffaelli et al., 2004) and the muscarine sensitive M-channel  $K_v7/KCNQ$  (Vervaeke et al., 2006).

Ca changes induced in local recurrent terminals by pyramidal cell firing have been resolved by imaging (Holderith et al., 2012; Sasaki et al., 2012). A single action potential induces a Ca signal of rise time less than 1 ms that decays over several 10 s of ms (Figure A.2). Ca entry occurs without failure even if it varies between trials at the same terminal and Ca elevations at neighboring terminals are poorly correlated. For a given terminal, the mean amplitude of Ca-signals is better correlated with the area of the active zone than terminal volume (Holderith et al., 2012).

CA3 axon terminals express receptors for transmitters which modulate Ca entry or later steps in release processes (FigureA.2). Receptors for the metabotropic glutamate receptor, mGluR7, expressed at active zones facing interneurons but not principal cells (Shigemoto et al., 1996) specifically control the excitation of inhibitory cells (Scanziani et al., 1998). The kainate receptor GluK1, reduces release by effects on both Ca entry and on G-protein mediated stages in transmitter release (Salmen et al., 2012). In contrast, presynaptic NMDA receptors enhance Ca entry and facilitate release at some synapses made by CA3 collaterals (McGuinness et al., 2010).

## A.6 Pre- meets post: synapses made by CA3 pyramidal cells with other CA3 cells

When a single spike induces Ca entry into a CA3 axon terminal, one, or none, or several vesicles of the excitatory transmitter glutamate are liberated. Release fails, when Ca enters a terminal but no transmitter is liberated, as shown by imaging Ca-entry (Figure A.2) via post-synaptic glutamate receptors (Koester and Johnston, 2005; Holderith

et al., 2012). Multi-vesicular release following a single action potential is most convincingly demonstrated when two distinct post-synaptic events can be resolved in time, as at some inhibitory synapses in the cerebellum (Auger et al., 1998). Analysis of variations in synaptic events over a range of liberation probabilities supports multi-vesicular liberation (Conti and Lisman, 2003; Christie and Jahr, 2006).

Glutamate, released from a pre-synaptic terminal, binds to post-synaptic receptors. The number of receptors per site has been estimated with physiological, imaging, and anatomical techniques. Post-synaptic sites facing terminals of CA3 pyramidal cell axons in young animals, all express NMDA (N-methyl-D-aspartate) receptors (Takumi et al., 1999). Glutamate uncaging onto post-synaptic sites activates 3–10 NMDA receptors (Nimchinsky et al., 2004). Semi-quantitative immunostaining studies and imaging agree that about 30% of post-synaptic sites possess no AMPA ( $\alpha$ -amino-3-hydroxy-5-methyl-4-isoxazolepropionic acid) receptors (Nusser et al., 1998; Takumi et al., 1999; Nimchinsky et al., 2004). At synapses where AMPA receptors are expressed, about 10 of them (Figure A.2) are estimated to be activated after a single pre-synaptic spike in acute slices (Nimchinsky et al., 2004), 40–150 in culture (Matsuzaki et al., 2001). AMPA receptors are present at recurrent synapses with most types of interneuron (Nusser et al., 1998). NMDA receptors are less frequently expressed at synapses with interneurons and may be absent at contacts with fast-spiking, parvalbumin containing cells (Nyiri et al., 2003).

There are two other important differences between synapses made with interneurons and with pyramidal cells. First, recurrent contacts tend to innervate pyramidal cell spines, while those with most types of inhibitory cell innervate dendritic shafts (Gulyás et al., 1993). Second, the AMPA receptor isoforms involved are different. AMPA receptor complexes at synapses formed with interneurons do not include the GluR2 subunit (Bochet et al., 1994; Geiger et al., 1995), resulting in faster kinetics (Miles, 1990), Ca-permeability, and a block by endogenous intraneuronal polyamines (Isaac et al., 2007).

## A.7 Pre- meets post in dual records

Double records from pre- and post-synaptic neurones at recurrent synapses between CA3 cells were first made to prove their existence directly. They remain the most persuasive means to examine how one neuron influences another. They have permitted definition of the number of synaptic contacts involved in a unitary connection and assessment of variability and changes in synaptic efficacy (Debanne et al., 2008).

Records from pairs of CA3 pyramidal cells in acute slices (Figure A.3) suggest one pyramidal cell excites 2–3% of possible pyramidal cell targets in a slice (Miles and Wong, 1986, 1987b). Odds are more favorable in organotypic slices. Connectivities are 30–60%

(Debanne et al., 1995; Pavlidis and Madison, 1999). The number of release sites involved in a connection may also be higher in organotypic cultures. One to three contacts have been validated by EM for synapses between pyramidal cells and interneurons recorded and filled with biocytin in slices. In contrast, light microscopy suggests 14–19 putative contacts may be involved in connections between CA3 pyramidal cells in organotypic culture (Pavlidis and Madison, 1999).

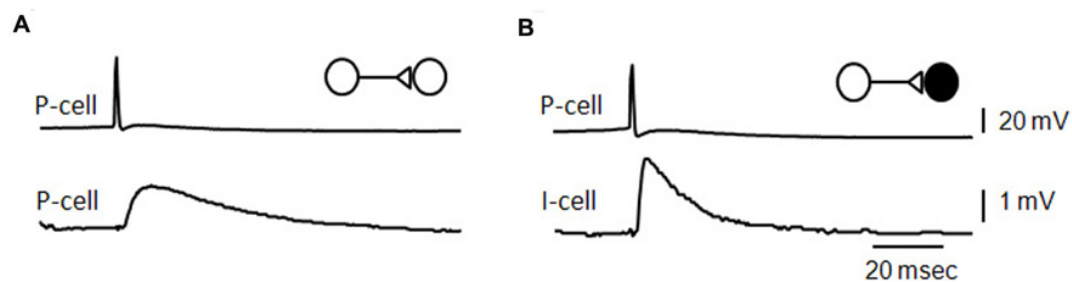


Figure A.3: **Unitary effects of recurrent excitatory synapses.** **A.** Average of EPSPs initiated in a CA3 pyramidal cell by single action potentials in a pre-synaptic pyramidal cell **B.** average of EPSPs elicited in a fast-spiking CA3 interneuron by action potentials in a pyramidal cell [an unpublished data Miles and Wong (B) adapted from Miles (1990)].

The mean amplitude of synaptic potentials is about 1 mV at connections between pyramidal cells in acute slices (Miles and Wong, 1986) and in culture (Debanne et al., 1995). EPSPs induced in fast-spiking interneurons (Figure A.3) are larger and faster than those initiated in pyramidal cells. Unitary synaptic current amplitude at connections made in culture can vary in the range 10–200 pA with an average near 30 pA (Pavlidis and Madison, 1999; Sasaki et al., 2012). In records from both acute slices and culture, events initiated successively at the same connection vary in amplitude. Transmission can fail, more often at connections with smaller averaged events. However pre-synaptic Ca entry never fails, even though it varies between successive action potentials (Holderith et al., 2012; Sasaki et al., 2012) and Ca signals are higher at terminals with a higher release probability (Koester and Johnston, 2005).

Synaptic events initiated sequentially at the same site vary in amplitude. This variability may have both pre- and post-synaptic components (Silver et al., 2003; Biró et al., 2005). Clear data on post-synaptic variability, is facilitated at connections with a single identified release site. At such a synapse, the variability in size of post-synaptic events was estimated at 20–50% (Gulyás et al., 1993). This variability might emerge from differences in the number of transmitter molecules released or in the activation of post-synaptic receptors.

The properties of recurrent synapses differ quite markedly from those of mossy fiber inputs, the other major source of excitation of CA3 pyramidal cells. A mossy fiber may

make 10–20 connections with different CA3 pyramidal cells (Claiborne et al., 1986). A recurrent collateral makes several thousand contacts with a much larger target population. Mossy fiber boutons contact proximal apical dendrites of CA3 pyramidal cells and have a diameter of 4–8  $\mu\text{m}$ . Each bouton may include 20–30 active zones, whereas a recurrent synapse may make one to three terminals on a post-synaptic cell. Finally mossy fibers contact apical dendrites near the CA3 soma, while recurrent synapses terminate at more distant dendritic sites resulting in smaller, slower somatic synaptic events. A mossy fiber input from one dentate granule cell can induce CA3 pyramidal cell firing and can so be termed a detonator synapse (Henze et al., 2002), whereas multiple spikes are needed to induce firing at recurrent synapses (Miles and Wong, 1987a).

## A.8 Short-term and long-term synaptic plasticity in double recordings

Records from pre- and post-synaptic cells at recurrent synapses have offered novel insights into activity dependent changes in synaptic strength over times lasting from milliseconds to hours.

Short-term plasticity (milliseconds to seconds) results from at least two functionally opposing processes. First, a single spike may facilitate transmission when the same synapse is activated again (Del Castillo and Katz, 1954). An enhanced release probability over several tens of milliseconds is ascribed to a residual elevation of intra-terminal Ca (Holderith et al., 2012; Sasaki et al., 2012). Second, and inversely, depression may result if few vesicles are available for release (Schikorski and Stevens, 1997; Shepherd and Harris, 1998). If they are replaced slowly (Stevens and Tsujimoto, 1995; Staley et al., 1998) the probability of a second release may be reduced by depletion. Both processes occur at connections between CA3 pyramidal cells (Debanne et al., 1996; Pavlidis and Madison, 1999). When a first spike induces a large event, a second synaptic response tends to be smaller due to depletion. Inversely a second EPSP tends to be larger after a small first event due to the residual Ca enhancement of release probability. Reflecting the underlying mechanisms, facilitation is maximal at 20–70 ms and terminates at about 500 ms, while depression can take several seconds to recover completely.

Long-term plasticity (minutes to hours) at different synapses varies in mechanisms of induction and expression. One of the most studied forms, long-term synaptic potentiation at Schaffer collateral synapses made by CA3 pyramidal cells with CA1 cells, is induced via the activation of NMDA receptors and expressed as the post-synaptic recruitment of AMPA receptors (Kerchner and Nicoll, 2008). Long-term changes in synaptic efficacy

seem to depend on similar mechanisms at recurrent synapses between CA3 pyramidal cells. Paired records from coupled CA3 cells have revealed some unitary details of this synaptic plasticity. The same connection can be potentiated or depotentiated (Debanne et al., 1998) by different temporal patterns of paired pre- and post-synaptic firing. About 20% of unitary interactions depend exclusively on NMDA receptors before potentiation (Montgomery et al., 2001), while both AMPA and NMDA receptors are activated after potentiation. Weak connections potentiate to a larger degree than initially strong connections (Debanne et al., 1999; Montgomery et al., 2001). Finally some connections between CA3 pyramidal cells do not seem to potentiate at all (Debanne et al., 1999; Montgomery and Madison, 2002).

## A.9 Transmission of recurrent excitatory signals on the membrane of a post-synaptic cell

Activation of membrane currents intrinsic to a post-synaptic cell by recurrent EPSPs affects how they sum, spread and eventually initiate firing. Initial evidence came from a prolongation of the decay of unitary EPSPs induced by pyramidal cell depolarization at subthreshold membrane potentials (Miles and Wong, 1986). In contrast unitary EPSPs initiated in fast-spiking inhibitory cells were not prolonged at depolarised subthreshold potentials (Miles, 1990). Work combining somatic records and synaptic stimuli with cell-attached records from dendrites, showed the activation of both inward currents, probably persistent Na channels, low-threshold Ca channels (Magee and Johnston, 1995), and outward currents, both inactivating and persistent (Hoffman et al., 1997). These currents have been more precisely described for EPSPs initiated by Schaffer collaterals (Lipowsky et al., 1996; Andreasen and Lambert, 1999; Perez-Rosello et al., 2011), as has evidence for a dendritic expression of the I-h current (Magee, 1999).

Distinct currents have been associated with specific effects on EPSP shape, summation, and spread. Na-channel activation near the peak of an EPSP tends to increase amplitude, while Ca-channels activated during the decay phase act to prolong EPSPs. The striking increase in dendritic expression of the I-h channel with distance from the soma (Lörincz et al., 2002) tends to equalize EPSPs impinging at proximal and distal sites (Magee, 1999). Dendritically expressed inactivating K-channels have been linked to less-than-linear summation of paired EPSPs impinging on different dendrites (Urban and Barrionuevo, 1998). Dual records from the soma and apical dendrites of CA3 pyramidal cells disclose two distinct regions of dendritic excitability (Kim et al., 2012). Fast Na-spikes are more easily initiated at distant sites corresponding to zones of recurrent

synaptic inputs, while excitability of more proximal dendritic sites is lower.

The role of intrinsic currents in shaping interneuron EPSPs may be quite different to that in pyramidal cells. Simulated EPSPs induce purely inward currents in pyramidal cells but rather induce inward-outward current sequences in interneurons (Fricker and Miles, 2000). So, while, EPSPs in pyramidal cells are prolonged, EPSPs in interneurons may decay more rapidly due to the activation of an outward current at subthreshold potentials.

Synaptic inputs to a neuron are significant to surrounding cells when they initiate firing. Summed EPSPs initiated by repetitive firing of a single CA3 pyramidal cell sometimes induce cause a post-synaptic pyramidal cell to fire (Miles and Wong, 1986). Spike-to-spike latencies are 10–15 ms, consistent with a role for recurrent excitatory synapses in the genesis of delayed (50–100 ms) population bursts (Traub and Wong, 1982; de la Prida et al., 2006). Recent work suggests spike-to-spike transmission may be limited to a few strong connections (Ikegaya et al., 2013).

Pyramidal cells induce interneuron firing more effectively and at shorter latencies of 1–3 ms (Miles, 1990; Csicsvari et al., 1998; Cohen and Miles, 2000). Interneuron EPSPs are larger and faster than recurrent EPSPs in pyramidal cells, and interneuron firing threshold is lower (Figure A.4). When interneurons are excited to fire, pyramidal cells may trigger di-synaptic IPSPs (Figure A.4) with high probability and considerable divergence (Miles, 1990; Csicsvari et al., 1998; Bazelot et al., 2010). While EPSP boosting mechanisms in interneuron dendrites are not clear, it is surprising that EPSPs induced from a single site (Gulyás et al., 1993) can induce firing. Even so, EPSP-spike coupling at single release site excitatory synapses with some cerebellar interneurons (Carter and Regehr, 2002) is also sufficiently strong that EPSPs control the timing of interneuron firing.

## A.10 Recurrent excitatory contributions to population activities in the CA3 region

Recurrent synapses transmit excitation from CA3 pyramidal cells to other pyramidal cells and to interneurons. They play a key role in operations and functions of the CA3 region, including the generation of physiological and pathological synchronous population activities.

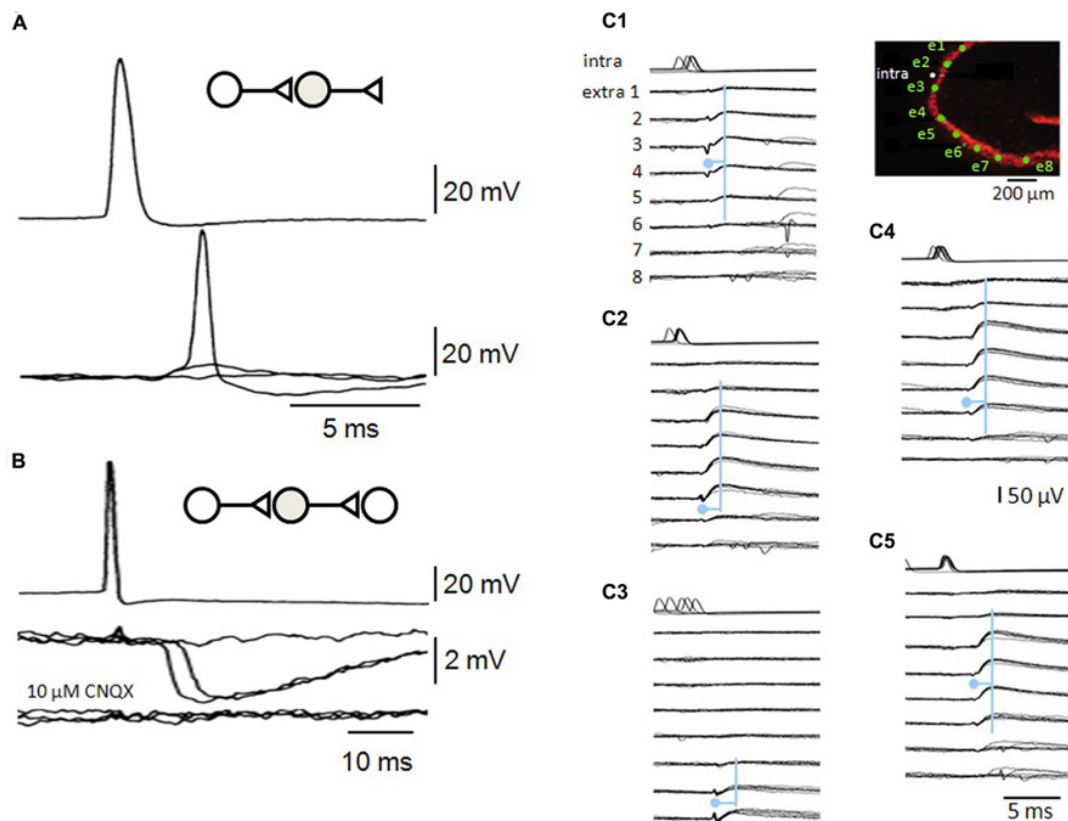


Figure A.4: **Recurrent inhibitory circuits in the CA3 region.** **A.** Post-synaptic responses of a fast-spiking interneuron to single pre-synaptic action potentials in a CA3 pyramidal cell. Responses include a failure of transmission, an EPSP and an EPSP that initiates interneuron firing. **B.** Di-synaptic inhibitory interactions between two CA3 pyramidal cells. Single action potentials in one cell induce IPSPs at variable latencies consistent with that of firing in (A), as well as some failures. Di-synaptic IPSPs were suppressed by the glutamate receptor blocker CNQX. **C.** A single pyramidal cell can initiate multiple di-synaptic IPSPs via firing in distinct interneurons. Records from a pyramidal cell (intra) and extracellular records from eight sites in st. pyramidale (extra 1–8, the diagram shows st. pyramidale in red and electrode sites in green). Field IPSPs were detected on electrodes 1–6 (C1), 2–7 (C2), 6–8 (C3), 1–7 (C4), and 2–6 (C5) repeatedly following single action potentials (traces are aligned on six overlapping field IPSPs for each trace). Field IPSPs are preceded by extracellular action potentials of short duration on electrodes 2–3 (C1), 6 (C2), 7–8 (C3), 6–7 (C4), and 5–6 (C5). The pyramidal cell may have initiated five distinct di-synaptic inhibitory interactions in these slice records (see Bazelot et al. (2010)).

## A.11 Interictal epileptiform rhythm

A key finding linking recurrent excitation to epileptiform activity was that stimulating any afferent pathway induced epileptiform firing in CA3 (Ayala et al., 1973). Population bursts occurred with a variable delay of 20–100 ms after the afferent response. (Traub and Wong, 1982) suggested that during the delay recurrent synaptic interactions within the CA3 population generate a population synchrony. Synchrony induced in disinhibited slices is complete in that all neurons tend to fire together with a field potential decorated with high frequency oscillations (Jefferys et al., 2012). Traub and Wong suggested recurrent circuits should possess two properties to generate such an event. Recurrent contacts should be divergent and one cell could cause more than one target neuron to fire. These points were verified with the demonstration that some single pyramidal cells could induce or entrain inter-ictal-like events (Miles and Wong, 1983, 1986, 1987a; de la Prida et al., 2006). Disynaptic feedback inhibition via CA3 pyramidal cell excitation of feedback interneurons, was shown to prevent the spread of firing by recurrent excitatory pathways (Miles and Wong, 1986, 1987a,b).

Recurrent synaptic function controls several features of the epileptiform activity induced by disinhibition. The duration of the population burst (20–80 ms) has been shown to result from transmitter depletion (Staley et al., 1998). The delay from one burst to the next (1–10 s) depends on the time for docked vesicles to be replenished (Staley et al., 1998, 2001). Procedures that induce persistent synaptic changes have persistent effects on the strength and frequency of network burst firing (Bains et al., 1999; Behrens et al., 2005).

Cellular properties also affect disinhibition induced synchrony by controlling transmission in chains of connected neurons. In slices, population bursts tend to be initiated in the CA3a region, where cellular excitability and recurrent connectivity are high (Wittner and Miles, 2007). In CA3a, spontaneous events are preceded by a field potential of duration about 50 ms (Wittner and Miles, 2007) during which excitatory synaptic events occur with increasing frequency. This delay is similar to that between single cell firing and a population event (Miles and Wong, 1983; de la Prida et al., 2006). Modeling work suggested that during this time activity in the pyramidal cell population increases in non-linear fashion (Traub and Wong, 1982). An epileptiform burst occurs when population activity exceeds a threshold frequency (de la Prida et al., 2006).

## A.12 Sharp-wave rhythm

Sharp waves (O'keefe and Nadel, 1978; Buzsaki et al., 1992) are field potentials of duration 100–150 ms, corresponding to a partial neuronal synchrony during behaviors including immobility and slow wave sleep. They are initiated in the CA3 region (Csicsvari et al., 2000) and have been associated with the consolidation of acquired events (Girardeau et al., 2009; Jadhav et al., 2012) represented as firing in specific groups of neurons.

Both recurrent excitatory interactions and the actions of specific interneurons have been implicated in the genesis of sharp waves (Buzsaki et al., 1992; Csicsvari et al., 2000). Sharp wave fields are enhanced by inducing long-term changes at recurrent synapses (Behrens et al., 2005). And yet, sharp waves are not identical with epileptiform events and do not depend on recurrent excitation alone (Liotta et al., 2011). Repetitive firing of peri-somatic interneurons may be a crucial element in sharp wave generation (Buzsaki et al., 1992; Klausberger et al., 2003). Gap-junctions have also been associated with sharp-waves, with the observation of spikelets in pyramidal cells and a blockade by gap-junction antagonists (Draguhn et al., 1998). However sharp waves persist, at reduced strength, in animals where the gap junction protein connexin 36 is genetically deleted (Pais et al., 2003). Possibly then, recurrent excitation of both pyramidal cells and interneurons (Hájos et al., 2013) may suffice to generate sharp waves.

## A.13 Theta and gamma rhythms

In contrast to sharp waves, theta fields (4–12 Hz) are generated when spatial memory representations are first acquired during movements (Vanderwolf, 1969; O'keefe and Nadel, 1978). Place-cells fire with theta oscillations and theta waves are also detected in rapid eye movement sleep.

Theta oscillations probably depend on signals generated outside the CA3 region. Signals from the septum may provide a sustained cholinergic excitation as well as glutamatergic (Huh et al., 2010) and inhibitory signals which selectively targeting hippocampal interneurons to disinhibit pyramidal cells (Freund and Antal, 1988; Toth et al., 1997; King et al., 1998). Synaptic connections within the CA3 region probably reinforce the rhythm via reciprocal interactions between pyramidal cells and some, probably peri-somatic, interneurons (Soltesz and Deschenes, 1993).

Gamma oscillations at 30–70 Hz may be superimposed on theta rhythmicity (Bragin et al., 1995; Csicsvari et al., 2003; Hasselmo, 2005). They are suggested to bind, or coordinate, activity of spatially dispersed neurons due to a single stimulus (Gray et al., 1989). In contrast to theta, gamma oscillations are generated within the CA3 region.

Reciprocal synaptic interactions between peri-somatic inhibitory cells and CA3 pyramidal cells via recurrent synapses are suggested to contribute both in vivo (Csicsvari et al., 2003) and in slice models of gamma induced by cholinergic agonists (Oren et al., 2006) or kainate (Fisahn, 2005). Gap junctions that transmit excitation between CA3 pyramidal cell axons may be another crucial factor in gamma generation (Traub and Bibbig, 2000; Traub et al., 2003).

## A.14 Comparison of recurrent connectivity in CA3 and other cortical regions

The hippocampal treatment of events, memories or representations may depend in part on the associative nature of the recurrent excitatory network between CA3 pyramidal cells. How do recurrent circuits in CA3 compare to those in other associative or sensory cortical regions?

The spatial extent of excitatory terminals seems to differ for recurrent synapses in associative, allocortical regions, such as CA3 and the olfactory cortex, and in six-layered primary sensory neocortex. CA3 pyramidal cell axons project longitudinally through most of the hippocampus (Lorente de Nó, 1934; Li et al., 1994). Local axons diffusely cover most of the olfactory cortex (Haberly, 2001; Franks et al., 2011; Poo and Isaacson, 2011). Connectivity within a six-layered cortex is certainly more complex, but overall may be more restrained in space. For instance, axons of layer IV pyramidal cells from sensory cortices tend to ramify locally within modules such as a single somatosensory barrel (Petersen and Sakmann, 2000; Feldmeyer, 2012). Superficial or deep layer pyramidal cells of primary visual or somatosensory cortex make longer range but often patchy projections terminating in regions occupied by cell groups of similar function (Gilbert and Wiesel, 1989; Holmgren et al., 2003; Ko et al., 2011; Feldmeyer, 2012).

The density of excitatory connections between pyramidal cells may be somewhat higher in sensory cortical modules than in associative allocortex such as CA3 or piriform cortex. Paired records from acute slices gave a value of 0.02–0.03 for the probability of a connection between two CA3 pyramidal cells (Miles and Wong, 1986) and recurrent connectivity in piriform cortex is estimated at 0.002–0.01 (Franks et al., 2011; Hagiwara et al., 2012). Estimates of connectivity are somewhat higher from paired records in slices of sensory cortex. The probability of connection between cells in different cortical layers ranges from 0.1 to 0.3 (0.2–0.3 in layer 4 of barrel cortex, (Lefort et al., 2009; Feldmeyer, 2012); 0.1 in layer 2/3 of neocortex, (Holmgren et al., 2003); 0.1 in layer 5 neocortex, (Markram et al., 1997).

An alternative way to define connectivity could be to measure the spatial distribution of terminals formed by the axon of a single cell. Terminals of some pyramidal cells in sensory cortex (Petersen and Sakmann, 2000) seem likely to show a more focal topology than those of the CA3 region (Ishizuka et al., 1990; Li et al., 1994). Data from paired records in slices indicates a lower local connectivity in CA3 than in sensory cortex. Lower values for recurrent connectivity may be a design feature to ensure sparse representations in an associative region.

Recurrent excitatory synapses may contact cortical interneurons selectively in both associative and sensory cortices. Paired records suggest connectivity from pyramidal cells to fast-spiking interneurons is higher than onto pyramidal cells (0.5–0.7 in neocortex layer 2, (Holmgren et al., 2003); in barrel cortex layer 2 ~0.6, (Avermann et al., 2012); 0.2 in piriform cortex layer 3, (Stokes and Isaacson, 2010). A higher connectivity as well as stronger signaling at single connections with GABAergic interneurons (Helmstaedter et al., 2008) protects against excessive synchrony, maintains stable population firing and sharpens signaling by imposing a sparse coding.

The strength of afferent and recurrent synapses may differ in both associative and sensory cortices. Mossy fiber synapses with CA3 pyramidal cells have more release sites (Claiborne et al., 1986) and stronger actions (Henze et al., 2002). Synapses from olfactory bulb onto piriform cortex cells are both stronger and less numerous than recurrent synapses (Franks et al., 2011; Poo and Isaacson, 2011). In barrel cortex however, recurrent connections between layer 4 pyramidal cells seem to be stronger (Feldmeyer et al., 1999; Feldmeyer, 2012) than thalamic synapses which excite the same cells (Bruno and Sakmann, 2006).

Thus recurrent networks of associative cortical regions have a wider spatial extent and a lower probability of connection between pyramidal cells than those in sensory cortices.

## A.15 The CA3 recurrent system as an associative network

Associative synaptic networks have been linked to the processes of completion and recall of stored information (Figure A.5). McNaughton and Morris (1987) noted that similar hypotheses have often been discovered (McNaughton and Morris, 1987). What do they assume? And how might they be tested?

Such hypotheses suppose that information, or a representation, or an event, or a memory, has a distributed existence as the correlated, or synchronous, discharge of a group of neurons (Hebb, 1949; Marr et al., 1991). Different informations presumably

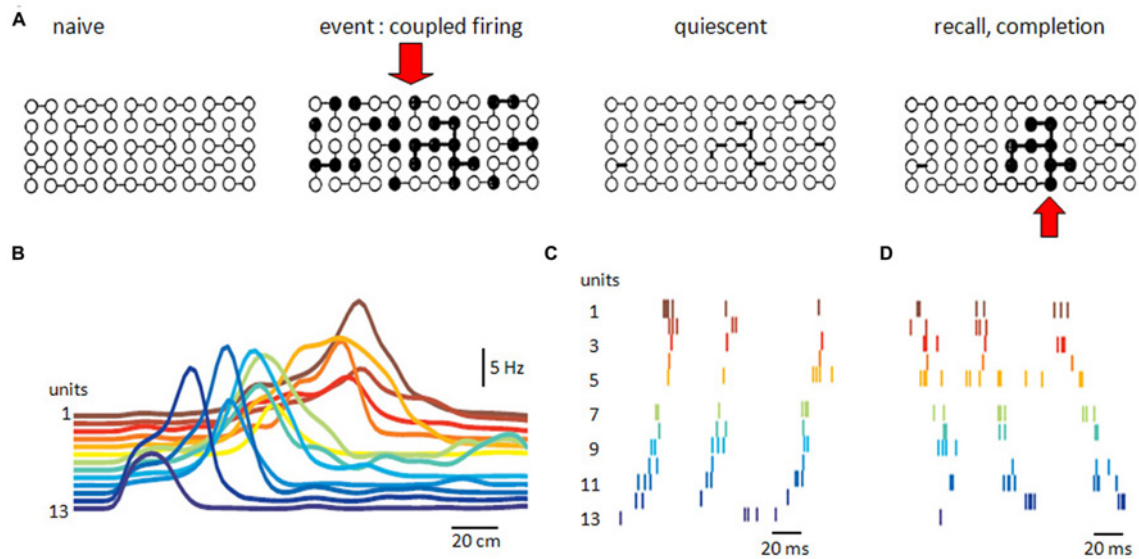


Figure A.5: Recurrent excitatory networks. **A**. Possible schema of connectivity and operations in a recurrent neuronal network. Some neurons are connected in the naive network. Coupled firing in a subset of neurons during an event reinforces synapses between them. Reinforcement persists during quiescence, until partial activation recalls or completes firing of the neuronal subset associated with the original event. **B**. Sequential firing of 13 pyramidal place cells as an animal passes through a space (horizontal axis is distance). Reactivation of sequential firing of these cells as **C**. forward replay or **D**. backward replay (adapted with permission from Diba and Buzsáki (2007)).

involve different groups, raising the question of how representations are constrained to be neuronally orthogonal (Marr et al., 1991; Rolls et al., 1998). They suppose that a way exists to associate or strengthen synaptic relations within such a group or ensemble of synchronously active neurons. It might correspond to the persistent synaptic potentiation which occurs when pre- and post-synaptic cells fire together (Hebb, 1949; Bliss and Lømo, 1973). They suppose that a full representation of an event can be recalled from some of its elements (Gardner-Medwin, 1976; McNaughton and Morris, 1987). The CA3 recurrent network where activity in some single cells can trigger population activities (Miles and Wong, 1983; Fujisawa et al., 2006) might be capable of operations similar to a cued recall (Figure A.5). The spatially widespread but lower connectivity of associative recurrent networks may favor this form of information storage.

Improved techniques to record and manipulate activity in large groups of neurons begin to suggest distributed ensembles may contribute to storage and recall. Using tetrodes to separate firing in 50–100 single units, Wilson and McNaughton (1994) showed that CA1 place-sensitive neurons that fired together during a spatial behavior, discharged synchronously again during the following episode of sleep (Wilson and McNaughton, 1994). Correlated firing in cell pairs was increased as animals learned a task and maintained

during replay. A specific role for recurrent synapses was established by genetically deleting NMDA receptor expression at recurrent synapses of CA3 pyramidal cells (Nakazawa et al., 2002, 2003). With the basis for persistent changes abolished, recall of spatial memories from partial cues was suppressed. Optical stimulation has recently been used to re-activate neurons associated with a representation (Liu et al., 2012). An ensemble of granule cells active during fear conditioning was labeled with a construction including c-fos which also induced expression of a light-sensitive opsin. Re-activating the sparse granule cell ensemble optically later, induced a fear response in a different context.

These data point to distinct neuronal operations associated with acquisition and recall. A two-stage memory system has often been postulated (James, 1890; Buzsáki, 1989). The two stages may occur during distinct brain and behavioral states. External representations, especially those associated with space (O'keefe and Nadel, 1978) and possibly also time (Huxter et al., 2003; Kraus et al., 2013) are acquired during theta activity. In contrast, recall or consolidation is linked with sharp-waves generated in CA3 (Buzsáki, 1989). Switching between these opposing behaviors might be achieved with distinct modulatory transmitters (Hasselmo et al., 1995) or, perhaps more economically, by external control of specific interneurons (Viney et al., 2013).

Acquisition and replay of ensemble activity were first described during theta and sharp waves respectively (Wilson and McNaughton, 1994). Several variants of the exact replay of neuronal firing sequences have now been distinguished most often in CA1 during sleep (Lee and Wilson, 2002; Matsumoto et al., 2013) and the awake state (Foster and Wilson, 2006; Diba and Buzsáki, 2007). Firing replay during sharp waves is increasingly linked to the consolidation of a memory or representation by transfer from the hippocampus to a more permanent storage in cortex (Rasch and Born, 2007; Nakashiba et al., 2009; O'Neill et al., 2010). During sharp waves of slow-wave sleep, similar firing sequences are detected in hippocampus and cortex (Ji and Wilson, 2007) and suppressing sharp waves during sleep interferes with consolidation (Girardeau et al., 2009).

The data on these forms of replay raises questions for future work. It needs to be re-examined in CA3. Many, but not all (Diba and Buzsáki, 2007), papers report data from CA1 with the caveat that the activity is likely to have originated in CA3. How is the apparent precision in firing maintained during the translation from CA3 to CA1? How is an appropriate sequence initiated in CA3? What neuronal and synaptic mechanisms can explain how a specific sharp wave is chosen, define the inhibitory and pyramidal cells that fire during it, and permit reversal of this sequence? Better techniques to define cellular and synaptic physiology in context of data on the activity of large numbers of neurons (Matsumoto et al., 2013) will be needed for the next steps to uncover the role of recurrent synapses and the functions of the CA3 region.

---

## Bibliography

---

- Andreasen, M. and Lambert, J. D. (1999). Somatic amplification of distally generated subthreshold epsps in rat hippocampal pyramidal neurones. *The Journal of Physiology*, 519(1):85–100.
- Auger, C., Kondo, S., and Marty, A. (1998). Multivesicular release at single functional synaptic sites in cerebellar stellate and basket cells. *The Journal of neuroscience*, 18(12):4532–4547.
- Avermann, M., Tomm, C., Mateo, C., Gerstner, W., and Petersen, C. C. (2012). Microcircuits of excitatory and inhibitory neurons in layer 2/3 of mouse barrel cortex. *Journal of neurophysiology*, 107(11):3116–3134.
- Ayala, G., Dichter, M., Gumnit, R., Matsumoto, H., and Spencer, W. (1973). Genesis of epileptic interictal spikes. new knowledge of cortical feedback systems suggests a neurophysiological explanation of brief paroxysms. *Brain research*, 52:1–17.
- Bains, J. S., Longacher, J. M., and Staley, K. J. (1999). Reciprocal interactions between ca3 network activity and strength of recurrent collateral synapses. *Nature neuroscience*, 2(8):720–726.
- Bazelot, M., Dinocourt, C., Cohen, I., and Miles, R. (2010). Unitary inhibitory field potentials in the ca3 region of rat hippocampus. *The Journal of physiology*, 588(12):2077–2090.
- Behrens, C. J., van den Boom, L. P., de Hoz, L., Friedman, A., and Heinemann, U. (2005). Induction of sharp wave–ripple complexes in vitro and reorganization of hippocampal networks. *Nature neuroscience*, 8(11):1560–1567.
- Biró, Á. A., Holderith, N. B., and Nusser, Z. (2005). Quantal size is independent of the release probability at hippocampal excitatory synapses. *The Journal of neuroscience*, 25(1):223–232.
- Bischofberger, J., Engel, D., Frotscher, M., and Jonas, P. (2006). Timing and efficacy of transmitter release at mossy fiber synapses in the hippocampal network. *Pflügers Archiv*, 453(3):361–372.
- Bliss, T. V. and Lømo, T. (1973). Long-lasting potentiation of synaptic transmission in the dentate area of the anaesthetized rabbit following stimulation of the perforant path. *The Journal of physiology*, 232(2):331–356.

- Bochet, P., Audinat, E., Lambolez, B., Crépel, F., Rossier, J., Iino, M., Tsuzuki, K., and Ozawa, S. (1994). Subunit composition at the single-cell level explains functional properties of a glutamate-gated channel. *Neuron*, 12(2):383–388.
- Bragin, A., Jandó, G., Nádasdy, Z., Hetke, J., Wise, K., and Buzsáki, G. (1995). Gamma (40-100 Hz) oscillation in the hippocampus of the behaving rat. *The Journal of Neuroscience*, 15(1):47–60.
- Bruno, R. M. and Sakmann, B. (2006). Cortex is driven by weak but synchronously active thalamocortical synapses. *Science*, 312(5780):1622–1627.
- Bucurenciu, I., Bischofberger, J., and Jonas, P. (2010). A small number of open Ca<sup>2+</sup> channels trigger transmitter release at a central GABAergic synapse. *Nature neuroscience*, 13(1):19–21.
- Buzsáki, G. (1989). Two-stage model of memory trace formation: a role for noisy brain states. *Neuroscience*, 31(3):551–570.
- Buzsáki, G., Wise, K., et al. (1992). High-frequency network oscillation in the hippocampus. *Science*, 256(5059):1025.
- Carter, A. G. and Regehr, W. G. (2002). Quantal events shape cerebellar interneuron firing. *Nature neuroscience*, 5(12):1309–1318.
- Christie, J. M. and Jahr, C. E. (2006). Multivesicular release at Schaffer collateral-CA1 hippocampal synapses. *The Journal of Neuroscience*, 26(1):210–216.
- Claiborne, B. J., Amaral, D. G., and Cowan, W. M. (1986). A light and electron microscopic analysis of the mossy fibers of the rat dentate gyrus. *Journal of comparative neurology*, 246(4):435–458.
- Cohen, I. and Miles, R. (2000). Contributions of intrinsic and synaptic activities to the generation of neuronal discharges in in vitro hippocampus. *The Journal of physiology*, 524(2):485–502.
- Conti, R. and Lisman, J. (2003). The high variance of AMPA receptor- and NMDA receptor-mediated responses at single hippocampal synapses: evidence for multiquantal release. *Proceedings of the National Academy of Sciences*, 100(8):4885–4890.
- Csicsvari, J., Hirase, H., Czurko, A., and Buzsáki, G. (1998). Reliability and state dependence of pyramidal cell-interneuron synapses in the hippocampus: an ensemble approach in the behaving rat. *Neuron*, 21(1):179–189.
- Csicsvari, J., Hirase, H., Mamiya, A., and Buzsáki, G. (2000). Ensemble patterns of hippocampal CA3-CA1 neurons during sharp wave-associated population events. *Neuron*, 28(2):585–594.
- Csicsvari, J., Jamieson, B., Wise, K. D., and Buzsáki, G. (2003). Mechanisms of gamma oscillations in the hippocampus of the behaving rat. *Neuron*, 37(2):311–322.
- de la Prida, L. M., Huberfeld, G., Cohen, I., and Miles, R. (2006). Threshold behavior in the initiation of hippocampal population bursts. *Neuron*, 49(1):131–142.
- Debanne, D., Boudkazi, S., Campanac, E., Cudmore, R. H., Giraud, P., Fronzaroli-Molinieres, L., Carlier, E., and Caillard, O. (2008). Paired-recordings from synaptically coupled cortical and hippocampal neurons in acute and cultured brain slices. *Nature protocols*, 3(10):1559–1568.

- Debanne, D., Campanac, E., Bialowas, A., Carlier, E., and Alcaraz, G. (2011). Axon physiology. *Physiological reviews*, 91(2):555–602.
- Debanne, D., Gähwiler, B. H., and Thompson, S. M. (1998). Long-term synaptic plasticity between pairs of individual ca3 pyramidal cells in rat hippocampal slice cultures. *The Journal of Physiology*, 507(1):237–247.
- Debanne, D., Gähwiler, B. H., and Thompson, S. M. (1999). Heterogeneity of synaptic plasticity at unitary ca3–ca1 and ca3–ca3 connections in rat hippocampal slice cultures. *The Journal of Neuroscience*, 19(24):10664–10671.
- Debanne, D., Guerineau, N., Gähwiler, B. H., and Thompson, S. M. (1995). Physiology and pharmacology of unitary synaptic connections between pairs of cells in areas ca3 and ca1 of rat hippocampal slice cultures. *Journal of Neurophysiology*, 73(3):1282–1294.
- Debanne, D., Guerineau, N. C., Gähwiler, B., and Thompson, S. M. (1996). Paired-pulse facilitation and depression at unitary synapses in rat hippocampus: quantal fluctuation affects subsequent release. *The Journal of Physiology*, 491(1):163–176.
- Debanne, D., Guérineau, N. C., Gähwiler, B. H., and Thompson, S. M. (1997). Action-potential propagation gated by an axonal ia-like  $k^+$  conductance in hippocampus. *Nature*, 389(6648):286–289.
- Del Castillo, J. and Katz, B. (1954). Statistical factors involved in neuromuscular facilitation and depression. *The Journal of Physiology*, 124(3):574–585.
- Diba, K. and Buzsáki, G. (2007). Forward and reverse hippocampal place-cell sequences during ripples. *Nature neuroscience*, 10(10):1241–1242.
- Draguhn, A., Traub, R., Schmitz, D., and Jefferys, J. (1998). Electrical coupling underlies high-frequency oscillations in the hippocampus in vitro. *Nature*, 394(6689):189–192.
- Engel, D. and Jonas, P. (2005). Presynaptic action potential amplification by voltage-gated na<sup>+</sup> channels in hippocampal mossy fiber boutons. *Neuron*, 45(3):405–417.
- Feldmeyer, D. (2012). Excitatory neuronal connectivity in the barrel cortex. *Frontiers in neuroanatomy*, 6.
- Feldmeyer, D., Egger, V., Lübke, J., and Sakmann, B. (1999). Reliable synaptic connections between pairs of excitatory layer 4 neurones within a single barrelof developing rat somatosensory cortex. *The Journal of Physiology*, 521(1):169–190.
- Fisahn, A. (2005). Kainate receptors and rhythmic activity in neuronal networks: hippocampal gamma oscillations as a tool. *The Journal of physiology*, 562(1):65–72.
- Foster, D. J. and Wilson, M. A. (2006). Reverse replay of behavioural sequences in hippocampal place cells during the awake state. *Nature*, 440(7084):680–683.
- Franks, K. M., Russo, M. J., Sosulski, D. L., Mulligan, A. A., Siegelbaum, S. A., and Axel, R. (2011). Recurrent circuitry dynamically shapes the activation of piriform cortex. *Neuron*, 72(1):49–56.

- Freund, T. F. and Antal, M. (1988). Gaba-containing neurons in the septum control inhibitory interneurons in the hippocampus. *Nature*, 336(6195):170–173.
- Fricker, D. and Miles, R. (2000). Epsp amplification and the precision of spike timing in hippocampal neurons. *Neuron*, 28(2):559–569.
- Fujisawa, S., Matsuki, N., and Ikegaya, Y. (2006). Single neurons can induce phase transitions of cortical recurrent networks with multiple internal states. *Cerebral Cortex*, 16(5):639–654.
- Gardner-Medwin, A. (1976). The recall of events through the learning of associations between their parts. *Proceedings of the Royal Society of London B: Biological Sciences*, 194(1116):375–402.
- Geiger, J. R., Melcher, T., Koh, D.-S., Sakmann, B., Seeburg, P. H., Jonas, P., and Monyer, H. (1995). Relative abundance of subunit mrnas determines gating and ca<sup>2+</sup> permeability of ampa receptors in principal neurons and interneurons in rat cns. *Neuron*, 15(1):193–204.
- Gilbert, C. D. and Wiesel, T. N. (1989). Columnar specificity of intrinsic horizontal and corticocortical connections in cat visual cortex. *The Journal of Neuroscience*, 9(7):2432–2442.
- Girardeau, G., Benchenane, K., Wiener, S. I., Buzsáki, G., and Zugaro, M. B. (2009). Selective suppression of hippocampal ripples impairs spatial memory. *Nature neuroscience*, 12(10):1222–1223.
- Gray, C. M., König, P., Engel, A. K., Singer, W., et al. (1989). Oscillatory responses in cat visual cortex exhibit inter-columnar synchronization which reflects global stimulus properties. *Nature*, 338(6213):334–337.
- Gulyás, a. I., Miles, R., Sík, a., Tóth, K., Tamamaki, N., and Freund, T. F. (1993). Hippocampal pyramidal cells excite inhibitory neurons through a single release site. *Nature*, 366:683–687.
- Haberly, L. B. (2001). Parallel-distributed processing in olfactory cortex: new insights from morphological and physiological analysis of neuronal circuitry. *Chemical senses*, 26(5):551–576.
- Hagiwara, A., Pal, S. K., Sato, T. F., Wienisch, M., and Murthy, V. N. (2012). Optophysiological analysis of associational circuits in the olfactory cortex. *Frontiers in neural circuits*, 6.
- Hájos, N., Karlócai, M. R., Németh, B., Ulbert, I., Monyer, H., Szabó, G., Erdélyi, F., Freund, T. F., and Gulyás, A. I. (2013). Input-output features of anatomically identified ca3 neurons during hippocampal sharp wave/ripple oscillation in vitro. *The Journal of Neuroscience*, 33(28):11677–11691.
- Hasselmo, M. E. (2005). What is the function of hippocampal theta rhythm? linking behavioral data to phasic properties of field potential and unit recording data. *Hippocampus*, 15(7):936–949.
- Hasselmo, M. E., Schnell, E., and Barkai, E. (1995). Dynamics of learning and recall at excitatory recurrent synapses and cholinergic modulation in rat hippocampal region ca3. *The Journal of neuroscience*, 15(7):5249–5262.
- Hebb, D. (1949). The organisation of behaviour: a neurophysiological theory.
- Helmstaedter, M., Staiger, J. F., Sakmann, B., and Feldmeyer, D. (2008). Efficient recruitment of layer 2/3 interneurons by layer 4 input in single columns of rat somatosensory cortex. *The Journal of Neuroscience*, 28(33):8273–8284.

- Henze, D. A., Wittner, L., and Buzsáki, G. (2002). Single granule cells reliably discharge targets in the hippocampal ca3 network in vivo. *Nature neuroscience*, 5(8):790–795.
- Herzog, E., Takamori, S., Jahn, R., Brose, N., and Wojcik, S. M. (2006). Synaptic and vesicular co-localization of the glutamate transporters vglut1 and vglut2 in the mouse hippocampus. *Journal of neurochemistry*, 99(3):1011–1018.
- Hoffman, D. A., Magee, J. C., Colbert, C. M., and Johnston, D. (1997). K<sup>+</sup> channel regulation of signal propagation in dendrites of hippocampal pyramidal neurons. *Nature*, 387(6636):869–875.
- Holderith, N., Lorincz, A., Katona, G., Rózsa, B., Kulik, A., Watanabe, M., and Nusser, Z. (2012). Release probability of hippocampal glutamatergic terminals scales with the size of the active zone. *Nature neuroscience*, 15(7):988–997.
- Holmgren, C., Harkany, T., Svennenfors, B., and Zilberter, Y. (2003). Pyramidal cell communication within local networks in layer 2/3 of rat neocortex. *The Journal of physiology*, 551(1):139–153.
- Huh, C. Y., Goutagny, R., and Williams, S. (2010). Glutamatergic neurons of the mouse medial septum and diagonal band of broca synaptically drive hippocampal pyramidal cells: relevance for hippocampal theta rhythm. *The Journal of Neuroscience*, 30(47):15951–15961.
- Huxter, J., Burgess, N., and O’Keefe, J. (2003). Independent rate and temporal coding in hippocampal pyramidal cells. *Nature*, 425(6960):828–832.
- Ikegaya, Y., Sasaki, T., Ishikawa, D., Honma, N., Tao, K., Takahashi, N., Minamisawa, G., Ujita, S., and Matsuki, N. (2013). Interpyramid spike transmission stabilizes the sparseness of recurrent network activity. *Cerebral Cortex*, 23(2):293–304.
- Isaac, J. T., Ashby, M. C., and McBain, C. J. (2007). The role of the glur2 subunit in ampa receptor function and synaptic plasticity. *Neuron*, 54(6):859–871.
- Ishizuka, N., Cowan, W. M., and Amaral, D. G. (1995). A quantitative analysis of the dendritic organization of pyramidal cells in the rat hippocampus. *Journal of Comparative Neurology*, 362(1):17–45.
- Ishizuka, N., Weber, J., and Amaral, D. G. (1990). Organization of intrahippocampal projections originating from ca3 pyramidal cells in the rat. *Journal of Comparative Neurology*, 295(4):580–623.
- Jadhav, S. P., Kemere, C., German, P. W., and Frank, L. M. (2012). Awake hippocampal sharp-wave ripples support spatial memory. *Science*, 336(6087):1454–1458.
- James, W. (1890). 77k principles of psychology.
- Jefferys, J. G., De La Prida, L. M., Wendling, F., Bragin, A., Avoli, M., Timofeev, I., and Da Silva, F. H. L. (2012). Mechanisms of physiological and epileptic hfo generation. *Progress in neurobiology*, 98(3):250–264.
- Ji, D. and Wilson, M. A. (2007). Coordinated memory replay in the visual cortex and hippocampus during sleep. *Nature neuroscience*, 10(1):100–107.

- Kandel, E. and Spencer, W. (1961). Excitation and inhibition of single pyramidal cells during hippocampal seizure. *Experimental neurology*, 4(2):162–179.
- Kerchner, G. A. and Nicoll, R. A. (2008). Silent synapses and the emergence of a postsynaptic mechanism for ltp. *Nature Reviews Neuroscience*, 9(11):813–825.
- Kim, S., Guzman, S. J., Hu, H., and Jonas, P. (2012). Active dendrites support efficient initiation of dendritic spikes in hippocampal ca3 pyramidal neurons. *Nature neuroscience*, 15(4):600–606.
- King, C., Recce, M., and OKeefe, J. (1998). The rhythmicity of cells of the medial septum/diagonal band of broca in the awake freely moving rat: relationships with behaviour and hippocampal theta. *European Journal of Neuroscience*, 10(2):464–477.
- Klausberger, T., Magill, P. J., Márton, L. F., Roberts, J. D. B., Cobden, P. M., Buzsáki, G., and Somogyi, P. (2003). Brain-state-and cell-type-specific firing of hippocampal interneurons in vivo. *Nature*, 421(6925):844–848.
- Ko, H., Hofer, S. B., Pichler, B., Buchanan, K. A., Sjöström, P. J., and Mrsic-Flogel, T. D. (2011). Functional specificity of local synaptic connections in neocortical networks. *Nature*, 473(7345):87–91.
- Koester, H. J. and Johnston, D. (2005). Target cell-dependent normalization of transmitter release at neocortical synapses. *Science*, 308(5723):863–866.
- Kopysova, I. L. and Debanne, D. (1998). Critical role of axonal a-type k<sup>+</sup> channels and axonal geometry in the gating of action potential propagation along ca3 pyramidal cell axons: a simulation study. *The Journal of neuroscience*, 18(18):7436–7451.
- Kraus, B. J., Robinson, R. J., White, J. A., Eichenbaum, H., and Hasselmo, M. E. (2013). Hippocampal time cells: time versus path integration. *Neuron*, 78(6):1090–1101.
- Le Duigou, C., Simonnet, J., Teleńczuk, M. T., Fricker, D., and Miles, R. (2014). Recurrent synapses and circuits in the CA3 region of the hippocampus: an associative network. *Frontiers in Cellular Neuroscience*, 7(January):1–13.
- Lebovitz, R., Dichter, M., and Spencer, W. (1971). Recurrent excitation in the ca3 region of cat hippocampus. *International Journal of Neuroscience*, 2(2):99–107.
- Lee, A. K. and Wilson, M. A. (2002). Memory of sequential experience in the hippocampus during slow wave sleep. *Neuron*, 36(6):1183–1194.
- Lefort, S., Tómm, C., Sarria, J.-C. F., and Petersen, C. C. (2009). The excitatory neuronal network of the c2 barrel column in mouse primary somatosensory cortex. *Neuron*, 61(2):301–316.
- Li, L., Bischofberger, J., and Jonas, P. (2007). Differential gating and recruitment of p/q-, n-, and r-type ca<sup>2+</sup> channels in hippocampal mossy fiber boutons. *The Journal of Neuroscience*, 27(49):13420–13429.
- Li, X.-G., Somogyi, P., Ylinen, A., and Buzsáki, G. (1994). The hippocampal ca3 network: an in vivo intracellular labeling study. *Journal of Comparative Neurology*, 339(2):181–208.

- Liotta, A., Çalışkan, G., ul Haq, R., Hollnagel, J. O., Rösler, A., Heinemann, U., and Behrens, C. J. (2011). Partial disinhibition is required for transition of stimulus-induced sharp wave-ripple complexes into recurrent epileptiform discharges in rat hippocampal slices. *Journal of neurophysiology*, 105(1):172–187.
- Lipowsky, R., Gillessen, T., and Alzheimer, C. (1996). Dendritic na<sup>+</sup> channels amplify epsps in hippocampal ca1 pyramidal cells. *Journal of Neurophysiology*, 76(4):2181–2191.
- Liu, X., Ramirez, S., Pang, P. T., Puryear, C. B., Govindarajan, A., Deisseroth, K., and Tonegawa, S. (2012). Optogenetic stimulation of a hippocampal engram activates fear memory recall. *Nature*, 484(7394):381–385.
- Lorente de Nó, R. (1934). Studies on the structure of the cerebral cortex. ii. continuation of the study of the ammonic system. *Journal für Psychologie und Neurologie*.
- Lörincz, A., Notomi, T., Tamás, G., Shigemoto, R., and Nusser, Z. (2002). Polarized and compartment-dependent distribution of hcn1 in pyramidal cell dendrites. *Nature neuroscience*, 5(11):1185–1193.
- Lorincz, A. and Nusser, Z. (2008). Cell-type-dependent molecular composition of the axon initial segment. *The Journal of Neuroscience*, 28(53):14329–14340.
- Magee, J. C. (1999). Dendritic ih normalizes temporal summation in hippocampal ca1 neurons. *Nature neuroscience*, 2(6):508–514.
- Magee, J. C. and Johnston, D. (1995). Synaptic activation of voltage-gated channels in the dendrites of hippocampal pyramidal neurons. *Science*, 268(5208):301.
- Markram, H., Lübke, J., Frotscher, M., Roth, A., and Sakmann, B. (1997). Physiology and anatomy of synaptic connections between thick tufted pyramidal neurones in the developing rat neocortex. *The Journal of physiology*, 500(2):409–440.
- Marr, D., Willshaw, D., and McNaughton, B. (1991). *Simple memory: a theory for archicortex*. Springer.
- Matsumoto, K., Ishikawa, T., Matsuki, N., and Ikegaya, Y. (2013). Multineuronal spike sequences repeat with millisecond precision. *Frontiers in neural circuits*, 7.
- Matsuzaki, M., Ellis-Davies, G. C., Nemoto, T., Miyashita, Y., Iino, M., and Kasai, H. (2001). Dendritic spine geometry is critical for ampa receptor expression in hippocampal ca1 pyramidal neurons. *Nature neuroscience*, 4(11):1086–1092.
- McGuinness, L., Taylor, C., Taylor, R. D., Yau, C., Langenhan, T., Hart, M. L., Christian, H., Tynan, P. W., Donnelly, P., and Emptage, N. J. (2010). Presynaptic nmdars in the hippocampus facilitate transmitter release at theta frequency. *Neuron*, 68(6):1109–1127.
- McNaughton, B. L. and Morris, R. G. (1987). Hippocampal synaptic enhancement and information storage within a distributed memory system. *Trends in neurosciences*, 10(10):408–415.
- Meeks, J. P. and Mennerick, S. (2007). Action potential initiation and propagation in ca3 pyramidal axons. *Journal of neurophysiology*, 97(5):3460–3472.

- Miles, R. (1990). Synaptic excitation of inhibitory cells by single ca3 hippocampal pyramidal cells of the guinea-pig in vitro. *The Journal of physiology*, 428(1):61–77.
- Miles, R. and Wong, R. (1986). Excitatory synaptic interactions between ca3 neurones in the guinea-pig hippocampus. *The Journal of Physiology*, 373(1):397–418.
- Miles, R. and Wong, R. (1987a). Inhibitory control of local excitatory circuits in the guinea-pig hippocampus. *The Journal of Physiology*, 388(1):611–629.
- Miles, R. and Wong, R. K. (1983). Single neurones can initiate synchronized population discharge in the hippocampus. *Nature*, 306(5941):371–3.
- Miles, R. and Wong, R. K. (1987b). Latent synaptic pathways revealed after tetanic stimulation in the hippocampus. *Nature*, 329(6141):724–726.
- Montgomery, J. M. and Madison, D. V. (2002). State-dependent heterogeneity in synaptic depression between pyramidal cell pairs. *Neuron*, 33(5):765–777.
- Montgomery, J. M., Pavlidis, P., and Madison, D. V. (2001). Pair recordings reveal all-silent synaptic connections and the postsynaptic expression of long-term potentiation. *Neuron*, 29(3):691–701.
- Nakashiba, T., Buhl, D. L., McHugh, T. J., and Tonegawa, S. (2009). Hippocampal ca3 output is crucial for ripple-associated reactivation and consolidation of memory. *Neuron*, 62(6):781–787.
- Nakazawa, K., Quirk, M. C., Chitwood, R. A., Watanabe, M., Yeckel, M. F., Sun, L. D., Kato, A., Carr, C. A., Johnston, D., Wilson, M. A., et al. (2002). Requirement for hippocampal ca3 nmda receptors in associative memory recall. *Science*, 297(5579):211–218.
- Nakazawa, K., Sun, L. D., Quirk, M. C., Rondi-Reig, L., Wilson, M. A., and Tonegawa, S. (2003). Hippocampal ca3 nmda receptors are crucial for memory acquisition of one-time experience. *Neuron*, 38(2):305–315.
- Nimchinsky, E. A., Yasuda, R., Oertner, T. G., and Svoboda, K. (2004). The number of glutamate receptors opened by synaptic stimulation in single hippocampal spines. *The Journal of neuroscience*, 24(8):2054–2064.
- Nusser, Z., Lujan, R., Laube, G., Roberts, J. D. B., Molnar, E., and Somogyi, P. (1998). Cell type and pathway dependence of synaptic ampa receptor number and variability in the hippocampus. *Neuron*, 21(3):545–559.
- Nyiri, G., Stephenson, F., Freund, T., and Somogyi, P. (2003). Large variability in synaptic n-methyl-d-aspartate receptor density on interneurons and a comparison with pyramidal-cell spines in the rat hippocampus. *Neuroscience*, 119(2):347–363.
- O’keefe, J. and Nadel, L. (1978). *The hippocampus as a cognitive map*, volume 3. Clarendon Press Oxford.
- Oren, I., Mann, E. O., Paulsen, O., and Hájos, N. (2006). Synaptic currents in anatomically identified ca3 neurons during hippocampal gamma oscillations in vitro. *The Journal of neuroscience*, 26(39):9923–9934.

- ONeill, J., Pleydell-Bouverie, B., Dupret, D., and Csicsvari, J. (2010). Play it again: reactivation of waking experience and memory. *Trends in neurosciences*, 33(5):220–229.
- Pais, I., Hormuzdi, S. G., Monyer, H., Traub, R. D., Wood, I. C., Buhl, E. H., Whittington, M. A., and LeBeau, F. E. (2003). Sharp wave-like activity in the hippocampus in vitro in mice lacking the gap junction protein connexin 36. *Journal of neurophysiology*, 89(4):2046–2054.
- Palani, D., Baginskas, A., and Raastad, M. (2010). Bursts and hyperexcitability in non-myelinated axons of the rat hippocampus. *Neuroscience*, 167(4):1004–1013.
- Pavlidis, P. and Madison, D. V. (1999). Synaptic transmission in pair recordings from ca3 pyramidal cells in organotypic culture. *Journal of neurophysiology*, 81(6):2787–2797.
- Perez-Rosello, T., Baker, J. L., Ferrante, M., Iyengar, S., Ascoli, G. A., and Barrionuevo, G. (2011). Passive and active shaping of unitary responses from associational/commissural and perforant path synapses in hippocampal ca3 pyramidal cells. *Journal of computational neuroscience*, 31(2):159–182.
- Petersen, C. C. and Sakmann, B. (2000). The excitatory neuronal network of rat layer 4 barrel cortex. *The Journal of Neuroscience*, 20(20):7579–7586.
- Poo, C. and Isaacson, J. S. (2011). A major role for intracortical circuits in the strength and tuning of odor-evoked excitation in olfactory cortex. *Neuron*, 72(1):41–48.
- Raffaelli, G., Saviane, C., Mohajerani, M. H., Pedarzani, P., and Cherubini, E. (2004). Bk potassium channels control transmitter release at ca3–ca3 synapses in the rat hippocampus. *The Journal of physiology*, 557(1):147–157.
- Ramón y Cajal, S. (1899). 1899-1904. textura del sistema nervioso del hombre y de los vertebrados. *Imprenta N. Moya. Madrid*.
- Rasch, B. and Born, J. (2007). Maintaining memories by reactivation. *Current opinion in neurobiology*, 17(6):698–703.
- Rolls, E. T., Treves, A., and Rolls, E. T. (1998). *Neural networks and brain function*. Oxford university press Oxford.
- Royeck, M., Horstmann, M.-T., Remy, S., Reitze, M., Yaari, Y., and Beck, H. (2008). Role of axonal nav1.6 sodium channels in action potential initiation of ca1 pyramidal neurons. *Journal of neurophysiology*, 100(4):2361–2380.
- Salmen, B., Beed, P. S., Özdogan, T., Maier, N., Jochenning, F. W., Winterer, J., Breustedt, J., and Schmitz, D. (2012). Gluk1 inhibits calcium dependent and independent transmitter release at associational/commissural synapses in area ca3 of the hippocampus. *Hippocampus*, 22(1):57–68.
- Sasaki, T., Matsuki, N., and Ikegaya, Y. (2012). Heterogeneity and independency of unitary synaptic outputs from hippocampal ca3 pyramidal cells. *The Journal of physiology*, 590(19):4869–4880.
- Saviane, C., Mohajerani, M. H., and Cherubini, E. (2003). An id-like current that is downregulated by ca2+ modulates information coding at ca3–ca3 synapses in the rat hippocampus. *The Journal of physiology*, 552(2):513–524.

- Scanziani, M., Gähwiler, B. H., and Charpak, S. (1998). Target cell-specific modulation of transmitter release at terminals from a single axon. *Proceedings of the National Academy of Sciences*, 95(20):12004–12009.
- Schaffer, K. (1892). Beitrag zur histologie der ammonshornformation. *Archiv für mikroskopische Anatomie*, 39(1):611–632.
- Schikorski, T. and Stevens, C. F. (1997). Quantitative ultrastructural analysis of hippocampal excitatory synapses. *The Journal of neuroscience*, 17(15):5858–5867.
- Sheng, Z.-H. and Cai, Q. (2012). Mitochondrial transport in neurons: impact on synaptic homeostasis and neurodegeneration. *Nature Reviews Neuroscience*, 13(2):77–93.
- Shepherd, G. M. and Harris, K. M. (1998). Three-dimensional structure and composition of ca3 cal axons in rat hippocampal slices: implications for presynaptic connectivity and compartmentalization. *The Journal of neuroscience*, 18(20):8300–8310.
- Shigemoto, R., Kulik, A., Roberts, J., Ohishi, H., Nusser, Z., Kaneko, T., and Somogyi, P. (1996). Target-cell-specific concentration of a metabotropic glutamate receptor in the presynaptic active zone. *Nature*, 381:442–458.
- Sik, A., Tamamaki, N., and Freund, T. (1993). Complete axon arborization of a single ca3 pyramidal cell in the rat hippocampus, and its relationship with postsynaptic parvalbumin-containing interneurons. *European Journal of Neuroscience*, 5(12):1719–1728.
- Silver, R. A., Lübke, J., Sakmann, B., and Feldmeyer, D. (2003). High-probability unquantal transmission at excitatory synapses in barrel cortex. *Science*, 302(5652):1981–1984.
- Soleng, A., Chiu, K., and Raastad, M. (2003a). Unmyelinated axons in the rat hippocampus hyperpolarize and activate an h current when spike frequency exceeds 1 hz. *The Journal of physiology*, 552(2):459–470.
- Soleng, A. F., Raastad, M., and Andersen, P. (2003b). Conduction latency along ca3 hippocampal axons from rat. *Hippocampus*, 13(8):953–961.
- Soltesz, I. and Deschenes, M. (1993). Low-and high-frequency membrane potential oscillations during theta activity in ca1 and ca3 pyramidal neurons of the rat hippocampus under ketamine-xylozine anesthesia. *Journal of neurophysiology*, 70(1):97–116.
- Spencer, W. A. and Kandel, E. R. (1961). Hippocampal neuron responses to selective activation of recurrent collaterals of hippocampofugal axons. *Experimental Neurology*, 4(2):149–161.
- Staley, K. J., Bains, J. S., Yee, A., Hellier, J., and Longacher, J. M. (2001). Statistical model relating ca3 burst probability to recovery from burst-induced depression at recurrent collateral synapses. *Journal of Neurophysiology*, 86(6):2736–2747.
- Staley, K. J., Longacher, M., Bains, J. S., and Yee, A. (1998). Presynaptic modulation of ca3 network activity. *Nature neuroscience*, 1(3):201–209.

- Stevens, C. F. and Tsujimoto, T. (1995). Estimates for the pool size of releasable quanta at a single central synapse and for the time required to refill the pool. *Proceedings of the National Academy of Sciences*, 92(3):846–849.
- Stokes, C. C. and Isaacson, J. S. (2010). From dendrite to soma: dynamic routing of inhibition by complementary interneuron microcircuits in olfactory cortex. *Neuron*, 67(3):452–465.
- Takumi, Y., Ramírez-León, V., Laake, P., Rinvik, E., and Ottersen, O. P. (1999). Different modes of expression of ampa and nmda receptors in hippocampal synapses. *Nature neuroscience*, 2(7):618–624.
- Toth, K., Freund, T., and Miles, R. (1997). Disinhibition of rat hippocampal pyramidal cells by gabaergic afferents from the septum. *The Journal of Physiology*, 500(Pt 2):463.
- Traub, R. D. and Bibbig, A. (2000). A model of high-frequency ripples in the hippocampus based on synaptic coupling plus axon–axon gap junctions between pyramidal neurons. *The Journal of Neuroscience*, 20(6):2086–2093.
- Traub, R. D., Pais, I., Bibbig, A., LeBeau, F. E., Buhl, E. H., Hormuzdi, S. G., Monyer, H., and Whittington, M. A. (2003). Contrasting roles of axonal (pyramidal cell) and dendritic (interneuron) electrical coupling in the generation of neuronal network oscillations. *Proceedings of the National Academy of Sciences*, 100(3):1370–1374.
- Traub, R. D. and Wong, R. (1982). Cellular mechanism of neuronal synchronization in epilepsy. *Science*, 216(4547):745–747.
- Urban, N. N. and Barrionuevo, G. (1998). Active summation of excitatory postsynaptic potentials in hippocampal ca3 pyramidal neurons. *Proceedings of the National Academy of Sciences*, 95(19):11450–11455.
- Vanderwolf, C. H. (1969). Hippocampal electrical activity and voluntary movement in the rat. *Electroencephalography and clinical neurophysiology*, 26(4):407–418.
- Vervaeke, K., Gu, N., Agdestein, C., Hu, H., and Storm, J. (2006). Kv7/kcnq/m-channels in rat glutamatergic hippocampal axons and their role in regulation of excitability and transmitter release. *The Journal of physiology*, 576(1):235–256.
- Viney, T. J., Lasztocki, B., Katona, L., Crump, M. G., Tukker, J. J., Klausberger, T., and Somogyi, P. (2013). Network state-dependent inhibition of identified hippocampal ca3 axo-axonic cells in vivo. *Nature neuroscience*, 16(12):1802–1811.
- Wilson, M. A. and McNaughton, B. L. (1994). Reactivation of hippocampal ensemble memories during sleep. *Science*, 265(5172):676–679.
- Wittner, L., Henze, D. A., Záborszky, L., and Buzsáki, G. (2007). Three-dimensional reconstruction of the axon arbor of a ca3 pyramidal cell recorded and filled in vivo. *Brain Structure and Function*, 212(1):75–83.
- Wittner, L. and Miles, R. (2007). Factors defining a pacemaker region for synchrony in the hippocampus. *The Journal of physiology*, 584(3):867–883.

Wong, R. and Traub, R. D. (1983). Synchronized burst discharge in disinhibited hippocampal slice. i. initiation in ca2-ca3 region. *Journal of Neurophysiology*, 49(2):442-458.

---

## List of Figures

---

2.1	Action potential . . . . .	3
2.2	$\text{Na}_v1.2$ and $\text{Na}_v1.6$ distribution in AIS . . . . .	10
2.3	Family of potassium channels . . . . .	12
2.4	Neuron Structures . . . . .	20
2.5	Action potential shapes differ if it is initiated in the axon or in the soma . . . . .	22
2.6	Hippocampal Cell morphology . . . . .	23
2.7	Expression of selected channels on AIS . . . . .	26
2.8	Burst firing in pyramidal cell . . . . .	27
2.9	Dendritic computation . . . . .	28
2.10	Action potentials in the soma and AIS . . . . .	30
2.11	Effect of TTX on recovery after activation of the action potential . . . . .	34
2.12	Neurons with the same channel compositions but different morphologies produce different firing patterns . . . . .	35
2.13	Oscillations in the hippocampus . . . . .	36
3.1	Theories of spike initiation . . . . .	65
3.2	Intracellular features of sharp spike initiation in multicompartmental models . . . . .	66
3.3	Extracellular field at spike initiation . . . . .	68
3.4	Currents at spike initiation . . . . .	71
3.5	Balance of currents at spike initiation . . . . .	72
3.6	Impact of intracellular resistivity $R_i$ on excitability . . . . .	73
3.7	Influence of soma size on spike initiation . . . . .	75
3.8	Somatic onset rapidness . . . . .	78
3.9	Active backpropagation is not necessary for sharp initiation . . . . .	80

3.10	Two-compartment model . . . . .	81
3.11	Sharpness of spike initiation in a small simulated neuron (axon diameter: 0.3 $\mu\text{m}$ ) . . . . .	83
4.1	Extracellular potential for models with shifted axon initial segment . . .	97
4.2	Width of extracellular AP . . . . .	98
4.3	Extracellular AP measured in midline between soma and AIS . . . . .	100
4.4	Profile of extracellular potential along soma and axon . . . . .	101
4.5	Dipole approximation graphics . . . . .	102
4.6	Axial current . . . . .	103
4.7	Dipole model . . . . .	105
4.8	Two cylinder model . . . . .	106
5.1	Detection and measurement of SPWs . . . . .	117
5.2	Single CA3 pyramidal cells trigger SPWs . . . . .	119
5.3	Synaptic events corresponding to SPWs and fIPSPs . . . . .	121
5.4	Evidence for activation of perisomatic inhibitory synapses during SPWs .	123
5.5	Single pyramidal cells induce firing in multiple interneurons . . . . .	124
5.6	Differences between initiated and spontaneous SPW fields . . . . .	126
5.7	Field inhibitory motifs during SPWs . . . . .	128
A.1	CA3 pyramidal cell axon and targets . . . . .	144
A.2	Anatomy and Ca handling at recurrent synapses between CA3 pyramidal cells . . . . .	147
A.3	Unitary effects of recurrent excitatory synapses . . . . .	150
A.4	Recurrent inhibitory circuits in the CA3 region . . . . .	154
A.5	Recurrent excitatory networks . . . . .	159

---

## List of Tables

---

2.1	Ion concentrations . . . . .	5
2.2	Na <sub>v</sub> channels in mammalian brain . . . . .	9
2.3	K <sub>v</sub> channels in mammalian brain . . . . .	14
2.4	Ca <sub>v</sub> channels in mammalian brain . . . . .	17